EXPERIMENTAL ANALYSIS OF THROUGH MASK ELECTROCHEMICAL MICROMACHINING PROCESS FOR GENERATION OF MICRO-TEXTURED SURFACES

Thesis submitted by

SUBRATA MAHATA

DOCTOR OF PHILOSOPHY (ENGINEERING)

DEPARTMENT OF PRODUCTION ENGINEERING

FACULTY COUNCIL OF ENGINEERING & TECHNOLOGY

JADAVPUR UNIVERSITY

KOLKATA-700 032

INDIA

2019

JADAVPUR UNIVERSITY
KOLKATA-700 032

Index No. 300/12/Engg.

TITLE OF THE THESIS:

Experimental Analysis of Through Mask Electrochemical Micromachining Process for Generation of Micro-Textured Surfaces

NAME, DESIGNATION & INSTITUTION OF THE SUPERVISOR:

Dr.B.BHATTACHARYYA
Professor, Dept. of Production Engg.
Jadavpur University
Kolkata – 700 032, India

LIST OF PUBLICATIONS:

International Journals:

1. "3D micro pattern generation by electrochemical micromachining (EMM) process", International Journal of Precision Technology, 4, Nos. 3/4 (2014) 192-211.

2. "Micro Dimple Array Fabrication by Through Mask Electrochemical Micromachining Utilizing Low-Aspect Ratio Mask", Journal of the Electrochemical Society, 165(3) (2018) E129-E137

3. "Influence of Electrochemical Micromachining Process Parameters during Fabrication of Varactor Micropattern", International Journal of Advanced Manufacturing Technology, 96 (2018) 411-427.

4. "Influence of Electrolytes on Surface Texture Characteristics Generated by Electrochemical Micromachining", Journal of Micromanufacturing, (2018) DOI: 10.1177/2516598418765355.

5. "Investigation into Suitability of Electrolytes during Microsurface Texturing by Electrochemical Micromachining", International Journal of Precision Technology 8, Nos. 2-4 (2019) 379-396.

6. "Fabrication of Different Micro Patterned Arrays by Through Mask Electrochemical Micromachining", Journal of the Electrochemical Society, 166(8) (2019) E217-E225.

7. "Experimental Investigation into Micro-Textured Surface Generation by Through Mask Electrochemical Micromachining", Journal of Surface Engineering and Applied Electrochemistry, 4 (56) (2020) (Accepted).

Book Chapters

1. "Micro-dimple Array Fabrication by Through Mask Electrochemical Micromachining", Lecture Notes on Multidisciplinary Industrial Engineering, M. S. Shunmugam and M. Kanthababu (Eds): Advances in Micro and Nano Manufacturing and Surface Engineering, 2019, Springer, 978-981-32-9424-0, 486068_1_En, (31).

LIST OF PATENTS: NIL

LIST OF PRESENTATIONS IN NATIONAL / INTERNATIONAL CONFERENCES/ WORKSHOPS:

International Conferences:

1. “Generation of 3D Fine Pattern Utilizing Electrochemical Micromachining Process”, Proceedings of the 8th International Conference on Precision, Meso, Micro and Nano Engineering (COPEN 2013), 13th-15th December 2013, NIT Calicut, Kerala, India (2013), pp 285.

2. “Investigation Into Electrochemical Micromachining Process For Fabricating 3D Fine Patterns In Air Lubricated Bearing”, Proceedings of the 5th International & 26th All India Manufacturing Technology, Design and Research Conference (AIMTDR 2014) December 12th–14th, 2014, IIT Guwahati, Assam, India (2014), pp 231-1.

3. “Fabrication of Island-Free Micro Dimple Arrays by Through Mask Electrochemical Micromachining”, Proceedings of the 10th International Conference on Precision, Meso, Micro and Nano Engineering (COPEN 2017), 7th-9th December 2017, IIT Madras, Chennai, Tamil Nadu, India (2017), pp 607.

4. “Investigation into Suitability of Electrolytes during Fabrication of Micro Dimple Pattern by Electrochemical Micromachining”, Proceedings of the 10th International Conference on Precision, Meso, Micro and Nano Engineering (COPEN 2017), 7th-9th December 2017, IIT Madras, Chennai, Tamil Nadu, India (2017), pp 595.

5. “Micro Dimple Array Fabrication by Through Mask Electrochemical Micromachining”, Proceedings of the 7th International & 28th All India Manufacturing Technology, Design and Research Conference (AIMTDR 2018) December 13th–15th, 2018, Anna University, Chennai, India (2018).

6. “Parametric Investigation into Electrochemical Micromachining for Generation of Different Microsurface Textures”, Proceedings of the 7th International & 28th All India Manufacturing Technology, Design and Research Conference (AIMTDR 2018) December 13th–15th, 2018, Anna University, Chennai, India (2018).

7. “Experimental Investigation during square micro-dimple pattern generation by Through Mask Electrochemical Micromachining”, Proceedings of the 11th International Conference on Precision, Meso, Micro and Nano Engineering (COPEN 2019), 12th-14th December 2019, IIT Indore, Indore, Madhya Pradesh, India (2019).(Accepted).

8. “Determination of the optimum process parameters through GRA during generation of circular micro-textured pattern by TMEMM”, Proceedings of the International Conference on Advancements in Mechanical Engineering (ICAME 2020), 16th-18th January 2020, Aliah University, Kolkata, West Bengal, India (2020).(Accepted).

JADAVPUR UNIVERSITY

FACULTY OF ENGINEERING & TECHNOLOGY
DEPARTMENT OF PRODUCTION ENGINEERING

CERTIFICATE FROM THE SUPERVISOR

This is to certify that the thesis entitled "EXPERIMENTAL ANALYSIS OF THROUGH MASK ELECTROCHEMICAL MICROMACHINING PROCESS FOR GENERATION OF MICRO-TEXTURED SURFACES" submitted by Shri SUBRATA MAHATA, who got his name registered on 9th April 2012 for the award of Ph.D. (Engg.) degree of Jadavpur University, is absolutely based upon his own work under the supervision of PROF.B.BHATTACHARYYA and that neither his thesis nor any part of the thesis has been submitted for any degree/diploma or any other academic award anywhere before.

____

Signature of the Supervisor
and date with Office Seal

Dedicated to my parents….

My pillar of strength and source of inspiration

For their faith in education, endless support,

love and encouragement

PREFACE

Micromanufacturing has become one of the focused areas of research in the recent years. Since industries from different fields are continually searching for the miniaturized products, the need to fabricate micro products from engineering materials becomes more apparent and necessary. In recent years, there has been a rapid development in micromanufacturing processes. Micromachining technology plays an increasing decisive and influential role in the miniaturization of components ranging from biomedical applications to chemical micro reactors and sensors. With the developments in MEMS, micro products are widely used in various fields namely electronics, aerospace, optical, biomedical, automotive, refrigeration and air conditioning etc. for manufacturing of micro components. Since, the miniaturization will continue till the existence of mankind, as long as people require effective space utilization with more efficient and better accuracy products, micromachining technology will still be more important in the future.

When ECM is used in microscopic domain for micromachining applications, it is called as Electrochemical Micromachining (EMM). EMM is an anodic dissolution process in which pulsed direct current with low voltage is applied between the metallic workpiece as anode and micro-tool electrode as cathode, immersed in an electrolyte with few microns of inter-electrode gap. The anodic material dissolves into metallic ions by the electrochemical reactions generating hydrogen gas bubbles on the cathode surface. Through Mask Electrochemical Micromachining (TMEMM) is categorized as one specialized type of EMM, which involves selective anodic dissolution of a metal or alloy through a mask in order to achieve a given shape and surface finish. The material removal is restricted by positioning a photoresist pattern, that is, masks on the metal surface; thus, dissolution is allowed from the desired portions of the metal surface only, i.e. workpiece surface.

The micro-scale surface topography of rolling mechanical elements plays an important role in the frictional power loss, the surface wear, the rolling contact fatigue (micro and macro scale pitting) failure etc. Micro-surface texturing is a process, which implements arranged micro-dimples of various shapes and patterns onto the contact surfaces. These dimples contribute mainly by acting as lubricant reservoirs to provide lubricant under the starved lubrication condition, and micro-hydrodynamic bearings to provide additional load-carrying capacity. In addition, the dimples can trap wear particles to reduce the third-body induced surface stress concentrations, friction and wear. Hence, this needs suitable micro machining method for machining of precise and accurate micro textured surfaces. TMEMM is a key micro

machining processes for the fabrication of simple as well as complex micro features on engineering materials, due to its advantages that includes better precision and control, less machining time, reliable, flexible, etc.. Geometrical shape, size, and surface quality of micro-dimples, fabricated on components affects its service life and running performance, hence fabrication of complex micro-textures on metallic surfaces in the range of tens to hundreds of microns in width and depth, with good shape accuracy, and surface quality is the focused area of research and needs further development.

From the past research findings, it is evident that fabrication of high-aspect-ratio patterned microstructures on metallic surfaces is still a challenging task for various available conventional and nonconventional micromachining techniques. Although researchers have already initiated some research work in the area of TMEMM, it still needs lot of independent research for achieving satisfactory control over TMEMM process parameters especially the mask thickness to fulfill the requirements of micro structuring. Considering the requirements of this research task, following objectives have been modulated for the work presented in this thesis:

(i) To develop experimental set-up of TMEMM for surface texturing of different micro textures as well as to prepare the experimental job samples through masking along with utilizing UV Lithography. The developed set-up should be capable of performing experimental investigations into various predominant processes for fulfilling the requirements of micro machining at different stages of experimentation.

(ii) To fabricate island-free micro-dimples by searching out the influence of predominant TMEMM process parameters i.e. applied voltage, pulse frequency, electrolyte flow rate, duty ratio and machining time, etc. on machining performance and dimensional uniformity in terms of undercut, average depth and surface roughness of the generated textured dimple array on stainless steel substrates utilizing low aspect ratio mask.

(iii) To identify most suitable range of TMEMM process parameters for fabrication of circular as well as square arrayed micro-textured patterned surfaces on stainless steel wafers by investigating the influence of various controllable process parameters such as mask thickness, duty ratio and machining time on machining accuracy and surface characteristics of the generated micro-patterned arrays. Moreover, attempt needs to be made to study the friction characteristics of the generated square and circular micro-textured patterned surfaces.

(iv) To fabricate high-aspect-ratio 3D micro arrayed structures with considerable level of precision employing low aspect ratio mask by developing the machining guidelines for TMEMM utilizing the developed experimental set-up by varying process parameters e.g. applied voltage along with electrolyte type and concentration on the machining accuracy and dimensional uniformity along with the surface roughness characteristics.

(v) To find out the best parametric setting of TMEMM for micro-pattern generation with minimum undercut, maximum dimple depth and minimum surface roughness using Design of Experiments (DOE) based on Taguchi Methodology.

(vi) To perform multi-objective optimization for searching out the optimal setting of TMEMM process parametric combination for simultaneous maximization of the dimple depth, minimization of the undercut and minimization of surface roughness utilizing Grey Relational Analysis. Micrographs of the micro-dimpled pattern generated at optimized parametric combination during experimentation needs to be observed in details and analyzed to ascertain the correctness of the optimization as well as conclusions made there on.

The thesis is structured in well-organized manner in such a way that chapter 1 outlines the review of past research on Through Mask Electrochemical Micromachining (TMEMM) and importance of TMEMM in engineering scenario. It also includes the challenges that are faced by the researchers during the periodical development of the said process, which forms the base for the framing of the objectives of the present thesis. Chapter 2 discusses the basic fundamentals of TMEMM process. Chapter 3 focuses on the development of TMEMM experimental set-up for generation of micro-dimple array of different geometries and the detailed experimental procedure for preparation of the samples required during the experimentation. Chapter 4 highlights fundamental experimentations during TMEMM utilizing the experimental set-up for analyzing the influences of the predominant TMEMM process parameters during the fabrication of island-free micro textured patterns and also study its effect on the dimensional uniformity and surface characteristics of the generated arrayed micro-textures. Chapter 5 incorporates the experimental investigations carried out during the generation of circular and square micro-dimples using low aspect ratio masks. A range of low thickness masks have been studied experimentally considering variable machining times including the surface topography of the generated micro-dimples. This chapter also includes the study of the friction characteristics between the micro-textured surfaces containing circular and square micro-patterns generated by TMEMM. Chapter 6 overviews the experimentation carried out for controlling characteristics of high aspect ratio

micro-textures during TMEMM. It includes in-depth study of some of the vital process variables for generation of High Aspect Ratio (HAR) microstructures within a short period of time. Chapter 7 include experimental investigation based on Taguchi method of robust design to find out the influence of the significant process parameters on machining accuracy i.e. undercut, dimple depth and surface roughness characteristics. It also consists of optimization of responses by searching out the most favorable parametric combination for decreasing undercut and surface roughness while increasing the dimple depth of the generated micro-patterned arrays. Moreover, this chapter also outlines about the multi-objective optimization of the studied responses through Grey Relational Analysis for simultaneous optimization of the responses. Finally chapter 8 consolidates the outcomes of the present research work along with the scope of the research in the area of TMEMM.

The researcher has attempted to justify the uniqueness of the present research work by exploring the possibilities of micromachining of various arrayed microfeatures on SS304 substrates utilizing through mask electrochemical micromachining process. The most salient and unique research finding that has been observed in the present research includes development of the TMEMM system set-up for arrayed island free micro-dimple pattern generation utilizing very thin photoresist masks. Analysis of fabricated micro-dimples of different geometrical contours utilizing low aspect ratio masks based on critical examination of various SEM micrographs to determine the influence of significant TMEMM parameters on machining accuracy and surface roughness during micromachining is another significant outcome. Single-objective optimization by Taguchi methodology based on Design of Experiments (DOE) and multi-objective optimization of TMEMM process parameter through Grey Relational Analysis will be significant contributions for opening up new insights to the applied researchers and manufacturing engineers working in the area of TMEMM. This research study also contribute by setting up most suitable TMEMM process parameters for machining of various micro-textures on thin stainless steel sheets. The study presented in this research work through the in-depth experimental investigations on through mask electrochemical micromachining of SS 304 may be useful for effective utilization of TMEMM process for various practical engineering applications.

Therefore, the researcher believes that the present research will provide a lot of possibilities to the researchers and scientists who are working in the area of TMEMM process and also provide guidance for indigenous development of TMEMM system for industrial purpose for precision micro-engineering applications.

ACKNOWLEDGEMENT

The insight of this thesis is certainly due to the contribution of several outstanding persons. The author wishes to express his deep sense of gratitude to the thesis supervisor Dr.Bijoy Bhattacharyya, Professor, Production Engineering Department, Jadavpur University, Kolkata for his constant guidance, helpful suggestions, continuous association, supports, encouragement and valuable advice at every aspect from the sprouting stage to the development stage of this research work. Without his constructive and timely advice, this thesis would have not been progressed as smoothly as it did towards its completion. The author indeed owes to him for his patience and valuable time which he has spent for the present research work.

The author gratefully acknowledges the co-operation and encouragement received from Dr. Biswanath Doloi, Professor, Dr. Shankar Chakraborty, Professor, Dr. D. Banerjee, Professor, Dr. Biplab Ranjan Sarkar, Associate Professor, Dr. A. S. Kuar, Head of the Department, and all the faculty members of Production Engg. Dept., Jadavpur University during the course of the research. Author would like to take this opportunity to thank Mr. Biswanath Das, Mr. Biswajit Pathak, Mr. Ravishankar Pramanik, Mr. Pravat Barik, and Mr. Subir Sanyal who supported all the time during developmental and experimentation stages.

Author gratefully acknowledges the support and co-operation of Dr. Rahul Shukla, Scientific Officer, Indus Synchrotrons Utilization Division, Raja Ramanna Centre for Advanced Technology (RRCAT), Indore for his endless support and co-operation for providing the laboratory facilities at RRCAT, Indore during preparation of the experimental samples. Thanks are also extended to the fellow students and research assistants of RRCAT, Indore, who, endlessly supported with their cordial assistance and valuable guidance during each and every stay at RRCAT, Indore.

Appreciation is also due to all fellow colleagues, Dr. V.U. Rathod, Dr. S.S. Anasane, Dr. Golam Kibria, Dr. Somnath Das, Nilanjan Roy, Subhrajit Debnath, Koushik Mishra, Sandip Kunar, Santosh Kumar, Abhishek Sen, R.M. Tayade, Sovan Maity, Hanimur Rahman, Vidyapati Kumar, and Goutam Roy for their constant co-operation, useful assistance and support during this research work. Author deeply extends thanks to Mr.Ramen Mallick, Deputy Chief Mechanical Engineer/Coaching, Eastern Railway, Kanchrapara, Mr.Animesh Ghosh, Assistant Works Manager/Coaching, Eastern Railway, Kanchrapara for their

humbleness and endless support during my period of study. The brawny support author has received from Mr. Sumit Pal, Senior Section Engineer/ Eastern Railway, Kanchrapara along with his valuable support as well as suggestions are beyond the acknowledgement. The author also likes to convey heartiest compliments to Mr. Subrata Nandi, Mr. Subrata Malakar, Mr. Kuntal Ghoshal, Eastern Railway, Kanchrapara Workshop for their consistent inspiration in completion of this research work.

Last but not the least, author would like to thank his parents, for their belief in education and endless support for higher studies and especially younger sister Jhulan for her warm wishes and constant support as well as inspiration, and all the family members for their constant encouragement in the pursuit of this research work. Without their understanding none of this would have been possible. It would have been very much difficult to complete this work without the support of his wife Mousami, who sacrificed her quality time and love during this tenure being as a primary source of strength and inspiration for him.

Finally, author sincerely thanks all of them who contributed directly or indirectly to this research work and helped the author in making the research work a success.

Subrata Mahata

VITA

The author, Sri Subrata Mahata, son of Mrs. Krishna Mahata & Mr. Niranjan Mahata was born on 29th December 1988 in a small village, Dabor in the district of Paschim Bardhhamaan, West Bengal. Author passed both the A.I.S.S.E.as well as A.I.S.S.C.E. from D.A.V. Public School, Rupnarayanpur, under the Central Board of Secondary Education in the year 2003 and 2005 respectively.

The author earned B.Tech. in Mechanical Engineering in the year 2009 from Mallabhum Institute of Technology, Bishnupur under West Bengal University of Technology with first class (DGPA-8.82). He was awarded the University Bronze Medal for securing 3rd position in the university. He completed his M.Tech. in Manufacturing Technology from National Institute of Technical Teachers' Training & Research, Kolkata in 2011 with first class. With a DGPA of 9.17, he secured the 3rd position in the university and was felicited with the University Bronze Medal.

The author qualified in the Graduate Aptitude Test in Engineering (GATE) in two successive years (2008 & 2009) with percentiles of 84.48 and 85.68 respectively, which entitled him to pursue his M.Tech with fellowship of AICTE, New Delhi throughout the tenure of two years.

Author joined the Department of Production Engineering as Senior Research Fellow under a project, "Optimization of Electrochemical Micromachining Process for 3D Fine Pattern Generation" sponsored by Bhabha Atomic Research Centre, Government of India in August, 2011. In April 2012, he got his name registered for Ph.D. (Engg.) in the Department of Production Engineering before joining Eastern Railway, Kanchrapara Workshop as Senior Section Engineer. He continued to pursue his research activities in the Department for completion of Ph.D. (Engg.).

Author is engaged in research work from 2011 onwards. He has published research papers in international journals and presented his work in international and national conferences. His research interests include micromachining and advanced manufacturing processes.

TABLE OF CONTENTS

		PAGE NO.
TITLE SHEET	------	i
LIST OF PUBLICATIONS	------	iii
CERTIFICATE FROM THE SUPERVISOR	------	v
PREFACE	------	vi
ACKNOWLEDGEMENT	------	x
VITA	------	xii
TABLE OF CONTENTS	------	xiv
Chapter 1 INTRODUCTION		
1.1 Introduction	------	01
1.2 Micromachining Processes	------	02
1.3 Electrochemical Micromachining (EMM)	------	06
1.4 Through Mask Electrochemical Micromachining (TMEMM)	------	09
1.4.1 Types of TMEMM	------	10
1.5 Review of Literature	------	14
1.6 Opportunities and Challenges in TMEMM	------	35
1.7 Objects and Scope of Present Research	------	36
Chapter 2 FUNDAMENTALS OF THROUGH MASK ELECTROCHEMICAL MICROMACHINING		
2.1 Introduction	------	39
2.2 Masking Methods and Materials	------	45
2.3 Metals and Electrolytes in TMEMM	------	47
2.4 Technical and Financial Considerations in TMEMM	------	54
Chapter 3 DEVELOPMENT OF TMEMM EXPERIMENTAL SET-UP AND PREPARATION OF EXPERIMENTAL SAMPLES		
3.1 Introduction	------	55
3.2 Components of the Developed TMEMM set-up	------	56
3.3 Specifications of the TMEMM set-up	------	60

3.4 Preparation of Experimental Samples ------ 63
3.4.1 Importance of SS304 in Engineering Applications ------ 63
3.4.2 Planning for Preparation of the Samples ------ 64
3.4.3 Mask Design and Fabrication ------ 65
3.4.4 UV-Lithography ------ 66

Chapter 4 INVESTIGATIONS INTO FABRICATION OF ISLAND-FREE MICRO-DIMPLE ARRAY BY TMEMM

4.1 Introduction ------ 70
4.2 Necessity of Island removal from dimple surface during generation of micro-textures ------ 70
4.3 Difficulties in conventional procedures for Island Removal in TMEMM ------ 71
4.4 Experimentation for investigating the effectiveness of low thickness mask (AZ4903) during fabrication of Island Free Micro Dimples ------ 71
4.4.1 Experimental Planning ------ 71
4.4.2 Experimental Methodology ------ 73
4.5 Experimental Results and Analysis for fabrication of Island Free Micro-Dimple array ------ 74
4.5.1 Effect of Electrolyte Flow Velocity ------ 74
4.5.2 Influence of Pulse Frequency ------ 80
4.5.3 Influence of Applied Voltage ----- 83
4.5.4 Influence of Duty Ratio and Machining Time on Dimple Characteristics ------ 86
4.6 Fabrication of Island-Free Micro Dimple Array based on Experimental Analysis ------ 91
4.7 Outcomes of the experimentation ------ 93

PAGE NO.

Chapter 5 GENERATION OF CIRCULAR AND SQUARE MICRO TEXTURED ARRAY BY TMEMM UTILIZING LOW ASPECT RATIO MASK

5.1 Introduction ------ 94
5.2 Importance of Mask Thickness in TMEMM ------ 95
5.3 Experimental Planning for Generation of Patterned Array of Different Geometries ------ 95
5.4 Experimental Methodology ------ 97
5.5 Experimental Results and Analysis for fabrication of Micro-Patterned Textured Array with different geometries ------ 98
5.5.1 Influence of TMEMM Parameters on Circular Micro-Patterned Textures ------ 99
5.5.2 Influence of TMEMM Parameters on Square Micro- Patterned Textures ------ 107
5.6 Fabrication of Circular and Square Micro-Dimple Array based on Experimental Analysis ------ 114
5.7 Analysis based on Friction Tests ------ 117
5.8 Experimental Outcomes ------ 119

Chapter 6 EXPERIMENTATION FOR CONTROLLING CHARACTERISTICS OF HIGH ASPECT RATIO MICRO-TEXTURES DURING TMEMM

6.1 Introduction ------ 121
6.2 Experimental Planning ------ 122
6.3 Experimental Methodology ------ 123
6.4 Experimental Results and Discussions for Controlling Aspect Ratio of micro-textures ------ 124
6.4.1 Effect of Applied Voltage and Electrolyte type on Undercut ------ 124
6.4.2 Influence of Applied Voltage and Electrolyte type on Dimple Depth (h) ------ 126
6.4.3 Influence of Applied Voltage on Surface Quality ------ 130

PAGE NO.

6.5 Fabrication of High Aspect Ratio (HAR) Micro-Textured Array of Circular Dimples based on Experimental Analysis ------ 131
6.6 Analysis based of Friction Tests ------ 133
6.7 Outcomes of the experimentation ------ 135

Chapter 7 EXPERIMENTATION FOR OPTIMIZING MACHINING ACCURACY AND SURFACE CHARACTERISTICS DURING CIRCULAR MICRO-TEXTURED PATTERN GENERATION

7.1 Introduction ------ 137
7.2 Experimental design based on Taguchi method ------ 138
7.2.1 Signal-to-Noise (S/N) ratio curve ------ 138
7.2.2 Analysis of Variance (ANOVA) ------ 139
7.2.3 Verification of Experiments ------ 140
7.3 Planning for Taguchi based Experimentation ------ 141
7.4 Procedure of Experimentation ------ 142
7.5 Experimental Results and Discussion ----- 142
7.5 1 Analysis based on S/N ratio curves ------ 142
7.5.2 Analysis of Variance ------ 145
7.6 Single Objective Optimization of Process Parameters ------ 147
7.7 Grey Relational Analysis ------ 149
7.8 Multi Objective Optimization of the desired responses ------ 150
7.9 Outcomes of the experimentation ------ 154

Chapter 8 GENERAL CONCLUSIONS

8.1. General Conclusions ------ 155
8.2. Future Scope of the work ------ 160

BIBLIOGRAPHY

Chapter 1

INTRODUCTION

1.1 Introduction

Miniaturization of the components and systems has established their importance in all spheres. Products are becoming smaller, lighter and more compact day by day. Further, standards and quality requirements are also ever rising with time. Micromachining is finding more applications in many products in the automotive, aerospace, medical device, jewellery, and consumables industries etc. In order to stay competitive, manufacturers have to produce parts that are less pricey, have superior surface finishes and meet ever increasing product quality requirements. Electrochemical Machining (ECM) is one of the processes gaining wider recognition in this sector to machine parts more accurately. ECM was initially utilized for machining hard and difficult-to-cut materials for machining of macro sized products. ECM has received much attention from emerging engineers and scientists working in the area of micromachining and microfabrication for electronic, bio-medical, aviation, and other related high-tech industries [1].

The importance of surface texture seems to be a compulsory necessitate for the manufacturing industry in today's scenario. Surface texturing is one potential response for improving the tribological characteristics of mechanical components. Surface textures improve tribological performance by acting as reservoir for lubricant, wear debris and by acting as hydrodynamic bearings. Surface textures also vary depending on the kind of technique employed. The design process for surface texturing is highly correlated to the particular functions of any application for which texturing is required. Since, texture quality is greatly affected by methods utilized, it is important to select such machining process, which not only satisfies the precision and accuracy of the generated micro-textures but also considers the techno-economic effects involved with it. Through Mask Electrochemical Micromachining (TMEMM) has already become an increasingly important machining technology for surface micro-texturing. From the research and development carried out till date, it is apparent that the effective utilization of ECM process in microscopic domain for surface structuring demands pro-extensive research for developing electrochemical machining technology, which can be used for generation of different micro textured surfaces. Figure 1.1 shows the chronological improvement in accuracy of ECM technology with respect to time.

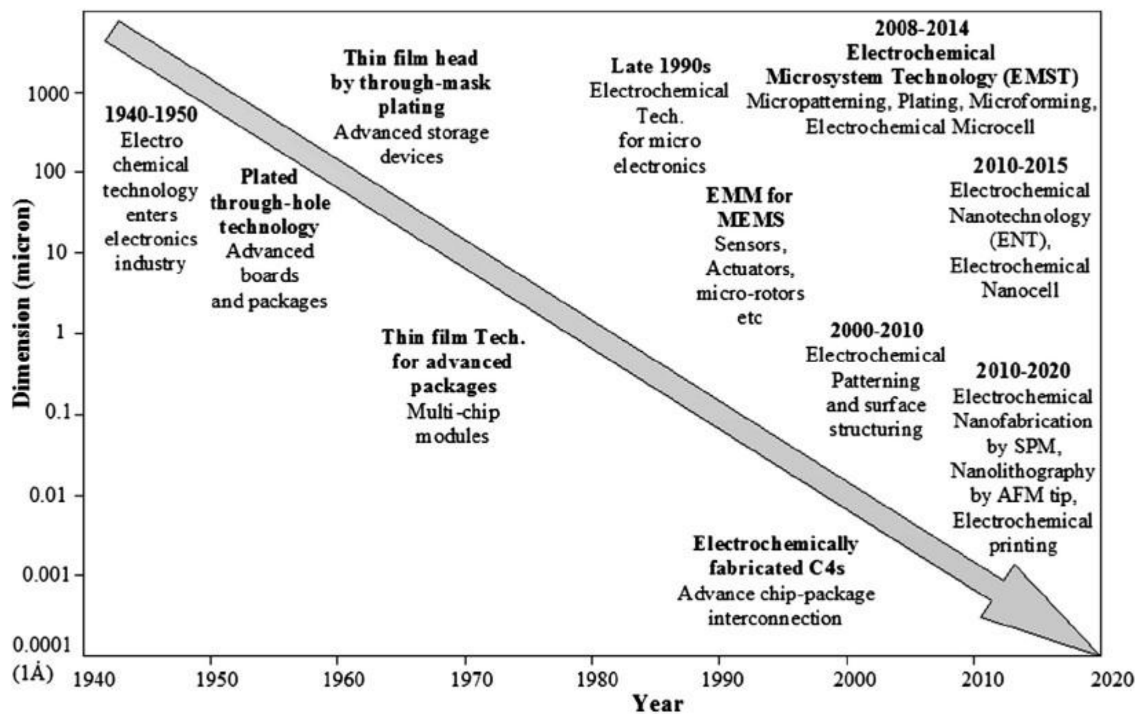

Figure 1.1: Chronological improvement of accuracy of ECM technology towards micro and nano range [2]

1.2 Micromachining processes

During the twentieth century, machining process has gained maturity in terms of the removal of specified amount from the workpiece in order to produce products more economically and accurately. In 1950s numerical control comes into picture in the field of manufacturing technology and opened the way for Computer Numerical Control (CNC) and Direct Numerical Control (DNC) machining. Further enhancement in machining accuracy, repeatability and flexibility in manufacturing process has been made possible with the advent of robotics in 1980s. Between 1980's and 1990's revolution in the field of computer and electronics industries accelerated the improvement in machining accuracy. Components of dimension in the order of micrometers (μm) were the increasing demands in the 1990s. As anticipated by Professor Taniguchi in 1983, the miniaturization technologies have moved into the nano-processing era, and now, even submicron precision is achievable from precise machining processes [3]. Figure 1.2 illustrates Taniguchi's prediction for achievable machining accuracy with time. This advancement has been made very clear in the semiconductor industry during the last three decades, where the number of components on an integrated chip has been doubled approximately in each 18 months time span. Today the semiconductor industries have revolutionized the field of electronics, telecommunications,

and computers. Micromachining can be placed in the group of precision machining and ultra precision machining.

Micro-machining is actually machining of small dimensions ranging from sub micron to micron. Such a smaller amount of machining is not easily achievable by a conventional technique where machining is done by the contact of tool and work piece. Achieving good surface finish is the major problem in conventional as well as some of the non-conventional machining methods.

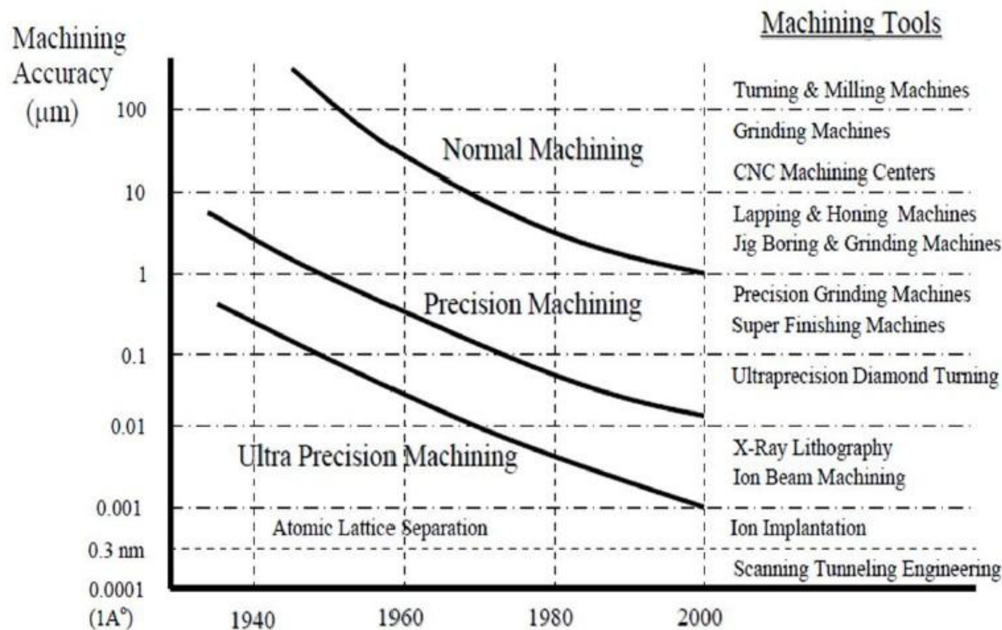

Figure 1.2: Machining accuracy with time by Taniguchi [3]

In recent years, with the development of Micro-electromechanical systems (MEMS) and multiple benefits of the micro systems such as low mechanical inertia, less thermal distortion, less mechanical vibration, low mass and weight, less space requirement, low cost of operation and less amount of material as well as energy requirements, microproducts are widely accepted in different engineering fields. Therefore, advanced engineering materials like stainless steel, titanium, titanium and nickel based alloys, aluminum alloys and super alloys etc. are used in fabrication of micro components because of their important properties like wear and corrosion resistant, good thermal conductivity, higher mechanical strength and bio-acceptability. Presently the market demand exists not only for micro parts but also for complex micro features on large components such as cooling holes in turbine blades, micro fins on large surface to increase heat transfer rate, etc. Hence, the objective of the miniaturization is either to create micro parts with better capabilities or to create micro features on macro components to enhance its functionality. Therefore, micro manufacturing

processes for advanced metallic materials needs further development for better applications in various fields.

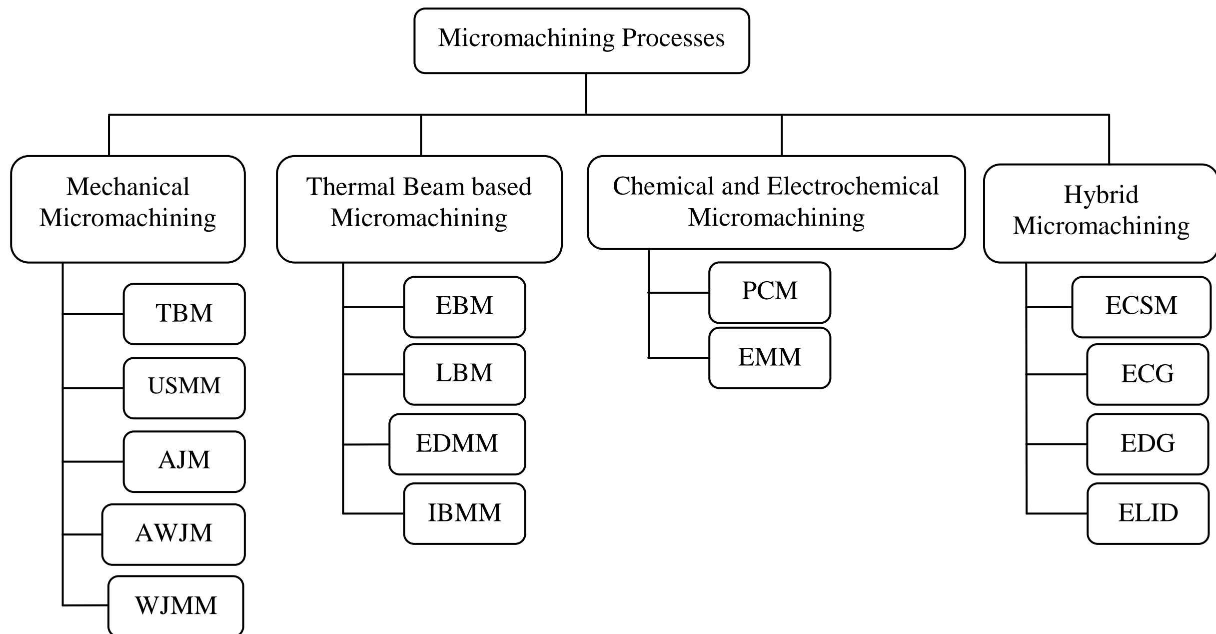

TBM: Tool Based Micromachining
AJMM: Abrasive Jet Micromachining
AWJMM: Abrasive Water Jet Micromachining
LBM: Laser Beam Micromachining
IBMM: Ion Beam Micromachining
EMM: Electrochemical Micromachining
ECG: Electrochemical Grinding
CHM: Chemical Machining

USMM: Ultrasonic Micromachining
WJMM: Water Jet Micromachining
EBM: Electron Beam Micromachining
EDMM: Electric Discharge Micromachining
PCMM: Photochemical Micromachining
ECSMM: ECM Spark Micromachining
EDG: Electric Discharge Grinding
ELID: Electrolytic In-Process Dressing

Figure 1.3 Different advanced micromachining techniques

Micromachining generally adopts a top down approach, which may involve various conventional as well as non-conventional machining techniques as exhibited in fig. 1.3. It may generate very small sized features such as micro holes, micro slots, and micro channels etc. on macro and micro parts, as well as micro components like micro gears, micro sensors, micro thermal devices, and computer chips down to nano size utilizing various techniques. Approaches towards micromachining are different for various methods to achieve an improvement. However these approaches are correctly directed towards micromachining with the following two guidelines.

(i) Micro-Cutting by conventional machining processes

In conventional machining, the basic methodology revolves around the removal of material in the micron level for the fabrication of microstructures. Here, selective material is removed from workpiece by mechanical force imparted by cutting tool through plastic deformation or brittle rupture. However, to maintain high level of precision is also an intricate task in the

conventional micro cutting. Now with the development of ultra-precision machine tools it is possible to achieve higher level of positioning accuracy, micromachining by cutting is achievable [4]. Several types of cutting processes are suitable for micromachining, e.g. drilling for micro holes, milling for microgrooves and micro 3D shapes, cutting for micro convex structures, micro grinding etc. are examples of conventional micro cutting process. The main drawbacks of conventional micromachining processes are high tool wear, rigidity requirement of the machine tool and heat generation at the tool-work interface, etc.

(ii) Micromachining by non-conventional processes

Non-conventional machining techniques has gained edge over conventional machining processes in micromachining applications due to its high precision and comparatively controlled micron size material removal. Supplementary advantage of non-conventional micromachining processes is that, there is partial or no physical contact between tool and workpiece. Laser Beam Machining (LBM), Ultrasonic Machining (USM), Electro Discharge Machining (EDM), Electron Beam Machining (EBM), Focused Ion Beam Machining (FIBM), Chemical Micro Machining (CMM) and Electrochemical Micromachining (EMM) are the typical examples of non conventional machining processes. These processes utilize either chemical or electrochemical energy, thermal energy, ultrasonic vibrations or combinations of these energies to machine the workpiece material.

Laser beam machining utilizes different laser sources such as CO_2-lasers, solid state lasers (e.g. Nd: YAG, copper vapor, diode lasers and excimer lasers for micromachining applications [5]. This process still has certain issues need to be dealt with e.g. non-uniform depth of cavity on vertical walls, heat affected zone (HAZ) etc. In EDM, sparks are generated between the two electrodes for material removal by erosion [6]. The said process requires the workpiece material to be conductive, while the hardness of the material is not a matter of concern. Tool wear is a foremost concern in this process in addition to thermal deformation of the machined surface. Material removal in micro USM is achieved by mechanical action of abrasives as well as erosion due to rapid pressure changes caused by the ultrasonic vibration of the abrasive slurry in the working zone. This process is suitable for the micro machining of hard brittle and inert insulators such as ceramics, glass, quartz, composites and precious stones and also for machining of fragile and porous materials such as graphite. Major problem in MUSM is the high tool wear ratio [6]. In EBM, high energy electron beam of high power density in the order of 1.55 $MWmm^{-2}$ [7] is focused on workpiece material. Material is removed by evaporation, causing thermal effects around the machining zone which restricts the aspect ratio of generated features. FIB machining is an alternative way of machining fine

structures. Ions from a plasma source are directed and focused onto the workpiece surface where removal of materials takes place through sputtering. In this way, 3D structures can be obtained in which spot sizes in the order of 10-50 nm are achieved. The material removal rates of the process are relatively low (of the order of some pm^3/s). Ions of inert gas like argon with high kinetic energy in the order of 10 keV are used to bombard and eject atoms from workpiece surface by elastic collision [6]. However, FIB is highly expensive and complex process. Chemical micro-machining (CMM) involves one or more chemical reactions by which a work piece substrate is oxidized to produce reaction products, which are carried away from the surface by the chemical medium. In CMM, both anodic and cathodic reaction takes place without external current on the reactive surface such that the rate of oxidation is balanced by the rate of reduction of the etchant groups. Difficulties of CMM process include lesser machining rate, use of highly corrosive electrolyte which causes relatively high ecological problems and safety hazards.

1.3 Electrochemical Micromachining (EMM)

When ECM is applied for machining of micron sized features it is called as electrochemical micromachining (EMM). EMM is an anodic dissolution process in which high frequency pulsed direct current with low voltage is applied between the metallic workpiece as anode and microtool as cathode, immersed in an electrolyte with few microns of inter-electrode gap. The anodic material dissolves into metallic ions by the electrochemical reactions generating hydrogen gas bubbles on the cathode surface.

With the development in MEMS, micro products are widely used in various fields namely electronics, aerospace, optical, biomedical, automotive, refrigeration and air conditioning etc. Machining of advanced engineering materials needs suitable micro machining method for the fabrication of precise and accurate micro parts. Traditional micro machining methods like turning, grinding, and milling have dimensional limitations for the cutting tools and fixtures, high tool wear, and poor surface quality. Whereas, non-traditional machining methods like EDM and LBM are thermal based, and results tool wear and heat affected zone respectively. LIGA process is limited to the fabrication of 2D micro structures and chemical machining process cannot be controlled properly in micro machining domain. Hence, EMM is the most suitable method for machining of micro features because of its important benefits like better precision and control, good surface quality without affecting metallic properties of work piece irrespective of the hardness of the material, no residual stress, no heat affected zone, and no tool wear i.e. micro-tools can be used repeatedly for longer period of time.

(i) Advantages of EMM

EMM has numerous benefits over other competing micro machining methods which can be categorized by product, material and advantages regarding machinery.

(a) Product advantages

(i) Machined micro features are free of burrs, and heat affected zone.

(ii) Since it is a noncontact type process, no stress developed in tool or workpiece surface.

(iii) High dimensional accuracy and better surface quality of machined micro features can be attained, since workpiece material is dissolved at atomic level by electrochemical reactions.

(iv) Complex 3D micro features can be machined by utilizing single micro-tool with the modern process monitoring capabilities.

(b) Material advantages

(i) Any metallic material can be machined irrespective of its hardness and toughness, since the anode dissolves by electrochemical reactions. The machining rate of material depends upon the atomic weight, valency, and the current passed through the circuit.

(ii) Metallic micro structure of workpiece material remains unaltered.

(c) Machinery advantages

(i) Less initial investment, as well as less running cost in comparison to competing micro machining processes.

(ii) The shape of the micro-tool electrode remains unaltered during the machining, since hydrogen gas evolution is the only reaction at the cathode.

(iii) Same micro-tool can be reused multiple times for machining of micro-features, since there is no tool wear, resulting low cost involvement in tool.

(ii) General limitations

(a) Because of the different specific requirements of the EMM process, machining setup for EMM is still under laboratory development. No ready to use commercial EMM set-up is available in market till date.

(b) Some electrolytes utilized during EMM may harm the environment, whereas eco-friendly electrolyte such as citric acid, mineral water, etc. can also be used in EMM for micro machining applications.

(c) Each product and material requires new research. So, mass production is essential for proper justification of the cost effectiveness of the process.

(iii) Types of EMM

EMM finds applications in aerospace, automobile, and other heavy industries for carrying out various micro-fabrications through shaping, milling, deburring, finishing as well as processing of thin films. EMM can be classified into two broad groups on the basis of degree of localization effect of the material removal mechanism as presented through fig. 1.4 i.e. Through mask EMM and Mask-less EMM.

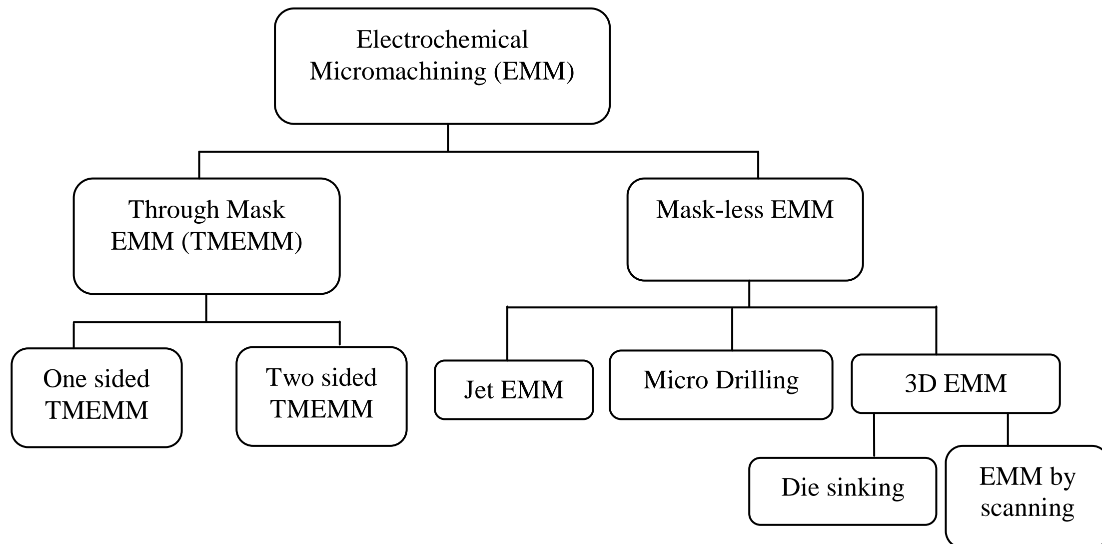

Figure 1.4 Detailed classifications of EMM techniques [2]

Through mask EMM can be again distinguished into one sided TMEMM and two sided TMEMM, whereas, Mask-less EMM can be classified to jet EMM, micro drilling and 3D EMM. Mask-less EMM achieves localized and directional material removal via different means such as a micrometer-sized cathode tool (μECM), an impinging electrolyte jet (Jet EMM), pulsed current (Pulse EMM), a focused laser beam (Laser enhanced EMM) or a combination of these methods. In this case, anodic dissolution is controlled by the current density distribution on the anode surface, which depends on various predominant machining parameters and anodic reaction pattern. Passivating electrolyte is suitable for mask-less EMM due to its ability to form transpassive oxide films and hence, metal removal is more selective and localized across the zone of work piece surface where it faces the tool. Metal removal is also, highly localized by the high frequency ultra short pulse width.

In jet EMM, an electrolyte jet is used as the machining tool. A stream of electrolyte flows through a nozzle acting as cathode, and impinges on the work piece, which is represented by an anode of the ECM cell. The jet EMM technique can be effectively utilized for generating micro patterns in metal foils.

In Capillary Drilling (CD), electrolyte is passed through a fine glass capillary to the cutting zone. A dilute solution of nitric acid as electrolyte is preferred for CD technique. The glass capillary contains very fine wire inserts such as platinum, which acts as a cathode. The hole produced by CD technique is in the order of below 0.5 mm diameter, which is smaller in diameter compared to Jet EMM. Large number of micro holes can be effectively drilled at a time in hard materials with multiple capillary tubes drilling assembly.

3D EMM can be utilized effectively for producing 3D parts by properly eliminating or compensating its stray current and micro sparking effect. Some of the most predominant factors, which influence the machining characteristics of 3D EMM are micro tool coating, inter electrode gap control, ultra-short pulse power, type of tool electrode etc. Electrochemical machining techniques, when utilized for generation of three-dimensional micro features, are known as 3D EMM [8].

1.4 Through Mask Electrochemical Micromachining (TMEMM)

Complexities of the microfeatures to be machined, accuracy level to be achieved as well as process productivity are some of the important criteria to be looked into during EMM. Flexibility of material removal by applying the principle of electrochemical technique is one of the main criteria to be considered during selection of the type of EMM to be used for the specific application.

Different types of EMMs have already been represented in fig. 1.4. In one of the specialized and industrially accepted technique, the material removal is restricted by positioning a photoresist pattern, that is, masks on the metal surface; thus, dissolution is allowed from the desired portions of the workpiece surface. This type of EMM technique is known as Through-mask EMM (TMEMM).

In TMEMM, anodic dissolution takes place at the work piece surface that lies at the bottom of the cavity created by the photo resist mask. Photo resist patterned metal work piece is made an anode in an electrochemical cell so that the exposed metal surface is removed by high rate anodic metal dissolution. In through-mask EMM, the localization of the material removal is secured by the photolithographic mask. As such, mask patterning process requires careful implementation of different steps that involve generation of master art work, surface preparation, choice of suitable photo resist and imaging.

Photolithography is a process used in micro-fabrication to selectively cover certain parts of a substrate with a so-called photolithographic mask, or photoresist [9]. Its basic steps involve the application of a light sensitive polymeric layer onto the workpiece, exposing this layer to

light with a desired pattern, and developing the exposed photoresist. In positive photoresists, the parts of the polymeric layer exposed to the light become soluble to the developer. In negative photoresists, the exposed area becomes insoluble to the developer. After the micro-fabrication step, which may be etching or deposition, the photoresist is removed chemically from the workpiece by a resist stripper. Selecting proper current density as function of substrate shape and cell geometry can significantly reduce the metal removal rate in the lateral direction. The continuing improvements in photolithography have made it possible for through-mask EMM to play an increasingly important role in micro-fabrication [10].

1.4.1 Types of TMEMM

In through mask EMM, a photolithographic mask is applied onto the workpiece and dissolution occurs only from areas not protected by the mask i.e., the localization of the material removal is secured by the photolithographic mask. There are no specific requirements concerning the shape or position of the counter electrode.

TMEMM may be one sided and two sided depending on the application of photo resist mask on one side or two sides of the work piece. The substrates in TMEMM typically consist of an insulating support layer topped with a metal layer, onto which a photolithographic mask is applied. The process using such a substrate is referred to as one-sided through-mask EMM. Figure 1.5 diagrammatically illustrates the phenomenon of one sided TMEMM. In two-sided TMEMM, the metal layer is sandwiched between two congruent layers of photolithographic mask. The etching process thus occurs on both sides of the metal layer.

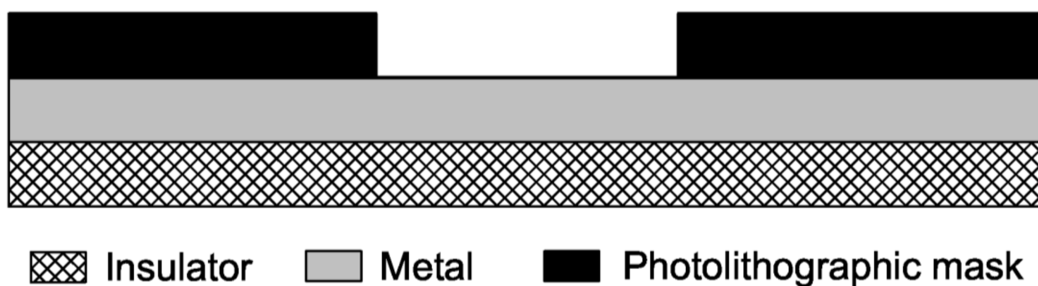

Figure 1.5: Typical photolithographically structured substrate (One sided TMEMM)

The assembly of the substrates in TMEMM causes an inherent drawback. Because the underlying support is insulating, the metal layer itself is the only electrical contact to the power source. The metal at the openings of the photolithographic mask is usually completely etched off. If the etching is non-uniform and higher etching rates occur at the brink of the workpiece, the electrical contact will be lost and the process will stop prematurely before the etching is finished in the middle of the workpiece. This results in the formation of a lump of residual material at the centre of the generated micro-feature known as “islands”. The

problem of island formation is treated as a certainty in the TMEMM. This problem does not apply if there is a continuous area or lane of photoresist running from the brink to the middle of the micro-feature, i.e., loss of electrical contact depends highly on the design of the workpiece. PCB designs usually have an open area along the edges and hence, a non-uniform distribution of the etching rate would cause loss of electrical contact.

The types of TMEMM are hereby discussed below in details:

(a) One-sided Through-Mask EMM

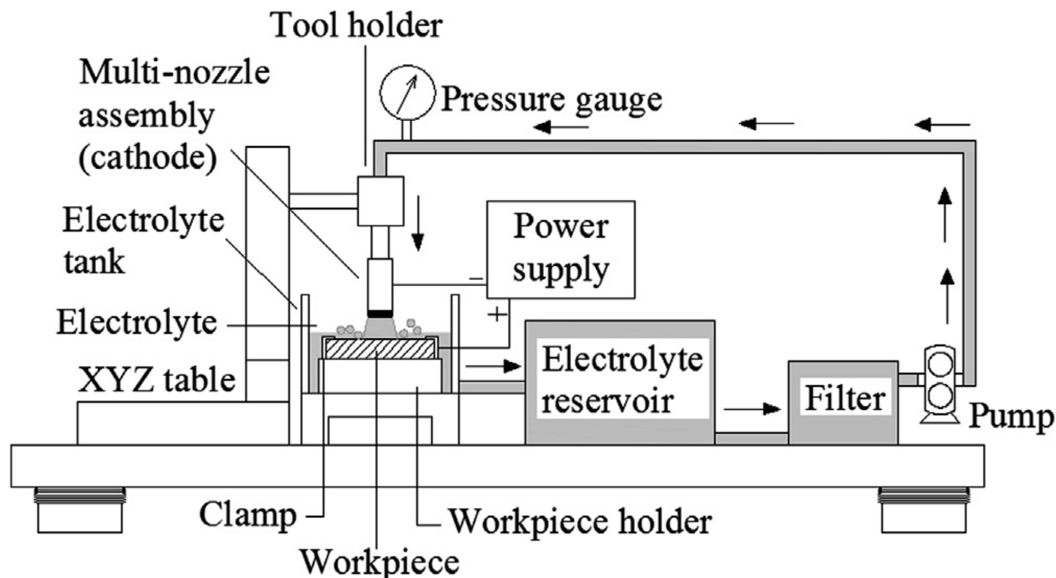

Figure1.6: Schematic diagram of the set-up of one sided TMEMM [4]

Figure 1.6 schematically exhibits the set-up details of the one-sided TMEMM technique. The workpiece is made the anode of an ECM cell and mounted on a holding device. The holding device is attached to a driving mechanism consisting of a precise XYZ microstage. The tool (cathode) of the ECM cell is represented by a multi-nozzle assembly that delivers electrolyte to the machining zone. The tool is fixed at a particular position in the machining chamber. The workpiece can be moved across the tool along any path to generate any complex profile, which to be created on the workpiece surface as per the design of the mask. The electrolyte supply system consists of reservoir, pump, and filtration units.

The workpiece is moved at a constant speed below the multi-nozzle tool. The gap between the multi-nozzle cathode and work sample, i.e. the Inter Electrode Gap (IEG) is kept constant between 0.5 and 2.5 mm and can be varied by utilizing the Z-axis movement of the micro-stage in the work table. A high-speed electrolyte from the multi-nozzle assembly impinges on the masked surface of the workpiece and removes the metal from the unmasked zone of the surface of the anode through electrochemical dissolution. The active area during

micromachining is defined by the electrolyte in contact with the sample. The electrolyte impinges to the surface of the sample and is directed downward, and flows from the side of the nozzle assembly that produces a non-uniform current distribution at the portion of the work sample in contact with the electrolyte. Hence, current density and so as the material removal rate attains a higher value in the impingement region and gradually reduces as a function of the distance from the region of impingement. The sample is scanned above the cathode to maintain an equal amount of metal removal from the unmasked portion of the workpiece surface by compensating the stray current effect. The sludge mainly consisting of the dissolved metal along with the heat generated in the inter-electrode spacing during the dissolution is removed by the flowing electrolyte.

Micro-nozzles can be fabricated on a thin metal foil by one-sided through-Mask EMM. Fabrication of nozzle plates by EMM involves cleaning of the metallic foil and application of photoresist on both sides of the foil. The photoresist on one side is exposed and developed to generate the initial pattern, consisting of an array of circular openings. A controlled one-sided TMEMM process is employed to fabricate flat-bottomed V shaped nozzles on the sample as shown in fig. 1.7. The photoresist on the backside of the foil acts as a protective insulating layer. By controlling the TMEMM parameters, nozzles of desired shapes can be fabricated. The final nozzle shape is determined by several factors that include undercutting, etch factor, dissolution time, and dissolution conditions. Pulsed power supply is found to be effective in achieving dimensional uniformity of an array of nozzles during one-sided TMEMM.

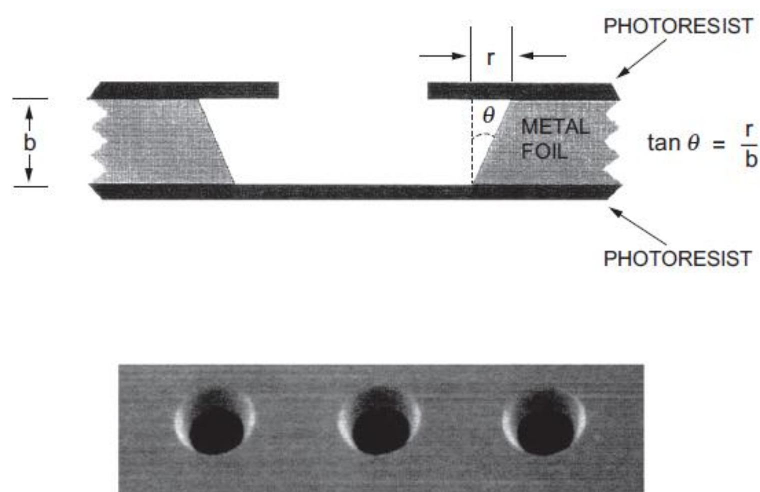

Figure 1.7: Basic features and array of micro-nozzles fabricated by one-sided TMEMM [11]

(b) Two-sided Through-Mask EMM

The set-up details of the two-sided EMM technique have been schematically exhibited in fig. 1.8. The experimental sample is held vertically in the machining chamber. The job is made

the anode of the electrolytic cell. The tool consists of two cathode assemblies mounted over the vertically held job. Highly localized anodic dissolution from the unmasked region of the two sides of the work piece is achieved by scanning the tool assembly over the work sample. The electrolyte flows through the tool assembly and passes across the surface between the cathode tool and masked workpiece anode. An extremely small IEG is maintained between the work sample and cathode, which provides uniform localized metal removal due to stable current flow distribution with negligible stray current effect. The cathode tool can be scanned back and forth across the masked anode at a suitable rate utilizing linear movement of a bidirectional stage. The electrolyte flow, IEG, and movement of the cathode tool can be altered as per specific design requirement of the mask pattern and sample sizes. The shearing flow from the top to the bottom and an impinging flow directed into the masked workpiece can be used depending on the aspect ratio of the feature to be generated on the masked work sample.

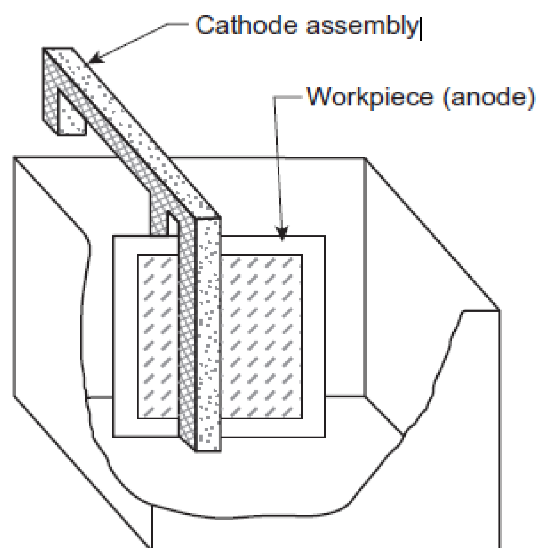

Figure 1.8: Schematic diagram of two-sided TMEMM set-up [12]

Compared to the widely employed chemical etching process, TMEMM offers better control and flexibility for microfabrication. A higher machining rate, the use of less corrosive electrolyte, and eco-friendly process are some of the advantages of TMEMM. Moreover, a wide range of materials, including high strength corrosion resistance alloys, can be machined by this technique. This method is a precise, parallel, and relatively fast process, capable of producing well defined surface patterning from the nanorange to microrange. However, a limitation of TMEMM is the low aspect ratio of the produced micro-features, due to the isotropic etching behavior. TMEMM is more increasingly recognized for the fabrication of electronic components, which involves high precision micromachining of thin metallic films.

A lot of research work to fabricate high-aspect-ratio micro-features of desired shape, size, and surface quality is going on in the world. Moreover, fabrication in a characteristic scale of tens to hundreds of micrometers with good shape accuracy and surface quality is a challenging task and needs further developments.

1.5 Review of literature

The progress of modern electronics technology towards smaller devices triggered the miniaturization of mechanical and optical parts like sensors, connectors, actuators or reactors. Applications of machining materials in micrometer and sub-micrometer scale are considered to be a key future technology. Presently researchers are trying to develop different processes for machining materials on micrometer and sub-micrometer scale with full control on shape and accuracy. In the newer challenges of micromachining, ECM has proved its compatibility over other non-conventional micromachining processes due to its prime process advantages.

Electrochemical micromachining (EMM) is one of modern age nontraditional micro machining processes, which removes the workpiece material through anodic dissolution and has capability to machine the micron sized features on any electrically conductive materials, irrespective of its mechanical and chemical properties as well as hardness. EMM has been applied successfully for machining of micro features on advanced engineering materials. However, application of principle of anodic dissolution in micro domain involves lots of complexities and process intricacies especially when EMM is utilized to generate micro features on advanced material such as stainless steel, titanium, other alloys etc.

Recently, surface texturing has gained momentum as a way to control the friction, which is involved in various applications and systems, such as components of internal combustion engines, dies and punches of the metal forming processes and MEMS. Surface-texturing can be in the form of arranged micro-dimples of various shapes and patterns onto the contact surfaces. These dimples contribute mainly by acting as lubricant reservoirs to provide lubricant under the starved lubrication condition and micro-hydrodynamic bearings to provide additional load-carrying capacity. In addition, the dimples can trap wear particles to reduce the third-body induced surface stress concentrations, friction and wear. Several surface modification techniques which are applied to improve bio-functional performances are coating of surfaces, making of textured patterns with variable geometries, creating micro/nano structures, surface grafting, combination of texturing and coating, etc. However, selection of the potential surface texturing technique that fulfills the desired performance characteristics is still challenging.

TMEMM is a highly complex electrochemical texturing process, combining metal shaping and finishing into one operation. Predicting the removal rate, the shape profile and the surface finish is not straightforward, because of the interaction between current distribution, mass transfer and surface films. Over the past few decades, a considerable amount of work has accrued, pertaining to the problem of shape-evolution modeling in particular. These studies are largely concerned with conditions corresponding or equivalent to diffusive mass transfer alone. This literature review highlights the status of the development in research activities carried out across the globe in various aspects of TMEMM. However, to exploit full potential of the TMEMM process, a considerable work in the area of micro surface texturing needs to be carried out. Further research is still needed to improve accuracy and repeatability of the said process not only to make it more acceptable to the industry by considerably reducing its economic involvements but also improving the control of the machining accuracy through in-depth study of the process parameters. Review of research highlights the status of development carried out in this area across the world in various aspects of through mask electrochemical micromachining namely:

(i) Developments of EMM process,

(ii) Fundamentals of TMEMM,

(iii) Mathematical Modelling and Simulations of TMEMM process,

(iv) Mask and Islands in TMEMM, and

(v) Recent Developments in TMEMM.

Comprehensive study of reported research documents has been carried out to identify the existing challenges in the respective areas, which will be helpful for identifying the problem areas of the present research work.

(i) Developments of EMM process

Electrochemical micromachining (EMM) has already emerged as one of the important micro-manufacturing techniques in the field of micro-engineering. In order to understand the fundamental concepts of electrochemical micromachining (EMM) process along with the various developments in the EMM process, in depth review of various research articles has been presented in the following discussion. Comprehensive study of EMM is also an equal importance before executing detailed investigation into TMEMM.

Osenbruggen et al. [13] extensively explained research studies on electrochemical machining and its application in micromachining. Authors designed experimental ECM equipment that consists of extensive measuring and control instrumentation for setting the machining voltage, short circuit protection, controlling tool feed and fluid flow control apart from

circulation and purification of electrolyte. The metal removal rate and accuracy depends on tooling, electrolyte, gap width, current density and electrolyte flow rate. It was experimentally justified by the authors that the accuracy can be improved by insulating the tool with SiC layers and an intermediate layer Si_3N_4 that are applied by chemical vapor deposition (CVD) process. Moreover, the use of pulsed voltage and small gap width also improved accuracy. Passivating electrolyte has been preferred due to its high dimensional accuracy. Complex shapes were produced very rapidly without tool wear, burring and mechanical stresses.

Chikamori [14] proved the possibility of applying ECM process for micromachining by maintaining very narrow inter-electrode-gap (IEG) so as to improve machining accuracy. IEG was kept at very small value such that the possibility of applying ECM process to micromachining increases. IEG can be decreased down to several microns by reducing machining voltage and electrolyte concentration. Author developed a controlled closed loop ECM experimental set-up for micromachining, which includes linear actuator, piezoelectric transducer, electrical system, monitoring sensors, etc. Influence of IEG, machining voltage and electrolyte concentration on accuracy and surface finish of the machined product were investigated through experimental analysis. A small hole of 170 μm on 0.2 mm nickel plate was drilled by electrochemical machining process with small machining voltage and maintaining small IEG. From the experimental results, it was observed that with increase in machining voltage, side gap also increased that reduced the machining accuracy. The author had given more focus on smaller IEG and optimized voltage, which increased the possibilities of applying ECM for micromachining range of applications.

Masuzawa [15] summarized the basic concepts and applications of major methods of micromachining. The basic characteristics of conventional and non-conventional micromachining methods were discussed based on different machining phenomena i.e. removal by mechanical force, removal by melting and vaporization, removal by ablation, removal by dissolution, plastic deformation, solidification, lamination and recomposition. Promising methods were introduced in detail hinting at suitable areas of applications, i.e. holes, pins, slots and 3D machining. Two approaches were presented towards micromachining, i.e. reduction of unit removal and improvement in equipment precision. Principles, advantages and disadvantages of various micromachining processes were explained clearly with the help of tabular columns. A comparative study of the various micromachining processes based on material removal mechanism had been carried out with the help of tabular representation.

Schuster et al. [16] explained the use of ultrashort pulses in electrochemical micromachining and it was suggested that micromachining precision can be increased to nano-range by the application of ultrashort voltage pulses. The pulse duration provided a direct control for setting the machining accuracy. Machining precision can be increased with shorter pulses, which was explained clearly along with their experimental work performed on copper sheet employing a cylindrical micro-tool. The ultra short pulses increased the current density and localize the dissolution process. During micromachining, the IEG was monitored by recording the current transient flowing through the cell. Authors also stressed the scope of ultrashort pulses in the area of three-dimensional microstructure generation. Three-dimensional micromachining was achieved by the application of ultra short voltage pulses of only nanosecond duration.

Bhattacharyya et al. [17] developed an EMM system, which was designed particularly for micromachining. The developed system consisted of mechanical machining unit, electrolyte flow system and electrical system. Mechanical machining unit comprises of micro-tool feeding device for feeding the tool, work holding platform for placing and holding the workpiece, and machining chamber in which tool and workpiece was submerged in electrolyte during electrochemical micromachining process. Electrical system consisted of step-down transformer to reduce the main power supply, rectifier to convert AC power supply to DC power supply, and pulse generator to provide the required pulse nature of power supply. The micro-tool was driven by stepper motor, which was controlled by microprocessor through various programs. Authors also introduced an electrolyte flow system to supply fresh electrolyte in the IEG for proper dissolution. The developed electrochemical micromachining set-up provides various advantages, which fulfilled the needs of the micromachining operations.

Lee et al. [18] developed a pulsed electrochemical machining (PECM) process model to predict the machining depth for the analysis of the inter electrode gap mechanism. Experiments had been carried out with NaCl and $NaNO_3$ electrolyte as well as direct and pulsed current. $NaNO_3$ electrolyte had proved better machinability than the other because of its ability to change appropriately to the transpassive state without forming pits on the surface of the workpiece. By using pulsed current, it is easy to control the machining accuracy precisely. Authors also presented an identification method for the machining depth by in-process analysis of the machining current and inter electrode gap size. The inter electrode gap characteristics including pulse current, effective volumetric electrochemical equivalent and electrolyte conductivity variations were analyzed based on the model and experiments.

Piotrowski et al. [19] investigated the mechanism of anodic polishing of titanium in methanol-sulfuric acid electrolytes using steady-state and impedance measurements. Authors also studied the effect of electrolyte composition, convection conditions, and temperature on the value of the limiting current. From the data analysis, authors found that the electropolishing of titanium in methanol-sulfuric acid electrolytes was mass transport controlled. Based on the observed variation of the limiting current density with electrolyte composition, authors suggested that the transport of dissolved tetravalent titanium species from the anode surface to the bulk solution is rate limiting. High-frequency impedance data also confirmed this mechanism and provided strong evidence of the presence of compact salt film at the anode surface under limiting current conditions. Authors also confirmed the passivation effect of surface film which was influenced by presence of water at a concentration in excess.

Ferri et al. [20] demonstrated the feasibility of performing the two-level EMM of titanium structures consisting of a large flat-bottomed central cavity with a grid pattern of small grooves and two smaller cavities connected to the central cavity by narrow channels. Authors investigated two types of problems related to this structure using model geometries. A test structure involving a large shallow cavity with a groove pattern at its bottom was successfully fabricated using two different process strategies, each of which required two applications of a photoresist and two etching steps. From the results obtained during single-step etching with a model geometry involving large cavities connected by small channels, authors concluded that under suitable conditions diffusion controlled dissolution of titanium leads to flat-bottomed cavities with a polished surface. During etching of narrow channels, the cylindrical diffusion of dissolution products away from the channel opening led to higher dissolution rates compared to large flat-bottomed cavities and a corresponding increase in etched depth. Authors calculated the current distribution along the microprofile and simulated the shape evolution of the grooves using a moving boundary simulation.

Ghoshal and Bhattacharyya [21] presented a novel approach of sinking and milling method for micro channel generation. In this method, micro tool moved vertically to final depth or required depth of machined feature followed by milling along the path of the micro features. Authors also developed simulation model for sinking and milling method in which equipotential curve distribution in the cross-sectional gap of micro tool and workpiece had been exhibited. Authors concluded that the sinking and milling method of micro-channel generation was better than the scanning method of micro-channel generation in terms of reduction of taper angle.

Rathod et al. [22] machined blind micro grooves of 500 µm deep in stainless steel utilizing indigenously developed EMM set-up. Authors investigated the influence of various predominant EMM parameters like applied voltage, pulse frequency, duty ratio, tool feed rate, and electrolyte concentration on the machining accuracy, i.e., width overcut, depth overcut, and material removal rate during fabrication microgrooves in stainless steel. To achieve better accuracy of microgrooves, authors recommended lower machining voltage, lower electrolyte concentration, higher pulse frequency, lower duty ratio, and higher tool feed rate.

Bannard [23] confirmed the difficulty in electrochemical dissolution of titanium due to the existence of corrosion resistant surface film of tenacious, passivating oxide from the experimental investigations and mentioned that the corrosion resistance created problem to the electrochemical dissolution of titanium in low voltage. Author also investigated the anodic dissolution of titanium alloys on variety of electrolytes based on potassium bromide. Author identified the dissolution mechanism of titanium and its alloys in aqueous electrolytes in either a 3- or a 4-valent process. Based on the polarization curve, author observed that once original passive oxide film has been ruptured, the active dissolution begins and it was controlled by limiting current. Authors identified that using NaCl as an additive to the KBr, slight improvements in the stray current attack properties of the electrolyte and in the surface finish were obtained.

Chiou et al. [24] designed and developed an EMM apparatus to fabricate a micro tungsten rod with high aspect ratio. The distilled water containing 2% wt NaOH have been taken as the electrolyte and an iron needle was used as the cathode. The rotating speed of the tungsten rod was controlled and adjusted by the first motor. The rotating speed had been set to be 200 rpm and 500 rpm. The bearing support and the first motor were attached to the linear slider, and this slider was driven by the screw of a non-rotating spindle type micrometer head. A synchronous belt had been used to connect the gear in the spindle of the second motor and the gear mounded on the spindle of micrometer head so that the slider could be driven by the second motor. With the help of developed set-up, authors fabricated an extremely thin straight rod of diameter 2 µm and radius of the tip of about 0.5 µm with the length of 240 µm, ratio of length to diameter of about 120.

Yang et al. [25] proposed a new EMM method, in which mineral water was used as an electrolyte. Authors investigated the use of mineral water as a promising solution which can be used in the production of MEMS, such as micro pins, by the method of ECMM. Investigators reported advantages of using mineral water as the electrolyte. Experimental

results presented with theoretical analysis for the fabrication of micro pins and micro hole drilling in the tungsten (WC) material. Authors successfully fabricated WC micro-pin with the diameter range of 20–30 μm from a WC pin of 300 μm diameter in 10 minutes. Furthermore, the machining properties using mineral water as the electrolyte were investigated and it was found that the response to an ultra short pulsed power supply was much faster than the conventional electrolytes, such as $NaNO_3$. It was also observed that it was more suitable when nano second pulse power supply was used.

Park et al. [26] carried out experimental investigation for air-lubricated hydrodynamic bearings on the specially built EMM system. Pulse electrochemical machining (PECM) process model was also developed to predict the machining groove depth by using in-process measurement of machining current as well as inter electrode gap size. Sodium nitrate ($NaNO_3$) showed its potential for achieving higher accuracy as compared to sodium chloride (NaCl). It was experimentally established from the graphs that the electrode gap increases with the increase in pulse duration and machining time whereas increase in electrode gap results lower machining groove depth. Experimental results showed that an optimum electrode gap of 0.1-0.15 mm had been considered for better electrolyte flow and electrochemical reactions.

Cagnon et al. [27] performed 3D micromachining of stainless steel using ultrashort voltage pulses on the experimental set-up, which comprised of the control of tool/workpiece interface potential, the electronics for providing ultrashort voltage pulses and features for 3D movement of the tool. Platinum wire of 50μm was used as tool; whose front face was mechanically polished with SiC and Al_2O_3 paper, and upper side of the tool was coated with thermoplastic wax to reduce the lateral flow of electrochemical currents. Interface potentials were adjusted by a Pt counter electrode and reference electrode. Mixtures of concentrated hydrofluoric and hydrochloric acid was selected as an electrolyte to prevent the formation of passive layer on the workpiece during the machining process so as to achieve submicron precision and high processing speed. The application of ultrashort voltage pulses keeps the resolution down to nanometer level. At 1.8 V and 5 ns pulse, structure was generated whose surface roughness was below 200 nm and radius of curvature at the edge reached below 500 nm. From the analysis of SEM micrographs and subsequent discussion, it was concluded that proper choice of electrolyte and proper adjustment of ECM parameters such as pulse duration and pulse amplitude allows the machining of stainless steel with extraordinary precision.

Rasmussen and McGeough [28] explained the role of overpotential at both anode and cathode electrode which had been a significant factor in electrochemical micromachining (ECMM)

process. The overpotential was categorized in terms of concentration, activation and resistance types. To account these overpotentials in ECMM, theoretical equations had been derived based on expression for Laplace, which accounts for the potential in the electrolyte between the anode and cathode together with equations for Ohm's and Faraday's law that accounted for current density in the inter electrode gap (IEG), the rate of anodic metal dissolution and cathodic gas generation. Authors concluded that 500 nm width grooves could be engraved on aluminium computer disks by use of single crystal diamond tools. Experimental and simulation studies indicated that depth of cut could be as small as 1-1500 nm and 0.1-10nm. Accuracies of 0.2 μm and 5nm r.m.s in roughness and diameters upto 1500 nm had been reported.

Sen and Shan [29] provided an overview of electrochemical hole-drilling processes, their critical features, range of their applications, and experimental and analytical investigations of the process. For drilling cross-holes and simultaneous drilling of multiple holes of different shapes, electrochemical hole-drilling processes had been considered as a better choice in comparison to all other non-traditional hole-drilling processes. The notable features of ECM drilling process included the absence of residual stresses and excellent surface finish which makes the process more attractive for components exposed to high temperature. Appropriate means of handling and disposal of electrolytes, optimum selection of process parameters, systematic analytical and theoretical modeling and analysis, control on geometry of the drill hole, and development of process control strategies were the main issues which needed further investigation for the commercial success of these processes in industry.

Forster et al. [30] proposed a newly developed ECM sinking process with vibrating tool electrodes to improve shape accuracy. Vibration of the tool was used to improve flushing conditions and shape accuracy. Some tests were conducted on the developed prototype die-sinking machine by using stainless steel and tool steel as work specimens. From the test results, it was observed that machining time and roughness had been decreasing with increasing electrolyte concentration. Measurement of generated cavity edge showed an edge angle of 87.8° and a lateral gap of 50 μm that proved the applicability of ECM-die-sinking process for micro-structuring of high stressed metals that were widely used in bio-medical applications.

Jain et al. [31] studied the effects of process parameters such as applied voltage, electrolyte concentration, pulse duty cycle, and feed rate on the machined hole diameter with a developed mathematical model. Authors utilized a sewing needle with 47 μm tip diameter as tool to machine various micro features. Authors also developed mathematical model to

establish quadratic relationship between hole diameter and the different machining process parameters. From the experimental observations and analysis based on mathematical model, authors concluded that as the voltage increased, the hole diameter increased, and as the feed rate increased, the hole diameter decreased because of less time available for machining. With the increase in electrolyte concentration, the hole diameter first increased and then decreased.

(ii) Fundamentals of TMEMM

Researchers across the world have attempted to understand the fundamental aspects of the TMEMM process for better control over the process, and for widening its engineering applications in various fields. Different research papers reporting basic principles, machining characteristics, process variation and applications of TMEMM in manufacturing industries have been comprehensively reviewed under this section.

Datta and Romankiw [32] discussed the basic principle and application of chemical and electrochemical micromachining (EMM) for fabrication of electronic components. Authors highlighted different types of chemical and EMM processes and comparison among them. Chemical micromachining have been widely used in the electronic industry for a variety of applications including fabrication of metallic parts, printed circuit boards and semiconductor devices on those days. EMM appeared to be very promising as a future micromachining technique, particularly in the fabrication of metallic parts where it offers several advantages including high speed, wider range of materials machining, and minimized safety problems. However better understanding of high rate anodic dissolution process was required for EMM to become a widely employed manufacturing process in the electronic industry.

Datta et al. [33] carried out experimentation and analyzed the results of jet and laser jet electrochemical micromachining on nickel and steel in NaCl and $NaNO_3$ electrolyte. In the absence of a laser beam, sodium nitrate ($NaNO_3$) electrolyte has been better suited for micromachining at high current densities, which yielded relatively high metal removal rate with minimum stray cutting compared to sodium chloride (NaCl) electrolyte. The use of a laser-jet significantly reduced the over cutting during micromachining in chloride solution. The influence has been more pronounced for steel than nickel. On the other hand, laser beam enhanced the oxygen evolution reaction in the nitrate solution.

Datta et al. [34] explained high rate anodic dissolution processes and the influence on thin film patterning in micromachining. The role of convective mass transport and current distribution on the surface finish and shape evolution was explained in detail. Depending upon the metal-electrolyte combination and operating condition, different reactions take place

at high current density, which significantly influences the micromachining performance. So understanding of the kinetics and stoichiometry of anodic reactions and their influences on mass transfer was essential to optimize the process parameters. Influence of current density on dissolution efficiency for different metal electrolyte combination had been exhibited graphically. As the current distribution can be controlled by controlling the photoresist dimension, electrical and hydrodynamic parameters; undercut can be drastically reduced, which increases the possibilities of applying ECM process for microfabrication. Several examples of the applications of mask-less and through-mask electrochemical micromachining were presented.

Datta and Harris [35] developed a high speed EMM process tool for microfabrication and compared with chemical etching in the areas of surface finish, undercut, material removal rate, etc. EMM process can be applied to all types of conducting materials including conducting ceramics, chemically resistant materials and semiconductors. Accumulation of reaction products in solution and depletion of both components are of little concern, thus making EMM as a simple and environmental friendly manufacturing process. Precision micro-tools development has been an important aspect that required careful understanding of hydrodynamics, current distribution and process parameters on EMM performance. It was experimentally established by the researchers that operating EMM at higher current density provided micro smooth surface and uniformity in pattern. High aspect ratio was achieved by increasing the electrolyte impingement at the surface.

Zinger et al. [36] carried out surface structuring of titanium with well-defined topographies at the micrometer and nanometer scales useful for biomedical applications. Authors coated mechanically polished titanium disks with a poly isoprene-based negative photoresist then it was exposed using standard UV mask aligner thereafter it was developed to define the initial patterns. Anodic dissolution of the titanium through the patterned photoresist was performed in a methanol-based 3M sulphuric acid electrolyte. During the experiments, authors experienced the formation of passive oxide film on surface of titanium due to initial decrease in current. Authors identified that rapid removal of the passive oxide film was possible when sufficiently high potential had been applied. Authors successfully demonstrated scale-resolved electrochemical surface structuring of titanium consisting of hexagonal arrays of closely spaced smooth hemispherical cavities of 10-100 μm by TMEMM of mechanically polished titanium surfaces.

Spieser and Ivanov [37] presented and discussed different problematic areas of EMM. Authors thoroughly addressed the problems met by the μECM technology developers and to

present the current state-of-the-art solutions. Authors addressed almost all issues of EMM such as process monitoring and control issues which included inter-electrode gap (IEG) control and optimization, IEG modeling machine tools, and control of the voltage at the electrodes etc. Authors also focused on issues such as machining strategies, power supply unit, electrode and workpiece preparation such as on machine and off machine electrode preparation as well as measurement. Authors especially emphasized on machine set-up with optical devices for setting up the position of the workpiece and measuring capabilities of the machine will be used to determine the position of the working coordinate system (workpiece coordinate system) in the machine coordinate system and the position of the programmed point from the cathode electrode in two dimensions (length and diameter). Authors proposed that the modern control systems with fuzzy logic and neural networks knowledge into the EMM system for a more efficient and accurate machining process may be employed. In order to improve the accuracy of EMM set-up, authors recommended that the design of a power supply should be capable of delivering ultrashort pulses and providing enough power to the IEG as per requirement, over-current protection had been considered a must and should be integrated into the power supply, and a quick communication protocol between the power supply and the control system is essential for the successful control of the μECM process.

Wang and Zhu [38] proposed a combined process of WEDM and ECM for fabrication of multiple tool electrodes. Here, authors first fabricated the square cross-section columns by wire EDM. Then, the square multiple electrodes were immersed in the electrolyte, and the current flows between anode and cathode. Based on the principle of electrolysis, the square microelectrodes eroded into cylindrical microelectrodes. After the preparation of multiple electrodes, they were applied to machine the micro-holes in micro-ECM. Researchers claimed that this process of multiple micro electrode fabrication can improve productivity of EMM of titanium by electrochemical process in micro domain.

Madore and Landolt [39] successfully demonstrated the feasibility of using through-mask electrochemical etching for producing high-precision 3D topographies on titanium (Ti), applicable to biological applications. Authors utilized through-mask electrochemical machining (TMECM) to produce well defined surface topographies in Ti for biological studies. Dissolution of Ti was performed in two electrolytes, an aqueous solution containing sodium bromide, commonly used in high-speed machining of titanium, and a methanol solution containing sulfuric acid. Authors also carried out chemical etching of Ti in a hydrofluoric acid solution. Authors found that regular pattern etched on a Ti surface at 5 V in the NaBr electrolyte by passing a charge of 4 C. However, regular shape and smooth surface

textures were obtained when titanium was dissolved at 8 V, i.e., at the mass transport limiting current density in the non-aqueous electrolyte consisting of 3 M sulfuric acid in methanol.

Landolt et al. [40] discussed the role of mass transport, current distribution, passivating films for shape control and surface smoothening in EMM. EMM is faster and permits machining of chemically resistant metals such as super alloys, stainless steel and titanium. In anodic metal dissolution, salt film mechanism and accepter mechanism have been identified. In salt film mechanism, the rate of transport of dissolving metal ions from the anode surface into the bulk had been rate limiting. In the accepter mechanism, the transport rate towards the anode of accepter species such as complexing ions or water had been rate limiting. These species reacted with the dissolving metal ions to form complexed or hydrated species. Authors noticed that EMM produced cavities with a smooth surface only at optimized current density. Authors presented some new developments in EMM like oxide film laser lithography (OFLL). Using OFLL, the usefulness of EMM could be extended to non-planar surfaces and to the machining of multilevel structures for device fabrication. Extremely narrow inter electrode gap and very short current pulses were applied to improve dimensional control.

Lu and Leng [41] developed a method of jet electrochemical micromachining (Jet-EMM) to machine high aspect ratio micro-holes on titanium and its alloys. Jet-EMM system comprising of pressurized tank connected to compression air was used to generate electrolyte jet flow through the metal nozzle; electric power was supplied between the nozzle and the workpiece using a high voltage amplifier to provide constant voltage control; and work stage holding the workpiece could provide vertical, horizontal movement and rotation in the horizontal plane. The electrochemical reactions occurred when the electrolyte connected the nozzle acted as a cathode to the titanium workpiece that acted as an anode during the machining process. Jet-EMM as well as TMEMM performed experiments on titanium surface to generate micro-holes. From the analysis, Jet-EMM proved its potential for use in surface patterning of titanium implants.

Nouraei and Roy [42] presented a maskless electrochemical microfabrication process. In this method, a substrate (anode) was placed in an electrochemical reactor in close proximity to a tool (cathode) carrying the micropattern. The experimental investigation involved the development of a mathematical model for anodic dissolution in acidified and non-acidified media from a substrate, which was tested and verified against experimental data. The results showed that selective etching in acidified media produces a surface topography that was sinusoidal, whereas a rectangular topography had been obtained in non-acidified media due to the formation of an oxide at the surface.

Schonenberger and Roy [43] described a process to transfer microscale patterns on a fully exposed substrate. The method used electrochemical means and a specialised electrochemical reactor for pattern transfer. This process used a metallic material with a resist pattern, which serves as an electrochemical tool. The substrate, which was fully exposed, had been placed facing the tool, within close proximity. Initial experiments involving copper as the tool as well as substrate material showed that microscale patterns could be transferred with good reproducibility. In the reactor, they were placed within a distance of 500 µm. The authors had successfully transferred micro patterns which were significantly smaller than the electrode gap, namely 50, 100 and 200 µm.

Zhang et al. [44] proposed a modified microscale pattern transfer process without photolithography of substrates, through the use of movable dry-film mask electrochemical micromachining for the production of micro-dimples. Authors investigated the influence of electrochemical micromachining parameters, e.g. applied voltage and machining time on the machining accuracy of micro-dimples produced using this technique. Experimental results indicated that the machining accuracy deteriorated with prolonged machining time and increasing applied voltage. It was also found that to obtain high machining accuracy when machining micro-dimples of similar depth, a combination of higher current density with reduced machining time was recommended.

Frankenthal and Eaton [45] developed a new electrochemical technique for etching platinum in the processing of silicon integrated circuits. A periodically varying potential had been applied to a silicon wafer in a room temperature hydrochloric acid solution. The waveform was designed to overcome problems associated with the passivation of the platinum surface and with the relatively high resistance of the metallization. The process possessed the following properties: the resolution of electroetched test patterns was good; the process was compatible with both positive and negative photoresists; the etch time was a few minutes for the platinum thicknesses commonly used in integrated circuits; the process lends itself to instrumentation for determination of the completion of platinum removal; the dissolved platinum had been recovered. Authors investigated that the electroetching process was also applicable to the etching of other noble metals and to the etching of metallization on other substrates.

(iii) Mathematical modelling and simulations of TMEMM process

Considering the importance of TMEMM in the industrial arena, researchers from various research institutes, laboratories and universities have attempted to develop the process through the variation of different process parameters. However, the results obtained from

different experimental investigations utilized for the development of mathematical models has been validated during generation of different precise micro features. Progress taken place in the area of mathematical modelling and simulation has been reviewed in details in this section.

West et al. [46] provided the simulation of the electrochemical etching of lines and holes into metal films that are inserted between photoresist mask and an insulating support. Moving boundary simulation was presented with the help of boundary element method. Comparisons of calculated shapes with experiment results showed that etching under primary current distribution condition can be achieved in practice. Two aspect ratios of photoresist thickness of cavity width were considered; large aspect ratio has been assumed and various metal film thicknesses were investigated in first case whereas in second case it was investigated and studied experimentally. Authors tried to represent an agreement between theory and experimental values, and presented some results such as:

(i) A stable numerical algorithm for moving boundary simulation of etching process was developed as to give accurate computational results.

(ii) The results of the etching process with the initial exposure of the supporting insulator to electrolyte have been summarized by design curve that gives the cavity width necessary to etch groove of desired shape, hole of desired radius into metal of given thickness.

Zhang et al. [47] developed a theoretical model using ultra short voltage pulse for finding out the major influencing parameters on the machining accuracy and quality in the micro-ECM. Based on theoretical model, time constant, pulse period, pulse on-time and the stationary overpotential had been considered as the major influence factors on the machining accuracy and quality in the micro-ECM with nanosecond pulse. Experimental system was constructed, which included machining process detection, movement control function, pulse power supply and electrolyte circulating device, and experiments of micro groove and micro letter were carried out. Experimental results showed that lower voltage amplitude and shorter pulse on-time could produce more accurate microstructure shape.

Zhu et al. [48] developed a modified through-mask EMM to produce micro dimple and hole array, in which mask with patterned insulation plate coated with metal film as cathode had been closely attached to workpiece plate. When voltage was applied across the workpiece and cathode film over which the electrolyte flows at high speed, hole or dimple array was produced. Modeling and simulation had been done to observe the current density distribution. The effect of process parameters i.e. insulation layer thickness, cell voltage, current density and machining time on the microstructure shape had been demonstrated numerically as well

as experimentally. In order to assess the effectiveness of micro-dimple array on friction coefficient, friction test were conducted under the normal load of 500 N and test results for the sample with micro-dimple array reduced friction coefficient successfully.

Raffelstetter and Mollay [49] presented the optimization of the shape evolution of a PCB in terms of uniformity. A hierarchic modeling strategy was applied which allowed predicting the shape evolution of complex patterned workpiece considering an auxiliary electrode. The auxiliary electrode was optimized in terms of its geometry and potential. The strategy splits the simulation into three spatial scales; macroscopic, mesoscopic and microscopic scale. Considering influences from the other scales, simulations were performed on each scale in a simplified way. It was shown quantitatively how an optimized auxiliary electrode could prevent a non-uniform shape evolution of trenches at different places on the workpiece. Modeling a PCB without any auxiliary means resulted in a significantly non-uniform shape evolution. Using an auxiliary electrode could dramatically improved uniformity, resulting in an etching process that would not suffer from loss of electrical contact. The optimization was performed with respect to the width, distance and mean current density. Investigating their current density in relation to the optimized parameters cleared up the interplay of the different extrema.

Qian et al. [50] proposed a modified TMEMM process to produce micro-dimples on the hard chrome-coated surface. Authors selected finite element method (FEM) to analyze the electric field and calculate the distribution of current density on the anode surface for the analysis of material removal by ECM. Experiments had been carried out to generate micro-dimples on the hard chrome-coated surface with copper tool and sodium nitrate electrolyte. From the results, it was noted that the dimple diameter enlarged with the increase in current density and the machining rate proceeded more and more slowly with prolonged machining time when the electrolyte concentration, pressure and electrolyte temperature was fixed. The current density between 40 and 50 A/cm^2 and optimized machining time were essential for good pattern transfer. To verify the effect of micro-dimples array on the hard chrome-coating sample, friction test were conducted under a normal load of 500 N and obtained lower value of friction coefficient for the surface. By controlling machining parameters, micro-dimple array were produced efficiently, and the method improved the machining efficiency.

Wang et al. [51] investigated a double-sided TMECM process in order to fabricate hole-array with low taper angle. A model of the double-sided TMECM had been established to simulate the hole-formation process. The simulation results indicated that the electric field of the double-sided TMECM was beneficial to reduce the taper angles of machined holes. In order

to verify the simulation results, experimental investigations of hole-formation were implemented. The experimental results indicated that the sidewall of machined hole could be close to the straight at a certain machining time. Finally, a 6x50 hole-array have been machined by double-sided TMECM onto Ti-6Al-4V sheet with thickness 0.5 mm which resulted in the maximum taper angle of only 2.52° in the hole-array.

(iv) Mask and islands in TMEMM

Masks are the vital element in TMEMM that plays a significant role in the shape evolution of the final microstructures. Since the micro features developed in the mask are directly replicated to the micro-textures on workpiece surface, hence material, shape, size and thickness selections are the important criteria's to be considered while selecting masks during TMEMM. The proper design of the mask is of utmost importance for removal of 'islands', which hinders the creation of a sound dimple surface on the generated micro-textures. State of art research in mask design as well as island removal techniques have been reported and discussed in depth in this section.

Kwon et al. [52] developed a mathematical model for simulating the wall profiles in through-mask EMM of invar alloy films. Wall profiles change during electrochemical etching was simulated using the boundary element method with assumption of negligible concentration variation of bulk solution and kinetic resistance at the electrode surface. Primary current distribution can describe the electrochemical etching system adequately based on the comparison with the experimental results for the case of small aspect ratio. Authors observed a small deviation between theoretical and experimental results, which might be due to the mass transfer effect and Joule heating effect. It was observed that machining with 5 V required more time than machining with 6 V. However, the wall profile becomes anisotropic and surface roughness improved due to increase in applied voltage to 7.5 V.

Shenoy and Datta [53] reviewed some of the fundamental aspects related to understanding of the high rate anodic dissolution process and their influences on thin film patterning by EMM. The role of convective mass transport, current distributions on the surface finish and shape evolution was discussed. Authors also developed a mathematical model to predict shape evolution during TMEMM. Boundary element method has been used to solve the laplace equation for electric potential with appropriate boundary conditions that describe the metal dissolution process under ohmic control. The influence of the mask wall angle on the evolution of the metal wall profile has been shown to diminish with increasing metal film thickness ratio. Several example of the application of maskless electrochemical micromachining and TMEMM were presented.

Shenoy et al. [54] presented experimental investigation to study the problems of island formation caused by loss of electrical contact. A mathematical model was developed to predict shape evolution during through-mask electrochemical micromachining. Laplace equation for potential was solved using boundary element method to determine the current distribution at the anode. The current distribution was combined with moving boundary algorithm to predict the shape of the evolving cavity. Also the effect of the photoresist artwork on shape evolution and island formation has been characterized by three parameters; aspect ratio, film thickness ratio and spacing-to cleaning ratio. It was established by the authors that the problem of island formation has been likely for a combination of low aspect ratio and low film thickness ratio and island formation can be avoided either by increasing the photoresist thickness or by introducing dummy artwork.

Chen et al. [55] generated micro-dimple arrays on titanium alloy surfaces utilizing TMEMM with a reusable mask of polydimethylsiloxane (PDMS). Authors employed $NaNO_3$ electrolyte to generate micro-dimple arrays on a titanium alloy surface mask. Researchers analyzed dissolution characteristic of the titanium alloy in $NaNO_3$ electrolyte as well as optimum machining parameters, viz. voltage, pulse duty cycle, pulse frequency and electrolyte temperature, were identified. Authors observed serious stray corrosion on the titanium alloy surfaces when the micro-dimple arrays were generated using direct current. Hence, pulsed current had been applied in TMEMM to obtain good quality micro dimple arrays. It has also been identified by the researchers that electrolyte temperature influenced the machining localization, an electrolyte temperature of 20°C, micro-dimples with a diameter of 110 μm and depth of 20 μm could be generated. Authors concluded that, machining parameters of applied voltage of 24 V, pulse duty cycle of 10% and frequency of 100Hz were appropriate to improve the machining quality.

Qu et al. [56] employed polydimethylsiloxane (PDMS) as a mask in TMEMM due to its chemical resistance, low cost, flexibility and high moulding capability. A vacuum-aided process was introduced to fill a PDMS gel into an SU-8 mould, and the PDMS gel was solidified in an oven. Then, the cured PDMS micro through-holes were peeled off of the SU-8 mould. PDMS micro holes with a minimum diameter of 50 μm and a thickness of 200 μm were obtained. Furthermore, the PDMS micro through-holes were then used as a mask to prepare a micro dimple array by TMEMM. Experiments were conducted to verify the feasibility of the proposed approach and the effect of applied voltage and machining time on the diameter and depth of the micro dimple was investigated.

Chen et al. [57] performed simulations to analyze the distribution of current density on an anode surface and predicted the anodic dissolution process under a thick mask. For reuse, the mask was fabricated from a PDMS layer measuring 200 µm in thickness. The simulations and experimental results verified that the island phenomenon had been avoided by use of a thick mask. In addition, the effects of the applied voltage on micro-dimple formation were experimentally investigated and the results indicated that the dimensions of micro-dimples were mainly determined by the applied voltage: the micro-dimple diameter increases with increasing voltage, and machining localization increases sharply. With prolonged machining time at constant voltage, only a slight increase in dimple diameter had been observed. Moreover, because of a current valve in the electrolyte, micro-dimples with a flat bottom had been obtained at low voltage, whereas micro-dimples with a round bottom had been generated at high voltage.

Chen et al. [58] presented that the oxygen bubbles produced on the workpiece surface during the machining could be employed to reduce undercutting. A thick mask was introduced to prevent escape of the oxygen bubbles from the micro-dimples. The experimental results showed an undercutting of only about 3 µm with a 250 µm thick polydimethylsiloxane (PDMS) mask. In particular, there was no increase in undercutting when the applied voltage and machining time were increased. An interesting phenomenon was observed in which there was little increase in depth with increasing voltage, whereas the depth increased with longer machining time. Authors established that, direct or pulsed current had been used to generate different depths of micro-dimple arrays with low undercutting by simply controlling the machining time, regardless of the applied voltage.

Qian et al. [59] experimented that the auxiliary anode consisted in the mask to reduce the lateral undercutting for improving localization of the surface texture. Numerical simulation of the current density distribution in the inter electrode gap was used to theoretically verify the proposed method, and the effect of the auxiliary anode on the localization was investigated experimentally. The experimental results indicated that the machining localization had been significantly improved by the auxiliary anode, and the etch factor was decreased with the increasing machining voltage.

(v) Recent developments in TMEMM

Increased demand of micro products and micro systems in various fields necessitates machining of micro features on various advanced engineering materials. Micro features like micro dimple arrays and 3D micro structures of different shapes and sizes needs to be fabricated on macro, as well as micro sized products for its practical applications. Recent

development along with other notable advancements in the field of TMEMM has been reviewed under this section which focuses on the innovations of this process of micromachining in various fields.

Kern et al. [60] presented an application of TMEMM by combining maskless UV and electron beam lithography in combination with robust SU-8 photoresist technology for increasing the flexibility in pattern shape and potential scale down of feature size on planar substrates. Authors claimed that with this technique, features with a gradient in etch depth had been possible in one single micromachining process. Authors utilized 3 M H_2SO_4 in methanol using a 2 electrode set-up in a jacketed and tempered glass cell. From the experimental outcomes, authors stressed that maskless UV and e-beam patterned SU-8 was highly suitable for planar electrochemical surface micromachining from submicron to several hundred microns feature scale, excellent chemical stability of SU-8 together with the flexibility of maskless UV lithography providing great freedom in the pattern design. Authors found that this TMEMM technique was suitable for patterning of highly curved surfaces with substrate material choice, good mask patterning speed and freedom in feature shape.

Chauvy et al. [61] reported a novel EMM process for generation of micro features on titanium. This EMM process was based on oxide film laser lithography (OFLL) which consisted of selective laser irradiation of an anodically formed oxide film. Authors also investigated transformations occur in oxide films on titanium during laser irradiation which permitted subsequent selective dissolution of the underlying metal. Authors employed excimer laser irradiation with two different pulse lengths of 280 ns and 20 ns on anodically formed oxide films on the surface of titanium. Selective electrochemical dissolution has been carried out with 3 M H_2SO_4 in methanol at 100°C. Based on the experimental observations, authors suggested that depending on irradiation conditions different mechanisms may be responsible for locally destabilizing the TiO_2 film in electrochemical micromachining based on OFLL.

Sjostrom and Su [62] presented micro patterning on titanium utilizing mask-less EMM. Authors demonstrated surface features such as micro grooves and generation on surface of pure titanium by a direct writing manner through moving a single-tip tool across the surface. Authors utilized an ethylene glycol (EG) electrolyte. Authors claimed that upon utilizing a water free electrolyte, some of the difficulties normally associated with EMM, such as heavy gas formation in the gap between the tool and the workpiece, were significantly reduced. Authors also formed array of pits of a depth of approximately 1-5 µm, which has possible applications in biomedical area.

McCrabb et al. [63] developed a pulse and pulse reverse through mask electrochemical machining process for fabrication of gas flow field channels on metal bipolar plates used in PEM fuel cells. The process involved patterning a photoresist mask on the surface of the bipolar plate to protect specific areas during the ECM process. The application of pulsed electric fields, as opposed to constant direct current (DC) electric fields provided an improved level of control through optimization of the pulse parameters. The influence of the through mask pulse and pulse reverse ECM processing parameters, such as electrolyte composition, flow rates, pulsed voltage, pulsed on-times and off-times on material removal rates, surface finish, accuracy and dimensional control for the channel fabrication were examined.

Chen et al. [64] used a polydimethylsiloxane (PDMS) mask in TMEMM for generating high-quality micro-dimple arrays. With a PDMS mask being used for generating micro-dimple arrays, three electrolyte flow modes were investigated and a modified forward mode with a multi-slit structured cathode had been proposed for the generation of arrays that possessed uniform micro-dimple distributions and dimensions. Using this method, arrays were generated with average micro-dimple dimensions of 106 μm diameter and 10 μm depth, with a low standard deviation (STDEV). In addition, the results showed that both direct current and pulsed current had been used to generate micro-dimple arrays with a high degree of localization, although pulsed current produced deeper micro-dimples.

Chun et al. [65] combined through-mask electrochemical machining with portion of photolithography process to fabricate micro-hole arrays on invar fine sheet. The sheet was coated with dry film photoresist. Two types of electrode, plate and mesh were used to compare the influence of electrode type. The sheet was coated with dry film photoresist with micro- sized through holes. The results were compared in regard to uniformity and taper angle. These results were used to improve TMEMM for invar fine sheet when it was applied to fabricate micro-hole arrays and help to obtain optical uniformity and desired taper angles.

Ahn et al. [66] optimized the TMEMM process to fabricate bumping mask by controlling the process parameters such as electrolyte temperature, cathode size, exposed cathode area and agitation speed. By controlling process parameters, the effect of current density distribution and mass transport had been investigated. After the TMEMM process, Optical Microscope and Field Emission Scanning Electron Microscope were used to analyze the result. As a result, the bumping mask which has 250.6 μm of average hole diameter with 2.8% of CV value and smooth surface was fabricated.

Zhang et al. [67] proposed a new method, sandwich-like electrochemical micromachining (SLEMM), to reduce overcutting of micro-dimples in diameter and to enhance the

dimensional uniformity of micro-dimple arrays. Experimental results showed that for a similar depth of 11 μm, the use of SLEMM leads to a reduction in micro-dimple diameter from 124.3 to 109.0 μm and a sharp increase in etch factor from 0.9 to 2.5, confirming that SLEMM was able to enhance the machining localization and machining accuracy of micro-dimples. Arrays of 1500 micro-dimples were generated by SLEMM. Finally, different types of surface textures involving hexagons, ellipses, and squares were fabricated using SLEMM.

Baldhoff and Marshall [68] presented electrochemical impedance spectra during the mass-transfer limited dissolution of commercially pure aluminum rotating disk electrodes in concentrated phosphoric acid. The influence of rotation rate and potential on the observed capacitive and inductive semi-circles and the presence of a salt film on top of the oxide film had been discussed. The impedance spectra were interpreted hypothesizing the presence of a compact, barrier-type Al_2O_3 film only. The capacitive and inductive features were explained in terms of the capacitive charging of the barrier film, the relaxation of a surface charge at the film/solution interface and the perturbation of the film thickness. The properties of the film such as electric field strength, half-jump distance and polarizability of the film/solution interface were calculated in agreement with literature values.

Wang et al. [69] developed TMEMM to fabricate micro-grooves on the surface of titanium alloy. The distribution of current density affected the micro-groove profile, and different mask aspect ratios can form different distributions of current density in through-mask EMM. Authors established that micro-grooves with semi-circular profiles can be fabricated by controlling the aspect ratio of the mask groove. The effect of mask aspect ratio on the micro-groove profile during through-mask EMM has been investigated by electric field simulation. From simulation results obtained in a series of experiments, the appropriate mask aspect ratio was found for fabricating semicircular micro-grooves.

Zhang and Qu [70] used SLEMM for generating micro-dimples, in which the cathodic tool keeps in close contact with the mask firmly laminated to the anodic workpiece surface. The shallow micro-dimples were machined with the electrolytic products accumulating on the workpiece surface. A porous metal cathode was employed in SLEMM resulting in an open unit, which removed electrolytic products and generated deep micro-dimples. Authors reported about the poor machining accuracy of micro-dimples obtained with stationary electrolyte over the porous cathode. However, Pulse EMM and different electrolyte flow modes were applied to improve the machining accuracy of micro-dimples generated in SLEMM with a porous metal cathode to investigate their influence on machining accuracy of micro-dimples. The experimental results indicated that pulse current power supply improved

the machining accuracy of micro-dimples, compared with direct current power supply.

1.6 Opportunities and challenges in TMEMM

The reduced size of electronic components has revolutionized the field of electronics, telecommunications, and computers which uses silicon as the base material in the fabrication of micro components. The micromanufacturing processes for machining of silicon based materials are highly developed and advanced. The material properties of silicon are not at par with advanced engineering materials for different applications such as microsurgery, biotechnology, life science, micro fluidics, high temperature environment, mechanical applications. Therefore for micro fabrication of structure metals like stainless steels, tool steels, nickel base alloys, titanium and titanium alloys etc., there is need to develop low cost, faster and realistic micromanufacturing process for micro machining of simple micro features, as well as high-aspect-ratio microstructures having smooth surfaces. Several micro machining techniques, such as electro-discharge machining, chemical etching, abrasive jet machining, and laser machining have been utilized to fabricate micro features like micro holes, microgrooves, and 3D micro features on metallic surfaces. However, these techniques have some limitations when employed in practical applications. For example, microtool wear and surface defects generated at the machined surfaces are the main challenges in micro-EDM. Laser micro machining is comparatively faster and accurate method, but heat affected zone around the machined surfaces are unavoidable. Also, the generated micro structure tapers with increase in depth due to reduction in penetration energy of laser at higher depths.

EMM has a capability to fabricate stress and crack free surfaces on any metallic materials irrespective of its hardness. Since EMM is non-contact type of machining, no tool wear takes place, which increases its scope for mass production. From various literatures, it is seen that high aspect ratio microstructures are preferred in applications like micro thermal devices, micro coolers, micro reactors etc., since it increases the effective contact surface area. Whereas, fabrication of high aspect ratio micro features is still a challenge because of the problems like taper formation with increase in depth, heat affected zone, sludge or burr removal etc. by conventional as well as non-conventional micro manufacturing techniques. In spite of the various benefits of the EMM, very less literature is available on machining of high aspect ratio micro features on metallic surfaces like micro dimples and microgrooves with higher accuracy as well as repeatability. Further, patterned micro-dimples are one of the basic micro features incorporated on various micro devices like MEMS, micro thermal devices, micro reactors, micro robots, etc. In recent years, micro products are widely used in various fields because of the developments in MEMS. The trend of product miniaturization

by incorporating multiple functions in the product is increasing rapidly and will occupy almost all the fields of applications in future. Patterning on the surfaces of workpiece materials by Through Mask Electrochemical Micromachining (TMEMM) is advantageous rather than implementing other non-conventional processes which suffers from high manufacturing cost, degradation of machined surface, stiff control of operating parameters in executing satisfactory design and several other noticeable problems. Micro-textured arrayed structure plays a significant role in modern manufacturing such as aviation, electronics, automobile as well as medical industries where patterned surfaces are of high demand. The arrayed micro-textures are indispensible for the development of microproducts for micro systems, MEMS, micro-moulds, micro coolers, micro thermal devices etc. Fabrication of higher depth arrayed micro-structures on metallic surfaces in a cost-effective manner is still a challenging task for various available non-conventional micro machining techniques.

From the past research findings, it is evident that effective utilization of TMEMM process for precision manufacturing demands for extensive research to investigate the influence of major process parameters on micromachining requirements. Although esteemed institutions and researchers all over the world have initiated some research, but still this area of micromachining utilizing low aspect ratio photoresist mask requires lot of in-depth independent research for achieving satisfactory control of dissolution process to achieve higher accuracy and precision during TMEMM process. Hence, attempts should be made to fabricate different types of complex patterns on advanced engineering materials, considering various benefits of TMEMM over other competing micro surface texturing techniques for enhancing the applicability of TMEMM in various spheres of engineering.

1.7 Objectives and scope of present research

From the past research works, it could be adjudged that effective utilization of Through Mask Electrochemical Micromachining process for precision micromachining needs in-depth research to investigate the influence of predominant controllable variables on microtexturing requirements. Moreover, few attempts has been made to generate high aspect ratio micro features on metallic surfaces like micro dimples and microgrooves with higher accuracy and dimensional uniformity. The aim of this research work is to study the Through Mask Electrochemical Micromachining process in detail and apply it for machining of complex microstructures with different geometries and contours on one of the advanced metallic surfaces. The work may concentrate on experimental set-up development for process monitoring and control, selection of the thickness of the mask for fabrication of arrayed micro-textured surfaces, investigations into influences of process parameters, machining of

high-aspect-ratio microstructures, and finally to develop the guidelines for machining micro features of different geometries and contours utilizing low aspect ratio masks. Such experimental results would be a powerful database for the optimization of the through mask electrochemical micromachining process and hence, of considerable interest in industry-related research and development. It could not only yield quantitative predictions but also allow for a deeper understanding of how the different process parameters act and would consequently reduce the need for trial-and-error experiments. From this perspective, considering various needs of TMEMM process for surface texturing, following objectives can be identified for the present research:

(i) To develop experimental set-up of TMEMM for surface texturing of different micro textures as well as to prepare the experimental job samples through masking along with utilizing UV Lithography. The developed set-up should be capable of performing experimental investigations into various predominant processes for fulfilling the requirements of micro machining at different stages of experimentation.

(ii) To fabricate island-free micro-dimples by searching out the influence of predominant TMEMM process parameters i.e. applied voltage, machining frequency, electrolyte flow rate, duty ratio and machining time, etc. on machining performance and dimensional uniformity in terms of undercut, average depth and surface roughness of the generated textured dimple array on stainless steel substrates utilizing low aspect ratio mask.

(iii) To identify most suitable range of TMEMM process parameters for fabrication of circular as well as square arrayed micro-textured patterned surfaces on stainless steel wafers by investigating the influence of various controllable process parameters such as mask thickness, duty ratio and machining time on machining accuracy and surface characteristics of the generated micro-patterned arrays. Moreover, attempt needs to be made to study the friction characteristics of the generated square and circular micro-textured patterned surfaces.

(iv) To fabricate high-aspect-ratio 3D micro arrayed structures with considerable level of precision employing low aspect ratio mask by developing the machining guidelines for TMEMM utilizing the developed experimental set-up by varying process parameters e.g. applied voltage along with electrolyte type and concentration on the machining accuracy and dimensional uniformity along with the surface roughness characteristics.

(v) To find out the best parametric setting of TMEMM for micro-pattern generation with minimum undercut, maximum dimple depth and minimum surface roughness using Design of Experiments (DOE) based on Taguchi Methodology.

(vi) To perform multi-objective optimization for searching out the optimal setting of TMEMM process parametric combination for simultaneous maximization of the dimple depth, minimization of the undercut and minimization of surface roughness utilizing Grey Relational Analysis. Micrographs of the micro-dimpled pattern generated at optimized parametric combination during experimentation needs to be observed in details and analyzed to ascertain the correctness of the optimization as well as conclusions made there on.

However, scope of the present research includes:

It has been observed that the adequate research work have not been made in past few years in the area of through mask electrochemical micromachining (TMEMM) process in a cost-effective manner. The developed TMEMM system set-up will not only be useful for fabrication of micro-textured surfaces consisting of circular as well as square dimples but also performing experiments to analyze the influence of different process parameters on micromachining performance including the surface characteristics. Moreover, all such experimentation needs precise control over the experimental and measurement procedures along with accurate designing and planning. The utilization of appropriate type and concentration of electrolyte will be quite useful for machining of high-aspect-ratio microstructures with negligible undercut and improved surface quality. By adopting suitable DOE based on Taguchi method, experimental analyses and the test results will be quite useful for planning suitable control strategy of the TMEMM operation. The process is feasible for mass fabrication of devices with patterned micro textures. Efforts to modify TMEMM have picked up in recent decades, and several process variants exist today. Nonetheless, more work is urgently needed to explore these options more extensively and to increase the range of applications. The process has been widely used within the field of micromachining, especially in relation to micro-electronics, micro-actuators and micro textured surfaces, but also for the manufacture of accurate as well as precise micro-textures on thin metallic sheets. Therefore, the present investigation in the area of TMEMM technique is highly admissible for EMM of stainless steel substrate with mask of lean thicknesses and will certainly be suitable for various micro engineering applications at a cost effective manner.

FUNDAMENTALS OF THROUGH MASK ELECTROCHEMICAL MICROMACHINING

2.1 Introduction

Through-mask electrochemical micromachining (TMEMM) is a non-conventional machining process, in which a metal substrate is made the anode in an electro-chemical cell and thereby dissolved. The substrate is covered with an insulating mask, a patterned thin film and hence partly protected. Metal dissolution proceeds only through the mask openings, thus replicating the mask pattern over the surface. Through-mask EMM has received much attention for fabrication of micropatterns, as well as for shaping and finishing of 2D microfeatures. The photoresist patterned metal workpiece is made an anode in an electrochemical cell so that the exposed metal surface is removed by high rate anodic metal dissolution. In through-mask EMM, metal dissolution takes place at the workpiece surface that lies at the bottom of the cavity created by the photoresist mask [52]. Through-mask EMM can be of two types, simultaneous removal of the metal substrate from single side or simultaneously both the sides. Figure 2.1 shows line diagrams of though-mask EMM process depicting one-sided etching and two-sided simultaneous.

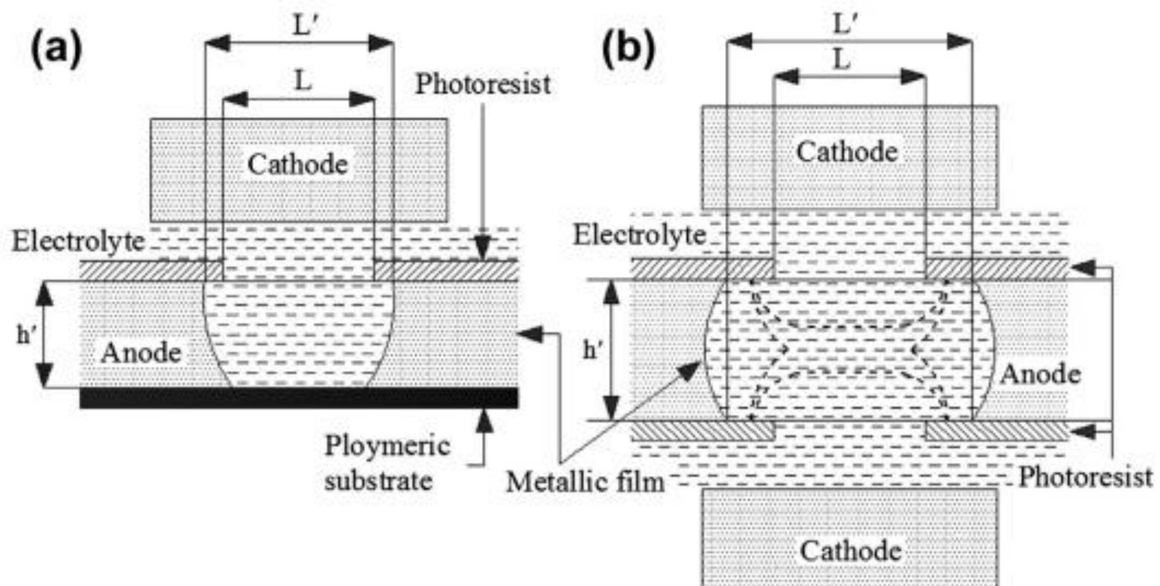

Figure 2.1: Through-mask EMM: (a) one sided and (b) two sided [2]

Through-mask EMM process involves the careful implementation of various steps that include production of the master artwork, surface preparation, choice of suitable photoresist, and imaging. The metal removal is isotropic in nature, and hence leads to undercutting below

the mask. During the designing of a photoresist mask, it is essential to have knowledge of the metal removal rate and the undercutting of the photoresist in through-mask EMM at different electrolytes and metal combinations. The most important influencing factor in the case of through-mask EMM is the etch factor (EF), which is defined as the ratio of the amount of straight through cut, that is, the thickness of metal substrate (h') to the amount of the undercut as expressed in equations 2.1 and 2.2 respectively:

For one-side etching,

$$\text{Etch Factor} = \frac{h'}{(L'-L)/2} \quad 2.1$$

For two-side etching,

$$\text{Etch Factor} = \frac{h'}{(L'-L)} \quad 2.2$$

Where, the photoresist undercut = L'- L

In TMEMM, the most important factors that govern the predominant machining criteria such as material removal rate, the shape profile and the surface finish of the workpiece are the conditions of mass transfer and the current distribution between anode and cathode. Both factors are intimately linked with each other, as they influence the presence and properties of surface films along the anode surface. In turn these dictate the mode of dissolution. An additional factor is the existence of an insulating mask, which, through its thickness as well as contour, also contributes towards effective anodic dissolution. Different salient characteristics in TMEMM are explained in details:

(i) Current distribution

During the initial stages of TMEMM, the distribution of the current density is highly non-uniform as the current is more concentrated at the edges than in the middle of the feature. As such, it leads to a maximum etch depth at the edge. As dissolution proceeds, the maximum of the current density distribution at the evolving surface starts to move toward the center of the feature due to metal surface under the photoresist drawing some of the current. The flow pattern of the electrolyte during through-mask EMM influences the convective mass transfer, which facilitates a high rate of metal dissolution at the center of the cavity, and then at the edge of the feature. Such a condition is beneficial as it can improve the anisotropy of the through-mask EMM process, which leads to minimization of the undercut of the photoresist. Current distribution in through-mask EMM can be modified by changing electrical and hydrodynamic parameters, which increase the possibility of fabricating high-resolution

features through utilizing high rate anodic dissolution of metals from a narrow cavity in processing advanced thin film materials for microfabrication.

In TMEMM, the current distribution must be described on different length scales simultaneously. These are the workpiece scale, the pattern scale and the feature scale. On the feature scale, only the geometry in the vicinity of a single aperture in the mask is taken into account, which extends at most to the neighboring features. Arrays of differently sized and spaced features constitute a pattern. The side-by-side arrangement of several such patterns on a single substrate conforms to the workpiece scale. Optimizing the current distribution, especially on the pattern and workpiece scale, is a necessity to minimize dimensional variations from feature to feature and from pattern to pattern.

The workpiece scale is concerned with the macroscopic current distribution within the electrochemical cell. As such, it is influenced by the cell geometry, the type and dimensions of the anode and cathode, as well as the presence and form of auxiliary electrodes. It is frequently characterized by edge effects, that is maxima and minima in the current distribution positioned along the workpiece edge and in the centre, respectively.

The pattern – scale current distribution describes variations in current density between different areas on the workpiece. Similarly to the workpiece scale, edge effects in the form of maxima in the current distribution are observed along the margins of a pattern. In general, maxima and minima in the pattern – scale current distribution emerge from spatial differences in the ratio of open to masked areas along the workpiece surface and from non-uniform spacing of adjacent features within a pattern.

(ii) Shape evolution

In TMEMM the formation of cavities and through-holes is governed by temporal and spatial variations in the rate of metal removal along the exposed metal surface. The local material removal rate is linked to the current distribution along the surface via Faraday’s law. The type of current distribution depends on the potential field between the electrodes and the boundary conditions along the surface. As stated, EF is the primary parameter that determines the localization of the microstructure generated during TMEMM. The control of EF during TMEMM depends on various parameters of electrochemical process as well as photoresist artwork parameters. Selecting a proper current density as a function of the substrate shape and cell geometry can significantly reduce the metal removal rate in the lateral direction. Figure 2.2 shows the shape evolution during through-mask EMM. Different geometrical

dimensions are shown during (a) cavity and (b) through-foil etching of a metal substrate through two different mask openings.

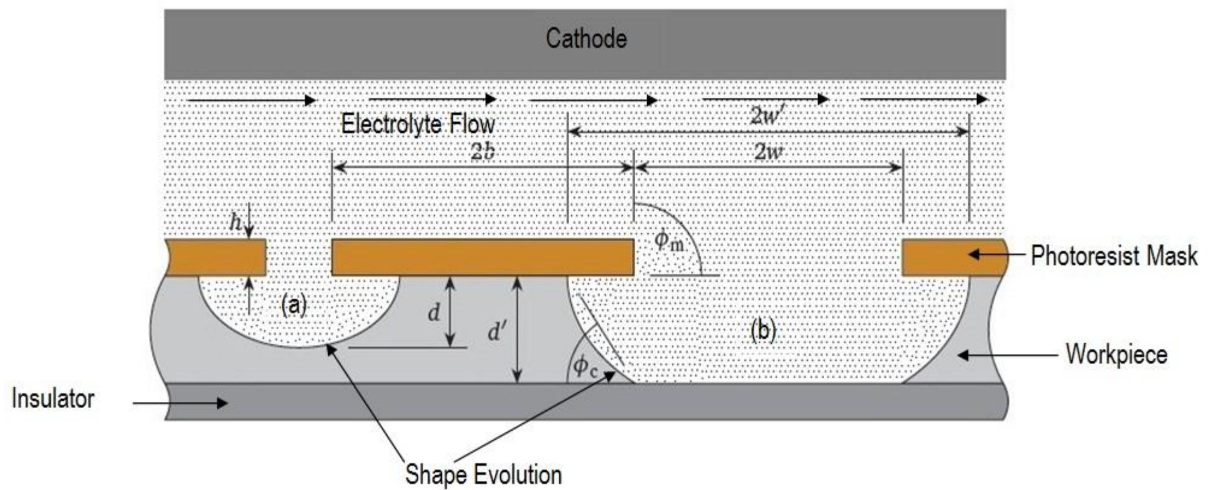

Figure 2.2: Schematic depiction of the shape evolution phenomenon during TMEMM

Shape-evolution studies distinguish between cavity and through-foil etching, and different parameters and length scales are of considerable importance in each case. These parameters are the spacing half-width (b), the metal-substrate thickness (d′), the maximum etch depth (d), the mask thickness (h), the mask-opening half-width (w), the final etch half-width (w′) and the mask wall angle (ϕ_m). In the case of cavity etching, the geometry of the problem is usually described by three scales. These are the aspect ratio of the mask opening (h/w), the spacing-to-opening ratio (b/w) and the ratio between the cavity depth and the mask-opening width (d/w). For through-foil etching, the film-thickness ratio (d′/w) and the cavity wall angle (ϕ_c) of the resulting aperture are also considered.

Apart from the assessment of the shape profile, the resulting cavities and through-holes are evaluated in terms of the undercut (U_c) of the mask and the etch factor (EF). The undercut is defined as the difference between the maximum half-width of the final etched cavity and the mask-opening half-width. The etch factor is defined as the ratio between the undercut and the maximum etch depth. Both the etch factor and undercut are relevant for the mask design. By taking into account the material removal underneath the mask, the mask openings can be sized to yield the desired cavity width at the end of the process [53]. The undercut and shape of the evolving surface will be governed by the following factors:

(i) Aspect ratio,

(ii) Spacing to opening ratio, and

(iii) Film thickness ratio, etc.

The aspect ratio of the mask opening is an important parameter which determines the shape of the feature. For a thick mask (aspect ratio i.e. $h/w > 0.5$), a flat-bottomed cavity forms at first, which subsequently acquires a hemispherical shape. The shape of the developing cavity will be an ellipse and maximum etch depth always remains in the cavity centre. This behavior is independent of neighboring features and thus the spacing-to-opening ratio. In contrast, for a thin mask ($h/w = 0.08$) the maximum etch depth is initially displaced from the centre. Accordingly, the profile reaches an inflection point. As the cavity deepens, the points of maximum etch depth move towards the centre and merge. For the latter case, adjacent features may exert a considerable influence on shape evolution, unless they are widely spaced ($b/w > 3$).

This difference in shape evolution stems from variations in the current distribution. For a high-aspect-ratio mask opening, the initial current distribution is practically uniform. As the metal surface recedes, a maximum in the current distribution forms at the cavity centre and remains there. In the case of a low-aspect-ratio mask opening, however, the initial current distribution is highly non-uniform; in particular, maxima occur along the edges. With an increase in the etch depth, the nature of current distribution becomes more uniform, and the maxima merge in the centre.

A shape-evolution study usually assumes different forms of mass transfer such as diffusion, forced convection and natural convection. During diffusive mass transfer, shape changes are solely governed by the geometry in the immediate vicinity of the mask opening e.g. immersion etching. In case the solution is strongly agitated, shape evolution is controlled by forced convection. The flow pattern in the presence of forced convection depends strongly on the shape of the cavity at hand e.g. jet and spray etching. If acceleration fields several magnitudes larger than earth's gravity is applied, shape evolution is dominated by natural convection e.g. in a centrifuge.

(iii) Surface finish

The average surface roughness after TMEMM is typically on the order of 0.07-1 μm. Important factors in determining the appearance of metal surfaces after electrochemical dissolution are current density, electrolyte flow rate and temperature, as well as the composition and structure of the metal or alloy.

In general, the magnitude of the current density along the anode determines the mode of metal removal, which is either characterized by active or mass-transfer-limited dissolution. Below the limiting current density the anode dissolves in the active state. Differences in the

orientation of crystal grains along the surface lead to variations in dissolution rate and thus expose crystal aspects. The resulting surface appears rough, dull and non-reflective. Conversely, anodic metal removal at the limiting current density leads to mass-transfer control. Variations in dissolution rate are suppressed and a smooth, polished and reflective surface finish is thus obtained. Complete mass-transfer control is necessary to achieve this phenomenon.

The composition and structure of the anode surface are also of importance in governing the surface finish, in particular during active dissolution. When machining pure metals or single-phase alloys, higher dissolution rates are observed in the vicinity of surface defects such as grain boundaries and metallic inclusions, resulting in grain boundary attack and pitting, respectively. In multi-phase alloys, different metallic phases often exhibit a distinct polarization behavior; thus, adjacent crystal grains belonging to different phases dissolve at varying rates. In all these cases, surface roughness increases rapidly. At higher current densities, however, specifically under mass-transfer control, such variations in the rate of metal removal are typically less pronounced or even suppressed completely. Nonetheless, when comparing mono and polycrystalline, as well as high and low purity materials, pure single crystals exhibit lower surface roughness after dissolution under polishing conditions than any other material type and composition.

Hydrodynamic effects due to electrolyte flow also play a major role in determining the surface finish, especially during mass-transfer-limited dissolution. The influence of hydrodynamic effects is magnified in TMEMM, where localized metal removal results in height differences along the surface over time leading to island formation. Consequently, non-uniform mass transfer ensues. This may be followed by partial removal of surface films, and thus incomplete polishing, or large-scale surface undulations.

2.2 Masking methods and materials

During TMEMM the anode surface is partially protected from dissolution by a patterned thin-film called mask. Today, several methods and materials are available to create the mask, including photo-sensitive polymers, metal oxides and inert silicones. Whichever material is used to fabricate the mask, it must satisfy several criteria to fulfill its purpose. The primary qualifying criteria for the mask material should be that it must be an insulator to enable preferential electrochemical dissolution through the mask openings. Secondly, the material must show sufficient chemical resistance to the electrolyte. In particular, its dissolution rate must be low compared to that of the anode material. To this end, a defect-free mask of

uniform thickness is advantageous. Thirdly, the mask should adhere firmly to the anode to facilitate accurate pattern transfer. Fourthly, the process and material cost need to be taken into account. Each of these points should be considered when making a choice of mask preparation. Some examples are illustrated below:

(i) Photoresists

The most widely used masking method is photolithography, which employs photo-sensitive polymer and resin coatings, known as photoresists. These are extensively employed in electrochemical micro fabrication, silicon micromachining and manufacture of intricate parts in aerospace, automotive, electronics and optical systems to name a few. The working principle of photolithography revolves around the fact that the structure of photo-sensitive polymers changes upon exposure to ultraviolet (UV) light.

Photoresists are divided according to the form, in which they are supplied, and the type of photochemical reaction, which occurs during exposure to UV light. Liquid resists are solvent-based, whereas dry-film resists are supplied in sheet or roll form. Both liquid and dry-film resists may be of positive-or negative type. UV exposure of positive resists leads to a decrease in molecular weight and thus an increase in solubility, either via photo-catalytic scission of polymer chains or photolysis of a photo-active sensitizer. In this manner, subsequent development creates a positive image of a design. For negative resists, when subjected to UV light, become less soluble, either due to cross-linking of polymer chains or the formation of products with higher molecular weight. Hence, a negative image forms after the development step.

Photolithography and photoresist-processing technologies are well-established and industrially approved, and many suppliers for equipment and materials exist. The requirement of resist depends solely on the application for which it is searched for. Furthermore, the parallel nature of the photolithography process enables the creation of multiple mask patterns simultaneously. But, this process also faces certain challenges. The necessary clean-room facilities and multiple processing steps create considerable capital and operational costs. The lack of an option to re-use the mask adds to these costs. Also, photolithography is largely limited to planar substrates. Though exposure equipment and photo-tools for non-planar substrates exist, these are geometry specific.

(ii) Oxide films

In response to the drawbacks of traditional photoresists and photolithography processes, resists based on oxide films, called oxyresists, were developed. The oxyresist technology

exploits the fact that some metals like aluminium and titanium naturally form adherent, passivating, nanometer-thin oxide films. These films can be grown artificially to much larger thickness via anodizing processes. Oxide films lend these metals their good corrosion resistance. Therefore, they were considered for use in TMEMM in conjunction with highly corrosive and aggressive electrolyte solutions, in particular for Al and Ti micromachining.

Several processes based on oxide films have been developed since the first inception of oxyresists. In the initial process variant, an oxide film is selectively formed on the metal by first applying and patterning a positive or negative photoresist via photolithography, which is followed by anodizing the exposed surface in a suitable solution. After stripping the photoresist, the oxide film remains and forms either a negative or positive image of the mask design. In this way, it acts as a protective mask during the successive electrochemical etching step. Instead, the photolithography step can be eliminated all together by the use of oxide film laser lithography (OFLL).

The cost-effectiveness of OFLL suffers from the serial nature of the laser-masking and marking process. Also, the investment and operating cost of the laser need to be taken into account. OFLL is limited to metals onto which a protective, adhering oxide film can be grown.

(iii) Polydimethylsiloxane (PDMS)

An additional negative aspect of the oxyresists is their lack of re-usability. Each substrate must again be treated to form a protective film, which is subsequently patterned and stripped in the end. If the mask were re-usable, these process steps could be omitted resulting in time and cost savings. The required re-usability, however, contradicts the criterion of good adherence between the mask and the substrate during the electrochemical dissolution step. One such candidate is a patterned silicone film made from polydimethylsiloxane (PDMS).

The creation of a PDMS mask requires the fabrication of a mould for casting. The mould corresponds to a negative image of the desired mask design. For example, if the mask should contain an array of linear trenches, then the mould includes line-shaped crests. Photolithography in combination with a negative-tone SU-8 photoresist may be employed for this step. PDMS gel is then cast into the mould, while applying a vacuum to quickly and thoroughly distribute the gel. After-wards the gel is allowed to cure and the resulting PDMS mask is de-molded.

While this process provides a low-cost, re-usable mask, a number of limitations exist as well. The chemical resistance of PDMS is limited, especially when exposed to concentrated acids

or alkalis. Accordingly, the use of PDMS masks is thus far limited to electrolytes consisting of neutral salt solutions. Furthermore, PDMS masks are hydrophobic in nature and good adhesion between the mask and the substrate is necessary; otherwise increased undercutting is observed.

2.3 Metals and electrolytes in TMEMM

(i) **Metals**: TMEMM is generally applicable to the machining of any electrically conductive material, be it a metal, semiconductor or conductive ceramic. The metals machined with this technique have been sequentially arranged along with their applications:

(a) Titanium - Biomedical implantable devices, e.g., dental and orthopedic implants and biomedical microsystems such as load bearing or drug containing devices are often made of titanium and titanium alloys. These materials offer biocompatibility, high fracture toughness and excellent corrosion resistance. TMEMM has received attention in the fabrication of biomedical implantable devices from titanium [39, 60]. The well-designed surface topographies obtained with EMM is a crucial advantage in this application. This is because the biomedical performance of titanium depends highly on the surface structure on the micrometer and nanometer scale. A special technique of TMEMM to titanium has been applied [61]. The researchers generated a defined surface oxide layer, which was subsequently structured by removing the oxide with excimer laser irradiation. The structured oxide functioned as lithographic mask in the machining process.

(b) Steel - Steel has a particularly broad field of application, and so has TMEMM of steel. Datta [11] discussed the production of nozzle plates for inkjet printer heads by through-mask EMM. Inkjet printing is based on ejecting the ink through nozzles by the pressure caused from the heating-up and vaporization of the ink constituents. The demands on the nozzles are a highly reproducible shape and dimension as well as the electrical and mechanical properties of the material. TMEMM meets these demands and offers a competitively-priced micromanufacturing process.

In hard disk drives, the information is stored on magnetic hard-disk platters. To read and write data, a slider with a magnetic head is moved along the platter. The slider is mechanically attached to a suspension, which is moved by an actuator arm. Through-mask EMM has received attention in the manufacturing of such slider suspensions. The slider suspension consists of an insulating layer which is sandwiched between steel and a copper layer. Both metal layers are etched through a photolithographic

mask. The specific advantage of TMEMM in this application is the potential to machine both metal layers with the same electrolyte in one fabrication step.

(c) Copper - Because of its high conductivity and electro migration resistance, copper is highly attractive for applications in microelectronics. PCBs, for instance, are usually made of this metal. Datta [11] discussed the fabrication of PCBs with TMEMM. A crucial advantage in this application is the ability to provide straight and smooth walls for copper lines of varying dimensions. Major drawbacks are the problem of island formation in large openings of the photoresist and the loss of electrical contact.

Another application of electrochemically machining copper through masks is the fabrication of cone connectors. Cone connectors are detachable electrical interconnections in electronic packaging applications and may be used to interconnect for example integrated circuits with PCBs and cards with each other or with cables. They are conical protrusion of specific shape and location, which may either contact with other cone connectors or with plane surfaces. For fabricating such shapes, the mask consists of photoresist dots placed at positions where the connectors are meant to evolve. TMEMM is a favorable technique for the fabrication of cone connectors because it yields well-defined, reproducible shapes and can be applied to a wide range of materials.

(d) Molybdenum - Two-sided TMEMM has received attention in the production of metal masks for screen printing [35]. Screen printing is a process where a metal paste is forced by a squeegee through the openings of a mask onto a substrate. In other words, the parts of the substrate where no paste should be applied are shielded, or screened, by the mask, which is where the term screen printing comes from. The design of the mask defines the pattern of the metallization. After the printing of the metal paste, the substrate is heated in order to obtain a solid metal pattern having good electrical properties. Molybdenum masks are used for the most demanding screen printing applications, because they provide better edge definition and paste release properties than alternative materials such as steel.

(e) Platinum- Frankenthal and Eaton [45] employed TMEMM in the manufacturing of silicon integrated circuits. They studied a metallization procedure which involves the sequential application of titanium, platinum and gold layer. The platinum and gold layers are patterned according to their functionality. This study demonstrates the potential of electrochemical etching through masks in the patterning of the platinum

layer. It uses an HCl-based electrolyte, whereas chemical etching uses aqua regia. Other attractive features regarding this application are better control of the etching endpoint, better reproducibility and higher etching rates.

Other materials for which through-mask EMM is an attractive fabrication technology include conductive ceramics, doped silicon and germanium semiconductors and various metals such as tantalum, tungsten, nickel, titanium, rhodium, aluminum and palladium.

(ii) **Electrolytes:** Electrically conductive solution which carries electricity through ions is termed as electrolyte. The electrolyte not only completes the electric circuit between the tool and workpiece, but also allows the desired machining reactions to occur. Generally, pure water is not conductor of electricity, but addition of any solvated ionic species makes it electricity conductive. The conductivity of an electrolyte solution depends on the concentration of the ions and behaves differently for concentrated and dilute electrolytes.

The electrochemical machining is mainly concerned with the interplay between the electricity and chemistry within a chemical environment which constitute the electrochemical cell. The electrochemical processes take place at the interface of electrode-electrolyte solution, usually bulk solution. In electrochemical cell, the electrode potential is used to dissolve workpiece materials. The mass transfer inside the electrochemical cell i.e. the dissolution of material depends on the hydrodynamic conditions for a given metal-electrolyte combination, and the dissolved mass transfer occurs in three different modes namely diffusion, convection, and migration. In electrochemical micromachining processes, the migration mode dominates the process mostly when very low concentration electrolytes are used, and the use of electrolyte circulation system is very limited. Electrolyte selection is an important task in EMM, and following points needs to be considered before electrolyte selection for specific application.

(a) Types of electrolytes

An electrolyte contains free ionic species that make it electrically conductive. The most typical electrolyte is an ionic solution i.e. acidic solution, basic solution, and salt solution but molten electrolytes and fused solid electrolytes are also possible. A liquid electrolyte provides better electrical conductivity than other electrolytes such as solid electrolytes and polymer electrolytes and consists of a salt or acid dissolved in a solvent or a mixture

of solvents. In TMEMM, the electrolytes are selected based on workpiece material used and the process requirements. The electrolytes are mainly classified into two categories, such as (i) passivating electrolytes containing oxidizing anions e.g. sodium nitrate, sodium chlorate, etc., and (ii) non-passivating electrolytes containing relatively aggressive anions such as sodium chloride. Passivating electrolytes are known to give better machining precision, offering machining of micro features with less side erosions. This is due to the formation of oxide films and oxygen evolution in the stray current region.

Various electrolyte solutions can again be broadly classified as aqueous and non-aqueous. Aqueous electrolytes are further divided into saline, acidic and alkaline solutions. Each of these groups has distinct advantages or areas of application.

Saline electrolytes are employed most frequently and for the widest range of materials, which includes the noble metals platinum, gold, silver, copper and their alloys. Non-noble metals include hafnium, molybdenum and zirconium. In addition, iron-nickel, nickel and titanium alloys, as well as a range of austenitic and martensitic stainless steels are machinable. The widespread application of saline electrolytes is based on their non-toxicity, low cost, and long-term stability. They are usually based on ECM solutions; thus, saline electrolytes contain NaCl, $NaNO_3$ or mixtures thereof and are used at or around room temperature. Advantageously, material removal in saline electrolytes only occurs, in case a potential or current is applied to the anode; otherwise the solution remains basically inert.

Acidic and alkaline electrolytes are typically made from viscous solutions of mineral acids like H_2SO_4 and H_3PO_4, and inorganic alkalis such as NaOH and KOH. Acidic electrolytes are advantageous in EMM because it produces soluble reaction products which can be removed easily from the inter-electrode gap without affecting the micro features of microtool. Parts machined in acidic and alkaline electrolytes often distinguish themselves by their superior surface finish. This is because frequently the specific metal-electrolyte combination permits mass-transfer limited dissolution polishing of surfaces is accomplished. Examples for this are molybdenum, nickel and niobium in acidic solutions, as well as tungsten in alkaline solutions.

Non-aqueous electrolytes comprise either salt-in-alcohol or acid-in-alcohol mixtures. The most common electrolyte constituents are H_2SO_4 or LiCl, which are dissolved in methanol or ethanol. These solutions are primarily applied to the machining of difficult-

to-etch metals and alloys, including nickel, tantalum, titanium, tungsten, and nickel-titanium alloys. The main incentive for the use of alcohol-based electrolytes stems from the fact that many of the above materials form inhibiting oxide films in the presence of small amounts of water-notably tantalum, titanium and nickel-titanium, which severely limits the dissolution process. Hence, water-free electrolytes should be used instead. In addition, initially present oxide films must be stripped first and their re-growth prevented, either via chemical or electrochemical means. Alcohol-based electrolytes have also proven useful when machining steels, cobalt and iron alloys, as well as aluminum. Nonetheless, their application is likely limited to metals and alloys, which are otherwise only machinable with difficulty. This is because specific safety concerns arise due to the toxicity, flammability and limited long-term stability of mixtures based on non-aqueous solvents.

Electrolytes are also classified as strong electrolyte and weak electrolyte based on degree of dissociation of solute. Strong electrolytes dissociates greatly for concentration ranging from very low to high values, whereas, for weak electrolytes dissociation of an electrolyte tends to unity at very low, limiting concentration, and reduces to about zero at high concentration.

(b) Electrolyte properties

The electrolyte at the IEG facilitates the electrochemical reaction. Therefore the electrolyte should:

(i) Ensure a uniform and high speed anodic dissolution,
(ii) Avoid the formation of a passive film on the anodic surface,
(iii) Not deposit on the cathode surface,
(iv) Have a high electrical conductivity and low viscosity to reduce the power used,
(v) Have good flow conditions in the narrow inter-electrode gap,
(vi) Be safe, nontoxic, and less erosive to the machine body,
(vii) Maintain its stable ingredients and PH value during machining,
(viii) Have minimum variation in its conductivity and viscosity due to temperature rise during machining,
(ix) Be less expensive and easily available,
(x) Possess less throwing power apart from basic properties like good chemical stability, high electrical conductivity, low viscosity, non-corrosive and inexpensive to increase the machining accuracy.

Apart from facilitating for electrochemical reactions, electrolytes have to perform various functions such as:

(i) Creation of an environment for anodic dissolution of workpiece material,

(ii) Conduction of the machining current,

(iii) Removal of the process by-products formed during machining

(iv) Carrying away the heat generated at inter-electrode gap, during machining to maintain constant temperature.

(c) Working life of electrolytes

The composition of the electrolyte begins to change with the progress of time during ECM. The major changes that may occur and their effects are detailed as follows:

(i) Loss of hydrogen, which may cause a reduction in electrical conductivity of the electrolyte and increase its pH value.

(ii) Loss of water, either by evaporation or carried off by evolved hydrogen gas, which may increase the concentration of the solution and thus may affect its electrical conductivity and its viscosity.

(iii) Formation of precipitate, which will reduce the concentration of the electrolyte and may affect its electrical conductivity.

(iv) Metal ions from the anode may pass into the solution and deposited on the cathode.

(d) Electrolyte concentration, temperature and flow

(i) Electrolyte concentration: The electrolytes in electrochemical cell carry electrical current by the movement of ions and the number of ions available for electrochemical reaction increases with increases in concentration. Therefore increased concentration of an electrolyte offers low resistance to flow of current resulting increased electrical conductivity. The magnitude of conductivity is determined by the type and number of ions present in the electrolyte. Hence, to compare the conductivities of the different electrolytes, the term electrolyte concentration is generally used, which can be applied to all electrolytes. Electrical current is carried out by the movement of ions in electrochemical cell. The rate of ionic movement is termed as the ionic mobility. Increase in electrolyte concentration increases machining current due to reduced electrolyte resistance. However further increase in electrolyte concentration reduces the electrical conductivity due to reduced ion mobility. Also increased density of electrolyte at

very high electrolyte concentration makes it difficult to remove the process by-products from narrow machining zone. Therefore dilute electrolytes are preferred in EMM of micro features.

(ii) Electrolyte temperature: During TMEMM of micro features, electrolyte concentration and temperatures are expected to be constant throughout the process for machining the micro structures with uniform features. Temperature of electrolyte at narrow IEG increases due to Joule's heating effect. Electrical conductivity of an electrolyte increases with increase in temperature because of increase in mobility of ions at increased temperature. Finally, increase in machining current due to reduced electrolyte resistance and due to increased temperature may generate micro features with varied characteristics like increased surface roughness, reduced machining accuracy, and higher MRR. Therefore, maintaining constant temperature of electrolyte during machining of micro features has its own importance.

(iii)Electrolyte flow: Machining of precise micro features by TMEMM demands micron sized tools with few micron of inter-electrode gap during machining. As per the requirements of the EMM process, fresh electrolyte needs to be supplied continuously at narrow inter-electrode gap by flushing out used electrolyte, for effective machining of micro features. Size of the microtools and IEG of few microns limits the movement i.e. flow rate of an electrolyte during machining. Higher flow rate of an electrolyte may vibrate the microtool in turn resulting in reduction of machining accuracy or controlled short circuit due physical contact with workpiece. Therefore, generally flowing electrolytes are recommended in machining of micro features by TMEMM, for improvement in precision and accuracy during micro machining of micro-textures.

2.4 Technical and financial considerations in TMEMM

In light of the resulting economy of scale, combining photolithography with electro-chemical etching processes i.e. TMEMM is expected to enable the fabrication of micro fluidic components in large quantities at low cost.

Indeed, cost savings are anticipated when TMEMM is considered. In the case of stainless steel, which is specially used for micro reactor fabrication, acidified ferric-chloride etchants can be substituted with concentrated NaCl electrolytes. Thereby, the requirements towards

equipment lining, safety precautions and waste disposal are reduced. TMEMM also helps in considerable time savings due to increased etch rates.

The isotropic nature of the PCM process leads to combined perpendicular and lateral etching, which result in large undercuts of the mask. Also, the etched metal surface is comparatively rough (0.5-5 μm). Therefore, channels and cavities are limited to shallow profiles and large widths in one-sided TMEMM. For the same reason, the minimum aperture size in double-sided TMEMM of thin sheets lies in the order of the sheet thickness. The dimensional tolerances also depend on sheet thickness and the design of the mask.

Compared to the widely employed chemical etching process, the TMEMM process offers better control and flexibility for microfabrication. A higher machining rate, the use of less corrosive electrolyte, and eco-friendly process are some of the advantages of TMEMM. Moreover, a wide range of materials, including high strength corrosion resistance alloys, can be machined by this technique. During machining of through-holes in thin metal foils, TMEMM produces burr-free edges and the mechanical properties close to the surface remain unchanged due to the absence of heat-affected zones and tool wear. This also results in a superior surface finish with sub-micrometer surface roughness.

Through-mask EMM is more increasingly recognized for the fabrication of electronic components as well as surface texturing, which involves high precision micromachining of thin metallic films. However, a limitation of TMEMM is the low aspect ratio of the produced microfeatures, due to the isotropic etching behavior, which needs deep investigation and further experimentation.

Chapter 3

DEVELOPMENT OF TMEMM EXPERIMENTAL SET-UP AND PREPARATION OF EXPERIMENTAL SAMPLES

3.1 Introduction

The escalating demand of arrayed microproducts in various fields have forced manufacturing industries to fabricate microproducts containing different surface textures from advanced engineering materials, in very short period of time. Electrochemical micromachining offers unique advantages over competing micromachining technologies and therefore finds ever-increasing application in all fields. Through Mask Electrochemical Micromachining (TMEMM) being a feasible process for fabricating geometrically well-defined micro patterned arrays of different shapes demands several technical specifications like arrangement and rigidness of mechanical structure, power supply requirements, workpiece and tool holding arrangements, in-process monitoring uniform IEG throughout the machining, etc. for the effective utilization of TMEMM process in the fabrication of arrayed microstructures on micro or macro products. There has been a few TMEMM system developed in research institutes, academic universities, as well as by commercial companies. Some of them are multipurpose systems or dedicated systems for EMM as well as for other non-traditional micromachining processes. Many research papers describe the machining capabilities of TMEMM for fabrication and generation of microstructures. Still as of today, there is no commercial, ready to use TMEMM machining set-up for micromachining applications. This is because of the electrochemical micromachining parameters which do not remain same for the different electrode-electrolyte combinations, and required shape and size of micro features and machining accuracy. Therefore for machining specific micro feature with desired machining accuracy, specific electrode-electrolyte combination is required, as well as demands for different machining strategy, which necessitates separate machining setup with varying capabilities. Keeping all above requirements in view, TMEMM system setup has been indigenously developed during the research programme.

A well-planned research program has been considered for the development of TMEMM system setup. Developed TMEMM setup has been successfully used in generation of island-free micro-dimple array of different geometry as well as fabrication of array of high-aspect-ratio micro-dimples on work piece samples by TMEMM which possess sufficient

dimensional uniformity as well as machining accuracy by maintaining the surface generated by machining.

3.2. Components of the developed TMEMM set-up

Machining of micro features in the form of micro-dimples by TMEMM necessitates different tasks to be done simultaneously in-tune with time or in coordination with each other. Hence, to develop a through mask electrochemical micromachining (TMEMM) setup, various subsystems along with their sub-components such as, machining cell along with workpiece and tool holding fixture, electrolyte flow system, power supply unit etc. have been interconnected.

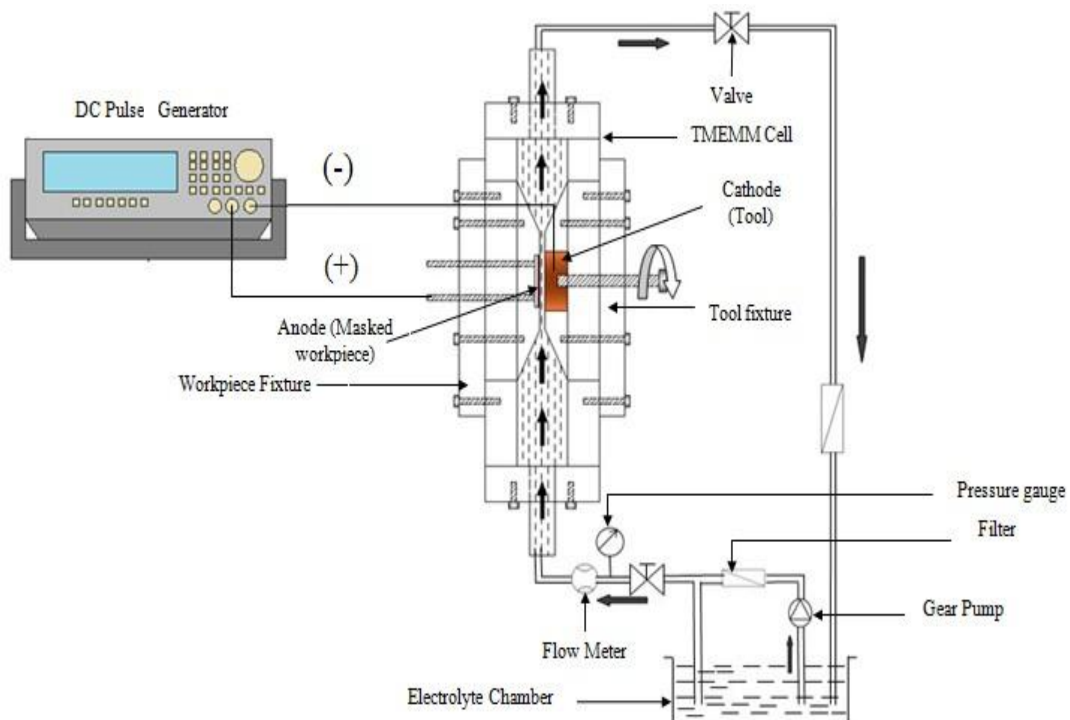

Figure 3.1: Schematic of the TMEMM experimental set-up with vertical cross flow electrolyte supply system

The schematic of the developed TMEMM experimental set-up is exhibited in fig. 3.1. Individual subsystems are described in detail in succeeding sections.

(a) TMEMM Cell

The TMEMM cell or the machining cell forms the foundation of the developed experimental set-up. It has three major components – workpiece holding device, tool holding device and the base, which integrates the workpiece holding device as well as tool holding device. All these three parts of the machining cell have been prepared with acrylic sheets (Perspex) such as to prevent its body from corrosion due to consistent

application of electrolytes. Figure 3.2 depicts design details of the machining zone with vertical cross flow electrolyte supply system consisting of its sub-assemblies:

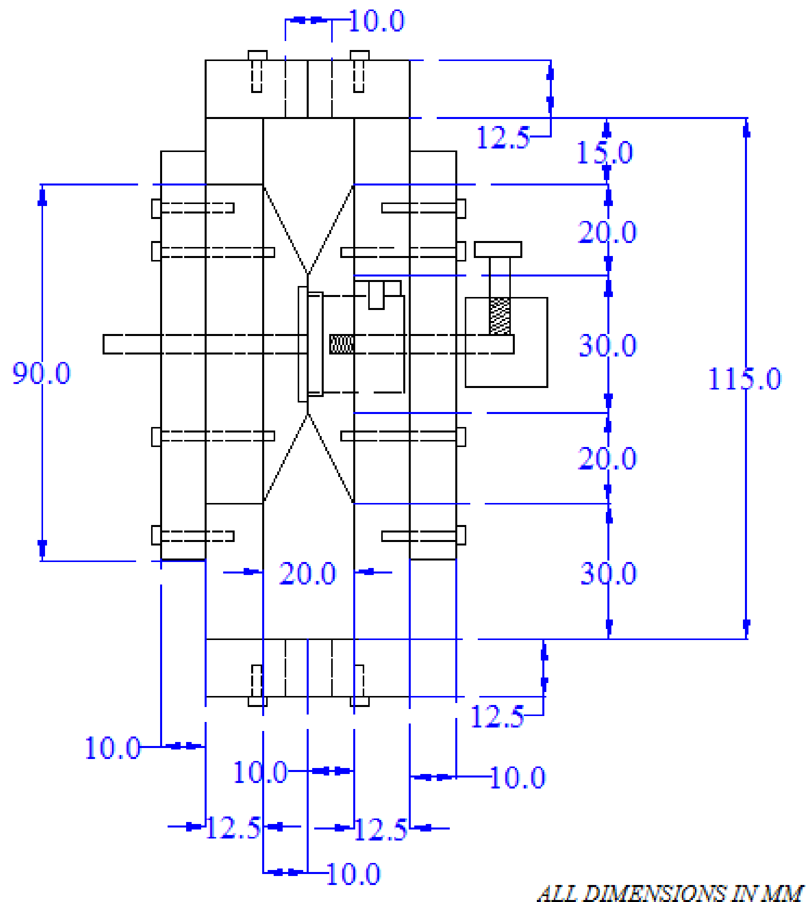

Figure 3.2: Design of machining zone with vertical cross flow electrolyte supply system

(i) **Base:** In addition to providing support to the workpiece as well as the tool holding device, the base holds the inlet and outlet electrolyte flow connections during machining etc. The inlet and outlet connections meant for electrolyte flow are made up of hollow stainless steel pipes of requisite diameters, that are press fitted with the base such as to allow the connections with electrolyte chamber to fix up rigidly during electrolyte flow while machining.

(ii) **Workpiece Holder:** It provides mechanical support to the masked workpiece (anode) during machining such that it is positioned just in front of the copper tool during machining. The experimental sample is fixed on the slot which was precisely made on the top of the workpiece holder of the specified thickness of the workpiece. The workpiece is held rigidly with two bolts such as to resist its dislocation and maintaining alignment during electrolyte flow. Figure 3.3 shows the dimensional details of the workpiece holder.

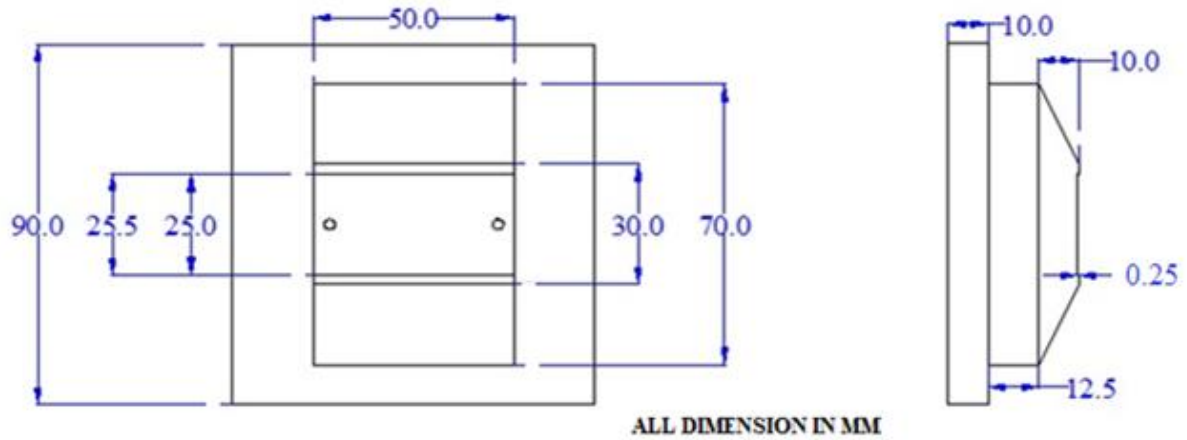

Figure 3.3: Specifications of the workpiece holder

(iii) **Tool Holder:** The cathode (copper tool of 12mm diameter) meant for accomplishment of the electrochemical reaction is held by the tool holding device. One cylindrical slot of the diameter of the tool has been cut in the top of the tool holder such that the tool can be accommodated onto it. Further, a through cylindrical slot in the bottom portion of the tool holder have been kept such that the shank of the depth micrometer could linearly retrace over it during adjustment of the inter electrode gap. Figure 3.4 dimensionally explains about the tool holder.

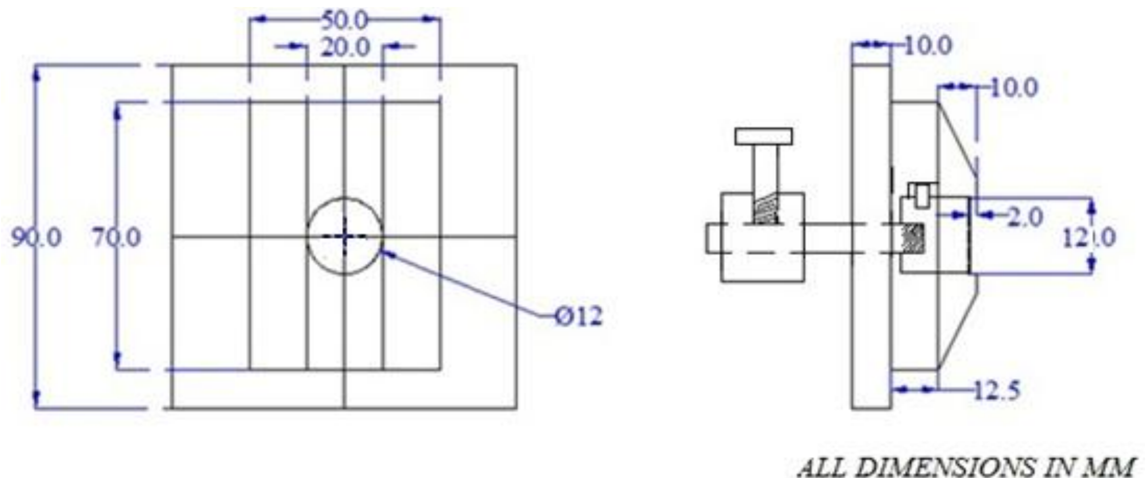

Figure 3.4: Specifications of the tool fixture

(b) Power Supply Unit

Power supply unit is a very important unit in the TMEMM system setup, since the nature of pulse and pulse parameters directly affect the machining accuracy of the generated micro-features. Machining takes place during pulse ‘on’ time only, and sludge removal from narrow machining zone mainly takes place during pulse ‘off’ time; therefore pulsed DC supply with short pulse period is preferred during TMEMM. Better control over

process needs pulse monitoring and control of the pulse parameters during machining operation. POA 75-4 rackmount four quadrant ultra high speed bi-polar power supply made by Matsusada Precision Inc., have been utilised for supply of power during the machining operations. It provides voltage in the range of +75 V to -75 V and current in the range of +4 A to -4 A.

(i) **Pulse generator:** Pulse generator generates DC pulses of required parameters and is the heart of power supply system. Continuous supply of the stable pulse patterns during machining is the prime function of a pulse generator. In the present system, function generator (Agilent 33250A, USA) has been used as source of pulses, which can supply pulse voltage of 10 V_{p-p}, pulse frequency up to 50 MHz, with capability to vary duty ratio. Various pulse parameters such as pulse period, pulse amplitude, pulse 'on-time' and 'off-time' i.e. duty ratio, pulse rise/fall times, positive or negative bias can be adjustable from a minimum to maximum value, resulting in different outputs for the same frequency.

(ii) **Digital storage oscilloscope:** Digital storage oscilloscope provides the online pattern of the supplied pulse along with the detailed information during machining. Digital storage oscilloscope has been used to monitor the machining conditions at the convergent machining zone, as well to detect the occurrence of short circuit if any between the copper tool and the masked workpiece by monitoring the nature of supplied pulse during initial IEG setting, as well as during machining to know the status of machining. Tektronix make TBS 1062 model having bandwidth of 60 MHz and a sampling rate of 1 GS/s has been used in the developed setup.

(c) Electrolyte Chamber and Flow System

Pump is used to lift clean electrolyte from the electrolyte chamber (storage tank) and supply electrolyte in the machining zone at desired pressure as shown in fig. 3.1. The electrolyte is supplied through the electrolyte supply ports. For the present research, cross flow electrolyte supply arrangement is used for experimentation. The electrolyte required for specific applications are prepared in the electrolyte chamber by mixing requisite amount of electrolyte with distilled water.

In EMM system it is necessary to maintain flow of electrolyte through small inter-electrode gap for accurate and precise machining. For this purpose smooth flow of electrolyte should be maintained and it is necessary to avoid blockage of small gaps. Hence electrolyte cleanliness is imperative. So it is necessary to ensure that piping

system does not introduce any foreign material like corroded particle, scale or pieces of broken seal material. Piping system used should be of non-corrosive material, therefore for the present experimentation piping material used is made from glass fibre reinforced plastic (GFRP). It is also necessary to maintain desired flow with required pressure. The electrolyte discharge rate is maintained by operation of flow control valves in the circulation system. The discharge rate of electrolyte can be controlled using by-pass valve provided in delivery path of pump and circulation piping. The digital flow meter is connected in the flow path system to measure discharge rate of flowing electrolyte.

(d) Inter electrode gap (IEG) control

The gap between the tool (cathode) and the workpiece (anode) is important factor to assure a stable metal removal in any micromachining processes. Although a higher range of IEG could be noticed in the TMEMM operations as compared with that found in EMM operations, the value lies in the range of 1500 μm to 2500 μm. A depth micrometer having a least count of 0.01 mm (10 μm) has been effectively used for minutely monitoring the IEG in the micromachining zone during the micromachining operation. The utilization of depth micrometer enhances the flexibility of adjusting the IEG during TMEMM experimentations.

3.3. Specifications of the TMEMM set-up

Complete dimensional details of the developed TMEMM system have already been pictorially presented in figs. 3.2, 3.3 and 3.4, that were taken into account during the design and development of the set-up developed for through mask electrochemical micromachining.

Figure 3.5 shows the actual photographic image of the sub components of TMEMM cell. Figure (a) and (b) represents the workpiece holding fixture and tool holding fixture respectively. Figure 3.6 depicts the assembled photographic view of the TMEMM cell with all sub components.

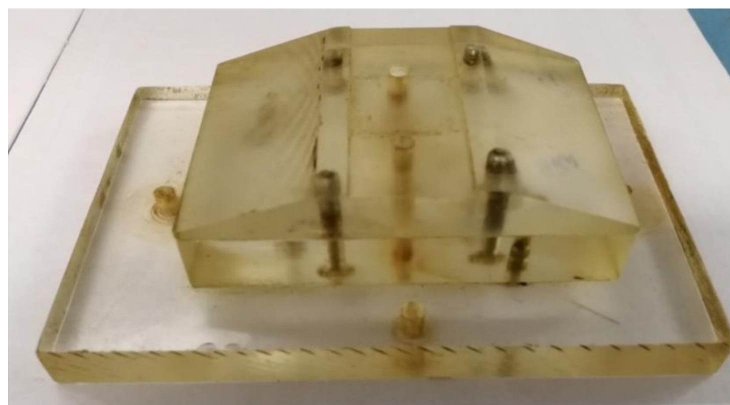

(a)

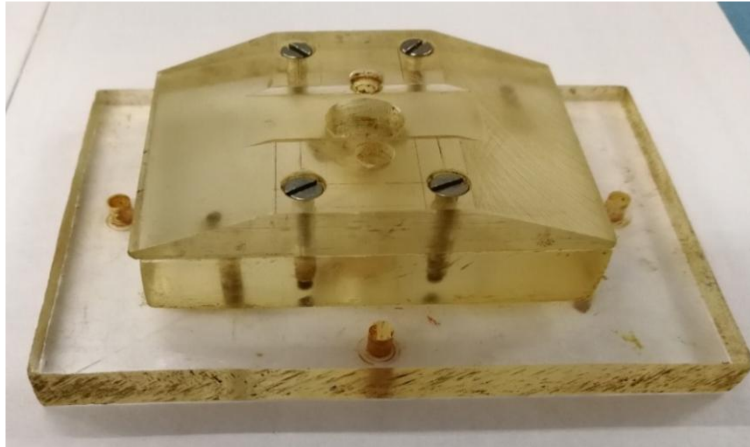

(b)
Figure 3.5: Actual picture of the (a) Workpiece holding fixture (b) Tool holding fixture

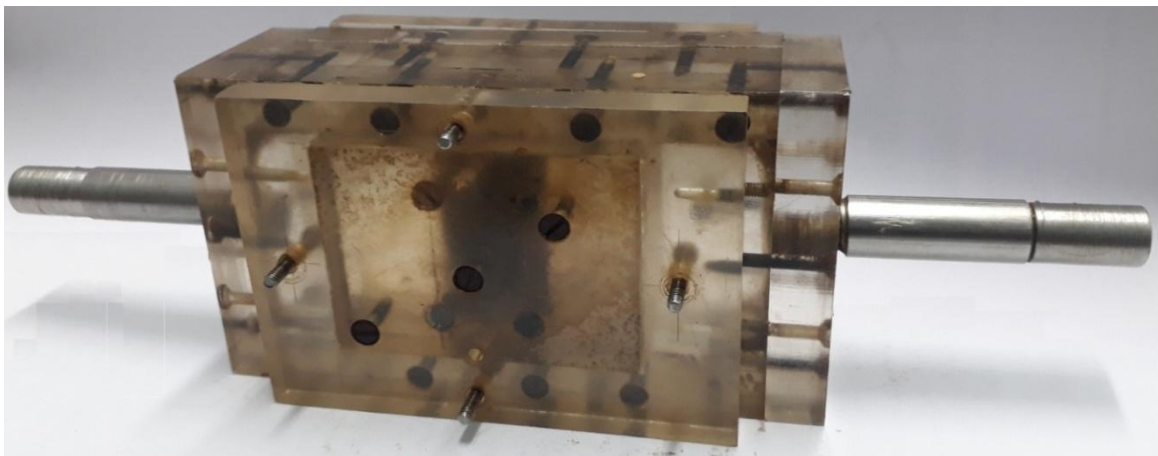

Figure 3.6: Pictorial representation of the Integrated TMEMM cell with all sub components

The power supply unit consisting all the interfaces for achieving controlled pulsed voltage during TMEMM have been pictorially illustrated in fig. 3.7.

Figure 3.7: Pictorial representation of the Power Supply Unit consisting of (a) Power Supply (b) Pulse Generator (c) Digital Storage Oscilloscope (d) Transformer

Photographic view of the indigenously developed TMEMM setup along with all the components have been exhibited in fig. 3.8. The components integrate to form the complete set-up which is utilized for carrying out various micro-texturing operations in TMEMM. A closer view of the TMEMM cell with electrical connections to anode and cathode and inter electrode gap monitoring unit have been depicted through fig. 3.9.

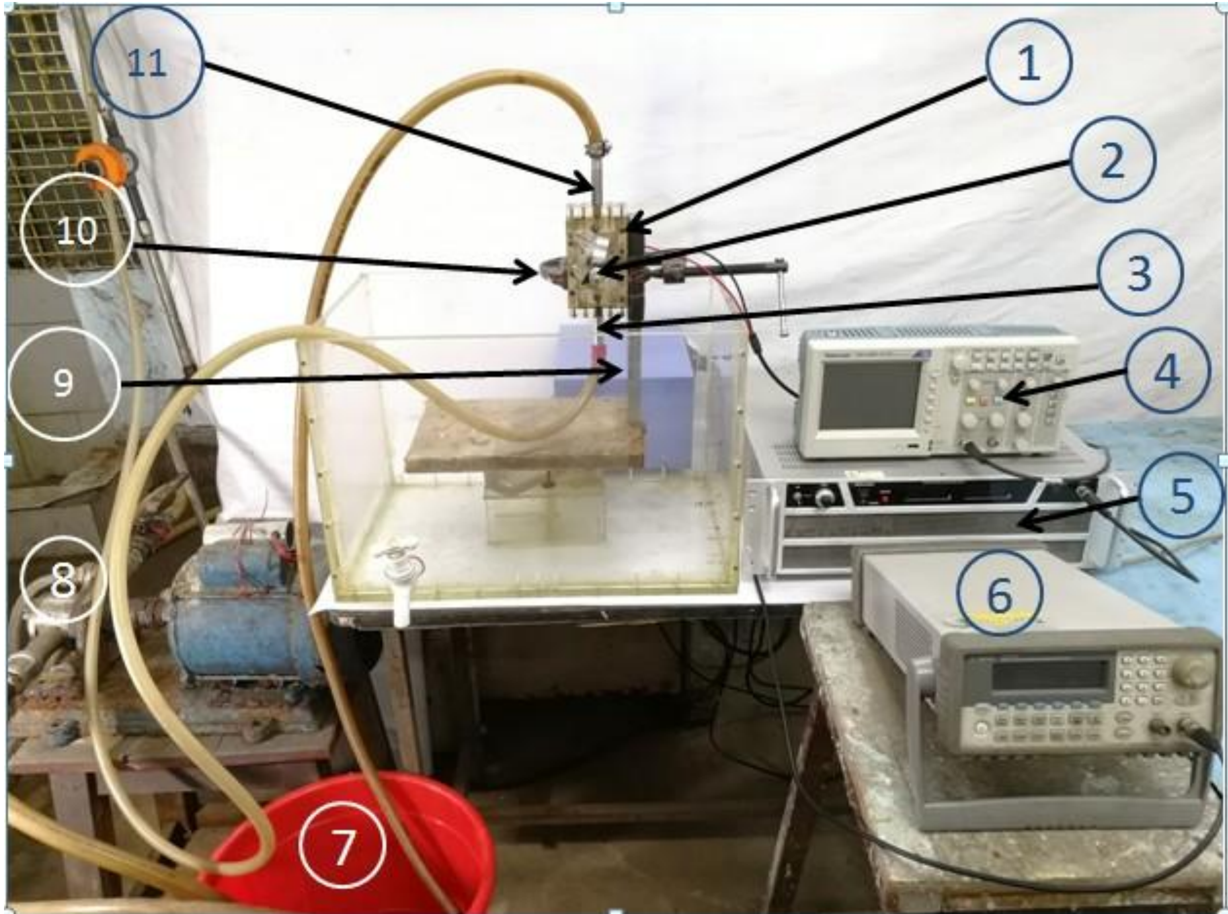

Figure 3.8: Actual photograph of the developed TMEMM experimental set-up, 1. TMEMM cell, 2. Depth micrometer, 3. Electrolyte inlet port, 4. Digital storage oscilloscope, 5. Power supply, 6. Pulse generator, 7. Electrolyte Circulation Chamber, 8. Electrolyte Circulation tank, 9. Fixture, 10. Clamp, 11. Electrolyte outlet port

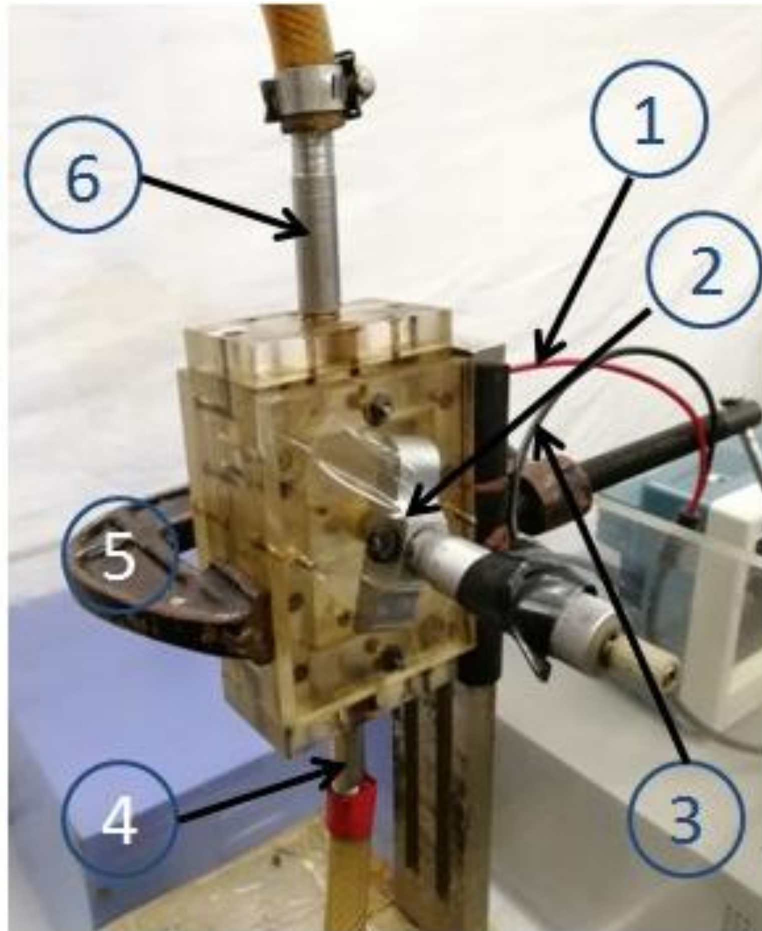

Figure 3.9: Closed View of the TMEMM cell showing 1.+ ve terminal connected to the workpiece, 2. Depth Micrometer, 3. –ve terminal connected to the tool, 4. Electrolyte inlet port, 5. C-Clamp, 6. Electrolyte outlet port

3.4 Preparation of Experimental Samples

Stainless Steel 304 has been considered as the workpiece material during the experimentation through TMEMM.

3.4.1 Importance of SS304 in engineering applications

Stainless steel (Grade-304) is the most versatile and widely used of all stainless steels. Its chemical composition, mechanical properties, weldability and corrosion/oxidation resistance provide the best all-round performance stainless steel at relatively low cost. It also has excellent low temperature properties and responds well to hardening by cold working. Grade 304 is readily roll formed into a variety of components for applications in the industrial, architectural, and transportation fields. SS 304 also has outstanding welding characteristics. Post-weld annealing is not required when welding thin sections. The austenitic structure also gives these grades excellent toughness, even down to cryogenic temperatures.

(a) Composition

Typical compositional ranges for grade 304 stainless steels are given in Table 3.1.

Table 3.1: Composition of SS304

Grade		C	Mn	Si	P	S	Cr	Mo	Ni	N
SS 304	Min	-	-	-	-	-	18	-	8	-
	Max	0.08	2.0	0.75	0.045	0.030	20	-	10.5	0.10

(b) Mechanical Properties

Typical mechanical properties for grade 304 stainless steels are given in Table 3.2.

Table 3.2: Mechanical Properties of SS304

Grade	Tensile Strength (MPa) min	Yield Strength 0.2% Proof (MPa min)	Elongation (% in 50mm) /min	Hardness	
				Rockwell B (HR B) max	Brinnel (HB) max
304	515	205	40	92	201

(c) Applications

SS304 is such a material which has versatile applications in engineering world. Different daily life applications that can be stated includes (i) Food processing equipment, particularly in milk processing & wine making (ii) Kitchen benches, sinks, troughs, equipment and appliances (iii) Architectural panelling, railings (iv) Chemical containers, including that of transport (v) Heat Exchangers (vi) Woven or welded screens for mining, quarrying & water filtration (vii) Threaded fasteners (viii) Springs (ix) Tanks and containers for a large variety of liquids and solids. (x) Process equipment in the aviation, mining, chemical, cryogenic, food, dairy and pharmaceutical industries such as medical implants etc.

3.4.2 Planning for preparation of the samples

SS304 sheets of size 50x50 mm^2 and having 200 μm thickness were carefully cut from a large sheet of SS304 of size 1ft x 1ft such that the sheets possess sufficient straightness and do not bend on corners. The samples were then cleaned with Isopropyl Alcohol (IPA) and coated with a negative photoresist AZ4903 using Spin Coater at different rpm for achieving coat of specific thickness. The coated samples were then baked followed by exposure through Ultra Violet Lithography (UV-Lithography) and developed for obtaining micro-scale patterns. The detailed procedure for UV-Lithography has been discussed later in this chapter. Each sample consists of micro-dimple arrays of diameter 65 μm. The entire process of lithography was carried out at Raja Ramanna Centre for Advanced Technology (RRCAT), Indore. A cylindrical copper tool of diameter 12 mm is utilized as cathode during experimentation.

Before use, samples were subjected to different cleaning treatments. Initially, the samples were rinsed with de-ionised (DI) water. Afterwards, the samples were ultrasonicated for 5 min. Isopropyl alcohol (IPA)/DI water was used for this purpose in a 1:1 (v/v) mixture. This was followed by rinsing with DI water and then with IPA, followed by drying in air. This was effective in removing any adhering debris or embedded particles. All samples intended for coating with photoresist underwent the above mentioned cleaning steps. The detailed procedure of fabrication of the samples required for experimentation has been described in Section 3.4.4.

3.4.3 Mask design and fabrication

AutoCAD is a tool for engineering drawing for variety of applications. Initially, the mask required for the specified application has been prepared in AutoCAD. Once the design is ready in AutoCAD then it is transferred on Coral DRAW for high resolution (10000 dpi) printing in polyester sheet. It was decided to accommodate sufficient circular as well as squares on 50 mm x 50 mm SS304 wafer for ease of fabrication and time saving. Figure 3.10 (a) shows a mask containing micro-holes as openings over it. The said mask has been prepared over polyester sheets after printing the design drawn in AutoCAD. It could be seen in fig. 3.10 (b) that nine experimental samples could be prepared after completion of a single UV-lithography process.

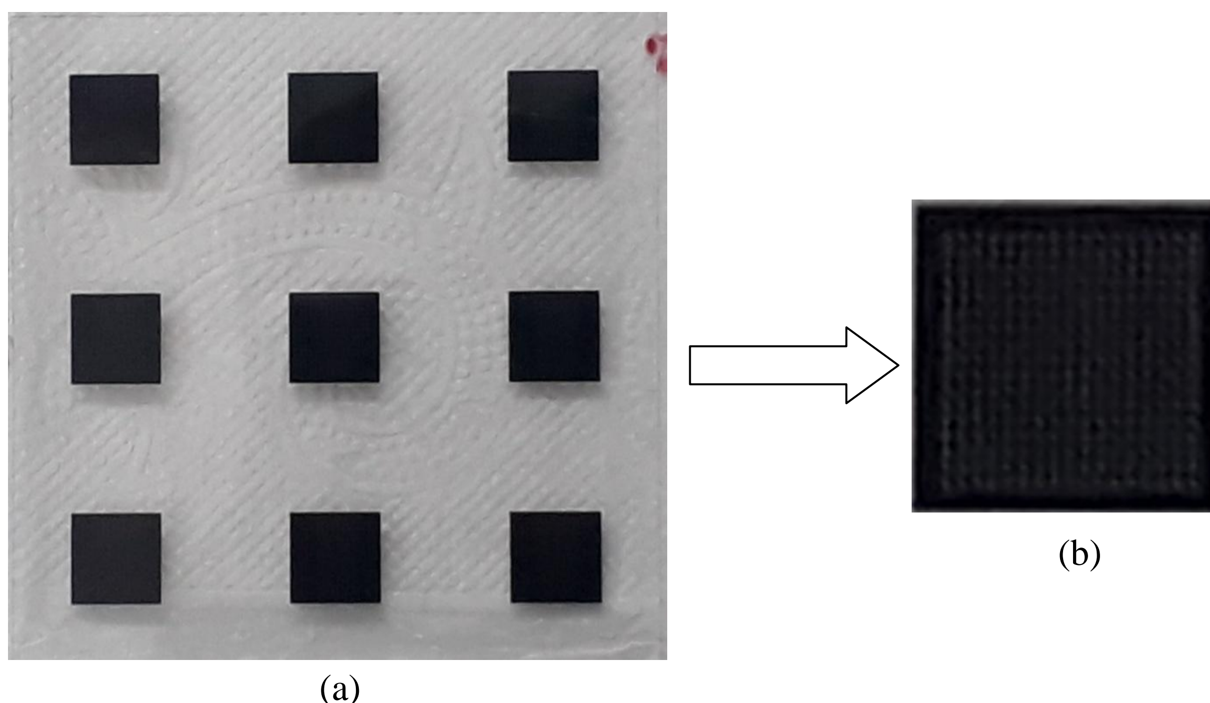

Figure 3.10: (a) A gelatine mask ($50x50mm^2$) to be used during lithography consisting of 9 similar imprints (b) Macroscopic view of a single masked portion

In addition to the desired pattern, each design also contained mask openings meant for alignment between the mask and the sample prior to ultraviolet (UV) exposure. These mask openings plays a significant role in the design topography of the geometrical features of the micro-texture patterns which are required to be replicated on the substrate after TMEMM process.

3.4.4 UV Lithography

UV lithography is perhaps the most commonly used photolithography technique in operation today. As the name implies, the basic concept of UV lithography centres around the properties and attributes of UV (ultraviolet) light.

UV Lithography is a process which uses UV light to transfer a geometric pattern from a photomask containing transparent and non-transparent regions for UV to a light sensitive chemical photoresist (PR) on the substrate. When particular wavelength of light is absorbed by the photoresist chemical changes occur in the photosensitive material and the image pattern on mask is transferred on a photo resist coated substrate. Light sensitive polymers that respond to light by cross-linking of their monomers (negative PR like AZ 4903, SU-8 etc.) or by breaking the polymer chains (positive PR like S-1813, PMMA etc.) are known as a photo resist. Figure 3.11 shows the schematic of photolithography.

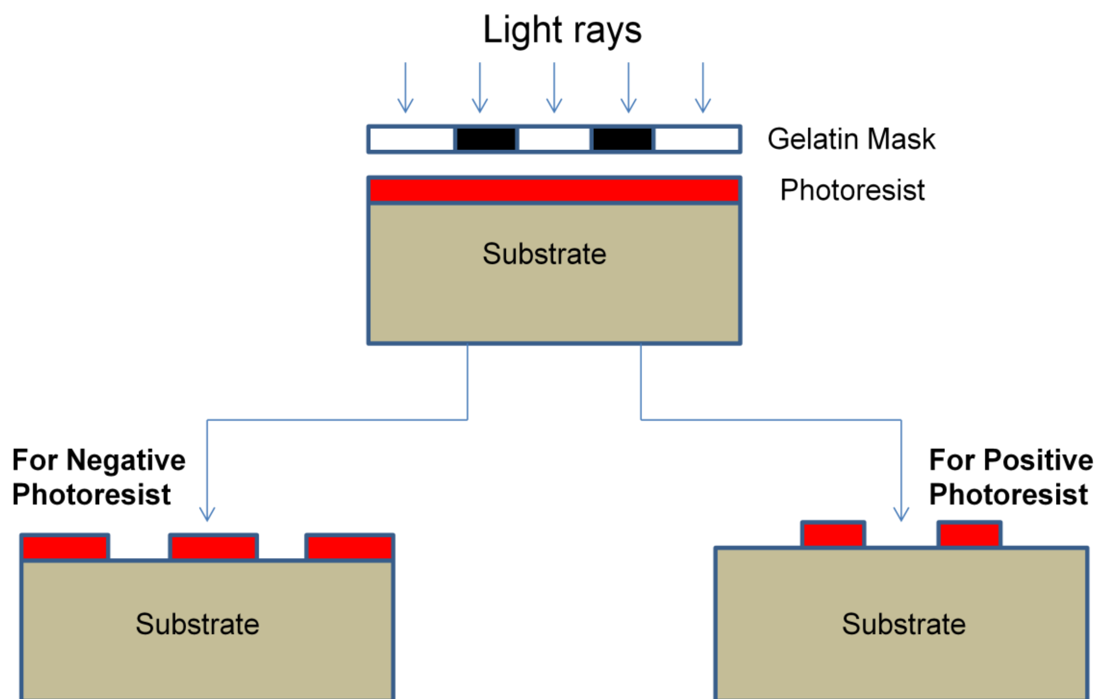

Figure 3.11: Schematic of photolithography process representing negative and positive PR reactions

Fabrication of experimental samples using UV lithography

Preparation of the samples required for experimentation is carried out in clean rooms, where air has been filtered out by particle contamination. Dust, bacteria and cells are micrometers in size and presence of which, will destroy the functionality of a microfabricated device. For this laminar flow table was used. In addition temperature, humidity, vibrations and electrical disturbances are kept under stringent control. The steps for preparation of the experimental samples using UV lithography are detailed below:

(i) **Cleaning**: Stainless steel substrate of dimension 50 mm x 50 mm x 200 μm (LxWxT) has been taken for UV mask fabrication. Substrate is properly cleaned in 1:1 solution of DI water and IPA for one hour. In cleaning process, organic and inorganic contaminations are removed from the surface of the substrate. Some common surface irritants include dust, fur, bacteria, water, and oil. Usually wet chemical treatment is used e.g. ultrasonication in acetone and IPA. The substrate is then heated to a temperature sufficient to remove any moisture that may be present on it due to rinsing in DI water.

(ii) **Photoresist application by Spin Coating**: The negative photoresist, AZ 4903 is applied over the SS wafer using spin coater. Spin coater gives a uniform thickness of PR. The photoresist solution is dispensed onto the substrate and the substrate is spun rapidly to produce a uniform thick layer due to the action of centrifugal force. The photoresist bonds uniformly to the surface, with the excess flying off during spinning. The spin coating process results in uniform thin layer. Two types of photoresists are available, positive PR and, negative PR, depending on their chemical composition and photo reaction. The photoresists are utilised according to requirements:

(a) **Positive photoresist**: A positive photoresist consists of three constituents; a photosensitive compound, a base resin and an organic solvent. Prior to exposure, the photosensitive compound is insoluble in the developer solution. After irradiation, the photosensitive compound in the exposed areas of the pattern absorbs energy, changes its chemical structure and transforms it into a more soluble species. After undergoing development, the exposed areas are completely dissolved. The examples of positive PR are PMMA, S-1813 etc.

(b) **Negative photoresist**: Negative photoresist are polymers combined with a photosensitive compound. Following exposure, the photosensitive compound absorbs the radiation energy and using chemical energy initiate a chain reaction

thereby causing cross linking of the polymer molecules. The cross-linked polymer has a higher molecular weight and becomes insoluble in the developer solution. After development the unexposed portions are removed. The examples of negative PR are SU-8 25, SU-8 2100.

(iii) **Prebake**: Prebaking is a process of heating the surface through a hot plate placed underneath the sample. Prebaking is normally done at 90°C to 100 °C for 30 to 60 seconds on a photoresist coated substrate to evaporate the excess coating solvent and to compact and harden the photoresist by reducing the residual stress in the film. In the instant case, prebaking has been carried out for 3 minute at 95°C.

(iv) **Mask Alignment:** The mask must be aligned correctly in reference to the surface. A photomask is a desired pattern that can be transferred onto a surface by means of light waves. The mask creates a sort of shadow between the light and the surface. No light passes through sections blocked by the mask. The mask is aligned with the help of a fixture developed for the said purpose. For UV exposure, the photomask is kept over the PR coated SS wafer. After that 3 mm thick glass is mounted and fixed with a fixture.

(v) **Exposure:** The photoresist, surface, and mask are subjected to UV light via a UV lamp. A band of 350 nm to 410 nm UV source with mercury light is used. UV exposure set-up used for lithography consists of mercury lamp, substrate mask holder, UV mask and PR coated resist substrate that are kept in close contact with each other. A 300 W Mercury vapour lamp was used as a UV source. It gives exposure in the UV wavelength band of 350 nm – 410 nm. The exposure is carried out for 140 seconds.

(vi) **Development**: The desired pattern is obtained by chemically removing the unexposed part (negative PR in this case) in a specific solution called developer. A developer solution is basically an etchant solution which removes the non linked polymeric chains of the photo resist. For Negative PR like AZ 4903, the molecules in the resist that are subjected to the most UV rays are bonded strongly together in long chains (polymerization). After the development process, the non-polymerized sections of the resist decompose and only the polymerized resist remains. During the development scissoned PR was washed off by the developer and unexposed region remain on the substrate. The complete development process continues nearly for 60 seconds.

(vii) **Post Bake**: The post bake is carried out to stabilize and harden the photoresist. It also removes any trace of development of chemicals over the substrate surface.

(viii) **Hard-bake**: If a non-chemically amplified resist is used, the resulting substrate is "hard-baked" typically at 90°C -120 °C for 20 to 30 minutes. The hard bake solidifies the remaining photo resist to make a more durable protecting layer.

A pictorial view of the finished product that was to be utilized during experimentation has been represented in fig. 3.12. Figure 3.12(b) shows image of a single experimental sample.

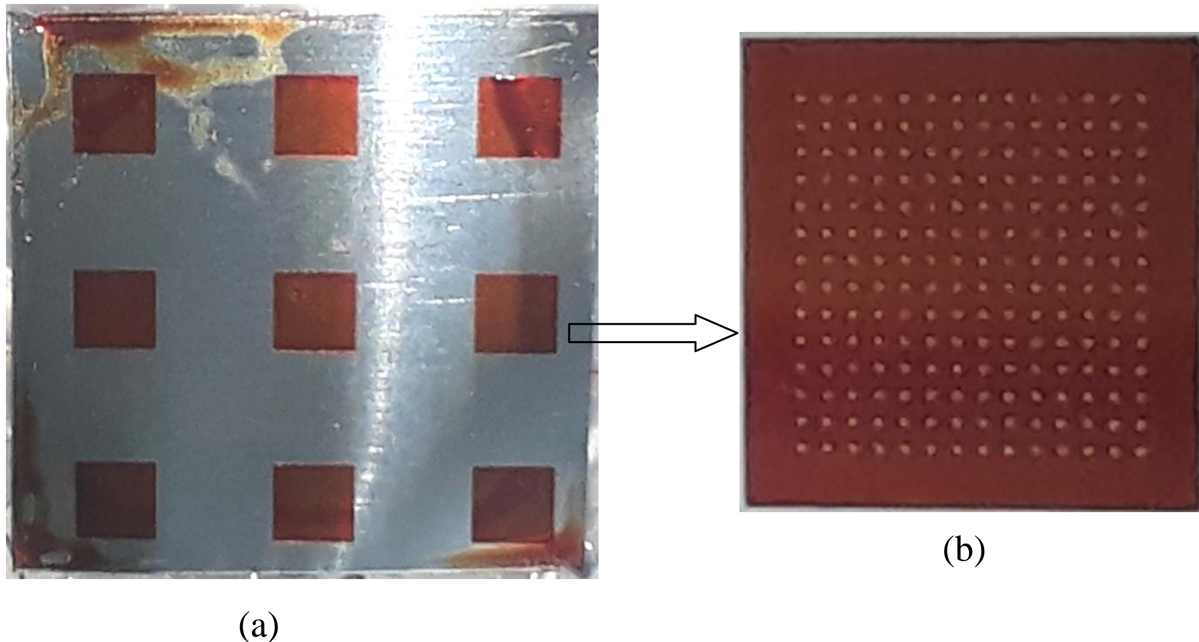

(a) (b)

Figure 3.12 (a) One specimen prepared after UV-lithography of SS304 with AZ4903 as mask (9 samples) (b) A single experimental sample after cutting of the specimen

Once the samples are ready for TMEMM after getting the desired pattern of PR coating, the samples are fixed in the workpiece holder of the experimental cell developed for TMEMM. After completion of machining, the features of PR are transferred onto the substrate. The photo resist is removed from the substrate with simple solvents such as acetone or IPA, which chemically alters the resist so that it will no longer adhere to the substrate. Optical inspection of the generated masked micro-textured surface has been carried out initially with Optical microscope (Leica DM2500, Germany). Talysurf CCI Non-contact 3D profilometer (Taylor Hobson) have been further utilised for precise measurements of the generated micro-surfaces. The analysis of the dimensions of the mask including geometry, resist thickness etc. could be accomplished with the software TALYMAP.

Chapter 4

INVESTIGATIONS INTO FABRICATION OF ISLAND-FREE MICRO-DIMPLE ARRAY BY TMEMM

4.1 Introduction

Micro-dimples are among the basic micro features that are indispensable in improving the tribological performance and reliability of various mechanical components. It is now receiving considerable attention in the electronics and other high-tech industries to produce metallic parts with microstructures. Through Mask Electrochemical Micromachining (TMEMM) is a feasible process for fabricating micro-dimple arrays with controlled size, location and density by maintaining surface texture. However, "Island formation" is one of the major barriers which not only hampers the surface quality but, in turn, weakens the effect of micro dimples during various engineering applications e.g. tribological, medical, aviation etc.

This chapter highlights in achieving island-free micro dimple array utilizing the most favorable machining parameters and AZ-4903, a negative photoresist, which is introduced as a mask due to its availability, low cost, chemical resistance and high flexibility. Pattern of micro-dimples free from islands imprinted on the mask are being replicated over SS 304 substrate with considerable repeatability.

4.2 Necessity of island removal from dimple surface during generation of micro-textures

Surfaces represent the boundary through which a large number of phenomena occur. The engineering fields involved by surface phenomena include chemistry, optics, mechanical engineering, electrical engineering and biomedical engineering etc. Many relevant industrial applications depend on surface properties. Surfaces are also the primary place of contact between biomaterial and its host organism. Roughness of the surface is a significant gauge of product superiority since it significantly controls the performance of mechanical parts as well as manufacturing cost. Surface roughness has an impact on the functional characteristic of the parts like lubrication, friction, wear, light reflection, heat transmission as well as it also affects mechanical properties like fatigue behavior, corrosion resistance and creep life etc.

In TMEMM, the electrical field intensity at the mask edge is much larger than that of the feature centre because of the marginal effect of the electrical field, which leads to a high current density at the edge. As such, the amount of material removal at the edge is more as compared to that at the centre of the dimple. As a result of which, non-uniformity in the

dimple surface could be noticed leading to formation of “island”. The problem of island formation is treated as a certainty in TMEMM.

However, it is utmost important to make the dimple surface free from islands to make it more convenient and utilizable for different tribological as well as engineering applications.

4.3 Difficulties in conventional procedures for island removal in TMEMM

It was experimentally investigated in previous research works that when TMEMM was carried out with a combination of a low aspect ratio and low film thickness ratio, island formation occurred due to loss of electrical contact. Island removal by employing masks of comparatively higher thicknesses i.e. 250 μm PDMS mask for generation of micro-dimple array free from islands have been studied upon the profiles of the generated micro-dimple arrays. Since, the phenomenon of island formation possess to be a hurdle towards sound micro dimple machining, so achievement of island-free micro dimples have always been a challenging task. While utilization of a 250 μm mask involves a considerable amount of expense, PDMS mask being hydrophobic in nature may restrict the electrolyte flow into the mask’s micro-holes, preventing ECM. This may lead to non generation of a sound dimple surface. As such, there is an urgent need to investigate TMEMM process utilizing thin mask of such a material which would possess sufficient adhesiveness with the workpiece so as to withstand the flow of electrolyte during through mask electrochemical micromachining.

To deal with various challenges during generation of island-free micro dimple array, AZ-4903, a negative photoresist can be introduced as a mask which will be readily available at low cost, chemically resistive and highly flexible. In order to achieve island free micro-dimple array, in depth experimentation along with detailed analysis is needed for which planned experimental investigations are to be carried out.

4.4 Experimentation for investigating the effectiveness of low thickness mask (AZ4903) during fabrication of island free micro dimples

4.4.1 Experimental planning

Keeping in view of the objectives of the present research work, the experimental observations and studies have been planned for conducting fruitful research analysis for deriving effective research findings. The experimental planning is aimed at investigation for dimensional uniformity as well as surface characteristics during generation of micro-dimple array in TMEMM.

EMM is one of the alternative machining processes that can be applied to the machining of advanced materials with surface textures for different applications. Many researchers have so

far concentrated on the process improvement in EMM and to the best of the author's knowledge, very less effort have been made to study surface characteristics of micro-textures generated using TMEMM.

To investigate the influence of TMEMM process parameters like applied voltage, electrolyte flow velocity, pulse frequency, and duty ratio, on dimple characteristics i.e. average dimple diameter and average dimple depth, the experiments have been systematically planned with machining parameters as shown in Table 4.1 and performed on the developed TMEMM set-up. The extreme limits of machining parameters i.e. upper and lower values were decided by performing trial experiments, and considering the experimental set-up capabilities. Keeping this objective into consideration, several basic experiments were performed utilizing developed cross flow electrolyte supply system in electrochemical micromachining. Experimental results based analysis on dimple characteristics have been presented in the following sections.

Table 4.1: Machining parameters for the experiments

Parameters	**Range**
Applied Voltage	8 V – 12 V
Electrolyte Flow Velocity	1.9 m/s – 7.6 m/s
Machining Frequency	1 kHz – 5 kHz
Duty Ratio	20% – 50%
Inter Electrode Gap (IEG)	2000 μm
Electrolyte Concentration	NaCl (10%) + $NaNO_3$ (10%)
Machining Time	90 s, 120 s

Approximately 40 micro-dimples for each sample were measured during analysis. Optical microscope (Leica DM2500, Germany), Talysurf CCI Non-Contact Profilometer (Taylor Hobson) and Scanning Electron Microscope (JEOL JSM 6360 and ZEISS EVO 40) were utilized to measure the machined surface characteristics and shape accuracy. 'TALYMAP' software has been utilized for analyzing the profiles of the generated micro-structures.

In TMEMM, geometric accuracy of the machined micro textures directly relates with the geometry of the micro features imprinted on the mask. Hence, geometrical deviations of the micro-dimples machined with different parameters have been analyzed with their scanning electron micrographs. The best machining parameters for machining circular shaped micro-

dimples have been searched out and further utilized for fabrication of island free micro-dimple array during TMEMM.

4.4.2 Experimental methodology

Procedural steps are necessary to follow, for conducting the planned set of experiments efficiently. The detailed steps followed for the different set of experiments are listed below:

(i) Copper tool (Cathode) of desired diameter has been prepared through turning and facing operations in the Lathe.

(ii) The masked workpiece (big) of size 50x50 mm^2 prepared through UV-Lithography have been equally cut into 9 small samples that are to be used during experimentation.

(iii) The mixed electrolyte solution of sodium nitrate ($NaNO_3$) and sodium chloride (NaCl) has been prepared as per the specified concentration and poured in the electrolyte chamber.

(iv) The constituents of the TMEMM set-up i.e. TMEMM Cell, workpiece holder, tool holder etc. are cleaned properly with cotton cloth, such that no difficulty arises when these three components mate to form the closed machining chamber.

(v) Experimental sample (Anode) is then fixed in the slot kept at the workpiece holder with fixing bolts on both sides of the top surface.

(vi) The copper tool (Cathode) is then mounted at the slot provided in the tool holder, which is designed in such a way that it is aligned over the workpiece (anode) when the machining chamber is ready after fitment. The bottom of the tool contains a cylindrical cavity which is the slot for the shank of the depth micrometer to enter such that upon rotation, the IEG can be accurately set during machining.

(vii) When the machining cell is ready after complete fitment of its accessories, then the electrolyte pipe connections are made after which the TMEMM cell is clamped rigidly on the stand of the machine base with a fixture which holds it firmly during experimentation.

(viii) Then after, the electrical connections i.e. positive terminal of the pulsed power supply with the workpiece extension bolt and the negative terminal of the power supply with the copper tool have been made.

(viii) The gear pump is then switched ‘on’ for fixation of the electrolyte flow velocity as per readings in the digital flow meter. The rate of inlet flow and outlet flow of the electrolyte is kept constant by adjusting the flow control knobs.

(ix) TMEMM process parameters like applied voltage, pulse period, duty ratio, pulse frequency, cut-off current, cut-off voltage, and electrolyte concentration are adjusted according to the desired experimental plan.

(x) The pulse power supply along with the stopwatch has been switched 'on' simultaneously. Micro-textures have been machined and process parameters like machining current and machining voltage have been noted down.

(xi) At the end of the TMEMM operation, power supply and the pump are switched off simultaneously, and electrolyte flow pipes as well as electrical connections are opened to make the TMEMM cell free.

(xii) The TMEMM cell is then dis-assembled into its three constituents.

(xiii) The workpiece sample is taken and cleaned with acetone and distilled water, dried in air and microscopic images of machined micro features have been taken for further analysis.

(xiv) The shape, geometry and surface integrity of the machined micro-structures during various sets of experiment have been observed and analyzed with the help of various profilometer images and SEM micrographs.

(xv) The results of all experiments have been noted down carefully for further analysis.

4.5 Experimental results and analysis for fabrication of island free micro-dimple array

The above mentioned process parameters have been studied in details and the influence of various process parameters such as applied voltage, pulse frequency, electrolyte flow rate, and duty ratio on dimple characteristics have been investigated varying one factor at a time. Hence, fabrication of island free micro dimple array by Through Mask EMM could be executed through detailed discussion of the experimental results.

4.5.1 Effect of electrolyte flow velocity

Initially, TMEMM was carried out using a static electrolyte i.e. electrolyte without flow as shown in fig. 4.1, in which both the cathode and the masked workpiece (anode) were immersed in the electrolyte and there was no additional arrangement to make the electrolyte flow. The electrolyte flows into the mask holes under its own gravity. As retrieved from research findings, a mixture of NaCl and $NaNO_3$ in specified proportion was chosen as the electrolyte and circulated for accomplishment of micro surface texturing experiments in TMEMM during this experimentation work. NaCl has been preferred for high material removal rate due to the availability of more ions for higher conductivity and $NaNO_3$ have been taken into consideration due to its machining accuracy. An Inter Electrode Gap (IEG) of 2000µm has been chosen for the experiments.

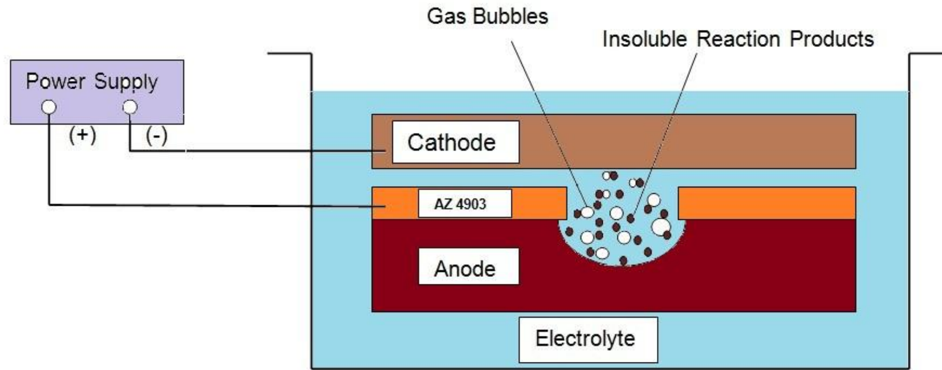

Figure 4.1: Schematic diagram showing TMEMM without flowing electrolyte

During the machining process, the metal dissolved at the anode workpiece, and at the same time, gas bubbles were generated. With prolonged machining time, small gas bubbles constantly grew into large bubbles and breaks. Debris and bubbles remaining between the electrode and the workpiece cause a bridge phenomenon which adversely affects the surface of the generated micro-dimples. This phenomenon is clear from fig. 4.1 wherein it is seen that the generated reaction products do not leave the machined surface after machining resulting in deterioration of the dimple surface. Although an IEG of 2000 µm was kept in the set-up, but the insoluble reaction products as well as gas bubbles could not escape from the generated dimple surface. As a result of which, a non-uniform as well as uneven surface could be found in the dimple surface after machining which is clear from fig. 4.2.

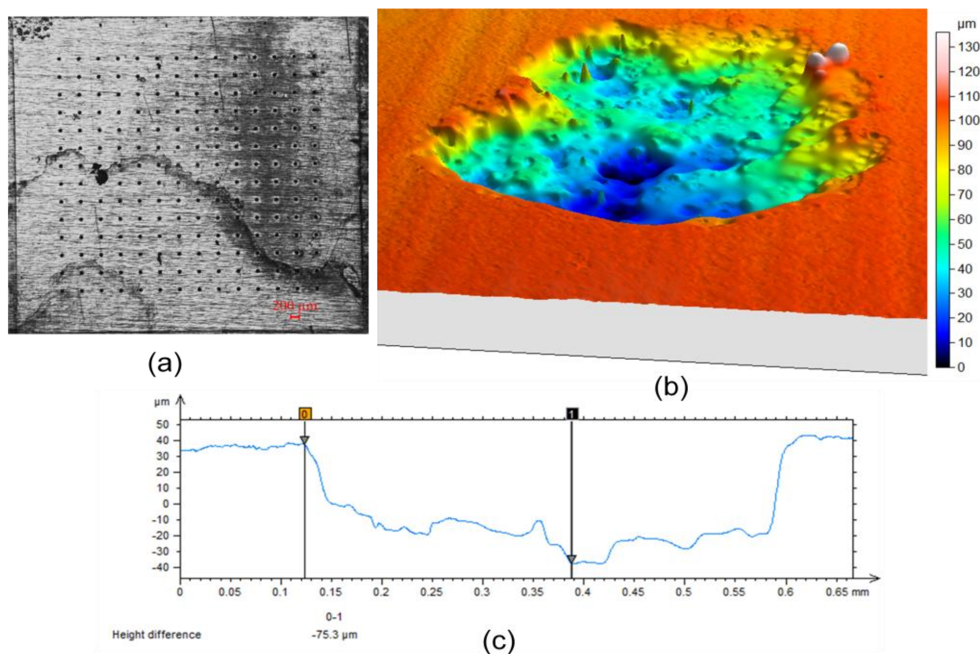

Figure 4.2: (a) Microscopic image (b) Profilometer image showing surface generated (c) Cross sectional view of the generated circular micro-dimple during TMEMM with static electrolyte

Figure 4.2 (a) shows the impressions created by the precipitates of sludge lying all over the sample surface when texturing have been carried out with static electrolyte. Further, fig. 4.2 (b) and (c) shows the profilometric image and cross sectional view of a generated circular micro-dimple. It could be easily noticed that the generated dimple surface is greatly affected when static electrolyte is used during TMEMM of micro-textured arrays. This is because the sludge generated during machining gets entrapped in the dimple surface due to stagnant nature of electrolyte and deteriorates the generated dimple surface. SEM micrograph in fig. 4.3 confirm the observations clearly showing the presence of a residual material in the respective centers of the generated micro textures, which contributes to the unevenness and non-uniformity of the surface generated in the textured circular micro textures.

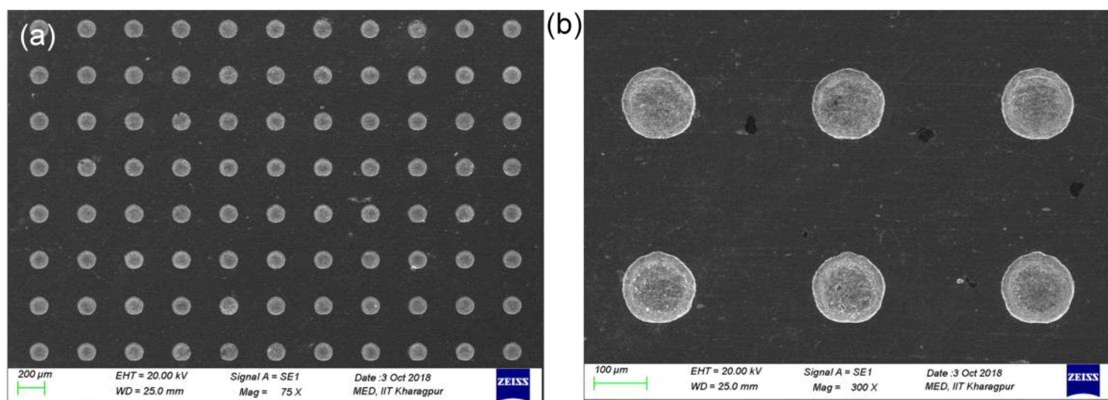

Figure: 4.3: SEM micrograph of micro-dimples generated using static electrolyte (a) 11x8 array (b) close view of some dimples generated by TMEMM with static electrolyte

Figure 4.3 (a) shows an array of approximately hundred micro-dimples. It could be clearly observed from fig. 4.3 (b) that material removal has primarily occurred from the edges leaving behind the materials at the centre. As such, the generated surfaces were very rough and uneven and highly ineffective in any engineering and tribological applications.

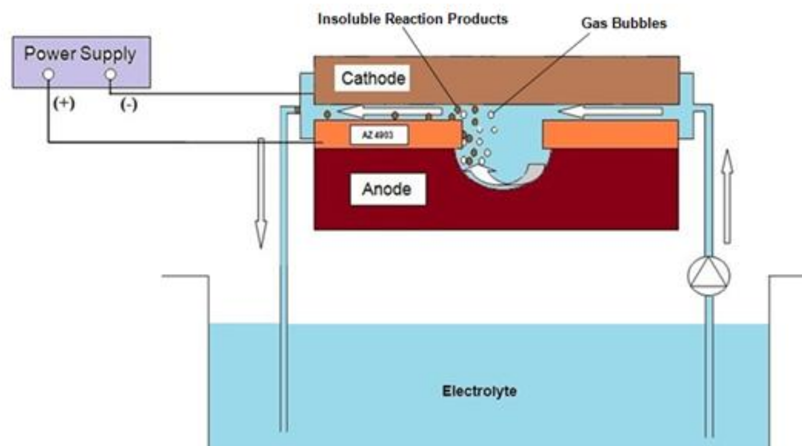

Figure 4.4: Schematic diagram showing TMEMM with flowing electrolyte

To combat with this situation, it was highly important to remove the debris and the gas bubbles from the machining zone. To force the electrolyte to flow through the IEG for efficiently flushing of the insoluble reaction products as well as the gas bubbles, an arrangement for flowing electrolyte has been proposed as shown in fig. 4.4. In the developed set-up, a gear pump has been introduced to carry out the flow of electrolyte from the electrolyte chamber to the TMEMM cell and then back to the chamber. Electrolyte was fed to the micromachining zone through a developed vertical cross-flow system.

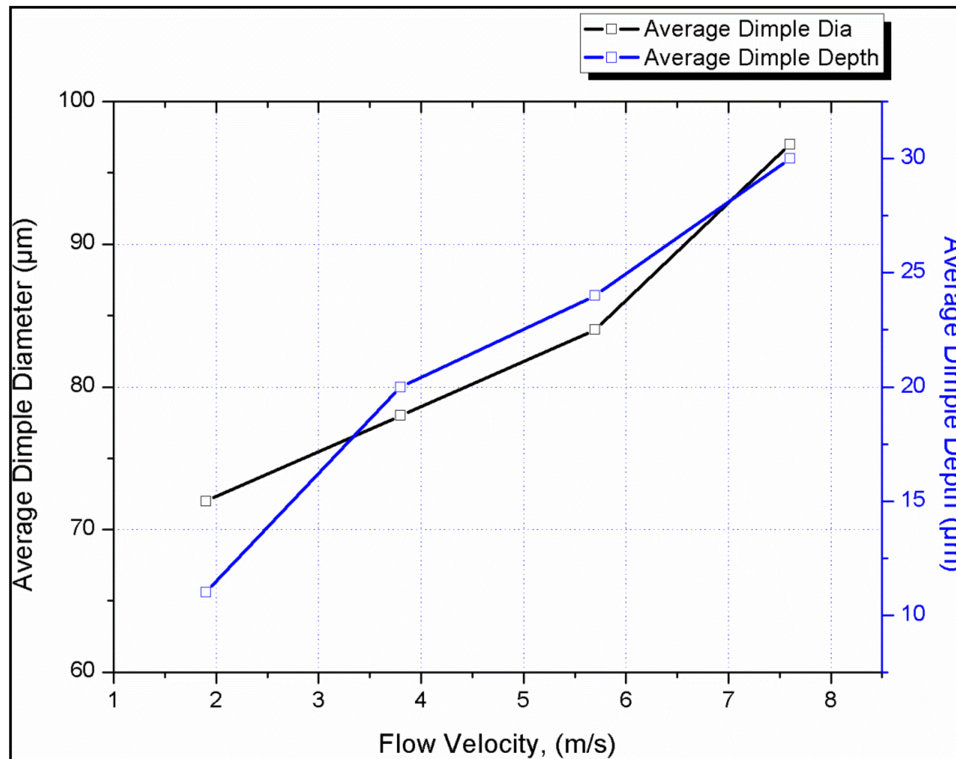

Figure 4.5: Variation of avg. dimple diameter and depth with electrolyte flow velocity

However, to assess the most favorable electrolyte flow velocity, experiments have been conducted with four different flow velocities i.e. 1.9 m/s, 3.8 m/s, 5.7 m/s and 7.6 m/s. Figure 4.5 plots the variations in average diameter and depth of the generated micro-dimples with the electrolyte flow velocity in the range of 1.9 m/s to 7.6 m/s, 12 V applied voltage, pulse frequency of 2 kHz, 30% duty ratio, mixed electrolyte concentration of 10%NaCl and 10%$NaNO_3$ for 2 minutes machining time. From the figure, it is revealed that average dimple diameter as well as the dimple depth increases with increase in electrolyte flow velocity. Gradual increase in the flushing capacity of the reaction products as well as the gas bubbles with increase in electrolyte flow velocity is the primary reason for the increase in the dimple diameter as well as the depth. When machining was initiated with 1.9m/s, material removal could only be noticed from the edges and the material remained almost intact at the centre.

This may be because of increased number of bubbles and more sludge generated at inter-electrode gap at lower flow velocity, which affects the removal of the material from the surface. Moreover, the non-uniform nature of current density allows the primary material removal from the edges and then after it turns to the centre. However, reasonable material dissolution could be noticed when the flow velocity reaches 3.8 m/s and the dimple surface showed no material lump on the surface generated after TMEMM as observed through the microscopic images.

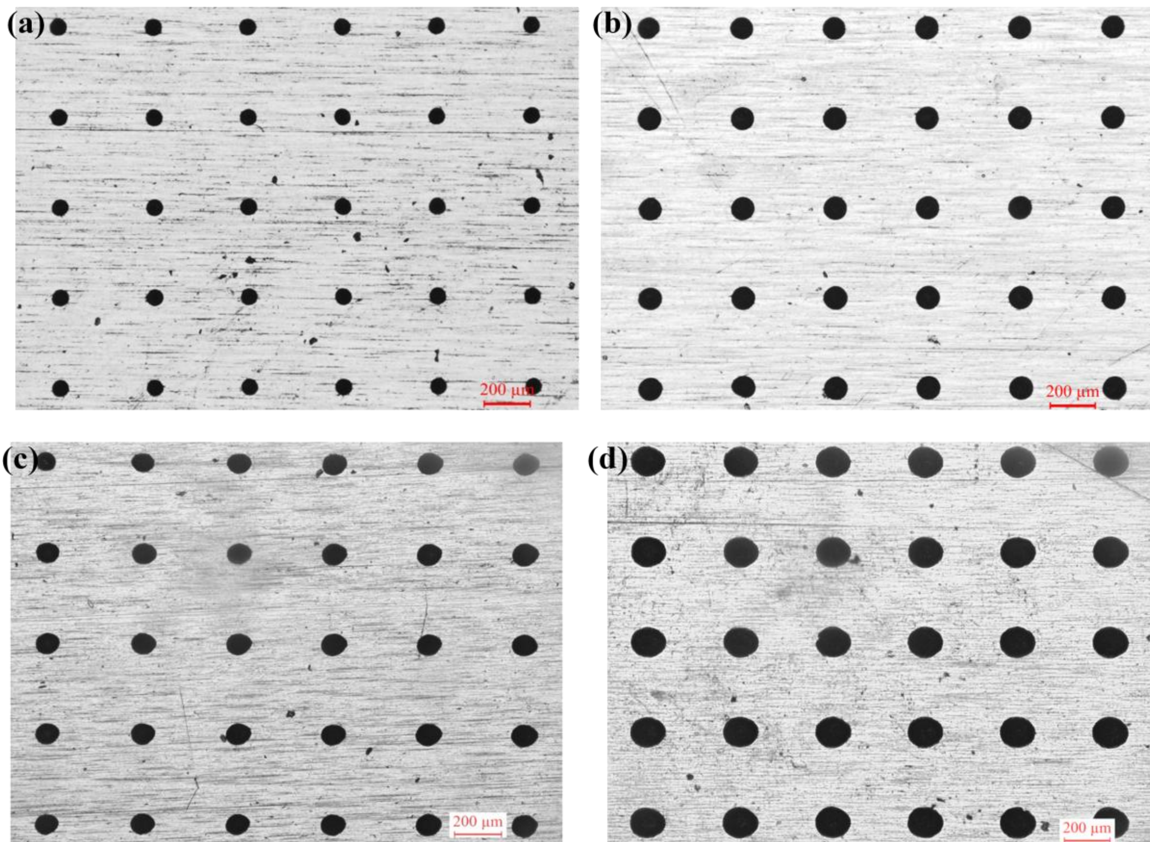

Figure 4.6: Microscopic images of micro patterned dimple array generated at different flow velocities, (a) 1.9 m/s (b) 3.8 m/s (c) 5.7 m/s (d) 7.6 m/s

Figure 4.6 depicts the microscopic images generated with varied flow velocities of electrolyte of 1.9 m/s V to 7.6 m/s, pulse frequency of 2 kHz, mixed electrolyte concentration of 10%NaCl and 10%$NaNO_3$ and 30% duty ratio. From the figure, it can be clearly seen that average size of the dimples present in the array increases as the flow velocity rises. Increased level of availability of fresh electrolyte in dynamic condition enhances the material removal in the generated surface of the dimple leading to increase in the diameter as well as depth of the dimples. But, it could be noticed from figs. 4.6 (c) and (d), that the shape of the micro-

dimples resembles ellipsoid structure which is in increased level at flow velocity, i.e. 7.6 m/s as compared to that of 5.7 m/s.

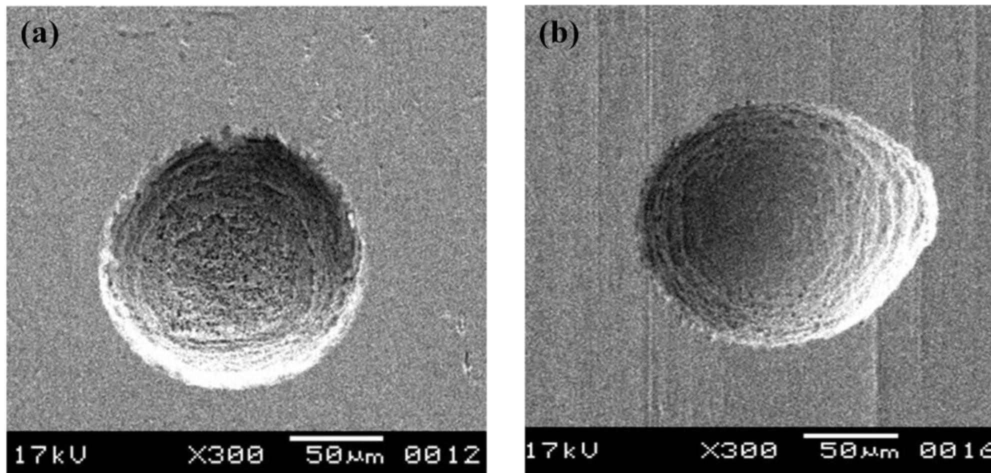

Figure 4.7: SEM micrographs of a single dimple machined at flow velocity (a) 3.8m/s (b) 7.6 m/s

It is quite evident from fig. 4.7 (b) that the material removal at high electrolyte flow velocity generates impression of the direction of electrolyte flow, leading to distortion in the dimensions of the generated micro dimples. Till 3.8 m/s, the dimples are circular in nature as depicted in fig. 4.7 (a), which establishes that 3.8 m/s is the most favorable value of flow velocity to be used for generation of island free micro-dimples possessing dimensional uniformity as well as machining accuracy.

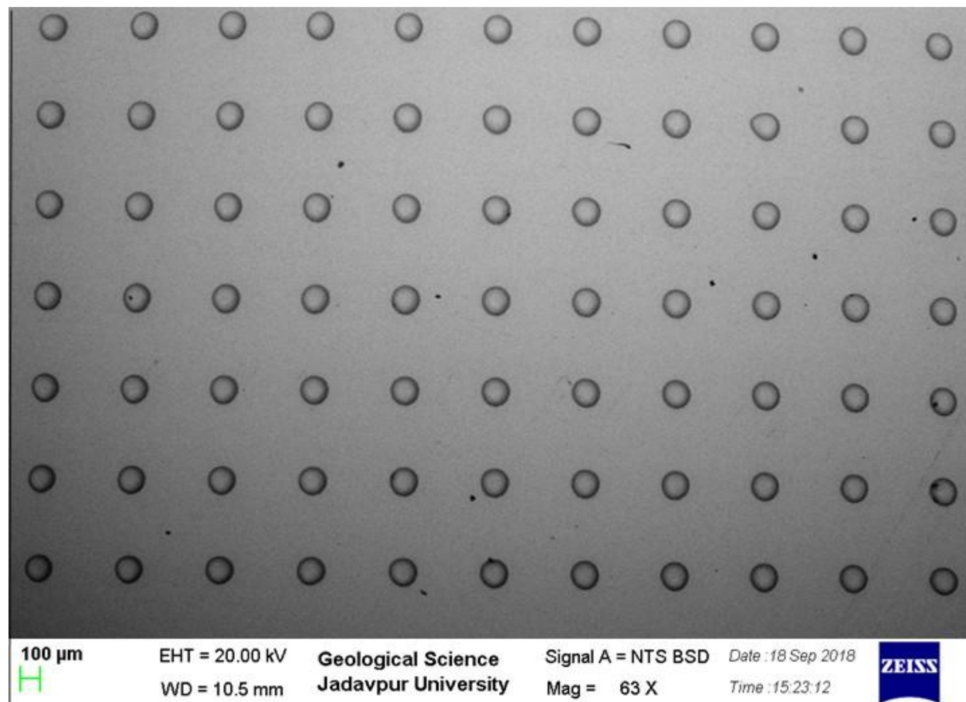

Figure 4.8: SEM micrograph of an array of dimples machined at 3.8m/s flow velocity

Figure 4.8 depicts the SEM micrograph of an array of dimples machined at an electrolyte flow velocity of 3.8 m/s. It could be noticed that dimensions of the circular micro-dimples are not disturbed and uniformity is maintained in the dimple geometrical characteristics when the samples are machined at this flow velocity. The SEM micrograph of the textured array shown in fig. 4.8 consists of the micro-dimples shown in fig. 4.7 (a).

4.6.2 Influence of pulse frequency

For investigating the influence of pulse frequency over dimple diameter and depth, masked SS304 substrates have been machined for 120 seconds with pulse frequency in the range of 1 kHz to 5 kHz, applied voltage of 12 V, 30% duty ratio, and electrolyte concentration of 10%NaCl and 10%$NaNO_3$.

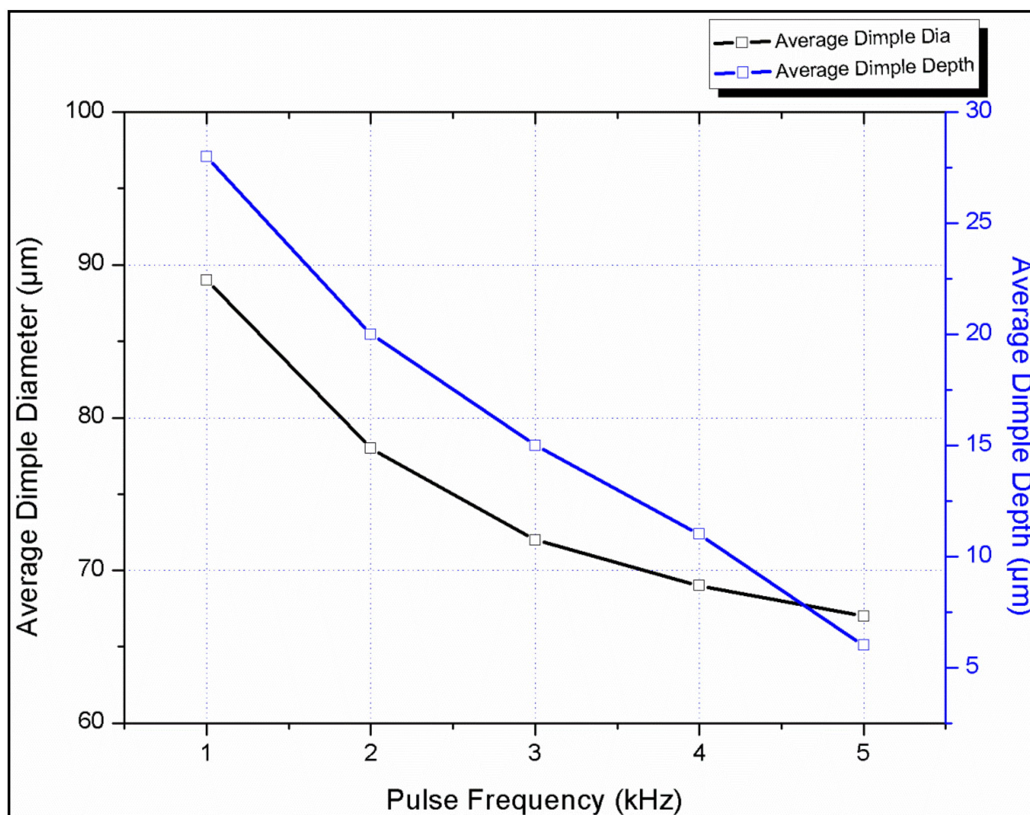

Figure 4.9: Variation of average dimple diameter and depth with pulse frequency

Figure 4.9 illustrates the variation in diameter and depth of the generated micro-dimple with respect to the applied frequency during TMEMM. It shows that both the diameter and depth of the generated dimples decrease with increase in applied frequency. Pulse period is the sum of pulse 'on' time and pulse 'off' time. For a fixed duty ratio, as applied frequency increases pulse period decreases with shorter machining on time and improves dissolution accuracy by localizing material dissolution. Hence, anodic dissolution in the dimple trench decreases which in turn decreases both the assessed geometrical characteristics of the micro-dimples.

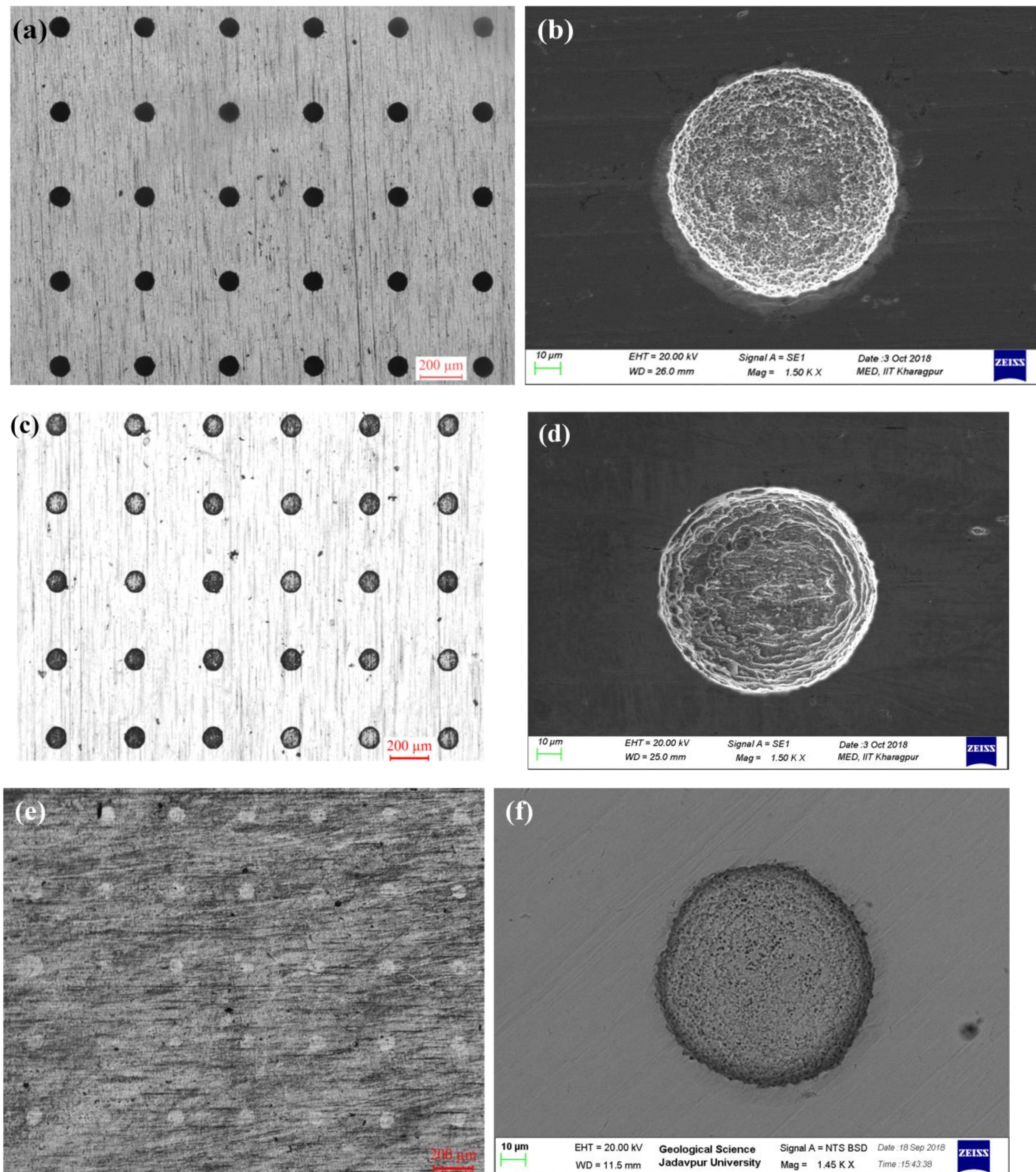

Figure 4.10: Microscopic images of micro-dimple patterned array and respective SEM image of a single dimple at different pulse frequency (a), (b) 1 kHz (c), (d) 3 kHz (e), (f) 5 kHz

Figure 4.10 shows the microscopic as well as the SEM micrographs of the SS304 samples after machining with pulse frequencies of 1 kHz, 3 kHz and 5 kHz, applied voltage of 12 V, 30% duty ratio, and a mixed electrolyte combination of 10%NaCl and 10%$NaNO_3$. It could be observed from figs. 4.10 (a) and (b), that sound dimple surface free from islands could be achieved when machining was carried out with frequency of 1 kHz & 2 kHz. However, machining with 2 kHz shows comparatively less electrochemical dissolution than texturing

with 1kHz. While machining with lower frequency i.e. longer pulse on time it increases the machining current which in turn increases current density and leads to the increased material removal from the dimple surface. When the frequency is increased at regular intervals after 1 kHz, the machining rate decreases due to decrease in the machining current, which hinders the material removal and this nature of machining can be noticed from figs. 4.10 (c) to (f). Therefore, to obtain island free micro-dimple array with good surface quality, machining with lower pulse frequency is desired.

It could be noticed from figs. 4.10 (e) and (f) that, least material removal could be observed when TMEMM was carried out at 5 kHz. It could be revealed from the figure representing single dimple that an imprint of the mask only representing the boundaries could be noticed in the generated micro-dimples. Due to the increment in the machining frequency, the pulse on time decreases gradually resulting in reduction in the material removal. This outcome is confirmed from figs. 4.10 (e) and (f) that practically no material removal takes place when TMEMM is carried out at higher frequencies. So, it is worthy to utilize lower range of pulse frequencies during machining of micro-textured patterns in TMEMM.

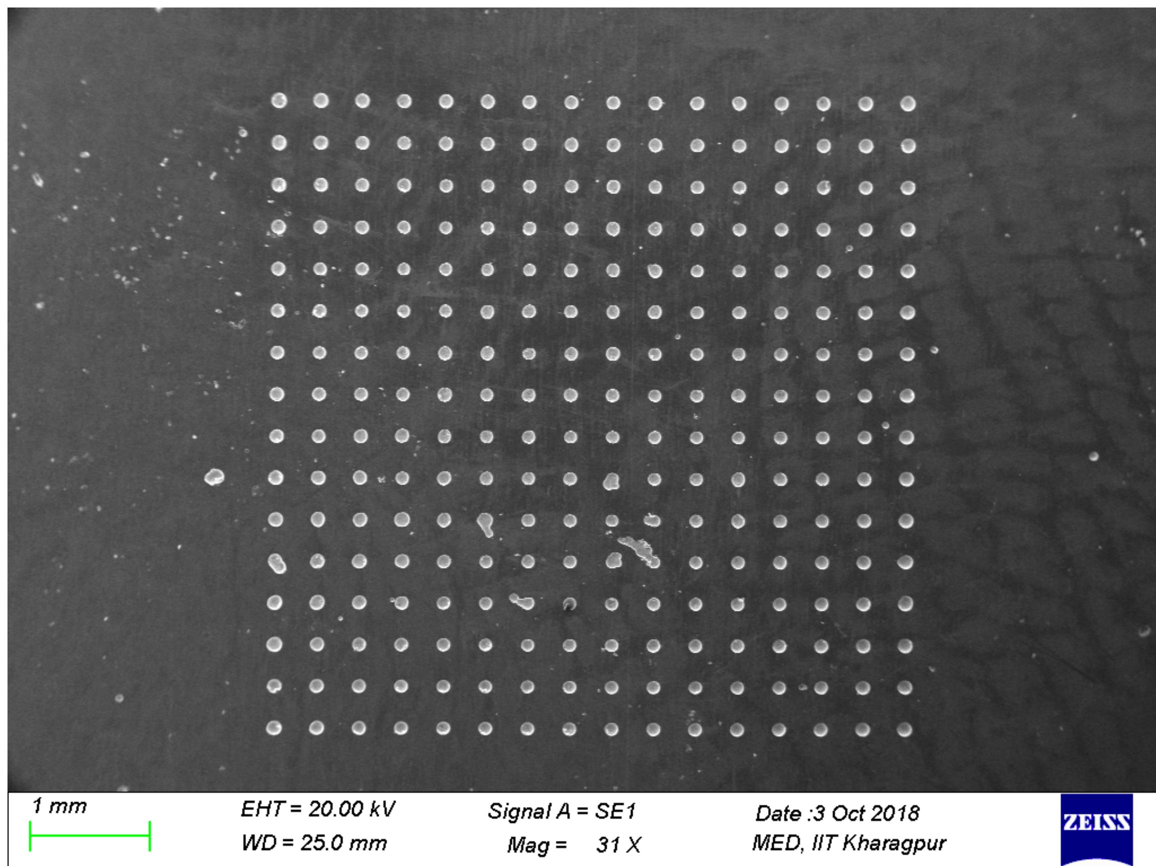

Figure 4.11: SEM micrograph of an array of dimples machined at pulse frequency 1 kHz

Figure 4.11 exhibits a complete array of circular micro-dimples generated at a pulse frequency of 1 kHz. It could be noticed that considerable and controlled machining has taken place in the generated micro dimples machined at lower range of frequencies making it applicable in various engineering applications.

4.6.3 Influence of applied voltage

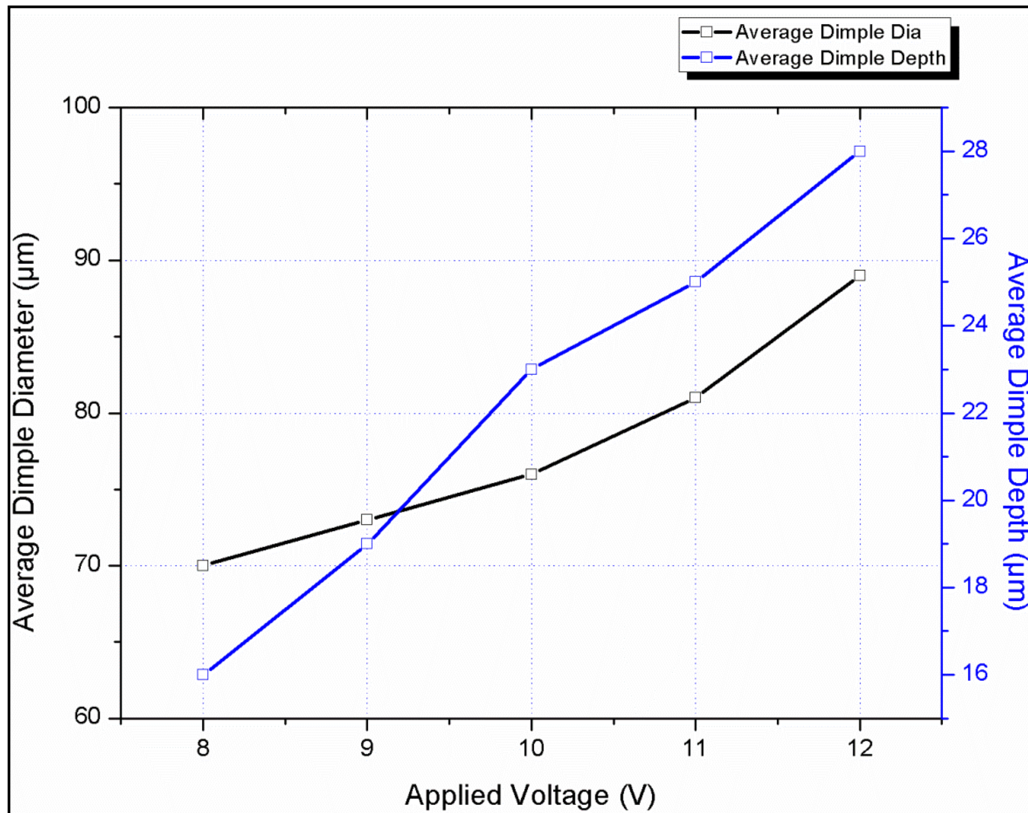

Figure 4.12: Variation of avg. dimple diameter and depth with applied voltage

Figure 4.12 plots the variations in average diameter and depth of the generated micro-dimples with the applied voltage in the range of 8 V to 12 V, pulse frequency of 1 kHz, 30% duty ratio, 3.8 m/s electrolyte flow velocity for 2 minutes of machining time. From the figure it is revealed that average dimple diameter as well as the dimple depth increases with increase in applied voltage. Increase in current density with increase in applied voltage commences faster material dissolution and results in the rise of removal of materials from the dimple crater resulting in the increase in the dimple diameter as well as depth. From the SEM micrographs shown in fig. 4.13, it is also observed that when the machining voltage reaches 10V, the islands disappeared from the dimple surface; establishing that10 V is the threshold value of the texturing during TMEMM. This may be because of increased number of bubbles and more sludge generated at inter-electrode gap at higher applied voltage, which affects the material dissolution process. So, when dimples have been machined with or above 10 V, the

dimple diameter along with depth, increases more rapidly leading to a sound dimple surface. However, the diameter should be kept within an approximation such that the measured undercut does not tip off a reasonable value leading to larger micro-dimple diameter and depth than expected.

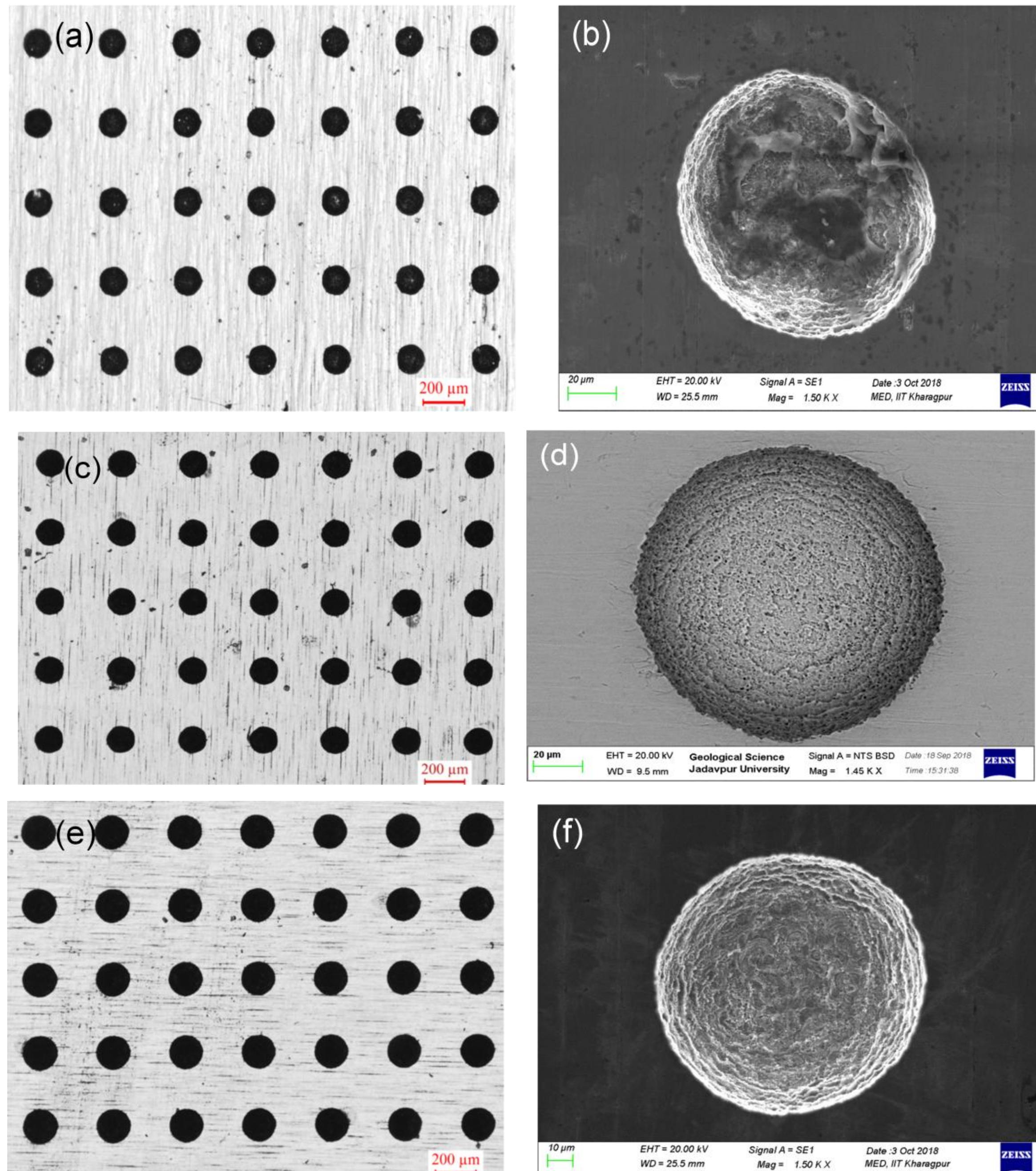

Figure 4.13: Microscopic images of micro-dimple patterned array and SEM micrograph of a single dimple at different applied voltage (a), (b) 8 V (c), (d) 10 V (e), (f) 12 V

Figure 4.13 depicts the microscopic images along with SEM images of single dimples generated with varied applied voltages of 8 V, 10 V and 12 V respectively, pulse frequency of 1 kHz, electrolyte concentration of 10% NaCl and 10% $NaNO_3$, electrolyte flow velocity of

3.8m/s and 30% duty ratio. From the figure, it can be clearly seen that average size of the dimples present in the array increases as voltage rises from 8 V to 12 V. Increased current density because of increased applied voltage leads faster material dissolution from the dimple surface. Hence, the average diameter and depth of the generated micro-dimple array increases as seen in fig. 4.12. However, it is clear from the figure that the dimples generated at applied voltage 8 V and 9 V contain islands (both in the form of residual material and material precipitate) because of the non dissolution of the material along the dimple surface. Also increased number of bubbles generated at cathode surface hinders the dissolution process causing non-uniform material removal resulting in poor surface quality. Hence, for achieving sound dimple surface with best surface quality, machining with a minimum voltage of 10 V is desired. However, selection of higher range of voltages shall affect the machining accuracy and lead to enhancement in the diameter and depth of the generated dimples by a large extent as depicted in figs. 4.13 (e) and (f). It could be revealed from fig. 4.13 (d) that micro-patterns textured with 10V possess better surface as compared to fig. 4.13 (b) and fig. 4.13 (f). As such, the applied voltage responsible for the generation of the dimple array as shown in fig. 4.13 (c) and single dimple as shown in 4.13 (d) i.e. 10 V is the most favorable applied voltage to generate precise micro textured surfaces with TMEMM.

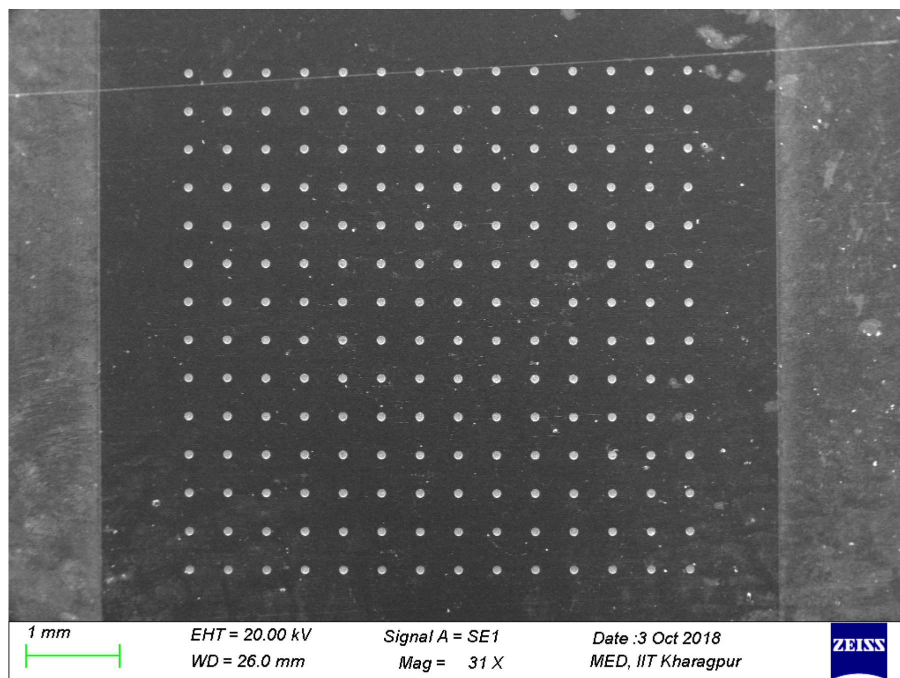

Figure 4.14: SEM micrograph of an array of dimples machined at applied voltage 10V

Figure 4.14 pictorially represents an array of micro-dimples machined with 10 V applied voltage. Dimensions of the generated micro-dimples are already been discussed in the graph

at fig. 4.12. The dimensions of the generated micro-dimples are purely application specific and finds ample utility in tribological applications.

4.6.4 Influence of duty ratio and machining time on dimple characteristics

Experiments have been conducted in the developed TMEMM set-up to analyze the effects of duty ratio and machining time during micro-dimple array fabrication. In order to attain a considerable island-free depth along with dimensional homogeneity in the generated micro-dimples, machining time is varied between 90 seconds and 120 seconds along with four levels of duty ratio (%) i.e. 20, 30, 40 and 50% respectively. Other process parameters i.e. applied voltage- 10 V, pulse frequency- 1 kHz, electrolyte flow velocity-3.8 m/s were finalized from experimental investigations of earlier sections in this chapter. Various dimple parameters such as undercut, depth and surface roughness characteristics (R_a and R_q) have been measured after the experiments. Moreover, the etch factor have been calculated to analyze the effects of duty ratio and machining time on the dimensional uniformity and isotropicity of the generated micro-dimples.

(i) Effect on Undercut

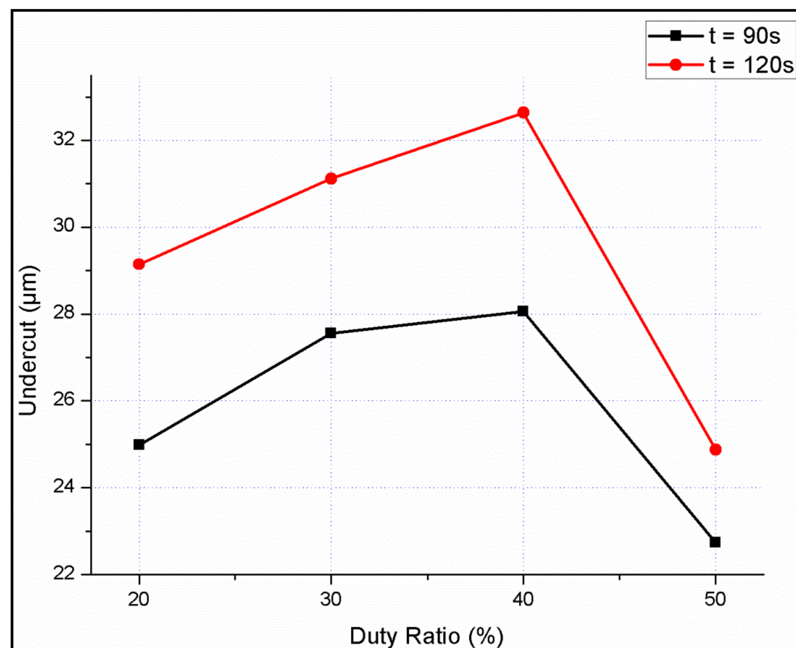

Figure 4.15: Effect of duty ratio on undercut

From fig. 4.15, it can be observed that with the increase in duty ratio, undercut increases gradually up to a certain value, and then decreases. With increase in duty ratio, current density increases and results in more material removal and causes increase in the undercut. When duty ratio exceeds 40 %, due to decrease in the pulse-off time, the oxygen bubbles

generated on the anode surface due to dissolution, gets entrapped under the mask. The slowing down of escape of oxygen bubbles results in increase in the inter-electrode resistance. As a result of which, the current decreases rapidly resulting major reduction in the undercut. Moreover, as the machining time (t) increases, the exposure time of the bare material (in between the mask opening) increases resulting in the rise in undercut.

(ii) Influence on dimple depth and etch factor

Previous researchers in this field of study has already established that, when a thin mask possessing micro-pattern is employed during TMEMM, due to significant influence of electric field, the intensity of electrical field at the edges of the mask is much larger than at the feature center, leading to higher current at the edge. As a result, non-uniform material removal is observed in the generated micro dimples. This in turn, had proved to be influential during the formation of islands in the dimple center.

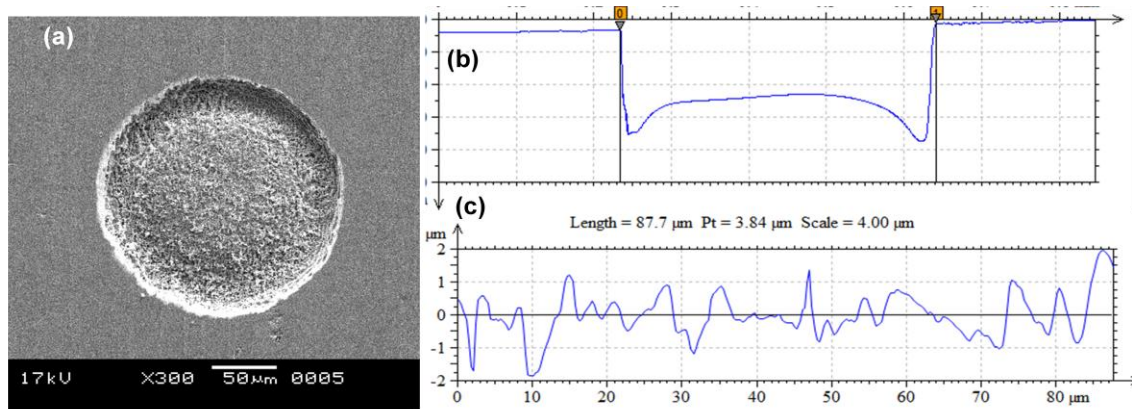

Figure 4.16: Micro-dimple prepared by TMEMM at less than 90s (a) SEM micrograph showing island at the centre of dimple (b) Surface profile of the formed dimple and (c) Surface characteristics of the generated micro-dimple

This phenomenon has been strongly observed in the initial phase of experimentation when the machining time is less than 90 s as shown in fig. 4.16 (a). Even few parametric combinations for 90 s machining time have also resulted in non removal of materials from the centre of the dimples. Figure 4.16 (b) shows the cross sectional view of surface profile of a generated micro-dimple in which a lump of material could be noticed at the centre of dimple. This is termed as “Island formation” in which more material gets removed from the edges as compared to the centre. It is considered as a negative aspect of a micro-dimple as it not only hampers the surface properties but also flattened the geometry of the fabricated micro-dimple. This aspect could well be observed from fig. 4.16 (c) which shows the irregularity in the surface roughness curve of the micro-dimple possessing island at the centre.

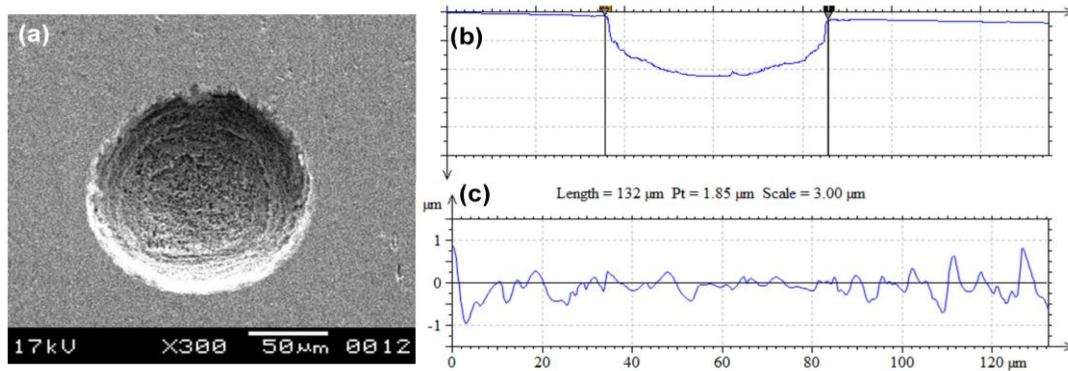

Figure 4.17: Micro-dimple prepared by TMEMM at most favorable parametric conditions (a) SEM micrograph showing micro-dimple (b) Surface profile of the formed dimple and (c) Surface characteristics of the generated micro-dimple

Keeping in mind the accuracy as well as material removal during machining, an electrolytic combination of 10%NaCl + 10%$NaNO_3$ have been considered during final experimentation. Moreover, the machining time is increased in steps and it is noticed that the island disappeared from the center of the dimple at 120 s as revealed in the SEM micrograph shown in fig. 4.17 (a). This is also confirmed from the cross sectional view of the surface profile that shows perfect pattern of micro-dimple with hemispherical bottom surface as presented in fig. 4.17 (b). As revealed in fig. 4.17 (c), the surface characteristics of the fabricated micro-dimple also verify the evenness of the surface of the micro-dimple as compared to fig. 4.16 (c). Hence mixed electrolytic consisting of 10%NaCl and 10%$NaNO_3$ along with prolonged machining time proved to be influencing parameters for achieving good quality micro-dimple patterns free from islands.

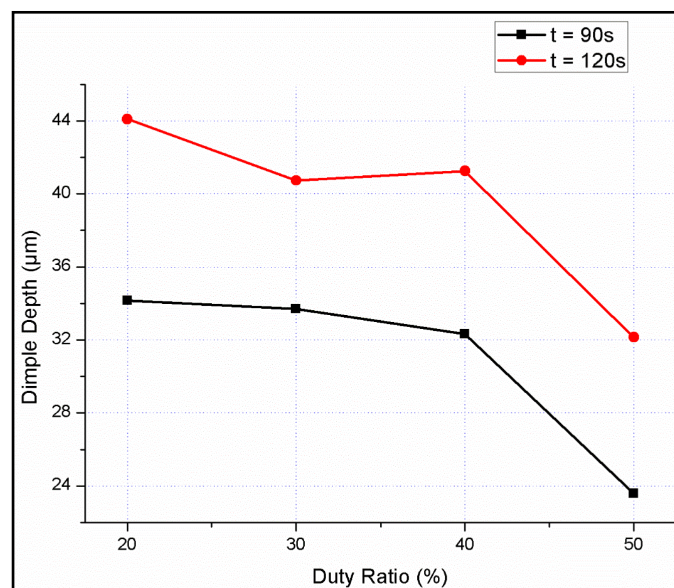

Figure 4.18: Effect of duty ratio on dimple depth

Figure 4.18 shows the depth variation in micro dimples at different duty ratios with changing machining times. It could be observed that as the duty ratio changes from 20% to 50%, the depth of the micro-dimples gradually decreases. At lower duty ratio, as pulse-off time is higher, the removed material gets sufficient time to leave the machined surface. As a result, the dimple depth is on the higher side. As duty ratio increases, the pulse-off time proportionately decreases causing hindrance in electrolyte exchange mechanism. This leads to reduction in depth of the micro-dimples at increased duty ratios. The dimple depths achieved while machining for 90 s is comparatively lower than that of the depths attained when the machining time was 120 s.

Machining localization is an influencing factor for micro-dimple formation and can be defined by etch factor. It is the sole way to determine the anisotropy of the TMEMM process. An etch factor of 1.0 indicates ideal isotropic material removal. A large etch factor implies small undercut and a controlled material removal could be observed beneath the mask opening, whereas a smaller etch factor implies large undercut where lateral material removal under the mask is much more.

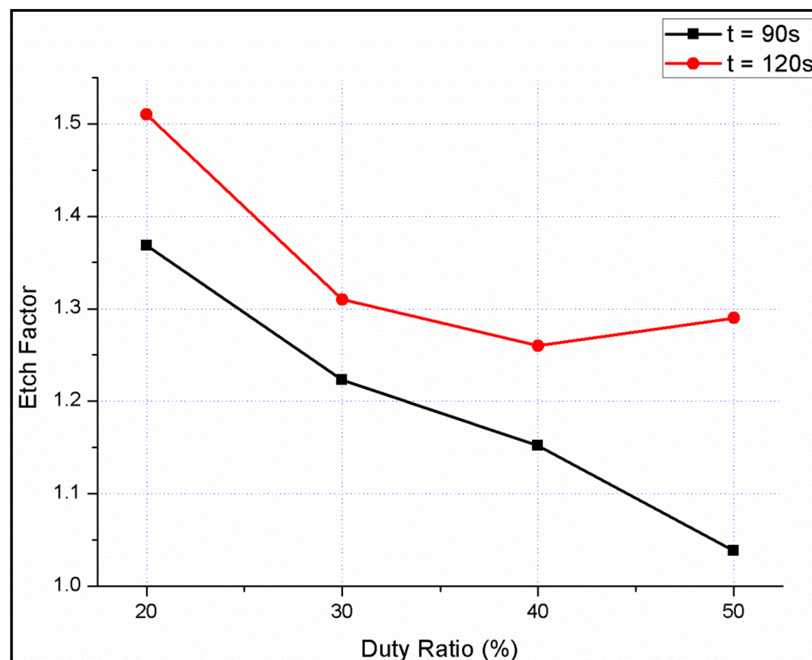

Figure 4.19: Effect of Duty Ratio on etch factor

Figure 4.19 plots the etch factors at different duty ratios. It could be noticed that etch factor reduces with increase in duty ratio. This aspect could be explained by the fact that as the pulse-on time increases, the stray current density also increases resulting in the increase in undercut, which decreases etch factor. When TMEMM was carried out at 90 s machining time, etch factor gradually decreases from 1.37 to 1.03. Whereas, in case of 120 s machining

time, etch factor have been found to be lowest at 40% duty ratio and after that there is a slight increment of 0.028 when the duty ratio was increased to 50%.

(iii) Influence of duty ratio and machining time on surface roughness characteristics (R_a and R_q)

After completion of the TMEMM experiments, the machined surfaces were held under the CCI Non-Contact Profilometer (Taylor Hobson) to investigate about two significant surface roughness characteristics (R_a and R_q) inside the periphery of the generated dimples. The non-contact profilometer with the help of high frequency light and precise lenses permits the measurement of the generated dimple surface consisting of the dimple boundaries alongwith the bottom surface.

Measurement of the roughness parameter of the implant surface morphology is important because its value influences the adhesion, adsorption and other significant surface properties of the material. During analysis in the CCI non contact profilometer, R_a, i.e. arithmetic average height value of the deviation of surface profile in relation to mean line and R_q, i.e. root means square roughness is the square root of the sum of the squares of the individual heights and depths from the mean line.

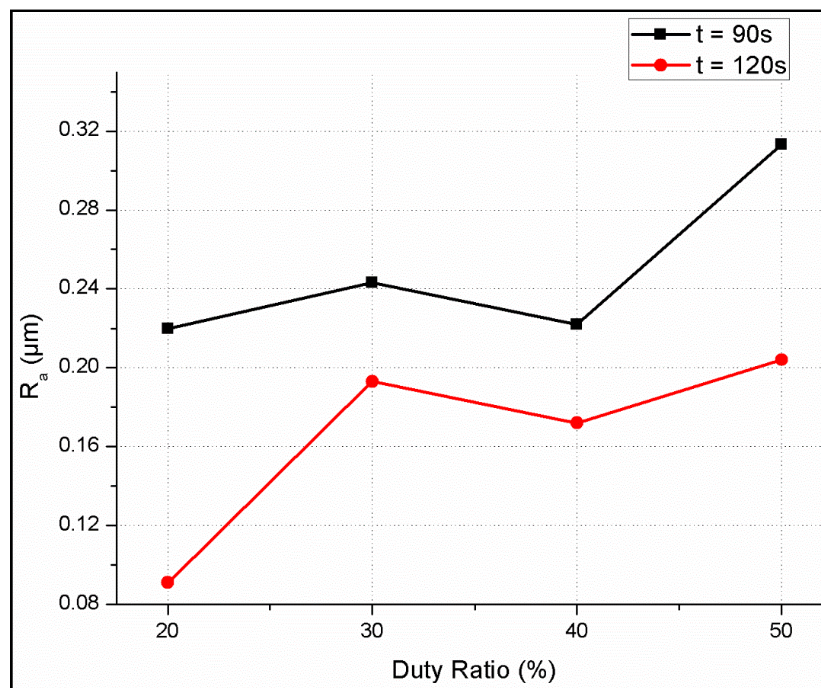

Figure 4.20: Effect of Duty Ratio on R_a

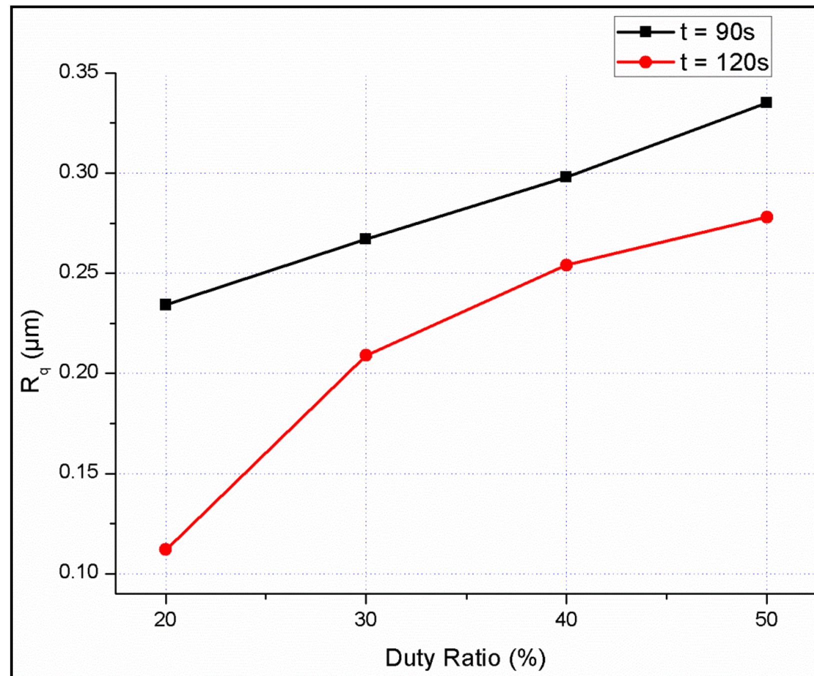

Figure 4.21: Impact of Duty Ratio on R_q

Figure 4.20 and fig. 4.21 explains about the nature of the machined surface at different duty ratios considering variations in R_a and R_q respectively. As duty ratio increases, both R_a and R_q showed an increasing trend. This is because the current efficiency and the total amount of electricity do not change when the same applied voltage and effective machining time are applied, and therefore the volume of material removed remains the same. However, the relaxation time to zero current is longer at a low duty cycle and the reaction products are removed more thoroughly by the flow of electrolyte.

As the duty ratio increases, the time of removal of the reaction products decreases gradually and hence, the surface integrity of the dimples machined at lower duty ratios are much finer than that machined at higher duty ratios. Therefore, a low pulse duty cycle is more suitable for generating micro-dimples with a better three-dimensional topography.

4.6 Fabrication of island-free micro dimple array based on experimental analysis

Based on the experiments conducted along with the thorough investigation of the results, it is obvious that fabrication of island-free micro-dimple array is feasible with this methodology of TMEMM. Figure 4.22 shows the SEM micrograph of the developed island free micro-dimple array fabricated under particular parametric combination i.e. machining voltage 10V, frequency 1 kHz, duty ratio 20%, electrolyte concentration 10% NaCl + 10% $NaNO_3$, electrolyte flow velocity 3.8 m/s and machining time 120 s.

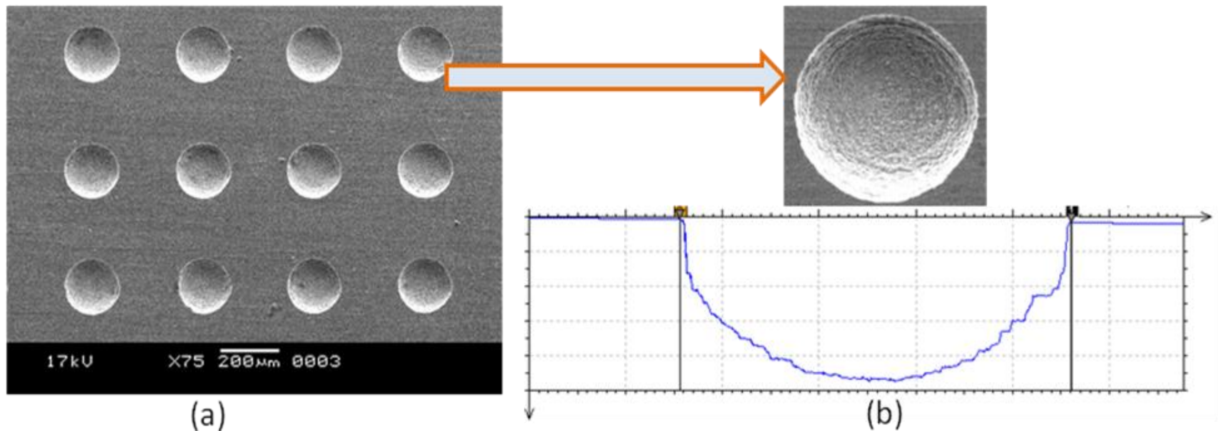

Figure 4.22: Island Free Micro-dimple (a) SEM Micrograph showing a 4x3 matrix along with a single dimple (b) dimple profile

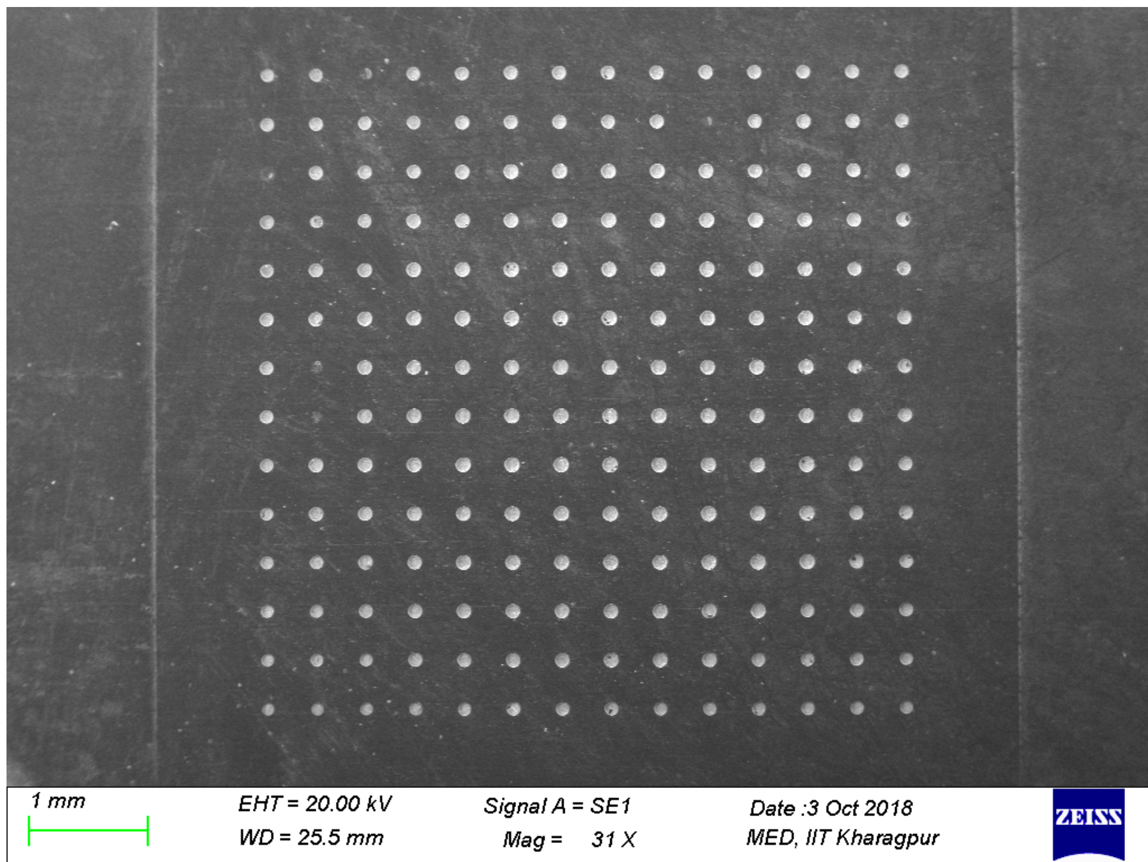

Figure 4.23: SEM micrograph of micro-dimple array machined at most favorable parametric combination

Figure 4.23 shows a complete matrix (17x17) of the generated patterned micro textures consisting of dimples. The workpiece sample is machined at the favorable combination of parameters as mentioned above which is obtained through detailed experimental analysis of each and every TMEMM parameters.

4.7 Outcomes of the experimentation

Micro-dimple arrays without island formation are generated over the sample covered with a mask with patterned micro holes of 65 µm diameter. It was experimentally established that formation of islands could be avoided even after using a thin mask of 16 µm thickness and well controlled shapes with smooth surface geometry can be achieved by prolonging the machining time to 120 s. A patterned mask of a noble mask material, a negative PR (AZ 4903), of very low thickness (16 µm) possessing strong adhesiveness with the substrate has been utilized during the experimentation. The developed TMEMM set-up with vertical cross flow electrolyte system generates micro-dimple array within a short period of time with improved dimensional uniformity. The controllable process parameters have been studied for searching out the suitable values for generation of island-free micro-textured pattern in the form of circular dimples. With the increase in duty ratio, while the value of undercut and the surface roughness rises, the depth of the micro dimples and the etch factor decreases. Formation of islands in the centre of the dimples could be restricted by enhancing the machining time and applying the mixture of NaCl and $NaNO_3$ as electrolyte. Moreover, utilization of thick masks for elimination of the island inside the dimples could be avoided by employing very thin masks resulting cost-effectiveness. Micro-dimple arrays measuring 97 µm diameter and 43.1 µm depth were successfully prepared with an applied voltage of 10 V, frequency 1 kHz, duty ratio 20% and a machining time 120 s.

Above discussion confirms about the most favorable value of TMEMM process parameters such as applied voltage, pulse frequency, electrolyte flow velocity, duty ratio and machining time to be considered during the generation of circular micro-dimple array free from islands. However, to fabricate micro-features with utmost accuracy as well as precision in TMEMM, thickness of the mask and its material is one of the parameter on which the final texture of the micro-structure lies. Since, a considerable amount of revenue is involved in the fabrication of the masked specimen mainly due to the expense incurred during procurement of the material to be used for mask, it is very much significant to search out for various alternatives to curtail the cost involvement in the material of mask such that this process of TMEMM can be economically more feasible for several industrial applications. Further, precise as well as accurate micro-features with various geometrical contours are also in great need to the modern manufacturing industry, which needs to be fabricated to enhance the applicability of TMEMM in engineering fields.

Chapter 5

GENERATION OF CIRCULAR AND SQUARE MICRO TEXTURED ARRAY BY TMEMM UTILIZING LOW ASPECT RATIO MASK

5.1 Introduction

Recent innovations in the area of micro fabrication have created a unique opportunity for manufacturing structures in the nm–µm range. Surface Texturing at the micron range e.g. micro-dimples, micro-grooves, micro-pillars and micro-prisms, etc. can be defined as a method for generation of specified texture e.g. dimple, square, grooved etc. on a surface. Patterned microstructures are among the basic micro features that are indispensable in improving the tribological performance and dependability of various mechanical components especially Micro-Electro-Mechanical Systems (MEMS). Micro-dimples have been extensively used in various industries for enhancement in the performance and usability of mechanical systems, such as improving biological, optical, tribological as well as thermal properties. The high aspect ratio of photoresist is responsible for non-uniform electric field distribution occurring over a workpiece, which finally leads to non-uniform removal of reaction products in TMEMM. So, understanding the need to investigate TMEMM process utilizing thin masks, experiments have been conducted utilizing a novel photoresist AZ 4903 and array of circular micro-dimples free from islands were fabricated with considerable repeatability and summarized in the previous chapter.

This chapter is a comprehensive study of TMEMM parameters by utilizing patterned masks of AZ-4903 of thickness range of 12 µm, 16 µm and 20 µm, possessing strong adhesiveness with the Stainless steel substrate. Experiments have been carried out to examine the effect of the employing thin masks on the geometrical profile of different patterned micro-dimples i.e. circular and square over different machining times. The effect of two vital process parameters e.g. duty ratio and machining time on dimple characteristics including undercut (U_c), dimple depth (d_d), etch factor (f_e) and specifically on two significant surface roughness characteristics (R_a and R_q) have been investigated during generation of array of micro circular as well as micro squared textured patterns. Further, friction analysis showing the alterations in the frictional co-efficient with increasing normal load at different dimple depths has been reflected in this chapter along with a comparison of the variation in the co-efficient of friction of the generated circular and the square micro-dimples with different depths.

5.2 Importance of mask thickness in TMEMM

In TMEMM, workpiece is covered by an electrically insulating patterned photoresist mainly, referred to as mask, involving the production of microsized feature arrays such as micro-dimples and micro-holes. In a standard TMEMM process, a nonconductive mask with a variety of perforated micro-patterns is formed on the workpiece to define the features to be reproduced. Micro-dimples are found to be a solution for reducing the coefficient of friction in mating surfaces. Mask dimensions, especially, its thickness and diameter plays a significant role in determining the size and shape of the final patterned textures. Moreover, it was experimentally studied by previous researchers that employing a mask of thickness ~ 250 μm could lead to the removal of islands present in the generated surface of the dimple. Since, the nature of current density distribution on the workpiece was non-uniform; the removal rate at the edges was faster than that at the center. So, masks of higher thicknesses were used up for disappearance of islands from the dimple surface. As such, it is extremely essential to study the impact of utilizing masks of lean thicknesses in TMEMM during fabrication of circular as well as square micro-dimples. Considering the necessity in curtailing the cost involved in the production of mask during TMEMM, a low cost negative PR (AZ-4903) have been selected and substrates are being coated with very lean thickness of the mask to understand the effects of mask thickness and machining time on various dimple characteristics.

5.3 Experimental planning for generation of patterned array of different geometries

In order to perform experiments as per detailed research planning, and considering the effects of various controllable parameters, a well planned research program has been taken up for experimentation in the developed set-up for executing through mask electrochemical micromachining which have already been discussed in Sec.3.2 of chapter 3. Stainless Steel 304 sheets of 200 μm thickness coated with AZ4903 possessing micro-scale pattern have been utilized for experimentation. Each sample consists of micro-dimple arrays of dimension 65 μm. A cylindrical copper tool of 12 mm diameter is utilized as the tool (cathode) during the experimentation.

Based on the past research findings, two significant parameters i.e. duty ratio and machining time have been considered as the influencing factors in this experimental set for TMEMM. Values of other TMEMM process parameters have been determined based on available research reports, mostly focused on the anodic dissolution of Stainless Steel. From the results obtained from experimental analysis of the previous chapter, the range of duty ratio is chosen

from 20-50%. Moreover, it has already been experimentally verified in the previous chapter that significant machining can be observed when the machining time reaches 90s. As such, two different machining times (t_m) i.e. 90 s and 120 s have been considered for the experiments to investigate its influence upon the machining performance and surface characteristics of the generated micro-textured patterns. The frequency of 2 kHz in the form of square pulses and electrolyte concentration of 10% NaCl + 10% $NaNO_3$ were fixed. Other parameters including the electrolyte flow velocity was also kept at optimized value as per experimental outcomes of chapter 4 i.e. 3.8 m/s, the back pressure was fixed at 0.04 Kg/cm^2. During the experimentation, three different SS304 substrates i.e. possessing thin masks of 12 μm, 16 μm and 20 μm thickness respectively and containing patterned micro holes and squares were employed during experimentation. Selected process parameters such as applied voltage, pulse frequency, electrolyte concentration, duty ratio, etc. have been represented in Table 5.1. Initially, Optical microscope (Leica DM2500, Germany) is used to measure the micro-dimple arrays. Talysurf CCI Non-Contact Profilometer (Taylor Hobson) is effectively utilized to measure the machined surface characteristics and analyze the profiles of the generated micro-structures. Scanning electron microscope (Zeiss EVO 40) was utilized to examine the fabricated micro-textured arrays.

To verify the effect of micro-dimples array on the sample surface, friction tests were performed in a multi tribotester apparatus (TR-25, DUCOM). During the test, samples were held stationary with the help of the attachment and made to slide against the rotating counter face roller. The speed of the roller and the duration of tests can be controlled via a computer attached to the tribotester. Load was applied by placing dead weights on the loading pan which was attached to a loading lever. During testing, the load was gradually increased to understand its impact on the co-efficient of friction. The loading lever is pivoted near the normal load sensor which helps in the measurement of effective normal load applied on the specimen. Each sample was driven by a motor to a rotational speed of 300 rpm for 300 s. Friction tests were carried out with normal load of 25 N, 50 N and 75 N respectively. The tests were conducted in both dry as well as wet conditions. During wet condition, the sliding contact zone was fully soaked in lubricating oil (Density – 0.898 g/ml, Kinematic Viscosity – 14 m^2/s, Dynamic Viscosity – 133 kg/m/s, Pour Point – -27°C, Flash Point – 193°C, Viscosity Index – 97)

Table 5.1: Experimental conditions during machining

Average diameter of micro-holes on the mask	65 µm
Workpiece Material	SS304
Thickness of workpiece	200 µm
Mask Material	AZ 4903
Thickness of patterned mask	12 µm, 16 µm, 20 µm
Machining Voltage	12 V
Duty Ratio	20%, 30%, 40%, 50%
Machining Frequency	2 kHz
Inter Electrode Gap	2000 µm
Flow Velocity	3.8 m/s
Electrolyte Concentration	10% NaCl + 10% $NaNO_3$
Machining Time	90 s, 120 s

5.4 Experimental methodology

The detailed procedure followed during the complete execution of the experimentation and analysis has been detailed in Section 4.5.2 in Chapter 4.

In TMEMM, the metal gets dissolved in both Z (Vertical) as well as X and Y (Lateral) directions, which results in undercutting as well as increase in micro-dimple depth. The Etch Factor (f_e) can be computed from equation 5.1, which is equal to the ratio of the etching depth of the micro-dimple to the undercut, is calculated to assess the machining localization of the micro-dimple:

$$\text{Etch factor, } f_e = d_d/U_c \quad (5.1)$$

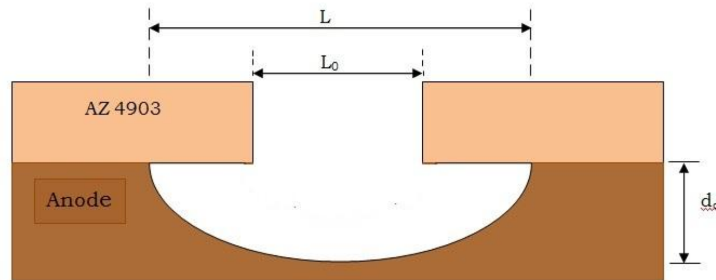

Figure 5.1: Schematic diagram showing Undercut

Where, d_d is the depth of the generated micro-dimple, U_c represents the undercut in the micro-holes of the mask as shown in fig. 5.1. Undercut, U_c can be calculated from equation 5.2 as the difference of the radius of the generated micro-dimples (L/2) to the radius of micro-holes patterned on the mask (L_0/2). A high f_e reflects high machining localization.

$$\text{Undercut, } U_c = \frac{(L - L_0)}{2} \quad (5.2)$$

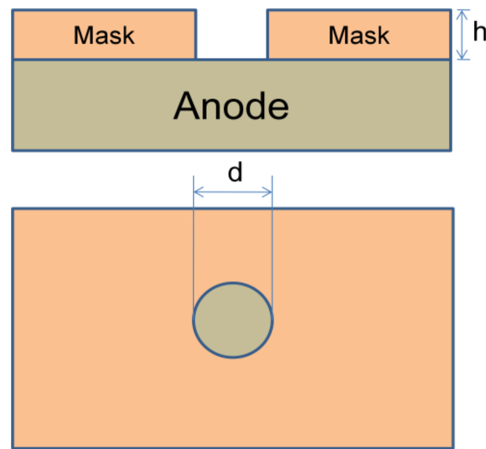

Figure 5.2: Side and Top View of the Anode and Mask prior to machining (single dimple)

The aspect ratio, AR, strongly influences the shape evolution of the micro dimples generated during TMEMM. AR can be mathematically evaluated from equation 5.3, which is the ratio of mask thickness (h) with the diameter of the dimple (d) as expressed in fig. 5.2.

$$AR = \frac{h}{d} \quad 5.3$$

It was experimentally demonstrated in previous research works that proper machining in TMEMM could be achieved only with high aspect ratio masks. As such, researchers utilized masks of relatively larger thicknesses to achieve microstructures with uniform geometry as well as topography. This novel methodology utilizes low aspect ratio masks along with a mixed electrolyte for fabrication of the micro-dimple array. Approximately 35-40 micro-dimples were measured while carrying out the analysis for each sample.

5.5. Experimental results and analysis for fabrication of micro-patterned textured array with different geometries

Experiments have been conducted in the developed TMEMM set-up to analyze the effects of duty ratio and machining time during circular as well as square micro-dimple array fabrication. In order to attain specified depth along with dimensional homogeneity in the generated micro-dimples, machining time was varied between 90 seconds and 120 seconds. In this research work, effect of utilizing three different types of masked samples along with impact of four levels of duty ratio under two machining times have been studied. Various dimple characteristics such as undercut, depth along with R_a and R_q have been measured after the experiments. In addition, the etch factor (f_e) is also calculated to observe the effects of selected machining parameters on the dimensional uniformity of the generated micro-dimples.

5.5.1 Influence of TMEMM parameters on circular micro - patterned textures

Fabrication of micro-textured array containing circular dimples have been thoroughly investigated in this chapter considering varying masks of thin ranges i.e. 12 µm, 16 µm and 20 µm to understand the effect of mask thickness. Although it was experimentally proved that island free micro-dimple array could be achieved with a prolonged machining time of 120s, but to understand the effects of the considered TMEMM machining parameters under different machining conditions during machining of squared micro-textures, the machining time of 90 s was experimentally studied in both the cases. The experimental results and discussions are detailed below:

(i) Influence of duty ratio and machining time on undercut (U_c)

Experiments were conducted to investigate the influence of duty ratio along with machining time on undercut at particular machining conditions i.e. machining voltage of 12 V, a mixed electrolyte having concentration of (10%NaCl + 10%$NaNO_3$) and 2 kHz frequency.

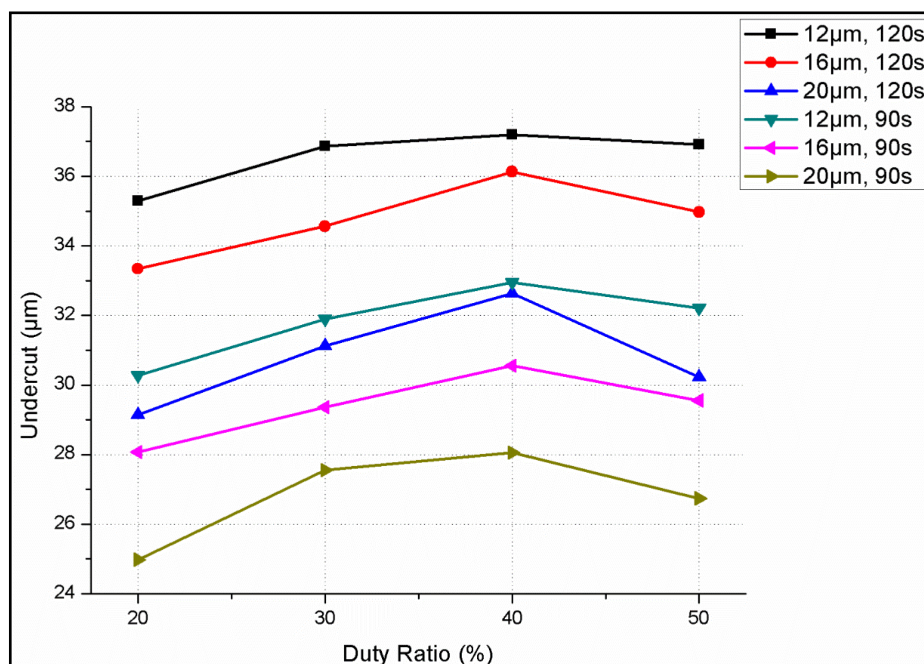

Figure 5.3: Effect of duty ratio on undercut at different machining times

From fig. 5.3, it is evident that with the increase in duty ratio, undercut gradually increases up to a certain value, and then decreases. The reason has already been detailed in chapter 4. The same nature could be observed with 12 µm and 20 µm masked specimens. It is also observed from fig. 5.3 that the U_c values at 90 s t_m is comparatively less than that for 120 s t_m. This can be explained by the fact that as the machining time increases from 90 s to 120 s, the exposure

time of the bare material in the mask opening increases resulting in the rise in undercut. Further, when machining is accomplished at 90 s t_m, lowest undercut of 24.98 µm is observed with 20 µm mask compared with 28.07 µm and 30.27 µm for 16 µm and 12 µm mask respectively. When machining time is increased to 120 s, U_c values ranges from 29.15 µm to 32.64 µm for 20 µm mask, 33.34 µm to 36.13 µm for 16 µm mask while it increases from 35.29 µm to 37.19 µm when TMEMM is done with 12 µm mask samples.

(ii) Influence of duty ratio and machining time on dimple depth (d_d)

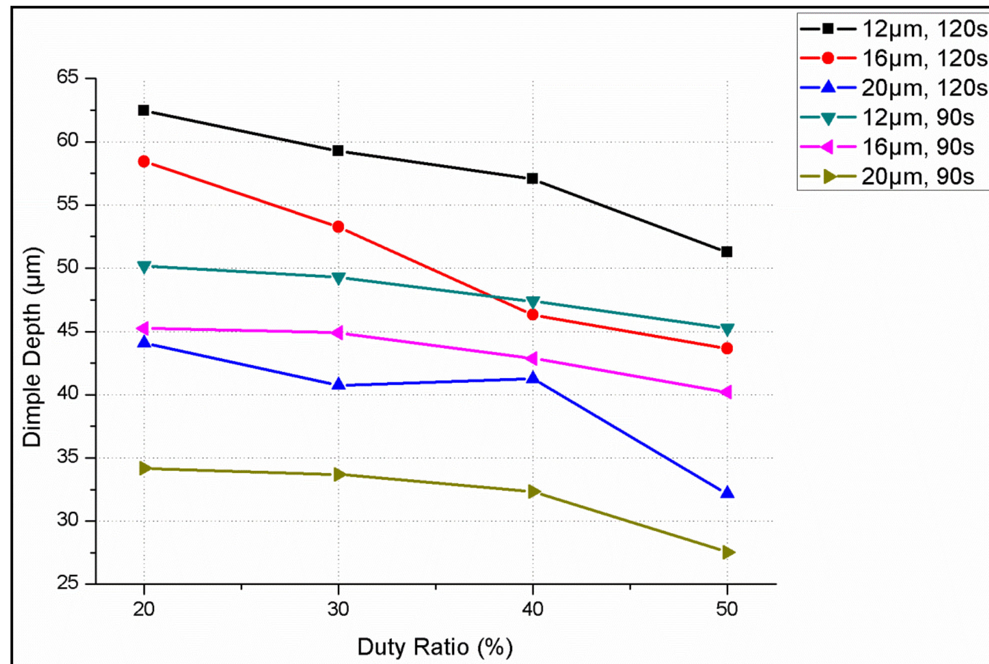

Figure 5.4: Effect of duty ratio on dimple depth at different machining times

Figure 5.4 shows the depth variation in micro dimples at different duty ratios with changing mask thicknesses at 90 s and 120 s machining time respectively. It could be observed that as the duty ratio changes from 20% to 50%, the depth of the micro-dimples gradually decreases from 20% to 40% duty ratio. At lower duty ratio, as pulse-off time is higher, the material removed during machining gets ample time to flush out from the machined surface. As a result, the dimple depth is on the higher side when TMEMM is carried out at 20% duty ratio. When duty ratio is gradually increased from 20% to 40%, the pulse-off time proportionately decreases leading to hindrance in electrolyte exchange mechanism leading to reduction in the depth of the fabricated micro-dimples. After the duty ratio crosses 40%, due to increase in pulse-on time, the pulse-off time decreases resulting in entrapment of sludge and gas bubbles within the generated micro-dimple. As a result, material removal in the ‘Z’ direction decreases, resulting in steep downfall in the dimple depth.

In TMEMM, material gets removed both from exposed areas as well as unexposed areas that are close to the exposed areas. This phenomenon is much stronger when the mask thickness is low. When TMEMM is conducted with thin mask i.e. 12 µm at different duty ratios, due to availability of high current for larger pulse on-time, material removed from the dimple surface is much more and the consequent depths of the micro-dimples are higher as compared to the micro-dimples fabricated with relatively thicker mask i.e. 16 µm and 20 µm respectively. When t_m is 90s, a maximum of 50.17 µm micro-dimple depth is observed when machining with 12 µm mask sample is carried out at 20% duty ratio with respect to 45.25 µm and 34.17 µm for samples with 16 µm and 20 µm mask respectively. The average value of micro-dimple depths minimizes to 27.54 µm, 40.21 µm and 45.25 µm at 50% duty ratio for the respective three masks in descending order. The corresponding maximum values of micro-dimple depths at machining time of 120s is found to be 62.46 µm, 58.42 µm and 44.10 µm for samples with mask thickness 12 µm, 16 µm and 20 µm respectively.

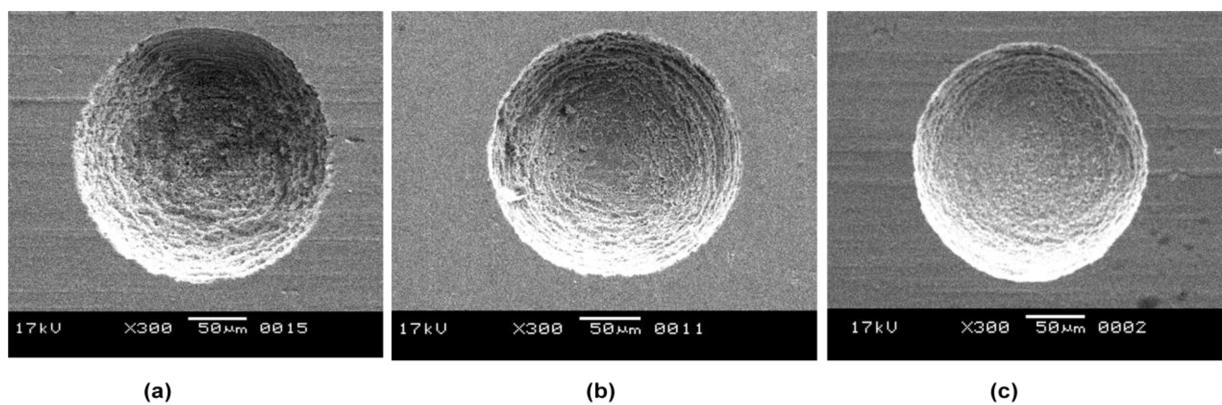

Figure 5.5: SEM micrographs showing micro-dimples generated under different mask thickness
(a) 12 µm (b) 16 µm and (c) 20 µm at 120 s t_m

When the thickness of the mask increased from 12 µm to 20 µm, the depth showed a relatively lower value. Figure 5.5 (a), (b) and (c) show SEM micrographs of three micro-dimples fabricated with three different mask thicknesses i.e. 12 µm, 16 µm and 20 µm at 120 s t_m. A minimum of 32.15 µm depth is achieved when TMEMM is carried out with a 20 µm thickness mask as compared to 43.15 µm and 51.24 µm in case of 16 µm and 12 µm mask thickness respectively. Moreover, the nature of material removal, when TMEMM is carried out with masked specimen having 12 µm mask thickness is comparatively much unorganized due to lack of uniformity in current distribution as compared to the other two masks. As a result, surface texture of the machined micro dimples with 12 µm mask thickness is much

rougher as compared to that of 16 μm mask and 20 μm mask thickness machined under same parametric setting, which is quite evident from fig. 5.5.

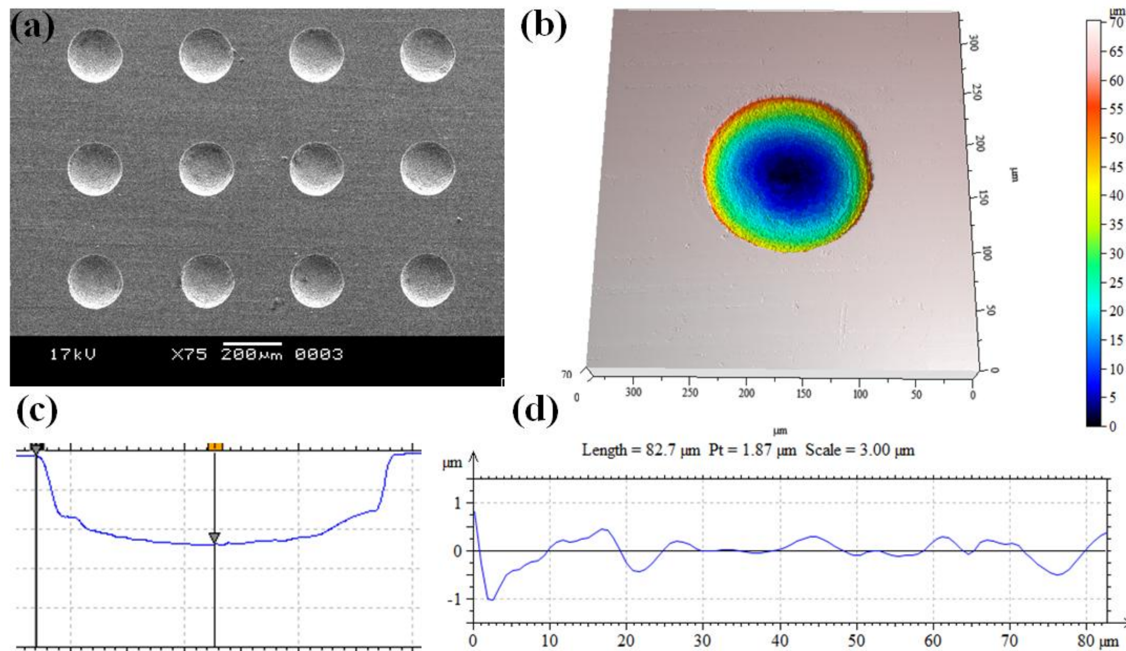

Figure 5.6: Micro-dimple array generated utilizing a 20 μm thick mask under favorable conditions (a) SEM micrograph of micro-dimple array (b) 3D profile of the generated micro-dimple (top view), (c) Side view (d) Surface characteristics of the generated micro-dimple

It has been experimentally established by previous researchers [64, 67,69,70] working in this domain that a PDMS mask of 250 μm thickness needs to be applied along with using $NaNO_3$ to restrict the formation of island in the centre of the dimples. However, for approximately same dimensions of micro-dimples, the islands disappeared when masks with relatively lesser thicknesses i.e. 20 μm thick is employed in TMEMM utilizing the mixed electrolyte of $NaNO_3$ and NaCl and prolonging the machining time. Figure 5.8 shows the microscopic images as well as the 3D profiles of the fabricated micro-dimple array. SEM micrograph at fig. 5.6 (a) shows the uniformity in the size of the dimples over the textured array. Figures 5.6(b) and (c) successfully establish the fact of non-formation of islands inside the dimple surface of the generated micro-array. Figure 5.6(d) shows the surface characteristics of the formed micro-dimple. The non-existence of islands attributes to the fact that the electrolyte chosen here is a combination of $NaNO_3$ and NaCl, wherein $NaNO_3$ is responsible for precise machining and the material removal is taken care by NaCl. Moreover, the usage of masks of thin range permits ample flow of electrolyte such that, the reaction products as well as gas bubbles gets removed both from the edges as well as the centre without any hindrance.

(iii) Influence of duty ratio and machining time on etch factor (f_e)

Machining localization is an indispensable factor for the formation of micro-dimples and can be described by etch factor (f_e). It is a unique approach to determine the anisotropy of the TMEMM process. An etch factor of 1.0 indicates the ideal isotropic material removal. A large etch factor implies small undercut and a controlled material removal is observed beneath the mask opening, whereas a smaller etch factor implies large undercut in which the material removed laterally under the mask is much more than the former one.

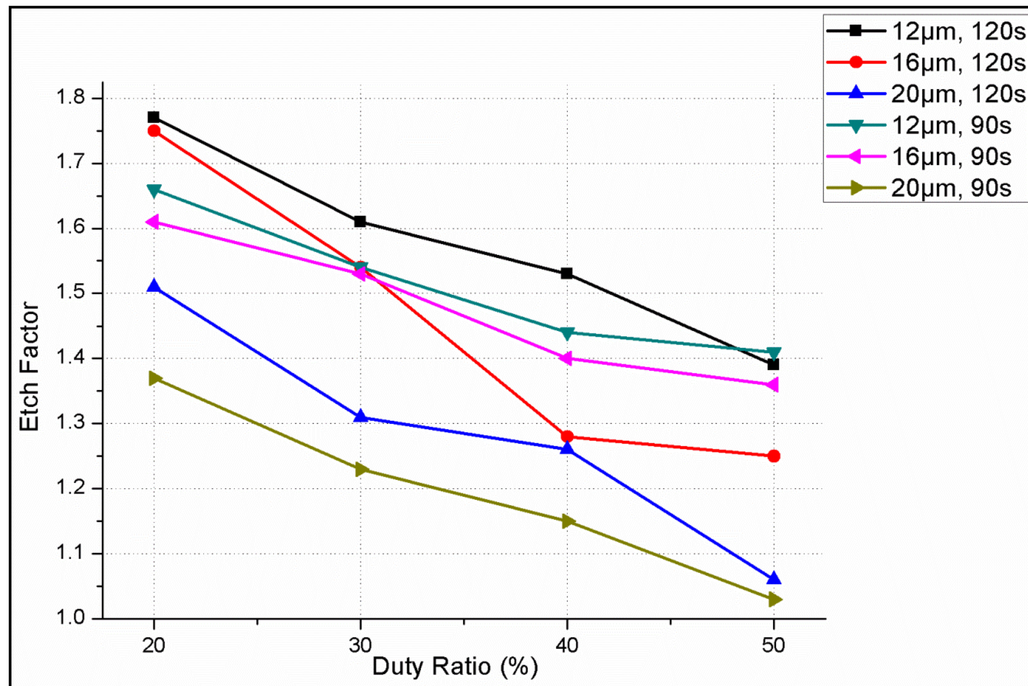

Figure 5.7: Effect of duty ratio on etch factor at two different machining times

Figure 5.7 plots the etch factors at different duty ratios. It could be noticed that etch factor reduces with increase in duty ratio. This aspect could be explained by the fact that as the pulse-on time increases, the stray current also increases resulting in the increase in undercut, resulting in decrease in etch factor. When TMEMM is carried out at 90 s machining time with varying mask thickness from 12 µm mask to 20 µm mask, the etch factor value gradually decreases from 1.66 to 1.37 at 20% duty ratio with respect to 1.41 to 1.03 at 50% duty ratio. When the machining time is increased to 120 s, similar decreasing trend in the nature of the graph is observed with duty ratios increasing from 20% to 50% as shown in fig. 5.7.

(iv) Influence of duty ratio and machining time on surface roughness characteristics (R_a and R_q)

Surface Roughness is one of the major parameter which defines the quality of the micromachining process. Since, the surface profiles of the fabricated micro-dimples play an important role towards various tribological applications, it is very much essential to look into the surface properties of the generated micro-dimples for increasing its acceptability as well as applicability in the engineering sphere. The arrayed micro-textured surfaces have been observed and measured by the Talysurf CCI Non-Contact Profilometer (Taylor Hobson) to investigate about two major surface roughness characteristics (R_a and R_q) inside the circumference of the generated micro-dimples.

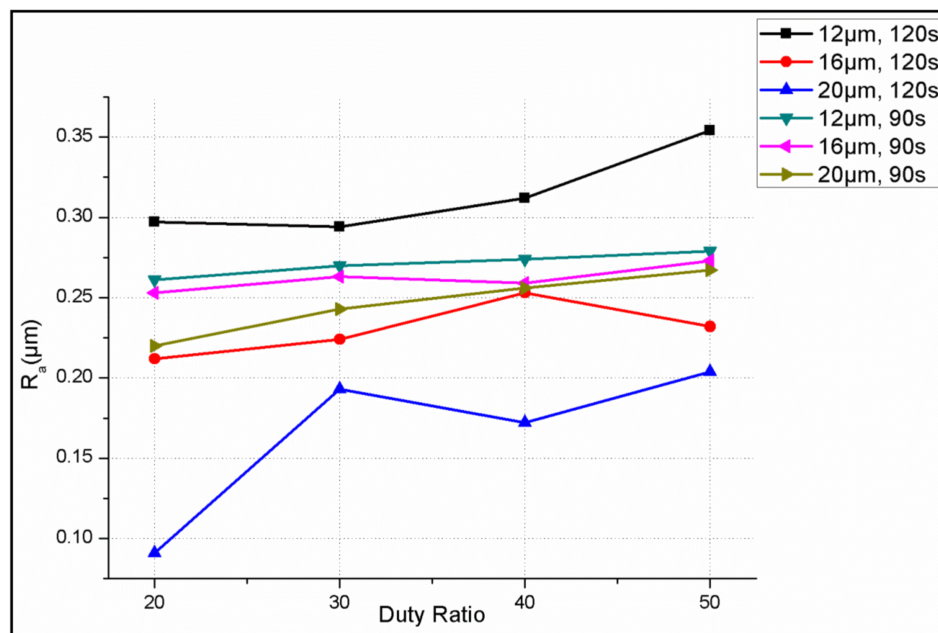

Figure 5.8: Effect of duty ratio on R_a at different machining times

Figure 5.8 reveals about the nature of the machined surface at different duty ratios machined at 90 s and 120 s respectively. As duty ratio increases, R_a of the surface generated during TMEMM gradually increases. This is due to the fact that, as the current efficiency and the total amount of electricity do not change when the same applied voltage and effective machining time are applied, the volume of material removed remains the same. However, the pulse off time is longer at low duty ratio and the reaction products are removed more efficiently by the flowing electrolyte, which enables controlled machining to achieve better surface condition.

As the duty ratio increases, this removal time of the reaction products decreases gradually and hence, the surface integrity of the micro-dimples machined at lower duty ratios are much

smoother (0.220 μm for 20 μm mask, 0.253 μm for 16 μm mask and 0.261 μm for 12 μm mask) than that machined at higher duty ratios.

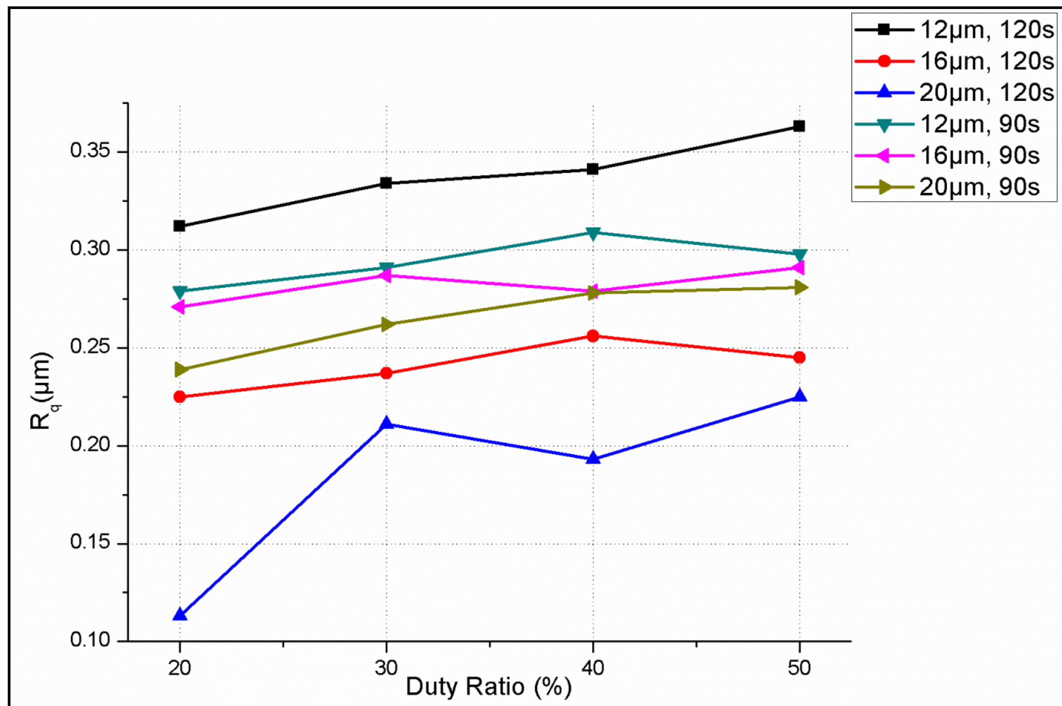

Figure 5.9: Effect of duty ratio on R_q at variable machining times

In addition to R_a, the values of the root means square component of the surface roughness, R_q have also been considered for investigation. Figure 5.9 plots the variation of R_q with increasing duty ratios and under three mask thicknesses and two machining times. During the analysis, 20% duty ratio has been found to be the most favorable for generation of circular micro-textured patterns with enhanced surface quality. This outcome is equally viable for all three masked samples. However, samples with 20 μm mask thickness have been found to be the best among the three different samples for generation of micro-textured circular micro dimples for t_m 120 s. Therefore, a low pulse duty cycle is more suitable for generating circular micro-dimples with a better three-dimensional topography. With the increase in machining time, more amount of fresh electrolyte comes in contact with the anode surface leading to the increasing in depth of the micro dimples and improving the surface roughness. So, it firmly complies with the results plotted in fig. 5.9.

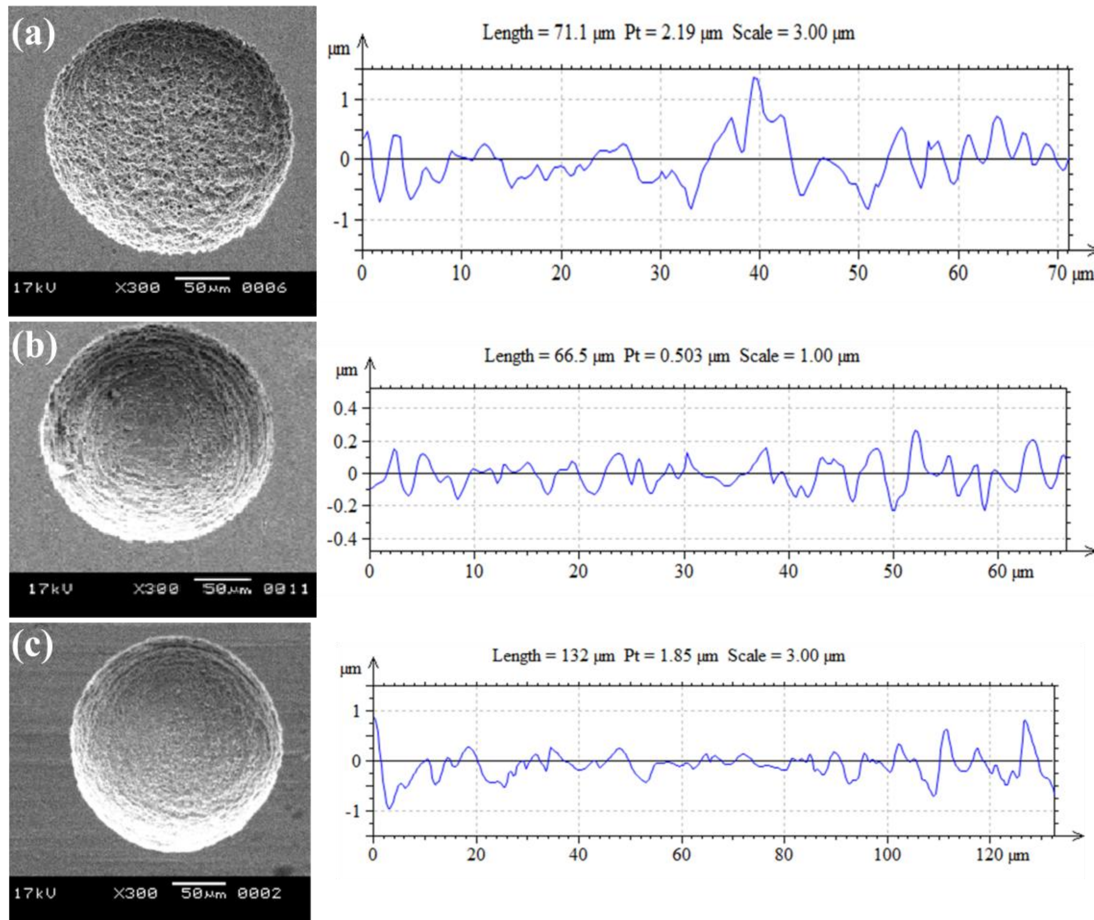

Figure 5.10: Micro-dimple fabricated with (a) 12µm (b) 16µm and (c) 20µm mask

When the mask thickness is less (12 µm), due to non uniform distribution of current, initially the material removal takes place from the interfacing edges. As the machining time increases, the current shifts from the interfacing edge towards the centre of the feature. As a result of which, the homogeneity of material removal is disturbed resulting in rough surface inside the generated dimple geometry. As the thickness of the mask gradually increases (20 µm), the effect of current distribution is comparatively less due to high mask aspect ratio. Although, the nature of material removal is identical, the amount of material removed is quite less than the former one. Further, due to high aspect ratio of the thicker mask, the non-uniformity in the distribution of current is comparatively less. As a result of which, the removal of materials from the dimple trench takes place in a rather controlled manner with the 20 µm masked samples as compared to the machining conducted with the 12 µm masked samples. As such, the generated micro-profile of the dimple array is relatively smoother as compared to that of 12 µm and 16 µm. SEM micrographs of the micro-dimples fabricated over samples with 12 µm, 16 µm and 20 µm mask along with their surface profiles are shown in fig. 5.10 (a), (b) and (c). It confirms that the surface roughness of the dimples machined under 20 µm

mask is much smoother in nature as compared to the dimples generated with samples possessing 12 µm mask and 16 µm mask. It is also clear from the SEM micrographs that the surface of the dimple machined with 20 µm mask is the best as compared with that fabricated with the thinner ones.

5.5.2. Influence of TMEMM Parameters on Square Micro- Patterned Textures

Experimental investigations have also been carried out during fabrication of square micro-dimple array. Similar set of experiments have been conducted to study the effects of duty ratio and machining time on undercut of the generated square micro-dimples. The machining conditions have been kept identical as considered during fabrication of circular micro-dimple array.

(i) Influence of duty ratio and machining time on undercut (U_c)

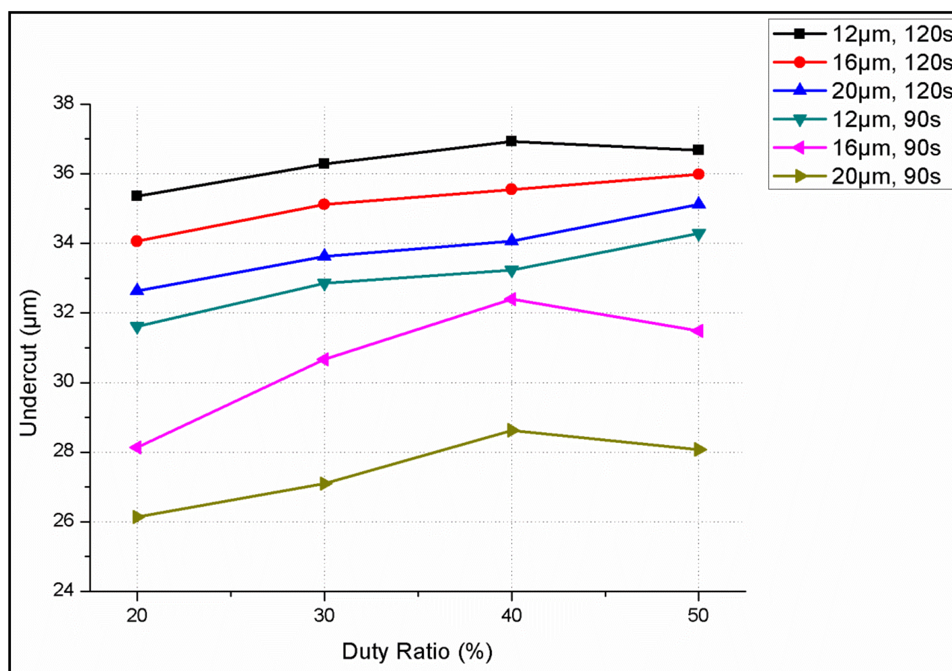

Figure 5.11: Effect of duty ratio on undercut at different machining times

Figure 5.11 shows the effect of duty ratio on undercut measured during the fabrication of the square micro-dimpled array at machining time 90 s and 120 s respectively. As duty ratio increases from 20% to 40%, U_c increases promptly for all the three masks at 90 s as well as 120 s. Since, the current flowing into the system increases and results in more material removal, U_c increases. When duty ratio exceeds 40 %, due to decrease in the pulse-off time, the oxygen and gas bubbles generated on the anode surface due to dissolution, gets entrapped under the mask. The slowing down of escape of oxygen bubbles results in increase in the inter-electrode resistance. As such, the current decreases rapidly resulting in steep reduction

in the undercut. Although the same trend could be observed during the TMEMM of circular micro dimples, but, it could be noticed that the average U_c values for circular micro-dimples is less than that of the square micro-dimples. This can be explained as, during the initial phase of TMEMM with the square micro-patterned mask, the current flux flow lines from the cathode comes vertically down through the edges and machining takes place along with the walls of the cavity thereby creating a box-type groove. After few seconds of machining, due to increase in current concentration around the edges and corners, the lateral material removal (X and Y axis) increases. This effect gradually reduces when machining is done with a comparatively thicker mask in which the higher aspect ratio of the mask hinders more material removal from edges leading to lesser undercut as compared to the circular micro-dimples.

(ii) Influence of duty ratio and machining time on depth (d_d)

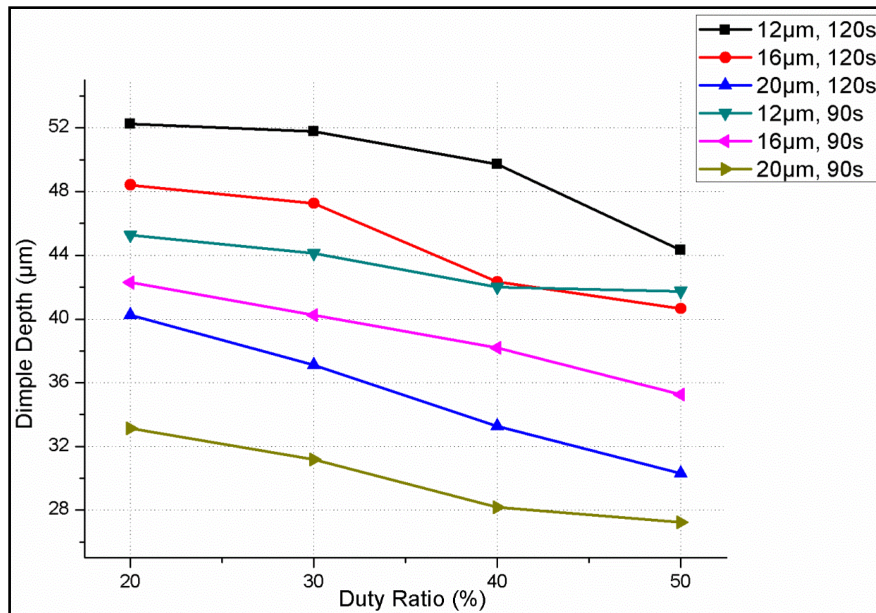

Figure 5.12: Effect of duty ratio on dimple depth at different machining times

Figure 5.12 shows the effect of duty ratio on the micro-dimple depth generated during fabrication of the dimpled array consisting of micro-squares at t_m, 90s and 120s respectively. As duty ratio increases from 20% to 50%, d_d decreased gradually form the order of 52.25 μm at 20% to 27.23μm at 50%. When TMEMM is carried out for 90s, the values of average micro-dimple depth ranges from 45.27 μm to 41.75 μm in case of 12 μm masked samples, 42.29 μm to 35.25μm in case of 16μm masked samples and 33.13μm to 27.23 μm in case of 20 μm masked samples. When machining time is increased to 120 s, a maximum of 52.25 μm depth is observed when machining with 12μm masked sample compared with 48.42 μm and 40.24 μm for 16 μm and 20μm masked sample.

The range of depths obtained during fabrication of circular micro-dimple array is on a higher side as compared to the square one. With the gradual increase in duty ratio, the pulse-off time decreases. As a result of which, the time required for flushing out of the reaction products continuously reduces which decreases the material removal from the 'Z' direction. This can be explained by the fact that due to the presence of edge and corner type geometry in squared dimples, the escape of the machined materials and gases gets hindered. As a result of which, the material removed vertically (Z direction) from the crater of the micro-dimples becomes lesser and lesser with the increase in duty ratio and as a result of which the dimple depths are on a lower range during generation of square micro-dimples as compared to circular patterned micro-dimples.

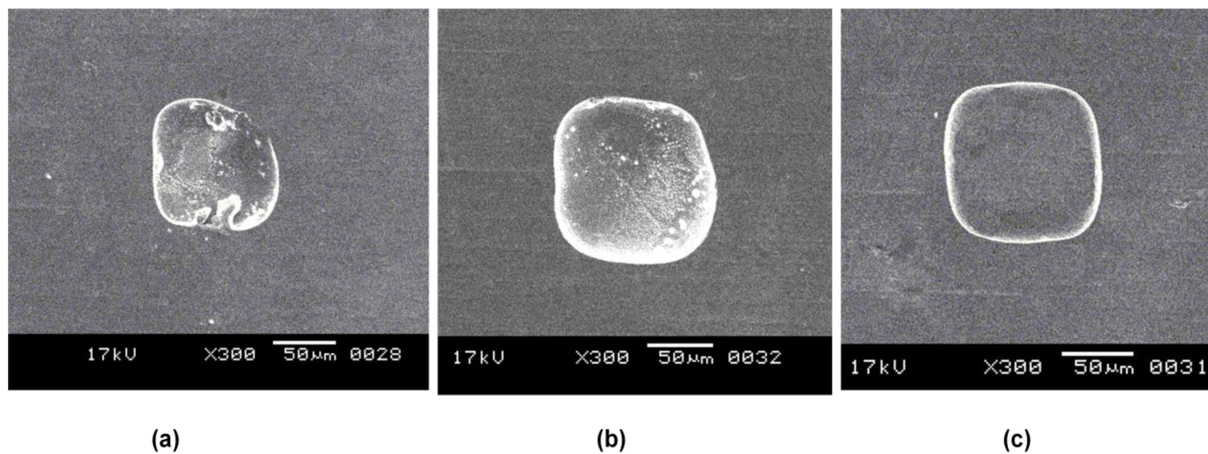

Figure 5.13: SEM micrographs showing square micro-dimples generated under different mask thickness at 120s machining time (a) 12 µm (b) 16 µm and (c) 20 µm

Figure 5.13 (a), (b) and (c) shows SEM micrograph of three square micro-dimples fabricated upon 12 µm, 16 µm and 20 µm masked samples at 120 s machining time under same parametric setting. A minimum of 30.29 µm depth is achieved when TMEMM is carried out with 20 µm thickness mask as compared to 40.66 µm and 44.32 µm in case of samples possessing 16 µm and 12 µm mask thickness respectively. When TMEMM is carried out with low thickness mask i.e. 12 µm, the current distribution being non-uniform, the removal of reaction products and gas bubbles from the dimple cavity is in highly unsystematic in nature leading to non-uniform dimple surface which is comparatively less when machining is executed with a comparatively thicker mask i.e. 16 µm and 20 µm respectively.

(iii) Influence of duty ratio and machining time on etch factor (f_e)

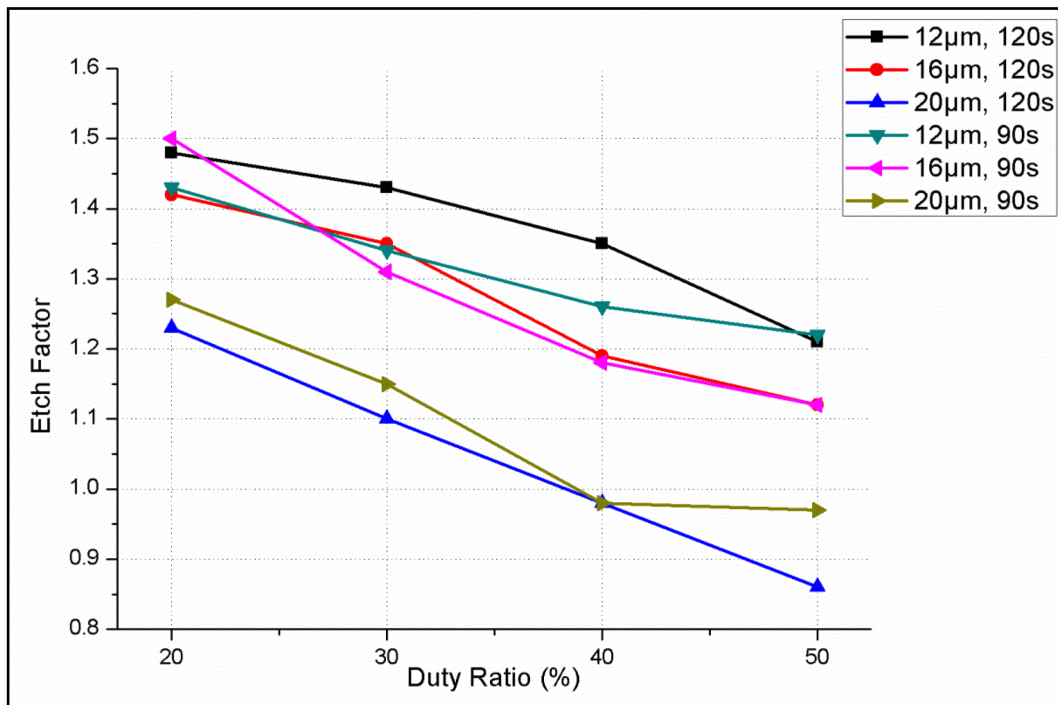

Figure 5.14: Effect of duty ratio on etch factor at different machining times

The etch factor i.e. the nature of isotropy can be defined as the ratio of depth of etch to the lateral etch (undercut). Figure 5.14 expresses the etch factors at different duty ratios at two machining times. It could be noticed that etch factor gradually reduces as the duty ratio is increased while machining is accomplished with both the masks. With varying mask thickness from 12 μm mask to 20 μm mask and machining for 90 s, the etch factor value lies between 1.27 to 0.97 for 20 μm masked sample with respect to 1.43 to 1.22 for sample possessing 12 μm mask. When the machining time is increased to 120 s, similar decreasing trend in the nature of the graph is observed with increasing duty ratios from 20% to 50%. The value of etch factor ranges from 1.48 to 0.86 for the samples machined for 120 s.

Since the etch factor for the square dimples are more closer to '1' than the circular micro-dimples due to the lesser range of depths, it could also be revealed that the fabricated square micro-dimples are more isotropic in nature as compared to that of circular textures.

(iv) Influence of duty ratio and machining time on surface roughness characteristics (R_a and R_q)

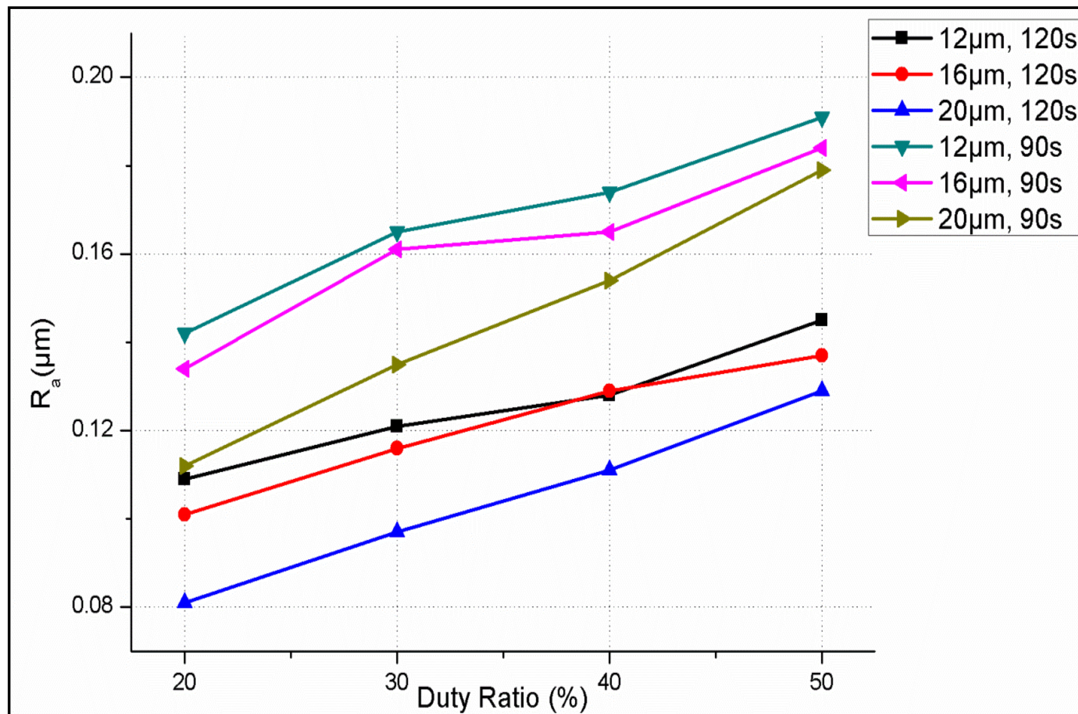

Figure 5.15: Effect of duty ratio on R_a at variable machining times

Figure 5.15 and fig. 5.16 plots the variation of surface roughness characteristics, R_a and R_q of the generated textured surface at different duty ratios. As duty ratio increases, both R_a as well as R_q gradually increases for all the three mask thickness. With the increase in duty ratio, the removal time of the reaction products decreases gradually and as a result of which, the organized nature of material removal is responsible for improvement in the surface integrity of the square micro-dimples machined at lower duty ratios as compared to the micro textured dimples machined at higher duty ratios. Therefore, a low pulse duty ratio is more appropriate for fabrication of micro-dimples with a better three-dimensional topography.

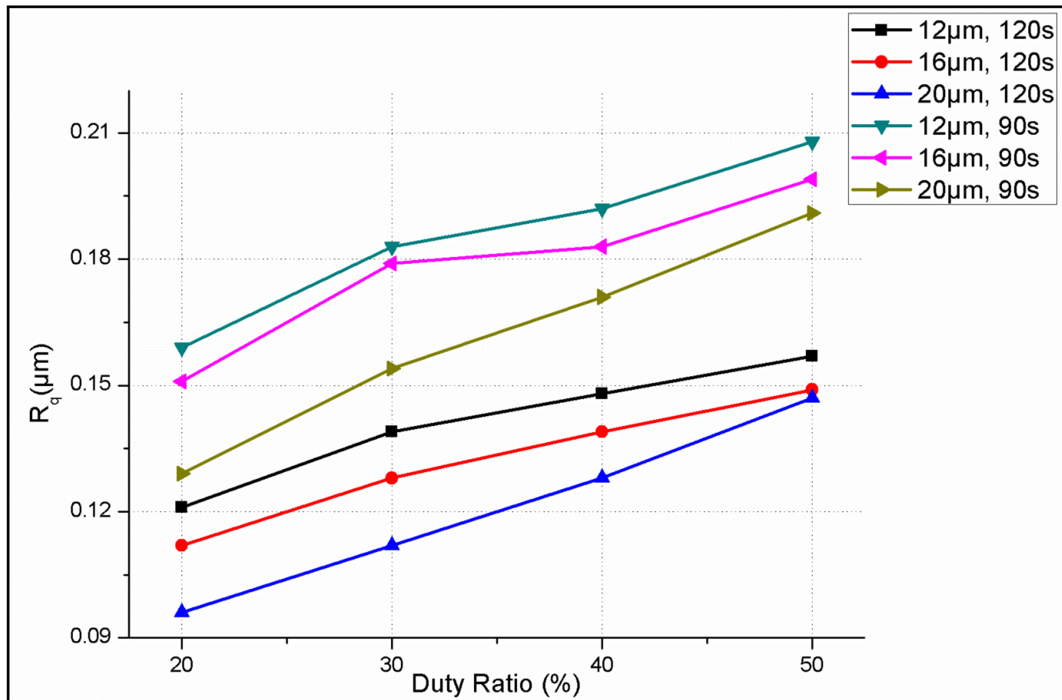

Figure 5.16: Effect of Duty Ratio on R_q at different machining times

Further, it could be seen that both R_a as well as R_q for all the samples (with three different masks) machined for 90 s is higher than that of the sample machined for 120 s. This is due to the fact that, as the current efficiency and the total amount of electricity do not change when the same applied voltage and effective machining time are applied, the volume of material removed remains the same. However, the pulse off time is longer at a low duty ratio and the reaction products are removed more efficiently by the flowing electrolyte, which enables controlled machining to achieve better surface condition. This concludes that machining time also plays a vital role in framing of the texture of a machined surface.

The same pattern of graphs has already been observed during the fabrication of circular micro-dimples. But, the range of both R_a and R_q of square micro-dimples are comparatively much less as compared to the circular micro-dimples. Since the dimple depths obtained while TMEMM of square patterns is lesser as compared to that of circular ones, the material removed from the dimple area is controlled and are also of lower ranges. As such, the surface roughness value is much more improved in the fabricated square micro-dimples as compared to the circular patterned array of dimples.

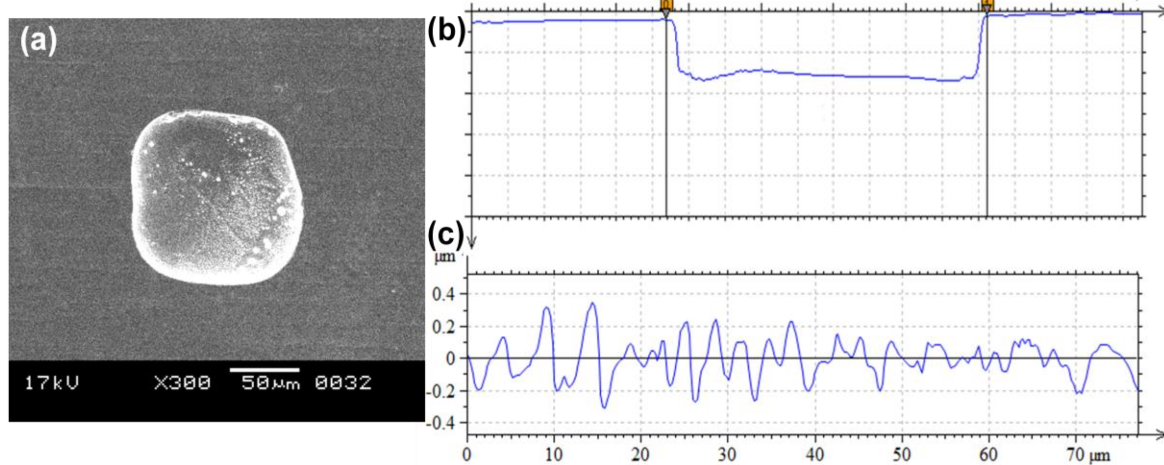

Figure 5.17: Square micro-dimple fabricated by TMEMM upon 16 µm mask at 120 s machining time (a) SEM micrograph (b) Surface profile of the formed micro-dimple and (c) Surface characteristics of the generated micro-dimple

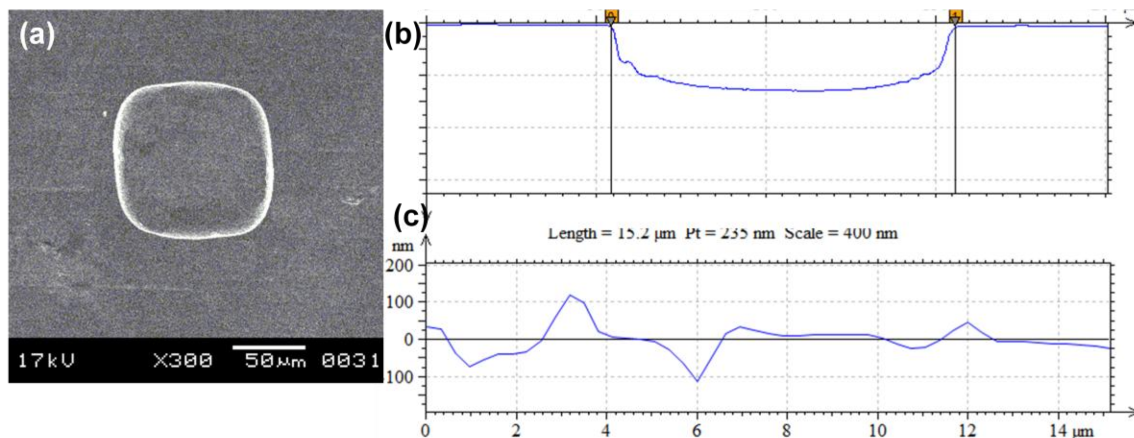

Figure 5.18: Square micro-dimple fabricated by TMEMM upon 20 µm mask at 120 s machining time (a) SEM micrograph (b) Surface profile of the formed micro-dimple and (c) Surface characteristics of the generated micro-dimple

Figure 5.17 and fig. 5.18 shows two square micro-dimples generated under same parametric combination utilizing 16µm masked sample and 20µm masked samples respectively. It could easily be noticed that when TMEMM is carried out with mask of low thickness, the removal of materials from the dimple surface is unorganized in nature due to non-uniform current distribution. As a result of which, more amount of materials are removed from the edges as compared with the centre. As such, there is unevenness in material removal resulting in formation of a very small material hump in the bottom surface of the generated dimple leading to unevenness as shown in fig. 5.17(b). The size of the island is much more in case of

12 μm masked sample. Hence, the dimple surface becomes very rough and uneven as confirmed by the surface profile in fig. 5.17(c).

On the other hand, when a comparatively thicker mask i.e. 20 μm mask is utilized during machining, the nature of removal of materials being organized in nature, the surface finish of the square micro-dimple formed after machining becomes uniform as depicted through fig. 5.18(b). Figure 5.18(c) reveals that the surface profile also complies with this aspect that the said textured surface is quite smooth and the surface roughness characteristics (R_a and R_q) are quite less as compared to that machined with 16μm masked sample.

5.6 Fabrication of circular and square micro-dimple array based on experimental analysis

Based on the experiments conducted along with the thorough investigation of the results, it is obvious that unlike circular micro-dimples, fabrication of square micro-dimple array is quite feasible with this approach of TMEMM. Moreover, duty ratio as well as machining time plays a substantial role in influencing the dimensions, geometrical topography and machining accuracy of the fabricated micro-dimple. Different machining times have been considered for the generation of island-free patterned micro arrays on SS304 surface.

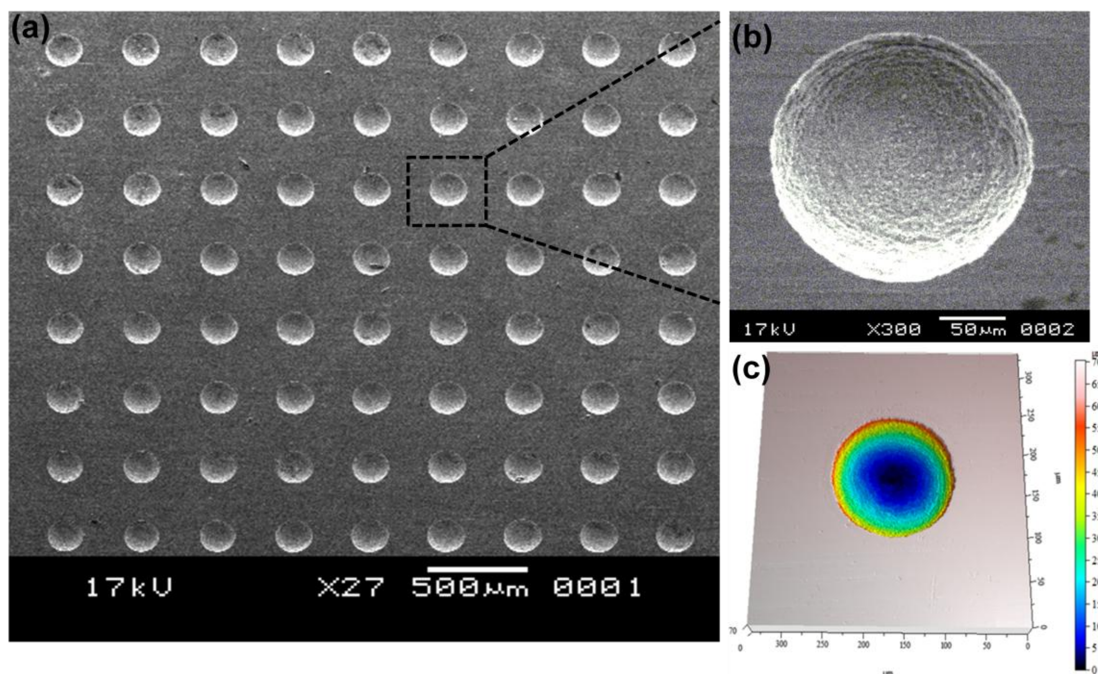

Figure 5.19 (a) SEM micrograph of the fabricated circular micro-dimple array generated with 20 μm mask at 20% duty ratio and 120s machining time (b) Single Dimple (SEM micrograph) and (c) 3D view showing surface profile of the micro-dimple generated by TMEMM

Figure 5.19 shows the pictorial representation of the micro-dimple array fabricated at 120 s machining time, where (a) represents the SEM micrograph of the full matrix of the generated circular micro-dimple array, (b) SEM micrograph of a single micro-dimple and (c) 3-Dimensional view of a generated micro-dimple.

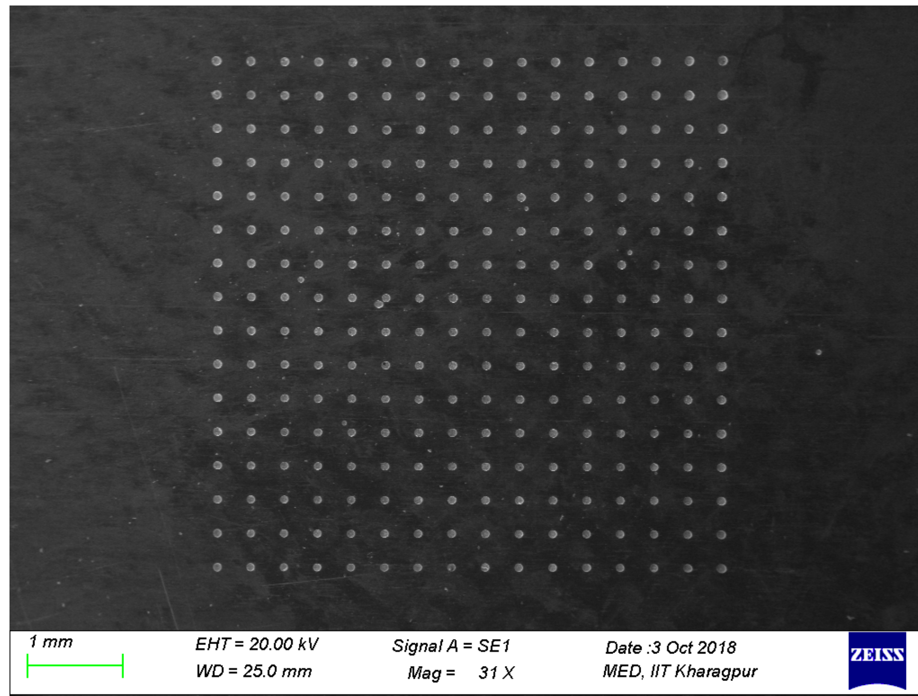

Figure 5.20 SEM micrograph of the complete micro-textured array of circular dimples generated with best combination of parameters

Figure 5.20 depicts the SEM micrograph of the full matrix of micro-patterned array containing circular textures generated when machined at the best parametric combination with a sample masked with 20 μm mask. Clear picture of the entire textured array proves the achievement of micro-texturing free from islands employing the proposed methodology of TMEMM.

Similarly, square micro-dimple array have also been generated as shown in fig. 5.21 (a) to (c). Island-free square micro-dimple arrays are effectively fabricated using 20% duty ratio by the application of an optimized electrolytic combination of NaCl and $NaNO_3$. Surface roughness characteristics (R_a and R_q) and dimensional uniformity of generated micro-textured surfaces has been found to be suitable when TMEMM is conducted under these parametric conditions. It is revealed from the experiments that 20% duty cycle along with 120 s machining time proved to be the most favorable conditions for micro-patterned array generation.

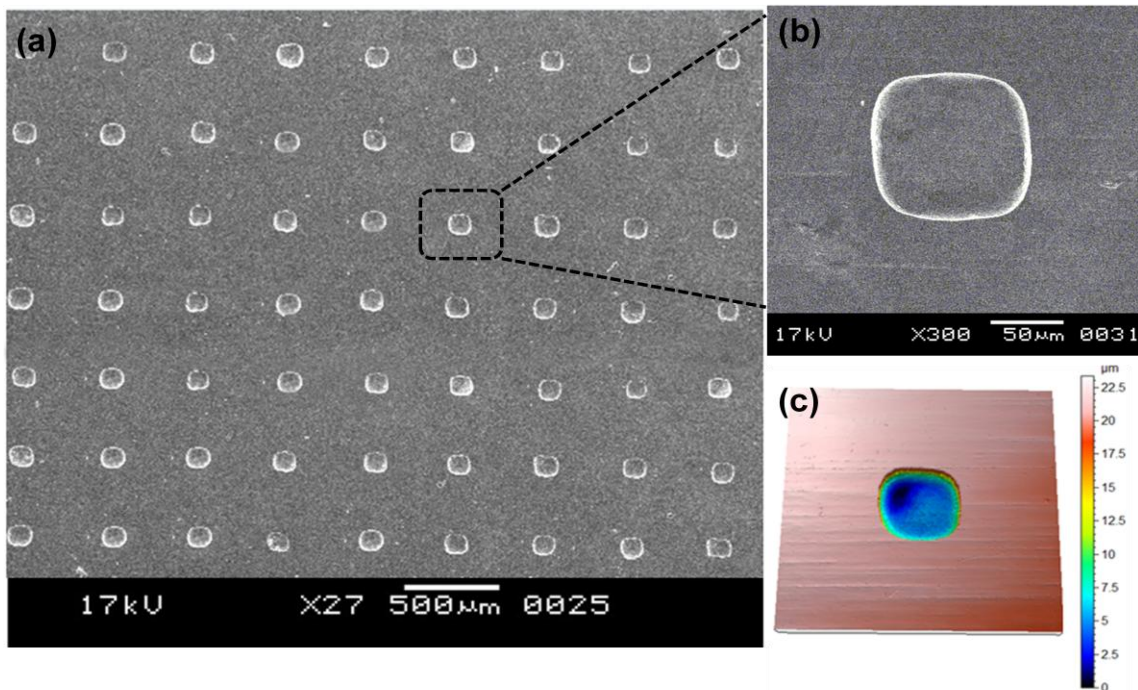

Figure 5.21: (a) SEM micrograph of the fabricated square micro-dimple array generated with 20 μm mask at 20% duty ratio and 120 s machining time (b) Single square micro dimple (SEM micrograph) and (c) 3D view showing surface profile of the micro-dimple generated by TMEMM

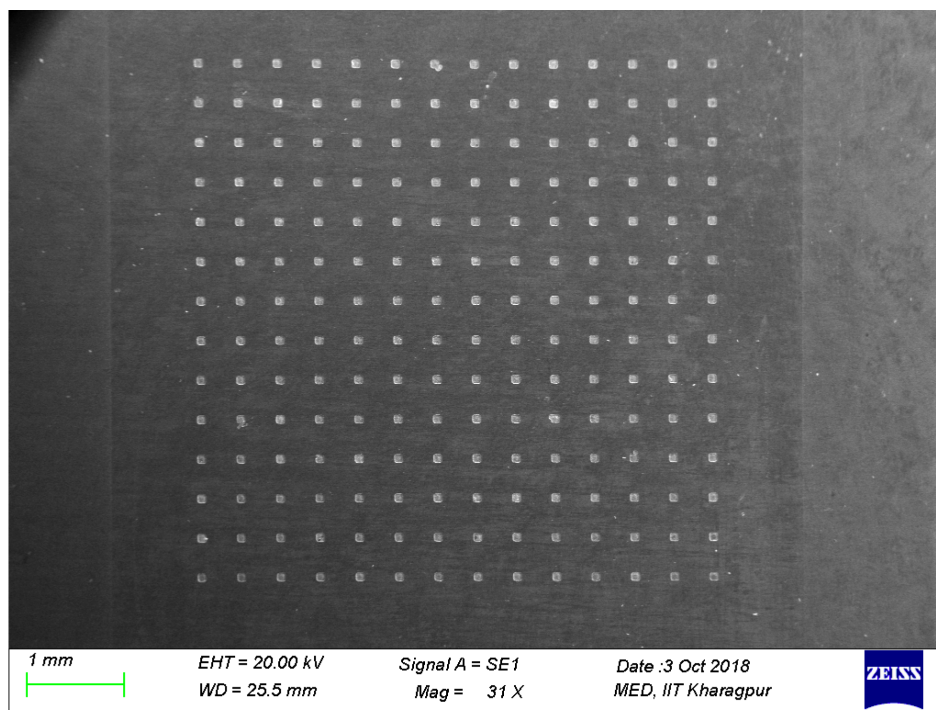

Figure 5.22: SEM micrograph of the complete micro-dimple array generated with best combination of parameters

Figure 5.22 illustrates the SEM micrograph of the full matrix of micro-patterned array containing squared textures generated when machined at the most suited parametric

combination with a sample masked with 20 µm mask. Textured array containing island-free micro-squares is achieved using TMEMM.

5.7 Analysis based on Friction Tests

In order to evaluate the effectiveness of the dimple depths generated in micro textured surface (circular as well as square), in-depth variation in the friction coefficient values under normal load (N) of 25 N, 50 N and 75 N have been studied using four different types of samples: (i) Non-dimpled sample, (ii) textured sample containing average dimple depths of 30 µm, (iii) textured sample containing average dimple depths of 35 µm and (iv) textured sample containing average dimple depths of 40 µm. Friction tests are conducted in both dry as well as wet conditions. The test results have been graphically plotted and the variation in the frictional co-efficient (µ) between the circular and squared micro-textured array studied for further analysis.

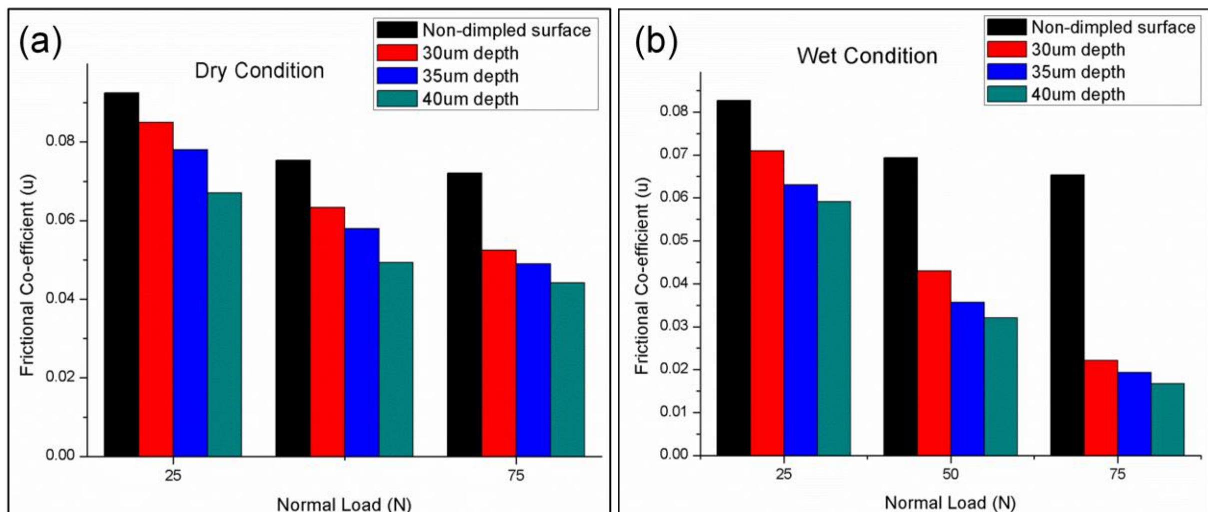

Figure 5.23: Effect of circular micro-dimple array on frictional co-efficient under different normal loads considering (a) dry condition (b) wet condition

The friction test results for the un-textured as well as samples with circular micro-dimple array of different depths are shown in fig. 5.23 (a) under dry condition and (b) under wet condition. Significant differences can be seen in the friction co-efficient of un-textured and textured surfaces.

With the application of lubricating oil, there was a noticeable reduction in the coefficient of friction. When the load was gradually increased from 25 N to 50 N and finally to 75 N, the frictional coefficient reduces from 0.071 to 0.0221 in case of micro-dimpled textured surfaces possessing circular dimples of 30 µm depth (average). With the increase in N, there is an increase in contact area between the structured surface and the load which finally results in

decrease in the frictional coefficient. Since, lubricant stored within dimples plays a significant role in minimization of the friction; the co-efficient of friction further reduces from 0.063 to 0.0193, when textured samples having average micro dimple depth of 35 µm are tested under different loads. This value further reduces from 0.0591 to 0.0167 for micro-dimpled surface having a texture depth of 40 µm. Moreover, it could be stated that with the increase in normal load, there is a considerable reduction in the coefficient of friction for textured samples with average depths of 30 µm depth and 40 µm depth respectively. Hence, it could be established that the micro-dimple array especially that with high aspect ratio had a great potential during friction reduction as it can be seen that the beneficial effect of micro-dimples enhanced as the dimple depth increases.

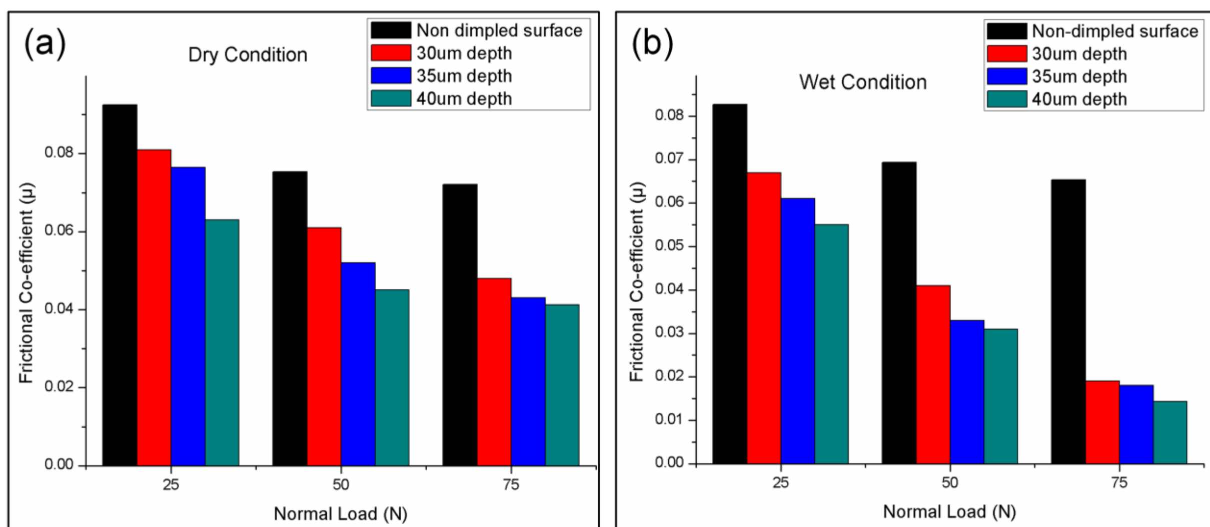

Figure 5.24: Effect of square micro-dimple array on frictional co-efficient under different normal loads considering (a) dry condition (b) wet condition

In parity with the previous analysis, the frictional analysis have also been carried out for the un-textured as well as samples with square micro-dimple array of different depths are shown in fig. 5.24 (a) under dry condition and (b) under wet condition. The friction behavior of the un-textured and textured surfaces containing micro-squares of different depths is discussed in details.

When lubricating oil was applied over the samples before initializing the tests, there was a noteworthy reduction in the coefficient of friction. When load is steadily increased from 25 N to 75 N, the frictional coefficient reduces from 0.067 to 0.019 in case of micro-samples possessing dimples of 30µm depth (average). This is because with the increase in the normal load (N), there is an increase in contact area between the structured surface and the load

which finally results in decrease in the frictional coefficient. This might be due to the fact that the textured surface could be used to provide lubrication, as well as to store wear debris efficiently, which is helpful for reducing the frictional co-efficient (μ). Since, lubricant stored within dimples plays a significant role in minimization of the friction; the co-efficient of friction further reduces from 0.061 to 0.018, when textured samples having average micro dimple depth of 35 μm are tested under different loads. These value further drops from 0.055 to 0.0143 for micro-dimpled surface having a textured depth of 40 μm. Therefore, it could be stated that with the increase in normal load, there is a considerable reduction in the coefficient of friction for patterned samples with average depths of 30 μm depth and 40 μm depth respectively.

After comparative analysis of the frictional co-efficient values for circular and squared micro-patterns, it could be inferred that the average frictional co-efficient of the samples with squares as micro-textures is comparatively less as compared to samples possessing circular micro-dimples as patterned micro textures. This nature can be noticed at both dry as well as wet condition. Due to the presence of edges and corners in the squared textures, the converging wedge in the square micro-dimples facilitated the formation of a lubricant film between the two surfaces, which further reduces the frictional co-efficient. Hence, the square dimple is the preferred choice for a textured surface to enhance the friction performance of a material.

5.8 Experimental Outcomes

TMEMM process for generation of circular and square micro-patterned array has been experimentally investigated with the help of thin PR masks. Based on the experimental findings as well as analysis of the micro-graphs, it is found that when the electrolyte concentration, flow velocity, applied voltage and frequency are fixed, the dimple diameter enhancement takes place with the increase in duty ratio along with the prolonged machining time. Circular as well as square micro-dimples are successfully generated by utilizing very thin mask of 20 μm thickness and machining for 120 s. Application of mask of thin ranges reduces the expenditure incurred during the process. Duty ratio for all the masks is varied from 20% to 50%. The results showed that with the increase in duty ratio, the depth of the generated micro-dimples gradually reduces.

The surface integrity of the dimples after TMEMM is also noticeable. Best surface is obtained during TMEMM with 20 μm masked samples with 20% duty ratio. R_a value for the fabricated circular micro-dimple has been found to be 0.091 μm whereas in case of square

micro-dimples, it reached to a minimum of 0.081 μm when machined at best parametric combination. From the detailed experimental analysis, it can be observed that the most favorable parametric setting i.e. electrolyte concentration 10% NaCl + 10% $NaNO_3$, voltage 12 V, frequency 2 kHz and duty ratio 20% generates best patterned micro-dimple array (for both circular as well as square) during TMEMM of stainless steel, when machined with a mask of 20 μm. Moreover, friction test results revealed that textured surfaces with micro-dimples play a key role in reducing the co-efficient of friction. Further, surfaces with square micro dimpled patterns considerably reduce coefficient of friction when subjected to increased normal loads in comparison with circular micro-dimples at various depths.

A simple novel process for fabrication of micro-dimple array by TMEMM by low aspect ratio masks has been demonstrated. The presented results demonstrate the feasibility of the proposed approach. Moreover, TMEMM can be considered as a feasible alternative in the generation of different micro-patterned arrays. An advantage of this present technique is that use of thick mask can be purely avoided resulting in considerable saving in the expenditure for the production of mask. Although square micro-dimples are beneficial considering its effectiveness towards friction reduction, the fabrication process is comparatively difficult considering the rounding off in the edges and corners. Whereas, circular micro textured surfaces are more acceptable to the manufacturing industry considering applicability point of view. However, further investigation in this field of surface texturing is also required to explore the possibilities of utilization of TMEMM for the fabrication of micro-patterns with higher depth and reduced undercut during surface structuring. Since, friction reduction has been one of the primary objectives of micro-texturing, effective utilization of TMEMM process parameters needs to be carried out for fabrication of high-aspect-ratio microstructures. Other controllable micromachining factors in TMEMM could be investigated to sort out many challenges in this field and increase the efficiency and performance of TMEMM towards micro-structuring.

Chapter 6

EXPERIMENTATION FOR CONTROLLING CHARACTERISTICS OF HIGH ASPECT RATIO MICRO-TEXTURES DURING TMEMM

6.1 Introduction

TMEMM is a process in which patterning on microstructures is carried out by selective material removal through photoresist masks. It has been an effective method for generating micro-textured arrays and acknowledges industrial acceptability. Compared to other processes, this method of electrochemical metal removal offers relatively better control, has higher machining rate and is more flexible for micro fabrication. Aspect Ratio (AR) has a significant contribution in influencing the current distribution at the initial metal surface and consequent shape evolution of the generated microstructure.

Micro texturing with dimples is one of the most established methods for the enhancement of lubrication and tribological performance. Surface areas covered with microstructures possessing high-aspect-ratio finds potential applications in a wide range of fields including heat transfer, adaptive aerodynamics, seal and bearing design, and composite materials. In the last few years, surface texturing has established to be an effective approach in engineering that result in enhancement in wear resistance, frictional coefficient, load capacity etc. Reserving lubricant is the basic perceptive of the lubricating mechanism of surface texture which includes micro-dimples, micro-grooves, micro-pillars, micro-prisms etc.

In this chapter, Through Mask Electrochemical Micromachining (TMEMM) is investigated to fabricate high-aspect-ratio circular micro-dimples utilizing a low cost photoresist. Since, the acceptability as well as applicability of circular micro-dimples is more in the present industrial world, generation of circular micro-textured surfaces have been taken into consideration in this set of research work. Experiments were performed with the help of indigenously developed TMEMM set-up to explore the suitable range of applied voltage to achieve controlled anodic dissolution during machining and to fabricate high aspect ratio micro dimples. Investigations were carried out to understand the influence of electrolyte type and concentration on the machining precision and surface characteristics of the generated high aspect ratio micro textured array. Further, friction test results were analyzed to figure out the alterations in the frictional coefficient of the micro-dimples with different depths as well as with non-dimpled samples.

6.2 Experimental planning

In order to perform experiments as per detailed research planning, and considering the effects of various controllable parameters, a well planned research program has been taken up for experimentation in the developed TMEMM set-up which have already been discussed in Sec.3.2 of chapter 3. Stainless Steel 304 sheets of 200 µm thickness coated with AZ4903 possessing micro-scale pattern. Each sample consists of micro-dimple arrays of dimension 65 µm. A cylindrical copper tool of 12 mm diameter has been utilized as cathode during the experimentation. Based on the knowledge incurred from the past research findings and conduction of trial experimental runs, it was learnt that high aspect ratio microstructures could only be fabricated when a longer etching time is maintained. But, prolonging the etching time may lead to increase in undercut and deterioration of surface of the generated micro-textures. Further, application of thin masks in TMEMM and creation of sound micro-patterned arrays have been considered to be a challenge in TMEMM. Hence, considering an urgent need to investigate TMEMM process utilizing thin masks and keeping in mind the utility of high aspect ratio microstructures in the present engineering scenario, in depth experimental investigation have been planned for generation of circular micro-textured patterns utilizing TMEMM.

In this chapter, two most influencing parameters which signify the dimension of aspect ratio in the microstructures e.g. applied voltage and electrolyte concentration has been considered during generation of micro-textured arrays by TMEMM. Samples possessing masks of 20 µm thickness have been investigated during experimentation. The range of applied voltage is chosen from 8-24 V, whereas, three different electrolytes viz. 10%NaCl + 10%$NaNO_3$, 10% $NaNO_3$, 20% $NaNO_3$ have been considered during experimental study. Duty ratio has been fixed as 20% considering the results of previous experiments. Other experimental conditions have been kept constant as discussed in Chapter-4 during the entire experimental schedule.

A mixed electrolyte with chloride and nitrate ions has also been experimented in TMEMM. $NaNO_3$ solution being a nonlinear electrolyte has been widely used for improving the machining accuracy in ECM. Further, the electrolyte being environmentally friendly is non-hazardous to the environment and equipment during machining. In this research work, $NaNO_3$ electrolyte with variable concentration along with a mixture with NaCl is experimentally studied during the generation of different surface geometries in the fabricated micro-dimple array in TMEMM. Patterned masks of negative PR (AZ 4903) of 20 µm thicknesses possessing strong adhesiveness with the substrate have been utilized during the

experimentation for generation of high aspect ratio patterned arrays containing micro-dimples. The effect of one of the most vital process parameter i.e. applied voltage along with changing electrolyte concentrations on undercut (U_c), dimple depth (d_d) and surface roughness (R_a and R_q) were investigated during micro-pattern array generation. Moreover, friction tests on the fabricated arrayed structures also need to be conducted to understand the effects of load as well as lubrication on the frictional coefficient. Selected process parameters such as applied voltage, pulse frequency, electrolyte concentration, duty ratio, etc. were represented in Table 6.1.

To validate the impact of micro-dimples array on the sample surface, friction tests were performed in a multi tribotester apparatus (TR-25, DUCOM). The machine details, its operating principle and the specifications of the lubricating oil have already been discussed in Chapter 4.

Table 6.1: Experimental Parameters for machining

Avg. diameter of micro-holes on the	65 µm
Thickness of patterned mask	20 µm
Workpiece Material	SS 304
Workpiece thickness	200 µm
Mask Material	AZ 4903
Applied Voltage	8, 10, 12, 14, 16, 18, 20, 22, 24 V
Duty Ratio	20%
Machining Frequency	2 kHz
Inter Electrode Gap	2000 µm
Electrolyte Concentration	10%NaCl+10%$NaNO_3$, 10% $NaNO_3$, 20% $NaNO_3$
Machining Time	120 s

6.3 Experimental methodology

The detailed procedure followed during the complete execution of the experimentation and analysis has been discussed in Section 4.5.2 in Chapter 4. The machining voltage had been varied with the interval of 2 V starting from 8 V up to 24 V and changing the electrolyte type and concentration. All other controllable process parameters have been kept at most favorable conditions as achieved through experimental investigations of earlier chapters.

6.4 Experimental results and discussions for controlling aspect ratio of microstructures

Experiments were carried out in the developed TMEMM set-up to explore the effects of duty ratio and mask thickness during micro-dimple array fabrication. Initially trial experiments

were conducted to fix the machining time such that a considerable depth of the micro-dimples could be achieved. Fixing the machining time to 120 s and duty ratio to 20%, experiments were carried out using patterned specimen of 20 µm mask thickness. Different dimple characteristics such as undercut, depth and surface roughness characteristics (R_a and R_q) were measured after the experiments. The results considered during the investigation of the various output parameters constitutes the average values of the dimples that were measured during analysis.

6.4.1 Effect of applied voltage and electrolyte type on undercut

In order to optimize the value of the voltage applied during machining, experiments on the influence of voltage on the machining accuracy of the formed micro-dimple were carried out while supplying different working voltages between the workpiece (anode) and the tool (cathode) utilizing three different electrolyte concentrations of 10% NaCl + 10% $NaNO_3$, 10% $NaNO_3$ and 20% $NaNO_3$. It is experimentally obtained that with the increase in voltage, undercut increases. Moreover, it could be found from the analysis of micrographs that proper machining would not occur until the applied voltage reaches 12 V. This nature of machining can be found in all the three electrolytes. An additional hump of materials could be noticed in the centre of the microstructures. The basis of this observation can be related to the machining principle of ECM, which states that electrochemical dissolution will not occur until and unless the applied voltage reaches a threshold value at which the dissolution reaction starts. In this study, 12 V can be obtained to be the threshold voltage. So, when TMEMM is carried out at less than 12 V, electrochemical dissolution process could not be completed and due to higher current density at the edges of the mask openings, initial material gets removed from the edges and then comes to the centre. The experimental results as expressed by the 3D image measured by the profilometer shown in fig. 6.1 (a) and cross sectional view of a generated micro dimple as in fig. 6.1 (c) along with SEM micrograph of the micro-dimple shown in fig. 6.1 (b) complies with the justification. Figure 6.2 (a) showing 3D image of a good micro-dimple machined at 12 V measured by the non contact 3D optical profilometer along with SEM micrograph at fig. 6.2 (b) and cross sectional view of the fabricated micro-dimple shown at fig. 6.2 (c) indicates that TMEMM can be utilized to machine micro-dimple array, which is also in line with the results plotted in fig. 6.3.

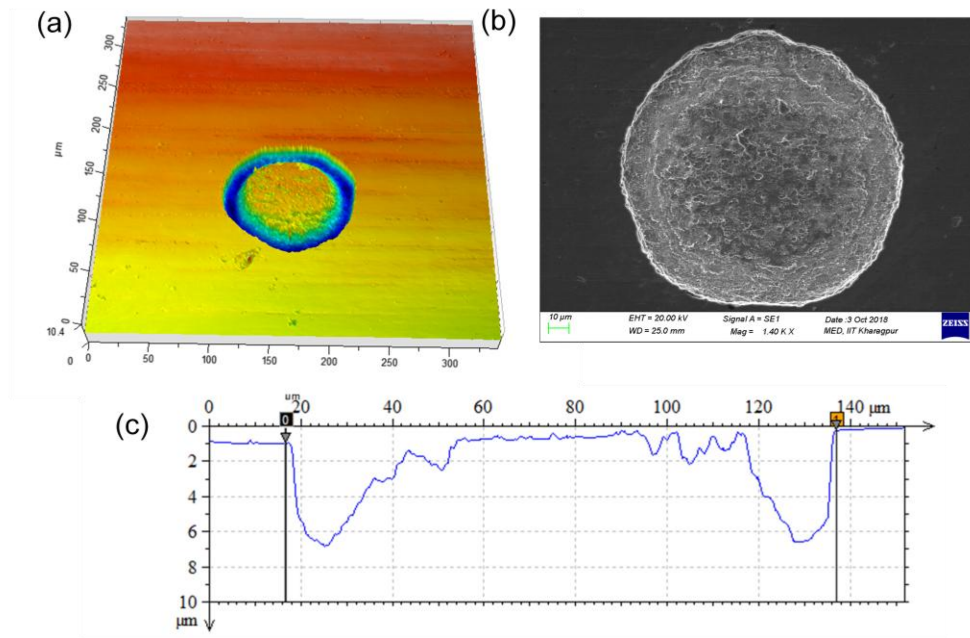

Figure 6.1: (a) 3D optical profile of a dimple machined at 8 V with 10%NaCl + 10%$NaNO_3$ showing island at the centre (b) SEM Micrograph of the generated micro-dimple (c) The cross sectional shape of the micro-dimple

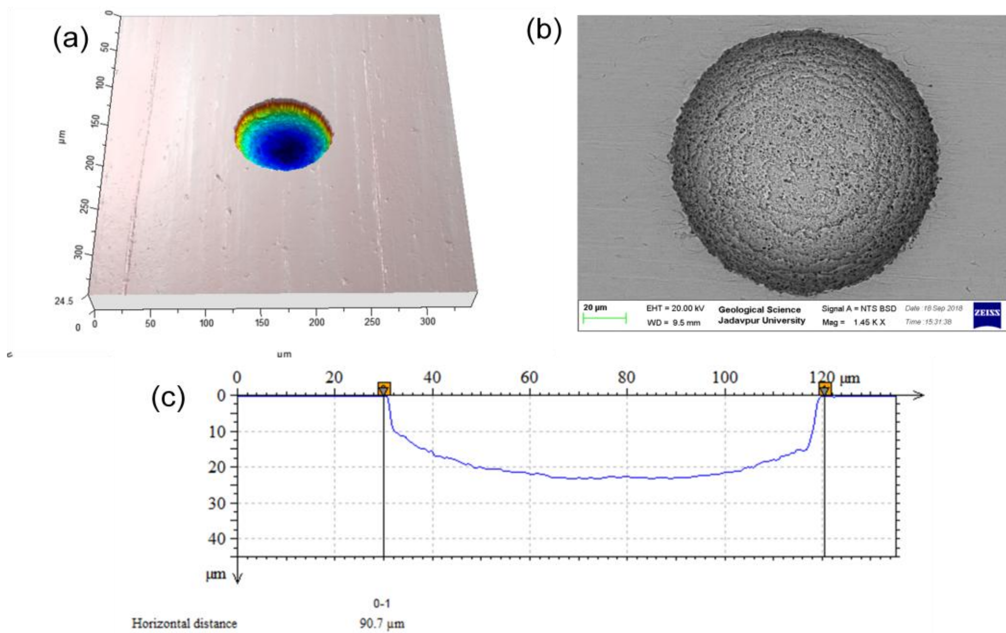

Figure 6.2: 3D optical profile of a good micro-dimple machined at 12 V with 10%NaCl + 10%$NaNO_3$ (b) SEM Micrograph of the generated micro-dimple (c) The cross sectional shape of the micro-dimple

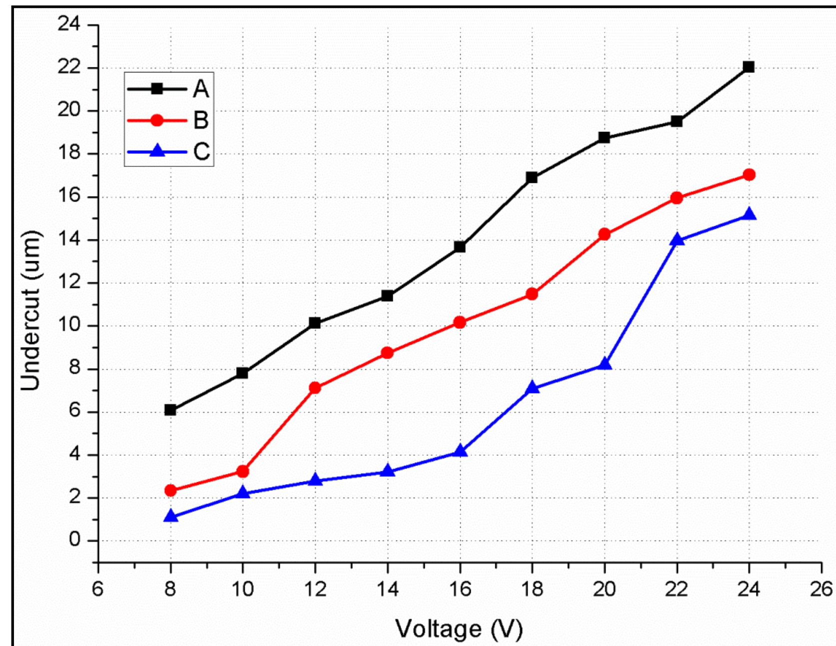

Figure 6.3: Effect of Voltage on Undercut considering three different electrolytes
A: 10%NaCl + 10%$NaNO_3$, B: 10%$NaNO_3$, C: 20%$NaNO_3$

Three different electrolytes viz. 10%NaCl + 10%$NaNO_3$, 10%$NaNO_3$, 20%$NaNO_3$ have been considered while carrying out the present research work. It could be found from the results that higher values of undercut could be noticed when TMEMM have been conducted by the mixed electrolyte concentration of 10%NaCl and 10%$NaNO_3$ followed by 10%$NaNO_3$ and 20%$NaNO_3$ respectively. The reason behind the nature of the material removal for the mixed electrolyte has already been detailed in Chapter 4. Since, $NaNO_3$ is passivating in nature, so, it forms a passivating layer over the material surface leading to improvement in accuracy during machining. As such, the undercut values for the samples TMEMMed with 10%$NaNO_3$ and 20%$NaNO_3$ are quite lower than that of the mixed electrolyte.

6.4.2 Influence of applied voltage and electrolyte type on dimple depth (h)

Figure 6.4 shows the depth variation in micro dimples at different machining voltages under three electrolytes. It could be observed that as the voltage increases from 8 to 24 V, there is a constant increase in the value of the average dimple depths. The concept of threshold voltage is also quite clear from the nature of the graphs which reveals a sudden hike in the depth values at or after 12 V with respect to micro dimples machined at 8 or 10 V. As the voltage increases, the material removal increases proportionately. With the duty ratio being 20%, the material removed gets sufficient time to leave the machined surface leading to a crater, which increases as the voltage increases. However, after 12 V, a continual increment in the depth values could be observed till 24 V.

Among the three electrolytes used, samples machined with 10% $NaNO_3$ shows the least values of average micro dimple depths ranging from 8.32µm to 29.06µm (from 12 V to 24 V).The values at 8 V and 10 V have not been considered due to the presence of islands inside the micro-dimple surface as already shown in fig. 6.3. Samples micro-machined with 20% $NaNO_3$ electrolyte shows dimple depth values that are in close proximity with the values of 10% $NaNO_3$ starting with 8.32 µm and ending with 29.06 µm. Higher range of dimple depths comes with the micro dimples which have been textured with the mixed electrolyte combination.

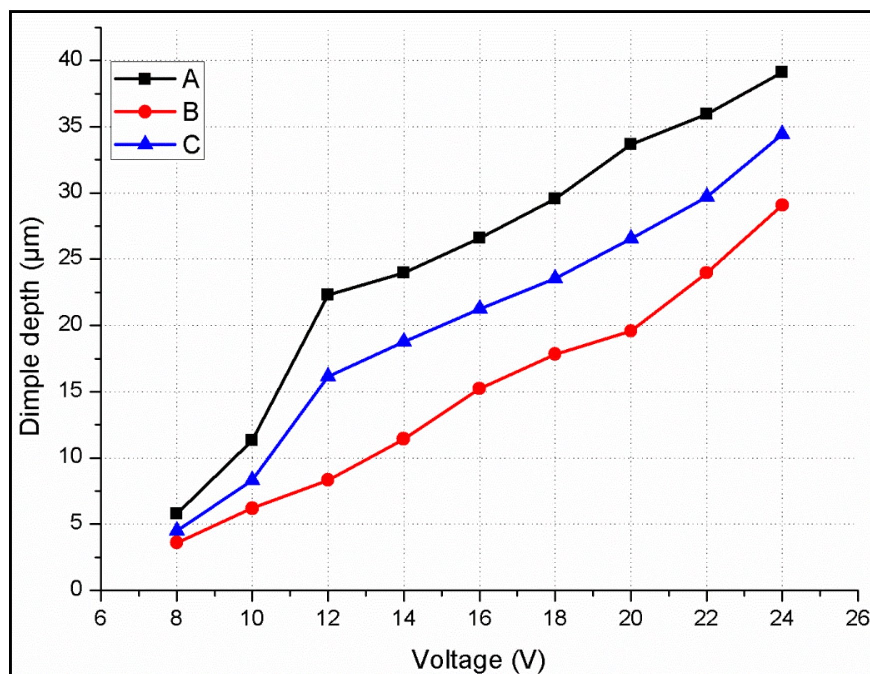

Figure 6.4: Variation of dimple depth with voltage and three different electrolytes
A: 10% NaCl + 10% $NaNO_3$, B: 10% $NaNO_3$, C: 20% $NaNO_3$

Figure 6.5 (a) shows the microscopic image of arrayed micro-dimple pattern along with two micro-dimples generated with an electrolyte concentration of NaCl (10%) + $NaNO_3$ (10%). It could be seen that dimensional uniformity is being maintained in the generated array. From the measurement achieved through non-contact profilometer, the average dimple diameter has been found to be 25 µm as illustrated in fig. 6.5 (b).

This average diameter of the micro-dimples reduces to 15 µm when TMEMM was carried out with 20% $NaNO_3$ electrolyte concentration as shown in figs. 6.5 (c) and (d) and gradually diminishes to 10 µm when machining was accomplished with 10% $NaNO_3$ electrolyte concentration as depicted in figs. 6.5 (e) and (f). In all the three cases, machining accuracy in

the form of dimensional uniformity is being maintained which is reflected from the microscopic and profilometric images of the micro-textured patterns.

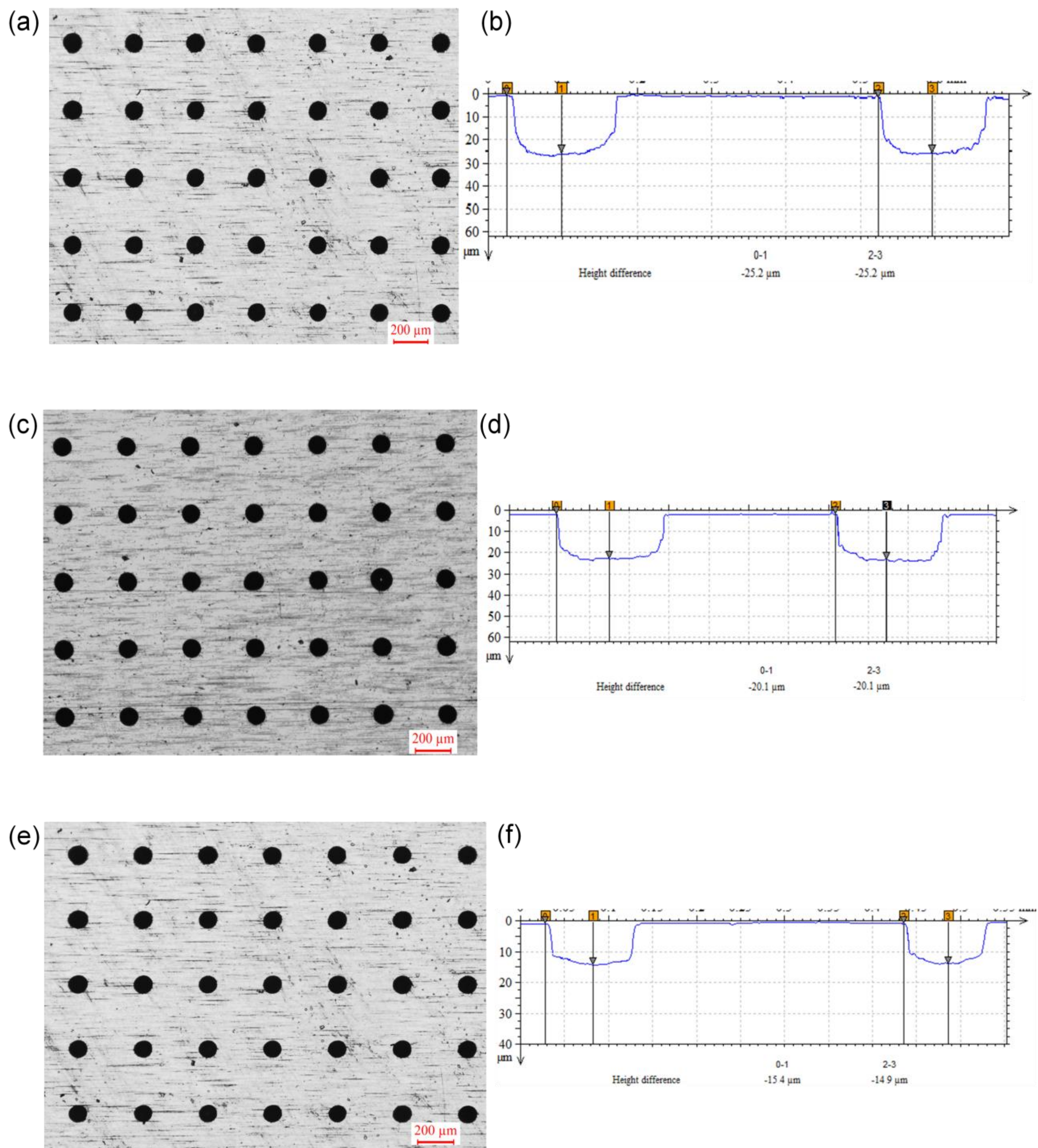

Figure 6.5: Microscopic Images of micro-dimple array generated at 16 V by (a) 10%NaCl + 10%$NaNO_3$ (c) 20%$NaNO_3$ (e) 10%$NaNO_3$ and corresponding profilometer measurements (b), (d) and (f) showing cross sectional view of the depths generated in the micro-dimples after 120 s

As discussed in earlier chapters, the aspect ratio (AR) is the sole parameter which strongly influences the shape evolution of the micro dimples generated during TMEMM and signifies

the quality of machining depth of a micro-dimple. Control of AR has been believed to be challenging task in TMEMM. AR can be mathematically evaluated from eq. 6.1, which is the ratio of dimple depth (h) with the diameter of the dimple (d) generated after machining.

$$\mathbf{AR} = {}^{\boldsymbol{h}}/_{\boldsymbol{d}} \qquad 6.1$$

It was reported in earlier researchers that proper machining in TMEMM could be achieved only with high aspect ratio masks. As such, researchers utilized masks of relatively larger thicknesses (250 µm) to achieve microstructures with uniform geometry as well as topography. In this methodology, mask of 20 µm thickness have been utilized and studied with three electrolytes for fabrication of micro-dimple array with comparatively high aspect ratio.

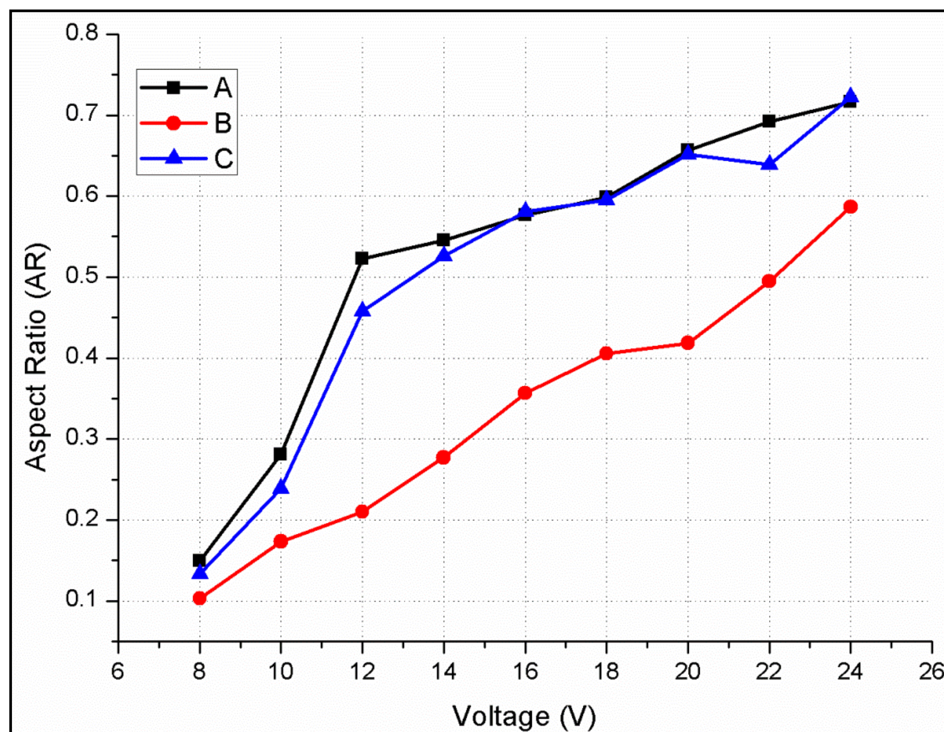

Figure 6.6: Impact on AR of the generated micro-dimples with voltage variation using three electrolytes during TMEMM (A: 10%NaCl + 10%$NaNO_3$, B: 10%$NaNO_3$, C: 20%$NaNO_3$)

It could be observed from fig. 6.6 that AR values of the micro-dimples generated by 10%NaCl + 10% $NaNO_3$ electrolyte and 20% $NaNO_3$ electrolyte are quite close to each other. Even the AR values of the two graphs nearly matches at 16, 18, 20 and 24 V respectively. On the other hand, the AR values of 10% $NaNO_3$ electrolyte bears a lower range of data than the other two starting with 0.103 and ending with 0.564. The nature of the graph is in accordance with fig. 6.4 where machining accuracy is being prioritized over material removal and the

least range of values for dimple depths were located with samples which have undergone TMEMM with 10% $NaNO_3$ electrolyte.

6.4.3 Influence of applied voltage on surface quality

After completion of the TMEMM process, the fabricated micro-dimple surface have been analyzed under the Talysurf CCI Non-Contact Profilometer (Taylor Hobson) to carry out investigation about the predominant surface roughness parameters, R_a and R_q inside the profile of the generated micro-dimples.

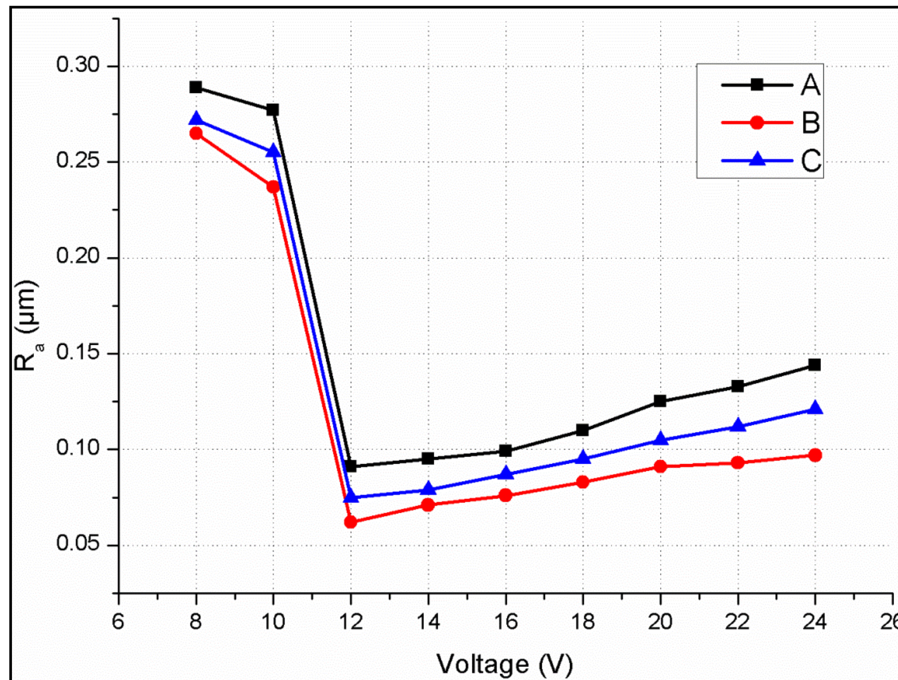

Figure 6.7: Effect of Applied Voltage on Ra under three different type and concentration of electrolyte, A: 10% NaCl + 10% $NaNO_3$, B: 10% $NaNO_3$, C: 20% $NaNO_3$

Figure 6.7 explains about the variation in the surface roughness characteristics, R_a of the textured micro-dimples at different machining voltages. As the voltage is increased from 8 V to 12 V, due to existence of islands in the vicinity of the micro-dimples, R_a decreases rapidly from 0.289 μm to 0.091 μm and then after reaches 0.144 μm at 24 V for the mixed electrolyte combination of 10% NaCl + 10% $NaNO_3$. Due to presence of more number of passivating ions in 20% $NaNO_3$, the surface accuracy of the said micro-dimples are on a slightly lower side than that of the samples machined with 10% $NaNO_3$. It could be inferred from the findings that best surface quality has been observed at threshold voltage (12 V) in all the three electrolytes which comes to 0.075 μm for electrolyte C but reduces to 0.062 μm for samples machined with electrolyte B.

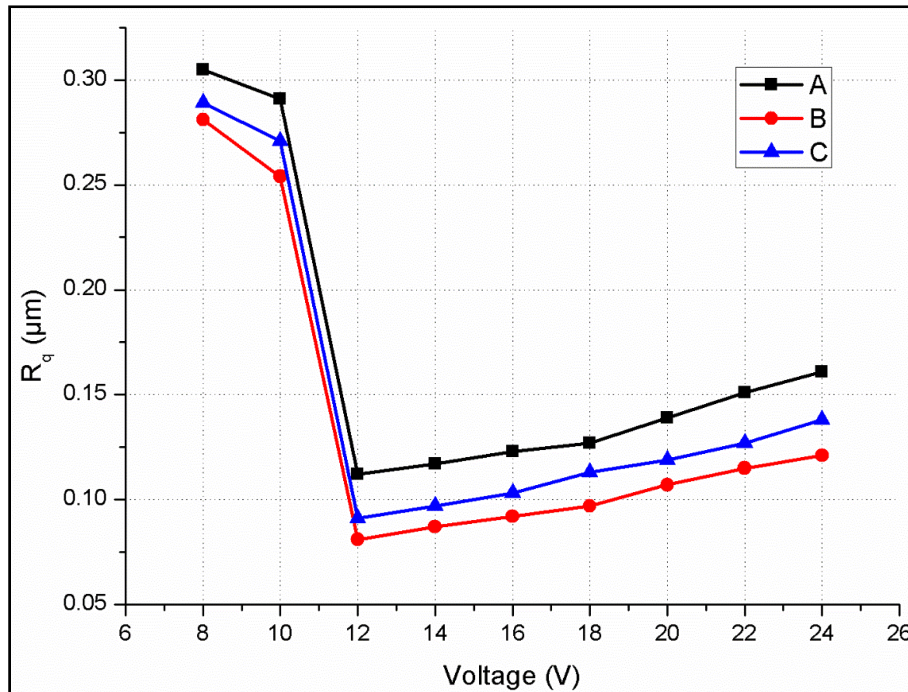

Figure 6.8: Effect of Applied Voltage on R_q under three different type and concentration of electrolyte, A: 10%NaCl + 10%$NaNO_3$, B: 10%$NaNO_3$, C: 20%$NaNO_3$

Figure 6.8 plots the variation in R_q with gradually increasing applied voltage. When the applied voltage is increased from 8 V to 24 V, R_q decreases from 0.305 µm at 8V to 0.112 µm at 12 V and then increases finally to 0.161 µm at 24 V for the mixed electrolyte combination of 10%NaCl + 10%$NaNO_3$. This initial decrease could be attributed to the presence of islands in the vicinity of the dimple surface, which is neutralized when the voltage reaches the threshold voltage, 12V. As such, lowest R_q has been observed at 12 V in all the three electrolytes which measures to 0.091 µm for electrolyte C in comparison to 0.081 µm for samples where texturing is carried out with electrolyte B.

6.5 Fabrication of high aspect ratio (HAR) micro-textured array of circular dimples based on experimental analysis

The experimental findings indicate that, with different machining parameters, the proposed methodology of TMEMM is feasible enough to fabricate accurate (possessing least undercut and higher depths) high-aspect-ratio micro dimples maintaining dimensional uniformity to be utilized in various tribological as well as other engineering applications. Moreover, electrolyte type and concentration as well as applied voltage have a significant influence on the generated micro-dimple dimensions.

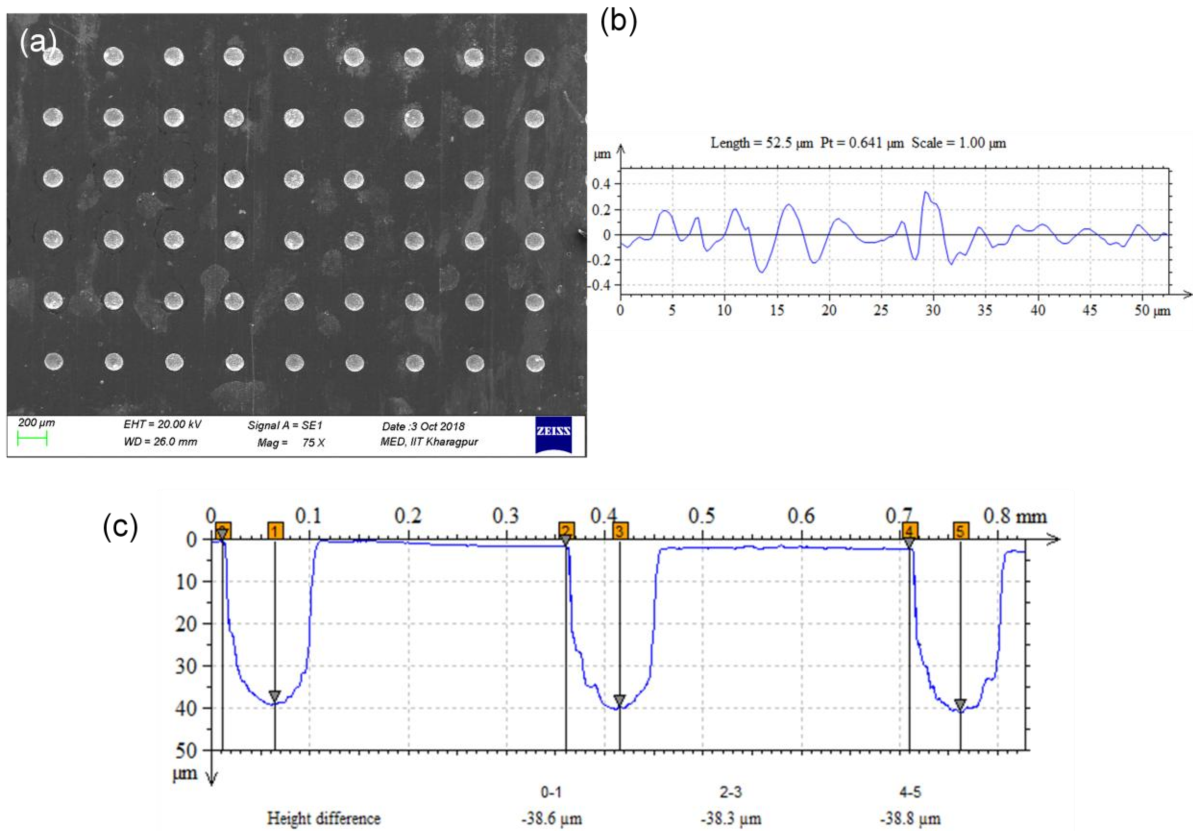

Figure 6.9: (a) SEM micrograph of micro-dimple array generated at 24 V with 10% NaCl + 10% $NaNO_3$ electrolyte (Electrolyte A) (b) Surface profile generated by TMEMM (c) Profilometer representation showing cross sectional view of the micro-dimple depths

Figure 6.9 shows the SEM micrograph of the micro-dimple array fabricated with the mixed electrolyte combination where (a) depicts a 9x6 matrix of micro-patterned structures, (b) symbolizes the surface profile of the one of the micro-dimples achieved after machining and (c) depicts the cross sectional depth profiles of the micro-dimples obtained from 3D non contact profilometer. The fabricated circular micro-textures possess depths in the range of 40 µm with a diameter of 109 µm leading to an AR of 0.7167.

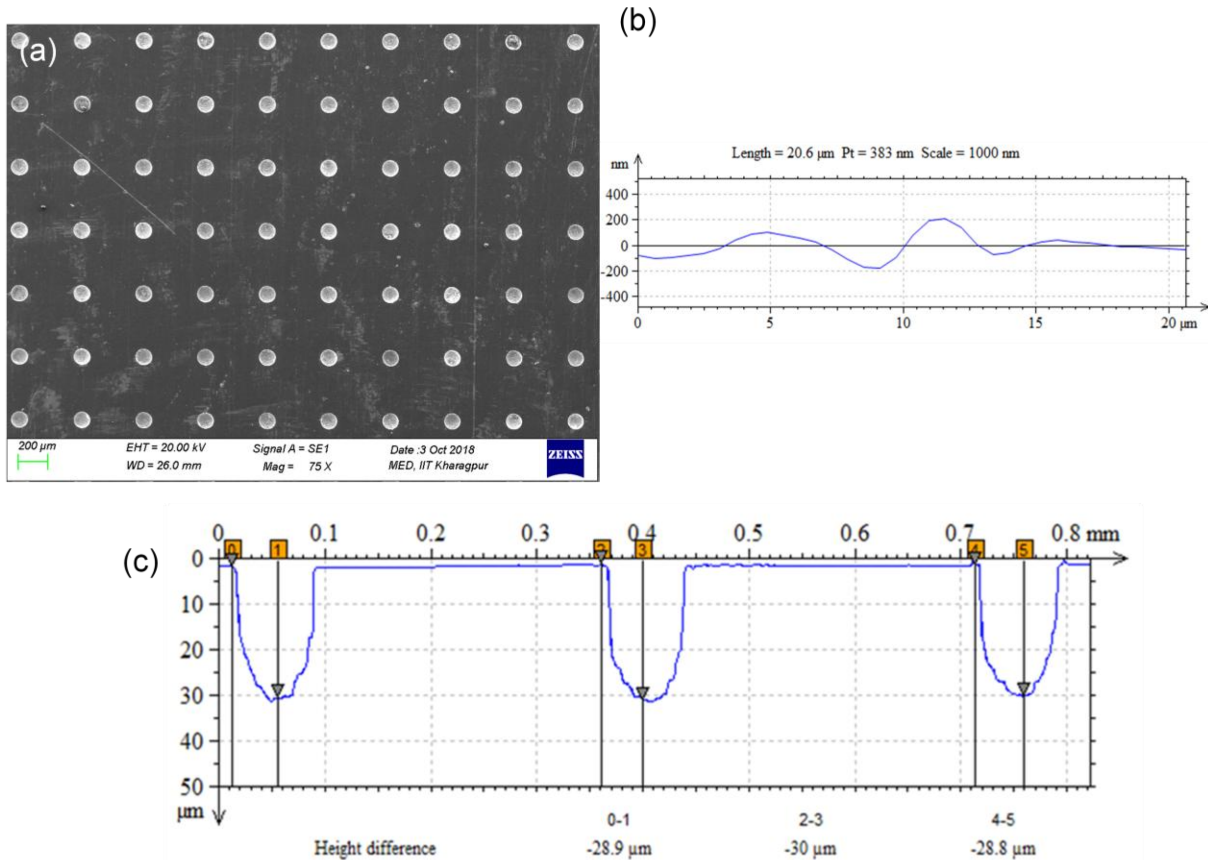

Figure 6.11: (a) SEM micrograph of micro-dimple array generated at 24 V with 10% $NaNO_3$ electrolyte (Electrolyte C) (b) Surface profile generated by TMEMM (c) Profilometer representation showing cross sectional view of the micro-dimple depths

When the same input parameters were considered TMEMM with 10% $NaNO_3$ electrolyte, the average dimple depths reduces to around 30 µm. However, there is a significant reduction in the dimple diameter, which results in AR of 0.5867. Figure 6.10 shows the micro-profiles fabricated under the said experimental conditions in which (a) expresses a 10x7 matrix of the micro-dimple pattern generated by TMEMM, (b) shows the quality of the dimple surface after machining and (c) represents the cross sectional profiles of the micro-dimple depths. The micro-dimples generated by 10% $NaNO_3$ electrolyte are of lesser diameters as compared with the micro-dimples generated by 10% NaCl + 10% $NaNO_3$ electrolyte, which can be observed from fig. 6.10 (a) and fig. 6.10 (c) respectively.

6.6 Analysis based on Friction Tests

In order to evaluate the effectiveness of the micro textured surface with high aspect ratio micro-dimples, in-depth investigation into the values of friction coefficient under three normal loads were carried out using four different types of samples: (i) Non-dimpled sample, (ii) textured sample containing average dimple depths of 15 µm, (iii) textured sample

containing average dimple depths of 20 μm and (iv) textured sample containing average dimple depths of 25 μm. Friction tests were carried out both under dry as well as wet conditions.

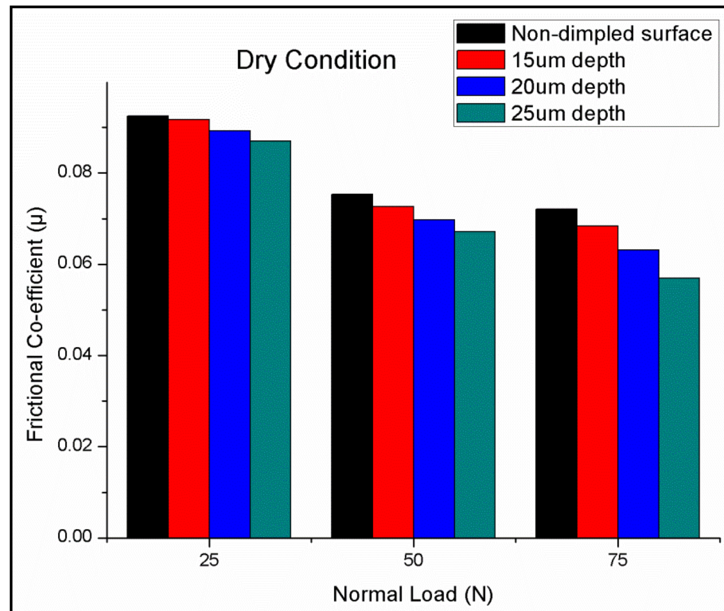

Figure 6.11: Effect of micro-dimple array on frictional co-efficient under different normal loads considering dry condition

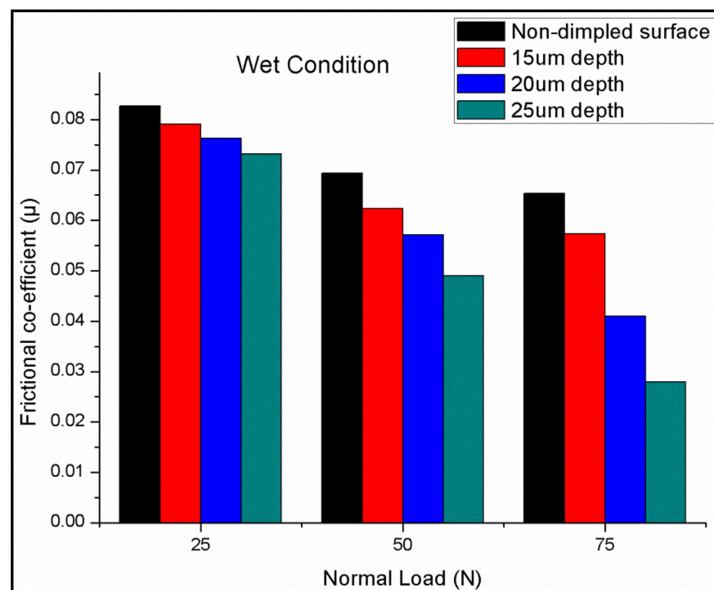

Figure 6.12: Effect of micro-dimple array on frictional co-efficient under different normal loads considering wet condition

The friction test results under dry condition and wet condition for the non-textured surface as well as samples with micro-textured array possessing different depths have been represented

in fig. 6.11 and fig. 6.12 respectively. Remarkable variations could be noticed in the friction behavior in tests with un-textured and textured surfaces.

With the application of lubricating oil, a noticeable reduction in the coefficient of friction could be noticed. When the load is gradually increased from 25 N to 50 N and finally to 75 N, the frictional coefficient reduces from 0.0791 to 0.0573 in case of micro-samples possessing dimples of 15 µm depth (average). This can be elaborated that, with the increase in normal load (N), there is an increase in contact area between the textured surface and the load which finally results in decrease in the frictional coefficient. Since, lubricant stored within dimples plays a significant role in minimization of the friction; the co-efficient of friction further reduces from 0.0763 to 0.041, when textured samples having average micro dimple depth of 20 µm are tested under different loads. These value further decreases from 0.0732 to 0.028 for micro-dimpled surface having a texture depth of 25 µm. Moreover, it could be stated that with the increase in normal load, there is a considerable reduction in the coefficient of friction for patterned samples with average depths of 15 µm and 25 µm respectively. Hence, it could be verified that the circular micro-textured array especially that with high-aspect-ratio possess a great potential during friction reduction as it can be seen that the beneficial effect of micro-dimples enhanced as the dimple depth increases.

6.7 Outcomes of the experimentation

From the outcomes, it has been observed that machining voltage of 12 V and above is sufficient to achieve continuous controlled dissolution. It was experimentally observed that patterned arrays containing micro-dimples with comparatively high-aspect-ratio have been successfully generated with this cost-effective technique of TMEMM utilizing 20 µm masked specimens and machining for 120 s. The result showed that with the increase in applied voltage, while the undercut and the depth of the micro dimples increases, both R_a and R_q initially decreases till 12 V and then gradually increases, although noticeable machining can be observed when applied voltage reaches 12 V.

When TMEMM have been carried out with same parametric settings, lowest range of undercut could be found with the samples machined with an electrolyte concentration of 20%$NaNO_3$ while the combination of 10%NaCl and 10%$NaNO_3$ have been analyzed to be the best electrolyte for achieving highest range of depths. Further, 10%$NaNO_3$ have been found out to be most suitable for achieving micro-dimples possessing best surface quality. 20%$NaNO_3$ have been found out to be best electrolyte for achieving highest aspect ratio microstructures among the three electrolyte combinations. Friction test results revealed that

dimpled high aspect ratio micro-textured surfaces play a significant role in reducing the co-efficient of friction. Further, surfaces with patterned micro arrays considerably reduce frictional coefficient when subjected to increased normal loads.

A comparatively economic and faster method of fabrication of micro-dimples possessing high-aspect-ratio have been experimentally investigated. A greater range of applied voltage along with different type and concentration of electrolyte have been studied during the experimentation schedule. However, it is felt that pulse frequency in a broader range need to be studied for achieving high-aspect-ratio micro-dimple patterned textures with least undercut and surface roughness and increased depth. As such, design of experiments needs to be carried out for searching out the parametric combinations for improving the machining accuracy and surface characteristics of the micro-dimples generated by TMEMM.

Chapter 7

EXPERIMENTATION FOR OPTIMIZING MACHINING ACCURACY AND SURFACE CHARACTERISTICS DURING CIRCULAR MICRO-TEXTURED PATTERN GENERATION

7.1 Introduction

The appealing and enigmatic properties of biological surfaces motivate people that a smooth surface is not always the best. Currently, the patterns of micro-dimples have attracted more attentions since such closed micro-textures with optimal dimensions are of high demand in several industries including electronics, aviation, medical etc. The advanced manufacturing techniques provide precision and freedom for the fabrication of micro-dimples, which enables the optimization of dimple geometry and distribution to achieving better tribological performances. Through Mask Electrochemical Micromachining (TMEMM) is one of the processes which provide the simplest guide way in achieving the requisite objectives of this engineering world.

Considering the present research objectives and findings achieved from previous chapters, the experimental studies and investigation have been planned to conduct successful research analysis for deriving effective research findings in context with the outcomes of the experimentation. The experimental planning is aimed at the generation of circular array of micro-dimples that cater the needs of micro-texturing in various industrial applications and studies the effect of different TMEMM process parameters such as applied voltage, pulse frequency and duty ratio on optimization of individual micro-dimple criterions i.e. machining accuracy (undercut and dimple depth) of the generated micro-dimple array, and surface roughness (R_a) of the generated micro-dimples. Taguchi Methodology is utilized for searching out the most favorable TMEMM process parameters through Design of Experiments (DOE) to achieve desired level of performance criteria through optimization of responses. Grey Relational Analysis (GRA) has been further applied to search out the best parametric combination that considers optimization of the desired responses simultaneously for accurate and precise micro-dimple array generation as well as gradation of the different parametric combinations and conduction of the optimal experiment to justify the genuinity of the findings.

7.2 Experimental design based on Taguchi method

During early 1960s, Dr. Genichi Taguchi developed the foundation of robust design and validated its basic philosophies [71, 72]. Taguchi's methodology provides the designer with a systematic and efficient approach for conducting small number of experiments to determine near optimum settings of design parameters. The main important task to be performed in robust design is measurement of quality during design and development, and efficient experimentation to find dependable information about the design parameters. Taguchi's method utilizes orthogonal arrays to study a large number of variables with a small number of experiments. The conclusions drawn from these small numbers of experiments are valid over the entire experimental range of the control factors and their settings. The method can reduce the research and development cost by simultaneously studying a large number of parameters. Taguchi method uses a statistical measure of performance called signal-to-noise ratio (S/N ratio), which is dependent on the quality characteristics to be optimized. The signal-to-noise ratio takes both mean and variability into account. After performing the statistical analysis of S/N ratio, an analysis of variance (ANOVA) needs to be employed for estimating error variance and for determining relative importance of various factors. Using the Taguchi method for parameter design, the predicted optimum setting need not correspond to one of the rows of the matrix experiment. Therefore, a confirmation experimental run using the predicted optimum levels for the control parameters being studied. The purpose is to verify the optimum conditions suggested by the matrix experiments do indeed give projected improvement. If the suggested and projected optimum values match, the suggested optimum condition will be adopted.

An orthogonal array for a particular robust design project can be constructed with the help of MINITAB software from the knowledge of the number of factors, their levels, and specific interactions. During this experimentation, L_9 orthogonal array have been performed according to the need. In L_9 array, 9 rows representing the 9 set of experiments, are to be conducted with 3 (three) columns at 3 (three) levels of the corresponding factors.

7.2.1 Signal-to-noise (S/N) ratio curve

S/N ratio is a mathematically transformed form for quality/performance characteristics, the maximization of which minimizes the quality loss and also improves (statistically) the additivity of control factor effects. For precision manufacturing, the objective is to minimise the actual value of performance characteristics in which smaller value indicates the better machining performance and it is addressed as "smaller the better" type problem. Similarly,

the actual value of performance characteristics in which higher value indicates the better machining performance and it is addressed as "higher the better" type problem. Thus minimisation of quality losses is equivalent to maximization of signal to noise ratio (S/N ratio).

In order to obtain optimal machining performance the "larger-the-better" quality characteristics, the S/N ratio for responses for j^{th} experiment is represented in eq. 7.1 as

$$\eta_j = -10 * \log_{10}\left(\frac{1}{n}\sum_{i=1}^{n}\frac{1}{{y_{ij}}^2}\right) \qquad 7.1$$

Similarly, in order to obtain optimal machining performance the "smaller-the-better" quality characteristics, the S/N ratio for responses for j^{th} experiment can be defined in eq. 7.2 as

$$\eta_j = -10 * \log_{10}\left(\frac{1}{n}\sum_{i=1}^{n}{y_{ij}}^2\right) \qquad 7.2$$

Where n is the number of replications and y^{ij} is the value of responses of ith replication test for j^{th} experimental condition.

7.2.2 Analysis of variance (ANOVA)

Different factors affect the performance to a different degree. The relative magnitude of the factor effects could be judged from the average S/N ratio for each factor level. A better feel for the different factors can be obtained by the decomposition of the variance, which is commonly known as analysis of variance (ANOVA).

ANOVA is used to investigate the machining parameters that have affected the observed values significantly. In this investigation, the analysis of variance (ANOVA) has been performed to determine the machining parameter, which has significant effect on the machining characteristics and also to find out the relative contribution of the machining parameters in controlling the responses of the TMEMM process. To accomplish ANOVA, the total sum of square deviation (SS_T) from the total mean S/N ratio (η_m), mean square (MS_i), sum of squares due to error (SS_E), mean square due to error (MS_E), variance ratio (F) and percentage of contribution (%) of each factor to the performance characteristics can be determined as:

$$\eta_m = \left(\sum_{j=1}^{N}\eta_j\right) / N \qquad 7.3$$

$$SS_i = \sum_{j=1}^{P}(\eta_m - \bar{\eta}_i)^2 \qquad 7.4$$

$$MS_i = \frac{SS_i}{DOF} \quad 7.5$$

$$SS_T = \sum_{j=1}^{P} (\eta_j - \eta_m)^2 \quad 7.6$$

$$SS_E = SS_T - SS_i \quad 7.7$$

$$MS_E = \frac{SS_E}{DOF} \quad 7.8$$

$$F = \frac{MS_i}{MS_E} \quad 7.9$$

$$P(\%) = \frac{SS_i}{(SS_T - SS_E)} \times 100\% \quad 7.10$$

Where,

N, Total number of experiments

η_j, S/N ratio at each parametric combination and

η_m, Grand mean of S/N ratio.

DOF, Degrees of Freedom

p, Number of main design parameter that affects the quality characteristics

$\bar{\eta}_i$, Mean S/N ratio at the optimal level

SS_i, Sum of square of ith replication

MS_i, Mean square of ith replication

SS_T, Total sum of square

SS_E, Sum of square due to error

MS_E, Mean square due to error

F, Variance ratio

P (%), percentage contribution (%) of each factor to the performance characteristics

7.2.3 Verification of experiments

The optimal combination level of machining parameters has been determined from the matrix experimentation. The final step is to predict and verify the improvement of the observed values through the use of optimal combination level of machining parameters. The predicted S/N ratio, η_{opt} can be calculated from eq. 7.11 as:

$$\eta_{opt} = \eta_m + \sum_{j=1}^{p} (\bar{\eta}_i - \eta_m) \quad 7.11$$

The difference between the optimal η (η_{opt}) calculated from the eq. 7.11 and experimental η obtained after texturing at optimal parametric conditions signify the authentication of experiments.

7.3 Planning for Taguchi based experimentation

Influence of significant process parameters i.e. applied voltage, pulse frequency and duty ratio on machining performance i.e. undercut, dimple depth and surface roughness were considered for Taguchi based experimentation during machining of patterned micro-dimple array. Specific experimental planning for Taguchi based experimentation has been discussed in this section. Keeping the aspect ratio of the micro-textures in mind, the undercut and surface roughness have been expected to be minimized and the depth has been expected to maximize. The detailed experimental conditions are shown in Tables 7.1 and 7.2.

Table 7.1: Variable machining parameters with their levels

Factors	**Symbol**	**Unit**	**Level 1**	**Level 2**	**Level 3**
Applied voltage (V)	1	V	10	11	12
Pulse frequency (kHz)	2	kHz	1	2	3
Duty ratio (%)	3	%	10	15	20

Table 7.2: Fixed machining parameters during experiments

Average diameter of micro-holes on the mask	65 µm
Thickness of the patterned mask	20 µm
Workpiece	SS 304
Thickness of the workpiece	200 µm
Material of the Mask	AZ 4903
Inter Electrode Gap (IEG)	2000 µm
Flow Velocity	3.8 m/s
Concentration of Electrolyte	NaCl (10%) + $NaNO_3$ (10%)
Machining Time	120 s

For analyzing the experimental responses based on Taguchi methodology, MINITAB software has been utilized.

7.4 Procedure of experimentation

The detailed procedure followed during the complete execution of the experimentation and analysis has been detailed in Section 4.5.2 in Chapter 4. Experiments were carried out as per chalked out plan and the outcomes are recorded for every experimental run. Here, undercut, dimple depth and surface roughness have been considered as three performance criteria of the

fabricated micro-dimples where undercut has been calculated by calculating the difference in radius of a micro-dimple before (with mask) and after machining (upon mask removal). This was accomplished initially with the help of Leica DM2500 optical precision microscope. Precise measurements of depth along with the diameter of the generated micro-dimples were carried out with the help of Talysurf CCI Non-Contact Profilometer (Taylor Hobson). All the textured samples were finally examined under scanning electron microscope (Zeiss EVO 40) for obtaining images. Surface Roughness characteristics have also been achieved from the profilometer scans.

7.5 Experimental results and discussions

TMEMM process criterions were measured during micro-patterned array generation on stainless steel workpiece, after each set of experimental run based on experimental planning as exhibited in Table 7.3. The considered performance criterions of TMEMM are undercut, dimple depth and surface characteristics measured through R_a (Centre Line Average). The mathematical formulations as well as computations required for maximization or minimization of responses and other analyses of the experimental data as accomplished by utilizing software, “MINITAB”, are listed in Table 7.3.

7.5.1 Analysis based on S/N ratio curves

In robust design, Taguchi philosophy of orthogonal arrays determines the effects of various process parameters efficiently. The analyses of experimental results have been carried out based on the values of signal to noise (S/N) ratios. The term signal represents the desired mean value of the output parameters and the term noise signifies the undesirable value for the responses. Three categories of S/N ratio are lower-the-better, higher the better, and nominal-the-best. In order to attain the most favorable machining outcome for undercut, the lower-the-better quality characteristic is considered. Similarly for dimple depth, higher-the-better and for surface roughness, lower-the-better quality characteristic have been considered respectively. All these outcomes pertain to improvement in aspect ratio of micro-textures. The computations have been done using eqs. 7.1 and 7.2 respectively. The analysis has been carried out utilizing MINITAB.

Table 7.3: DOE with experimental results and respective S/N ratio of responses

Expt. No.	DOE			Undercut (µm)	S/N Ratio (dB)	Dimple depth (µm)	S/N Ratio (dB)	Surface Roughness (µm)	S/N Ratio (dB)
	V	kHz	%						
1	10	1	10	9.1055	-19.1861	19.83	25.9465	0.3522	9.0634
2	10	2	15	5.7377	-15.1747	11.46	21.1837	0.4542	6.8557
3	10	3	20	5.5392	-14.8689	16.14	24.1581	0.267	11.4698
4	11	1	15	10.4696	-20.3985	21.92	26.8168	0.2993	10.4598
5	11	2	20	11.0483	-20.8659	14.04	22.9473	0.476	6.4479
6	11	3	10	7.8404	-17.8867	17.58	24.9004	0.653	3.7017
7	12	1	20	18.2651	-25.2324	21.46	26.6326	0.1333	17.5050
8	12	2	10	6.1879	-15.8308	13.44	22.5680	0.547	5.2403
9	12	3	15	13.8909	-22.8546	21.84	26.7851	0.251	12.0065

(i) Parametric influence on undercut, U_c

Table 7.3 shows the experimental results for undercut and the corresponding S/N ratio. Since the experimental design is orthogonal, it is possible to figure out the effect of each machining parameter at different levels.

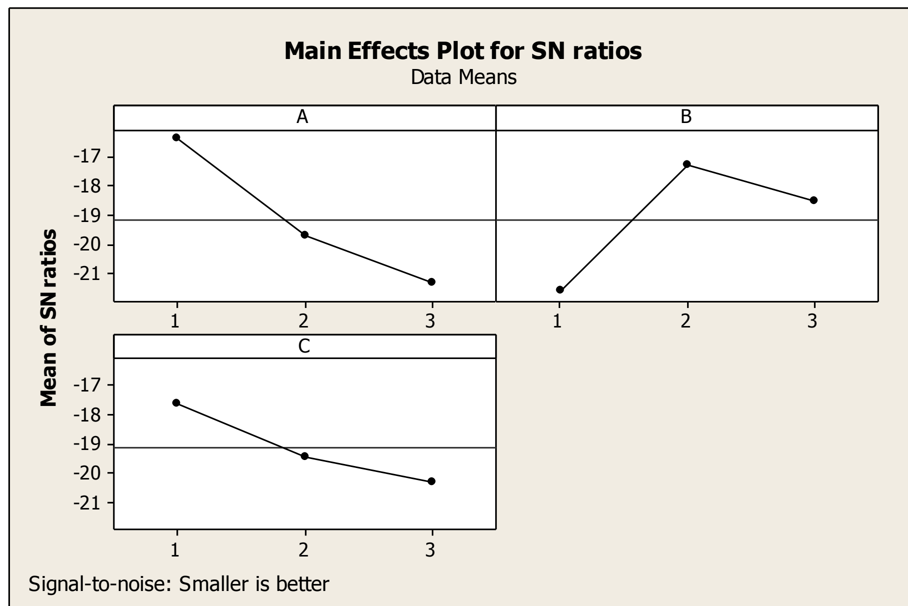

Figure 7.1: S/N Ratio graph for undercut

The average S/N ratio for each of the levels of all machining parameters taking undercut as response is graphically exhibited in fig. 7.1. The highest average S/N ratio gives the minimum undercut. It is clear from the S/N ratio response graph that for achieving minimum undercut, the optimum condition of machining is $A_1B_2C_1$ i.e., applied voltage of 10 V, pulse frequency of 2 kHz and duty ratio of 10%.

(ii) Parametric influence on dimple depth, D_d

Table 7.3 also depicts the experimental results for average dimple depth and the corresponding S/N ratio for each experimental run. The mean S/N ratio for dimple depth for all the factors at different levels is determined. The S/N response graph for dimple depth is shown in fig. 7.2.

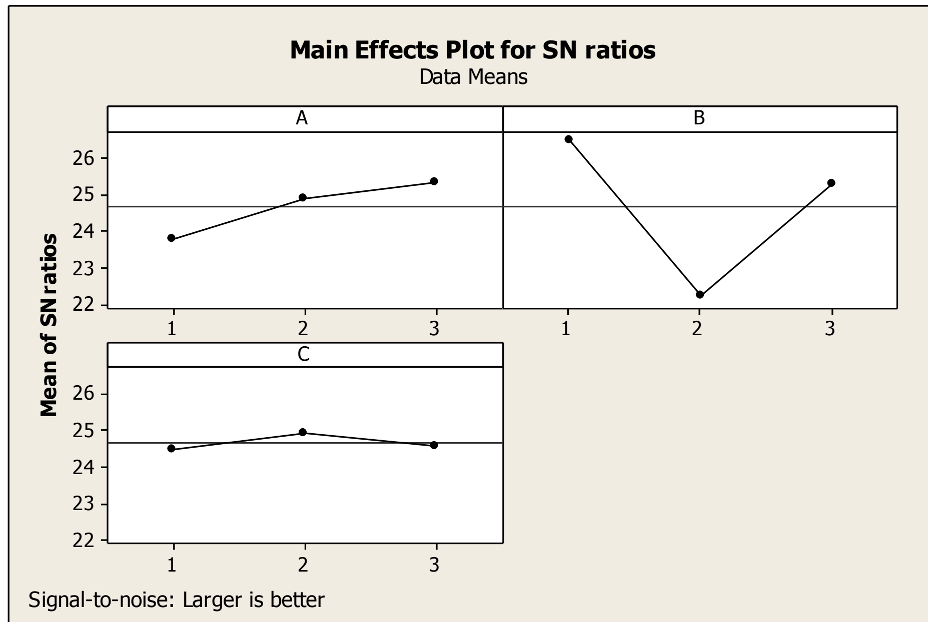

Figure 7.2: S/N Ratio graph for dimple depth

The greater average S/N ratio corresponds to the maximum depth. From the S/N ratio response graph, it can be concluded that the optimum parametric combination for maximization of dimple depth is $A_3B_1C_2$ i.e. applied voltage of 12 V, pulse frequency of 1 kHz and 15% duty ratio.

(iii) Parametric influence on surface roughness characteristics, R_a

The experimental results for R_a and the corresponding S/N ratio have been represented through Table 7.3. The mean S/N ratio for R_a for all the factors at different levels is determined. The S/N response graph for R_a is shown in fig. 7.3.

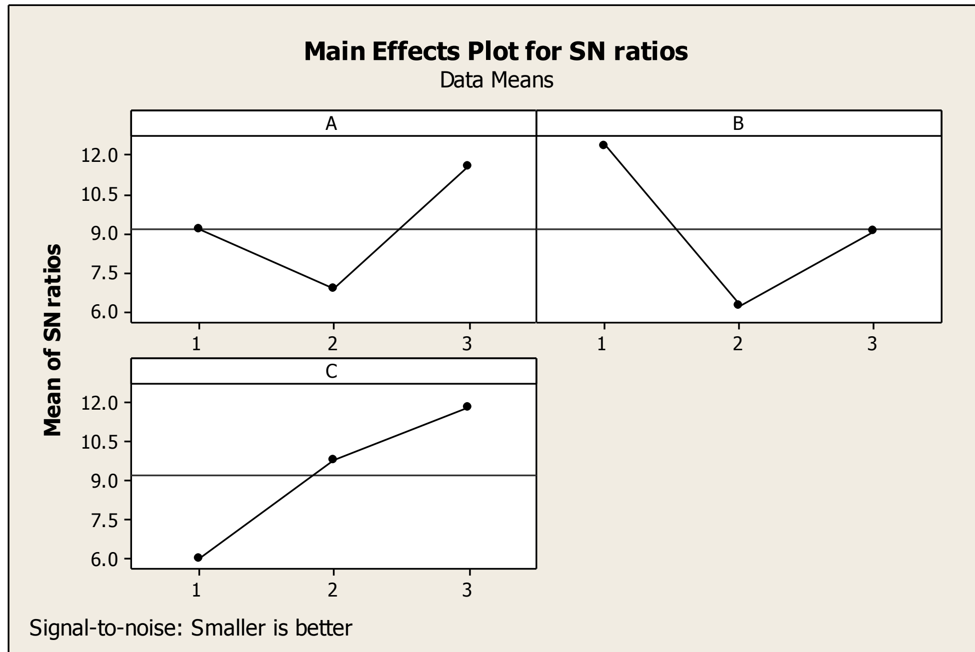

Figure 7.3: S/N Ratio graph for Surface Roughness (R_a)

The average S/N ratio for each of the levels of all machining parameters taking R_a as response is graphically exhibited in fig. 7.3. The highest average S/N ratio gives the minimum R_a. It is clear from the S/N ratio response graph that for achieving minimum R_a, the optimum condition of machining is $A_3B_1C_3$ i.e., applied voltage of 12 V, pulse frequency of 1 kHz and duty ratio of 20%.

7.5.2 Analysis of variance

In this investigation, the analysis of variance (ANOVA) has been performed to determine the significant machining parameters and to find the relative contribution of machining parameters in controlling the responses of the TMEMM process. To accomplish ANOVA, the total sum of squared deviation (SS_T) from the total mean S/N ratio (η_m) can be determined from eq. 7.6. The total sum of SS_T can be differentiated into two sources: (i) the sum of squared deviations due to each machining parameters (SS_A, SS_B and SS_C) and (ii) the sum of squared error (SS_E).

To perform F (variance ratio) test, the mean squared deviation due to each design parameter is calculated. The mean of squared deviation is equal to SS_T, divided by the number of DOFs associated with the design parameters. The value of F for each design parameter is the ratio of the mean squared deviation to the mean squared error. The percentage contribution by each of the design parameters is a ratio of the value of F of each design parameters to the total sum of the values of F for all the design parameters. Although the mathematical formulations involved in the accomplishment of ANOVA are shown in Eqs. 7.3 to 7.10, all

the data incorporated in the respective ANOVA tables have been taken after analysis in the software.

The result of ANOVA for undercut is shown in Table 7.4. The calculated value of F in ANOVA table is used to measure the relative effects of the factors. The larger the value of F, the more significant that factor becomes for controlling the responses of the TMEMM process. So the value of F can be utilized to rank order of the contribution of factors. From the results of ANOVA at Table 7.4, it is reflected that the applied voltage is the most influencing factor for controlling undercut. The pulse frequency follows the applied voltage in terms of percentage contribution, while duty ratio is the least contributor to the undercut during the generation of micro-dimple array in TMEMM.

Table 7.4: Results of ANOVA for undercut

Source	**Machining Parameter**	**DF**	**Seq SS**	**Adj MS**	**F**	**% contribution**
A	Applied voltage (V)	2	53.77	53.77	2.03	46.37
B	Pulse frequency (kHz)	2	39.02	39.02	1.47	33.65
C	Duty ratio (%)	2	23.16	23.16	0.87	19.98
Error		2	26.48	26.48		--------
Total		8	142.43			100

Table 7.5 shows the results of ANOVA for dimple depth, D_d. It is also found that the pulse frequency is the most inevitable as well as significant factor for controlling the dimple depth fabricated by TMEMM process, that contributes in bulk towards maximization of dimple depth. The applied voltage has mild effect on D_d followed by duty ratio compared to other machining parameters of the said process. The contribution order of the machining parameters for D_d is pulse frequency, applied voltage, duty ratio.

Table 7.5: Results of ANOVA for dimple depth

Source	**Machining Parameter**	**DF**	**Seq SS**	**Adj MS**	**F**	**% contribution**
A	Applied voltage (V)	2	14.916	7.458	2.93	12.31
B	Pulse frequency (kHz)	2	102.642	51.321	20.14	84.71
C	Duty ratio (%)	2	3.615	1.808	0.71	2.98
Error		2	5.096	2.548		-------
Total		8	126.270			100

The ANOVA results for R_a are tabulated in Table 7.6. It could be noticed from the table that the duty ratio contributes the most for shaping the dimple surface generated by through mask EMM. Although, the machining frequency has similar effect on R_a as duty ratio, while the impact of applied voltage can be considered to be the least as compared to other machining parameters.

Table 7.6: Results of ANOVA for surface roughness characteristics, R_a

Source	Machining Parameter	DF	Seq SS	Adj MS	F	% contribution
A	Applied voltage (V)	2	0.043687	0.021903	9.13	20.83
B	Pulse frequency (kHz)	2	0.080099	0.040050	16.69	38.18
C	Duty ratio (%)	2	0.085875	0.042938	17.89	40.99
Error		2	0.004800	0.002400		------
Total		8	0.214580			100

7.6 Single objective optimization of process parameters

The optimal parametric settings for different responses during generation of micro-dimple array are based on Taguchi method of robust design. The parameter settings of TMEMM process for achieving different optimum criterions i.e. for minimum undercut is applied voltage of 10 V, pulse frequency of 2 kHz and duty ratio of 10%; for maximum dimple depth is applied voltage of 12V, pulse frequency of 1kHz and 15% duty ratio; for minimum R_a is applied voltage of 12 V, pulse frequency of 1 kHz and duty ratio of 20% based on S/N ratio curves.

The predicted S/N ratio using the best machining parameters for undercut can then be obtained and the corresponding minimum undercut can be calculated using eq. 7.2. Table 7.7 shows a comparison of the predicted undercut with the actual undercut using the optimal machining parameter setting and a good agreement between the predicted and the actual undercut could be observed. The increase in S/N ratio from the initial machining parameters to the optimal parameters is 12.6554 dB which means that the undercut of the micro-dimple array decreases to 4.29 times of the initial value. An undercut of 7.3919 µm could be observed when TMEMM is conducted at the most favorable parametric combination of $A_1B_2C_1$ i.e., applied voltage of 10V, pulse frequency of 2 kHz and duty ratio of 10%.

Table 7.7: Results of confirmation experiment for undercut

	Initial Cutting Parameter	Optimal Machining Parameters	
		Predicted	Experimental
Level	$A_2B_2C_2$	$A_1B_2C_1$	$A_1B_2C_1$
Undercut (µm)	31.734	4.4907	7.3919
S/N Ratio	-30.0305	-13.0463	-17.3751

Improvement of S/N ratio = 12.6554 dB

Prediction error in S/N ratio = 4.3288 dB

Table 7.8: Results of confirmation experiment for dimple depth

	Initial Cutting Parameter	Optimal Machining Parameters	
		Predicted	Experimental
Level	$A_2B_2C_2$	$A_3B_1C_2$	$A_3B_1C_2$
Dimple Depth (µm)	9.656	23.4496	21.68
S/N Ratio	19.6959	27.4027	26.7212

Improvement of S/N ratio = 7.7068 dB

Prediction error in S/N ratio = 0.6815 dB

The predicted S/N ratio using the best machining parameters for the dimple depth can be obtained from eq. 7.1 and the corresponding maximum dimple depth can be calculated using eq. 7.2. Table 7.8 shows a comparison of the predicted dimple depth with the actual dimple depth using the optimal machining parameter setting and it could be observed that the predicted and the actual dimple depth are in good equivalence with each other. A comparison of the predicted dimple depth and the actual dimple depth using the finest machining parameter setting is shown in Table 7.9. The predicted dimple depth is consistent with the actual dimple depth. The increase in the S/N ratio from the initial to the optimal machining parameters is 7.7068 dB and therefore the improvement in dimple depth is 31% of the initial value.

Table 7.9: Results of confirmation experiment for R_a

	Initial Cutting Parameter	Optimal Machining Parameters	
		Predicted	Experimental
Level	$A_2B_2C_2$	$A_3B_1C_3$	$A_3B_1C_3$
Surface Roughness (µm)	0.421	0.1333	0.173
S/N Ratio	7.5144	17.505	15.239

Improvement of S/N ratio = 7.7246 dB

Prediction error in S/N ratio = 2.266 dB

An attempt has been made to generate a micro-patterned array of circular micro-dimples at overall optimal parametric setting i.e. 12 V, 1 kHz and 20% for achieving minimum R_a. The predicted S/N ratio using the optimal machining parameter for R_a can be obtained from eq.7.11 and the corresponding minimum R_a can also be calculated using eq.7.2. Table 7.9 shows a comparison of the predicted R_a with the actual R_a using the optimal machining parameter setting. It could be established that the predicted and the actual R_a complies with each other. The increase in S/N ratio from the initial machining parameters to the optimal parameters is 7.7246 dB which means that the improvement in R_a of the micro-dimple array is 0.248 μm with respect to the initial value.

7.7 Grey Relational Analysis

Grey relational analysis (GRA) as introduced by Deng [73] is an impacting measurement method in grey system theory that analyzes uncertain relations between one main factor and all the other factors in a given system. In the case when experiments are ambiguous or when the experimental method cannot be carried out exactly, grey analysis helps to compensate for the shortcomings in statistical regression. Grey relational analysis is actually a measurement of the absolute value of the data difference between sequences and it could be used to measure the approximate correlation between sequences.

In GRA, grey relational grade (GRG) is primarily employed to show the relationship between the sequences. If two sequences are the same, the corresponding GRG value becomes 1. The GRG value also measures the degree of influence that the comparability sequence has over the reference sequence. If a particular comparability sequence is more important than the other comparability sequences with respect to the reference, the GRG value for that comparability sequence and reference sequence will be higher than the other values. Thus, in GRA, multi-response variables are converted into a single GRG value, thus simplifying the optimization procedure. In the grey relational analysis, data pre-processing is first performed in order to normalize the raw data for analysis. The linear normalization of the experimental results is performed in the range between zero and unity, in order to reduce variability, and make the data dimensionless and comparable, which is also called the grey relational grading. Data pre-processing is thus a way of converting the original sequence to a comparable sequence. The following equations are applied for data pre-processing depending on the type of the considered criterion, i.e. eq. 7.12 for larger-the-better (higher values are preferred) and eq. 7.13 for smaller-the-better (lower values are desired) quality characteristics.

$$x_i^*(k) = \frac{x_i(k) - \min x_i(k)}{\max x_i(k) - \min x_i(k)} \quad i = 1,2,...,m \text{ and } k = 1,2,...,n \qquad 7.12$$

$$x_i^*(k) = \frac{\max x_i(k) - x_i(k)}{\max x_i(k) - \min x_i(k)} \qquad 7.13$$

Where $x_i(k)$ and $x_i^*(k)$ are the observed and normalized data respectively for i^{th} alternative and k^{th} criterion. After data normalization, the grey relational coefficient (GRC) is computed to express the relationship between the ideal (best) and the normalized data as expressed in eq.7.14.

$$\xi_i(k) = \frac{\Delta_{\min} + \zeta\Delta_{\max}}{\Delta_{0i}(k) + \zeta\Delta_{\max}} \qquad 7.14$$

Where $\Delta_{0i}(k)$ is the absolute value of the difference between $x_i^0(k)$ and $x_i^*(k)$ ($x_i^0(k)$ is the ideal sequence). The distinguishing coefficient (ζ) lies between 0 and 1, and is mainly responsible to expand or compress the range of GRC values. Generally, $\zeta = 0.5$ is preferred. On the other hand, $\Delta_{\min} = \forall j^{\min} \in i \forall k^{\min} \left\| x_0(k) - x_j(k) \right\|$ is the smallest value of Δ_{0i}; and $\Delta_{\max} = \forall j^{\max} \in i \forall k^{\max} \left\| x_0(k) - x_j(k) \right\|$ is the largest value of Δ_{0i}. A higher GRC value for an alternative indicates that it is closer to the optimal solution with respect to a particular criterion. The GRG value is then determined by finding out the average of the GRC values corresponding to each criterion as shown in eq. 7.15.

$$\gamma_i = \frac{1}{n} \sum_{k=1}^{n} \xi_i(k) \qquad 7.15$$

Where n is the number of criteria/attributes. A higher value of GRG for a particular alternative symbolizes its superiority over the others for a said application.

7.8 Multi objective optimization of the desired responses

GRA have been applied over the experimental data to search out for the most favourable combination of parameters that are responsible for simultaneous optimization of the desired responses i.e. minimization of undercut and surface roughness along with maximization of dimple depth. In the present study, minimum undercut and surface roughness, and maximum dimple depth are indications of better performance. For data pre-processing in the grey relational analysis process, dimple depth has been considered as the “higher is better”. Undercut and surface roughness criterion i.e. R_a were taken as the “lower is better”. All the sequences after data pre-processing using eq. 7.12 and 7.13 have been listed in Table 7.10.

Table 7.10: Normalized matrix for TMEMM process

Exp. No.	Experimental Data			Normalized Data		
	U_c (μm)	D_d (μm)	R_a (μm)	U_c	D_d	R_a
1	9.1055	19.83	0.35223	0.7198	0.80019	0.5787
2	5.7377	11.46	0.45417	0.9844	0	0.38257
3	5.5392	16.14	0.267	1.0000	0.44742	0.7427
4	10.4696	21.92	0.2993	0.6126	1	0.67935
5	11.0483	14.04	0.476	0.5671	0.24665	0.34056
6	7.8404	17.58	0.653	0.8192	0.58509	0
7	18.2651	21.46	0.133275	0.0000	0.95602	1
8	6.1879	13.44	0.547	0.9490	0.18929	0.20395
9	13.8909	21.84	0.251	0.3437	0.99235	0.77349

The grey relational coefficients and grade values for each experiment of the orthogonal array were calculated by applying eqs. 7.14 and 7.15 respectively. The grey relational co-efficient (GRC) and the grey relational grades (GRG) for the respective experimental runs have been shown in Table 7.11.

Table 7.11: GRC and corresponding GRG values for TMEMM process

Expt. No.	U_c	D_d	R_a	GRG
1	0.64083	0.71448	0.54271	0.63267
2	0.96976	0.33333	0.44746	0.58352
3	1	0.47502	0.66024	0.71175
4	0.56343	1	0.60927	0.72423
5	0.53596	0.39893	0.43124	0.45538
6	0.7344	0.5465	0.33333	0.53808
7	0.33333	0.91916	1	0.75083
8	0.90748	0.38147	0.38579	0.55825
9	0.43242	0.98493	0.68822	0.70186

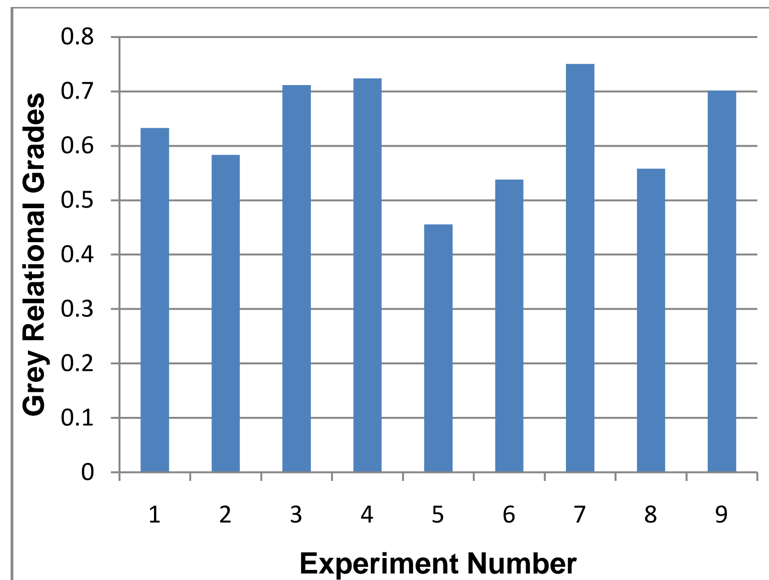

Figure 7.4: Bar Chart showing Grey Relational Grades of corresponding experiments

According to the performed experimental design, it is clearly observed from Table 7.11 that the experiment no. 7 has the highest grey relational grade. Therefore, experiment no. 7 provides the near optimal parametric combination for this TMEMM process for simultaneous optimization of all the three responses and is the optimal machining parameters' setting for minimum undercut, surface roughness and maximum dimple depth simultaneously (i.e. the best multi-performance characteristics) among the nine experiments.

In addition to the determination of optimum texturing parameters, the response table for the Taguchi method is used to calculate the average grey relational grade for each level of the TMEMM parameters. The procedure for calculation of average GRG for all levels is: (1) grouping the grey relational grades by factor level for each column in the orthogonal array; (2) taking the average of them. The average GRG values have been shown in Table 7.12.

Table 7.12: Response table for Grey Relational Grades

Process Parameters	Average Grey Relational Grade by factor level			Max-Min
	Level 1	Level 2	Level 3	
Applied voltage	0.64265	0.57256	**0.67031***	0.09775
Pulse frequency	**0.70258***	0.53238	0.65056	0.17019
Duty ratio	0.57633	**0.66987***	0.63932	0.09354

Since the grey relational grade represents the level of correlation between the reference sequence and the comparability sequence, the greater value of the grey relational grade means that the comparability sequence has a stronger correlation to the reference sequence at this level of the factor. In other words, regardless of category of the performance characteristics, a

greater grey relational grade value corresponds to better performance. Therefore, the optimal level of the process parameters is the level with the greatest grey relational grade value. An asterisk (*) marked with the respective GRG values indicates that the level value results in a better texturing performance. Based on the grey relational grade values shown in fig. 7.4 and the respective data incorporated in Table 7.12, the optimal TMEMM performance for multiple responses is obtained for the combination of applied voltage of 12 V, pulse frequency of 1 kHz, and duty ratio of 15%. As listed in Table 7.12, the difference between the maximum and the minimum value of the grey relational grade of the texturing parameters indicates the significance of the role that every controllable factor plays over the multi-performance characteristics. It is shown that the performance characteristics are mainly affected by pulse frequency. Moreover, the experimental values of the desired responses at this optimal parametric combination are shown in Table 7.13.

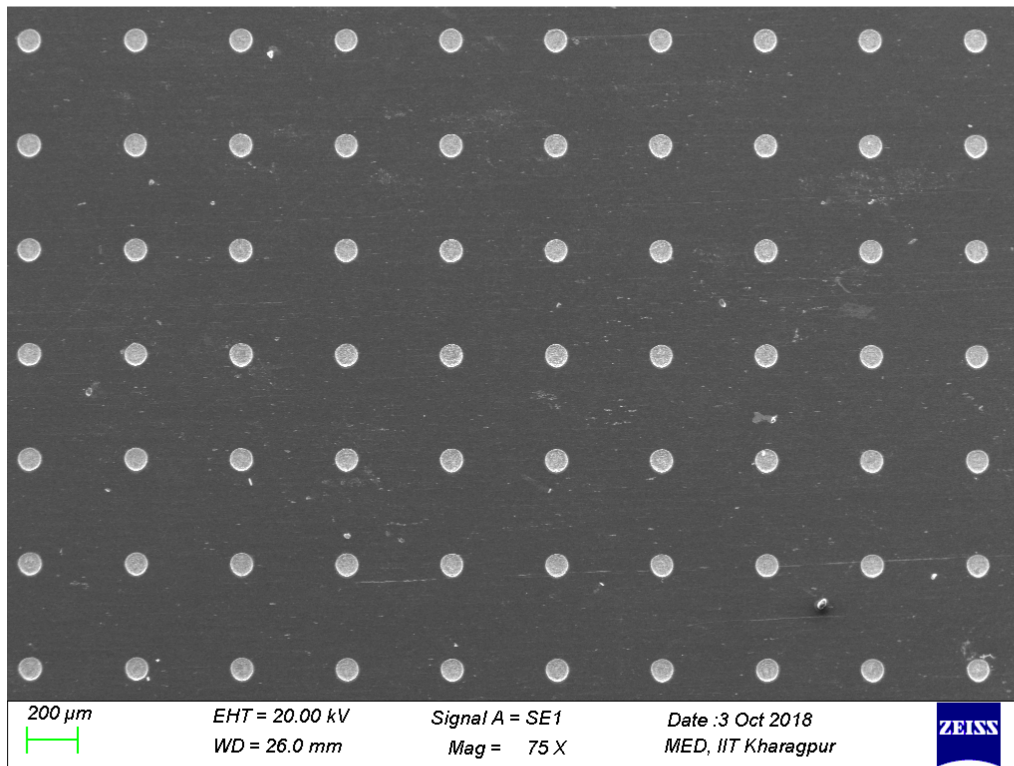

Figure 7.5: Micro-Dimples patterned array with simultaneous optimized responses formed at the optimized parametric combination

With these optimal settings as presented in Table 7.13, through mask electrochemical micromachining have been conducted. SEM micrograph of the patterned array of micro-dimples generated at optimal parametric combination has been illustrated at fig. 7.5.

Table 7.13: Experimental values of responses at optimal settings

Experimental values at Applied voltage-12 V, Pulse frequency-1 kHz, Duty ratio-15%	Undercut (μm)	Dimple depth (μm)	Surface Roughness (μm)
	14.5271	20.73	0.312

7.9 Outcomes of the experimentation

Taguchi method of single objective parametric optimization is introduced for the optimization of the TMEMM process parameters for generation of micro-dimple arrays. From the experimental results, S/N ratio and ANOVA analysis, it is observed that the applied voltage, pulse frequency and duty ratio are the three influential parameters (in rank order based on percentage contribution) which significantly affect the undercut of the generated micro-textures. For achieving minimum undercut of 7.3919 μm, the optimal level of parametric conditions is 10 V, 2 kHz and 10% for applied voltage, pulse frequency and duty ratio respectively. For attaining maximum dimple depth of 21.68μm, the optimum parametric condition is 12V, 1 kHz and 15%. Here, pulse frequency plays a major part in the maximization of dimple depth followed by applied voltage and duty ratio. The optimal parametric combination for minimization of R_a of 0.173 μm is 12 V, 1 kHz, 20%, where duty ratio and pulse frequency contributes equally followed by applied voltage. The improvement in the quality characteristics of TMEMM process is ensured by the confirmatory test results that establishes the validity of the analysis.

Multi-objective optimization has been performed to search out the optimal setting of TMEMM process parametric combination for maximization of the dimple depth, minimization of the undercut and R_a with Grey Taguchi Approach. After thorough analysis of the experimental data, it is found that experiment number 7 (12 V, 1 kHz and 20%) provides the near optimal parametric combination for this TMEMM process for simultaneous optimization of all the three responses and is the optimal machining parameters' setting for minimum undercut i.e. 18.2651 μm as well as surface roughness characteristics, Ra i.e. 0.133 μm and maximum dimple depth i.e. 21.46 μm simultaneously (i.e. the best multi-performance characteristics) among the nine experiments. Based on the grey relational grade values, the optimal TMEMM performance for multiple responses is obtained with a parametric combination of 12V applied voltage, 1 kHz pulse frequency and 15% duty ratio. Further, it is also found that among the three process parameters, the performance characteristics are mainly affected by the pulse frequency during experimentation.

GENERAL CONCLUSIONS

8.1 General Conclusions

Effective utilization of electrochemical dissolution process in through mask electrochemical micromachining (TMEMM) for precision micro-texturing demands an extensive research for investigating the influence of major process parameters on micro-texturing performance. The present research mainly consists of the development of experimental system set-up, preparation of experimental samples, development of technique for generation of island-free micro-dimple patterned array, experimental investigation into the influence of various process parameters on micro-texturing criteria i.e. machining accuracy; analyzed in terms of undercut, dimple depth and etch factor along with surface characteristics during generation of circular micro-textured surfaces. From the experimental results, best texturing parameters have been obtained and machining of various micro textures suitable for practical applications have been demonstrated. Moreover, generation of high-aspect-ratio micro-dimples has also been studied through experimental investigations utilizing significant TMEMM process parameters. However, within the limitation of resources, the following conclusions may be drawn:

(i) From the present study, it is clear that Through Mask Electrochemical Micromachining is one of the key micro machining methods, which can be utilized for machining of patterned micro-textures on advanced engineering materials whose industrial and commercial applications in specialized fields are rapidly expanding. TMEMM can be advantageously employed for machining of micro-structures of different geometries that have specific applications in different spheres.

(ii) Successful development of the TMEMM experimental system set-up has been made for effective analysis of the influences of various significant electrochemical phenomena during micromachining. The indigenously developed system set-up consist of different subcomponents namely TMEMM cell comprising of the base along with workpiece and tool holder, pulse power supply unit, electrolyte supply system and inter electrode gap control and monitoring system etc. The developed experimental set-up is capable of generation of micro-textures over the experimental job samples which were

meticulously prepared through precision design and development process of UV-lithography.

(iii) TMEMM process parameters have been experimented during generation of micro dimple array over SS304 samples employing a noble material i.e. AZ-4903, a negative photoresist, as mask, due to its availability, low cost, chemical resistance and high flexibility. An economical way of fabrication of circular micro-textures over metal surface by TMEMM utilizing low aspect ratio mask has been successfully presented. It was experimentally established that formation of islands could be avoided even after using a thin mask of 16 μm thickness. Further, well controlled shapes with smooth surface geometry can be achieved by prolonging the machining time. A patterned mask of a negative PR (AZ 4903) of very low thickness i.e. 16 μm, possessing strong adhesiveness with the substrate has been utilized during the experimentation. It was experimentally found from the SEM micrographs that micro-dimple array without islands can be successfully generated using a 16 μm thin mask utilizing TMEMM parameter setting i.e. applied voltage of 10 V, pulse frequency of 1 kHz, electrolyte flow velocity of 3.8 m/s, mixed electrolyte concentration of 10% NaCl and 10% $NaNO_3$, and duty ratio of 20% by prolonging the machining time to 120 s with considerable repeatability maintaining dimensional uniformity.

(iv) One of the significant contributions of present research is the generation of island-free micro-dimple arrays over stainless steel, i.e. SS304 substrate covered with a mask consisting patterned micro holes.The duty ratio along with the machining time have been further investigated for understanding its effect on the average undercut and average dimple depth of the generated patterned surfaces containing micro-textures. Further, the surface roughness characteristics (R_a and R_q) of the generated micro-dimples were experimentally investigated during the present research work. With the increase in duty ratio, while the value of undercut and the surface roughness rises, the depth of the micro dimples and the etch factor decreases. Island free micro-dimple arrays measuring 97 μm diameter and 43.1 μm depth, 0.091 μm R_a and 0.112 μm R_q were successfully generated utilizing TMEMM.

(v) Circular and square micro-patterned array were successfully generated and influence of the mask thickness on the machining performance and surface roughness characteristics has been experimentally studied. Low aspect ratio masks of three different thicknesses have been utilized during experimentation to study its influence on surface structuring

during TMEMM. When the electrolyte concentration, flow velocity, applied voltage and pulse frequency were fixed, with the increase in mask thickness from 12 µm to 20 µm, the dimple diameter along with the average depth of dimple decreases. It was also inferred from the SEM micrographs that, circular and square micro-dimples with best dimple surface having R_a of 0.091 µm and 0.081 µm and R_q of 0.113 µm and 0.096 µm respectively were successfully generated by machining for 120 s with electrolyte concentration 10% NaCl + 10% $NaNO_3$, voltage 12 V, pulse frequency 2 kHz and utilizing mask of 20 µm thickness. Application of mask of thin ranges, which reduces the expenditure incurred during the process, is another remarkable contribution of the present set of research.

(vi) Frictional analysis has been carried out to understand the effect of texturing on the generated surfaces in which the surfaces were subjected to friction test with increasing normal loads. It was noticed after the friction analysis that, when the surfaces with circular patterned micro dimples were subjected to a maximum normal load of 75 N, the frictional co-efficient gradually reduces from 0.0221 to 0.0167 with increasing dimple depths from 30 µm to 40 µm. This value further reduces from 0.019 to 0.0143 for surfaces containing square micro-texture arrays. As such, it was inferred that surfaces with square patterned micro dimples are more effective in reducing the frictional coefficient when subjected to increased normal loads as compared to surfaces containing circular patterned micro-textures, which is another noteworthy contribution of the present research.

(vii) High-aspect-ratio micro textured surfaces were successfully generated with the help of indigenously developed TMEMM set-up through exploring the suitable range of applied voltage along with electrolyte type and concentration on the machining precision and surface roughness of the generated micro-textures. 3D micro-textured arrays with an average depth of 40 µm possessing an aspect ratio of 0.7167 have been successfully fabricated with electrolyte concentration 10% NaCl + 10% $NaNO_3$, while an aspect ratio of 0.5867 was achieved when the texturing was carried out with 10% $NaNO_3$ electrolyte. The experimental results showed that with the increase in applied voltage, while the undercut and the depth of the micro dimples increases, R_a and R_q initially decreases to 0.091 µm and 0.112 µm till 12 V and then gradually increases to 0.144 µm and 0.161 µm respectively at 24 V, although it could be observed from the

SEM micrographs that noticeable machining can be observed when applied voltage reaches its threshold value i.e. 12 V.

(viii) Upon experimental investigation, it was found that, when TMEMM was carried out under similar parametric combinations, lowest range of undercut could be found with the samples machined with an electrolyte concentration of 20% $NaNO_3$ while the combination of 10% NaCl and 10% $NaNO_3$ have been analyzed to be the best electrolyte for achieving highest range of depths. Further, it was noticed from the SEM micrographs and profilometer images that 10% $NaNO_3$ have been found out to be most suitable for achieving micro-dimples possessing best surface quality and 20% $NaNO_3$ have been found out to be the best electrolyte for achieving highest aspect ratio microstructures among the three electrolyte combinations. When the textured surfaces were subjected to friction test, it was observed that surfaces with patterned micro arrays reduces frictional coefficient when subjected to increased normal loads and the rate of reduction is more during wet condition as compared to dry condition. After analysis of the friction tests, it was observed that the frictional co-efficient reduces from 0.0791 to 0.0573 for dimples with 15 µm depth, 0.0763 to 0.041 for 20 µm depth and 0.0732 to 0.028 when the average dimple depths ranges around 25 µm, when subjected to increased normal loads from 25 N to 75 N.

(ix) Parametric optimization of the TMEMM process parameters for generation of circular micro-patterned arrays utilizing Taguchi method is one of the valuable contributions of the research work. From the ANOVA analysis, it was found that applied voltage is the most significant factor for minimization of undercut while pulse frequency plays a dominant role in the enhancement of the dimple depth. Moreover, pulse frequency and duty ratio contributes equally towards improvement in the surface of the generated circular micro-textured dimples.

For achieving minimum undercut i.e. 7.3919 µm, the best level of parametric conditions according to S/N ratio graphs is $A_1B_2C_1$ i.e., the applied voltage of 10 V, pulse frequency of 2 kHz and duty ratio of 10%. For attaining minimum dimple depth i.e. 21.68 µm, the optimum level of parametric conditions is $A_3B_1C_2$, i.e., applied voltage of 12 V, pulse frequency of 1 kHz and duty ratio of 15%. The most favorable parametric combination for minimization of surface roughness characteristics, R_a i.e. 0.173 µm is $A_3B_1C_3$ i.e. 12 V applied voltage, 1 kHz pulse frequency and 20% duty ratio. The improvement in the quality characteristics of TMEMM process is ensured by

the Taguchi method of parametric optimization as the confirmatory test results establish the validity of the analysis.

(x) Multi-objective optimization has been performed to search out the optimal TMEMM process parametric combination for simultaneous maximization of the dimple depth, minimization of the undercut and surface roughness characteristics, R_a with Grey Relational Analysis. After thorough analysis of the experimental data, it was found that experiment in which applied voltage of 12 V, pulse frequency of 1 kHz and duty ratio of 20% were considered, provides the near optimal parametric combination for simultaneous optimization of all the three responses. Based on the grey relational grade values, the optimal TMEMM performance for multiple responses is obtained for applied voltage, 12 V; pulse frequency, 1 kHz; and duty ratio, 15% combination. It was also found that among the three process parameters, the performance characteristics are mainly affected by the pulse frequency during experimentation. Micrographs of the micro-dimpled pattern generated at optimized parametric combination during experimentation were observed and analyzed to ascertain the correctness of the optimization.

Therefore, it is evident that the present research consisting of development of TMEMM set-up, experimentations for micromachining of various arrayed micro-textures on SS304 substrates utilizing through mask electrochemical micromachining process will be quite useful for analyzing the influence of various process parameters for achieving suitable control over the TMEMM process during machining of micro-textured surfaces and high-aspect-ratio microstructures. The present experimental findings will also be useful for both the design and manufacturing engineers to assess the necessary information required while machining different micro textured surface for practical applications.

The research activities on TMEMM will open up many challenging possibilities for effective utilization of the developed TMEMM system set-up for micro-dimple pattern generation employing thin photoresist masks. In depth experimental investigations on through mask electrochemical micromachining of SS304 may be useful for effective utilization of TMEMM process for various practical applications and opening new possibilities to the researchers working in the area of TMEMM. Finally, the research in the area of micromachining will be an important substitution and will fulfill various urgent needs of the modern electronic, automobile, mechanical, bio-medical and related precision industries especially in the area of micro surface texturing.

8.2 Future scope of the work

As long as miniaturization of products continuous to be the trend of the present technological advancement, TMEMM will play a critical role in the area of micro surface structuring. The process has been widely used within the field of micromachining, especially in relation to micro-electronics, micro-actuators and micro structured surfaces, but also for the manufacture of thin precision parts along with specified surface texture. At this stage, researcher feels that more research and development is needed in this specialized area of micro surface texturing to make the TMEMM process more successful for precision micro manufacturing applications.

Hence, further scope of research includes:

(i) Development of CNC automated TMEMM set-up for precise control and online monitoring of the machining process for generating free formed three-dimensional microstructures on advanced as well as difficult to cut materials and especially on semiconductors.

(ii) A feasibility study under technical and economic criteria is needed to assess the potential commercial interest in TMEMM to identify the major cost components with regard to capital expenditure and operation including analysis of potential environmental impacts.

(iii) Further investigations with other engineering metals and alloys needs to be carried out for improving certain shortcomings during micromachining for generating different micro-textured surfaces.

(iv) Surface structuring on large surface area as well as on free form surface needs in-depth experimental investigation utilizing TMEMM, which may be beneficial for various engineering applications.

However, the researcher trusts that the present investigation and subsequent discussions will provide insight to the researchers, scientists and engineers who are working in the area of Through Mask Electrochemical Micromachining. It can also provide direction for indigenous development of TMEMM system including fabrication of different patterned micro-textured arrays and its practical industrial applications which are highly in-demand in advanced engineering scenario for precision micro-engineering applications.

BIBLIOGRAPHY

1. John F. Wilson, Practice and Theory of Electrochemical Machining, 1971, John Wiley and Sons Inc., USA.

2. B. Bhattacharyya, "Electrochemical Micromachining for Nanofabrication, MEMS and Nanotechnology", 2015, William Andrew publications, Massachusetts, USA.

3. N. Taniguchi, Current status in and future trends of ultra precision machining and ultrafine material processing. Annals of the CIRP, 1983, 32 (2): 573-582.

4. Z. Lu, T. Yoneyama, Micro cutting in the micro lathe turning system, International Journal of Machine Tools and Manufacture, 1999, 39 (7): 1171-1183

5. M. Gower, N. Rizvi, Applications of laser ablation to micro engineering. Proceedings of SPIE, High-power laser ablation Ill, 2000, 4065:452-460.

6. V. K. Jain, Advanced Machining Process, 2002, Allied Publishers Pvt. Ltd, New Delhi

7. J.A. McGeough, Advanced Methods of Machining, 1988, Chapman and Hall, London.

8. J. Kozak, D. Gulbinowicz, Z. Gulbinowicz, The Mathematical Modelling and Computer Simulation of Pulse Electrochemical Micromachining. Engineering Letter, 2008, 16:4, EL 16 4 14.

9. C. F. Coombs, Printed Circuits Handbook. McGraw-Hill, New York, 2001.

10. M. Datta, D. Landolt, Fundamental aspects and applications of electrochemical microfabrication. Electrochimica Acta, 2000, 45: 2535-2558.

11. M. Datta, Fabrication of an array of precision nozzles by through-mask electrochemical micromachining. Journal of the Electrochemical Society, 1995, 142 (11): 3801-3805.

12. M. Datta, Micro fabrication by electrochemical metal removal. IBM Journal of Research and Development, 1998, 42 (5): 655–669.

13. C. Van Osenbreggen, C.A. de Regt, Electrochemical micromachining. Philips Technical Review, 42 (1985) 22-32.

14. K. Chikamori, Possibilities of electrochemical micromachining. International Journal of Japan Society of Precision Engineering, 1998, 32 (1): 37-48.

15. T. Masuzawa, State of the art of micromachining. Annals of the CIRP, 2000, 49 (2): 473-486.

16. R. Schuster, V. Kirchner, P. Allongue G. Ertl, Electrochemical micromachining. Science, 2000, 289: 98-101.

17. B. Bhattacharyya, B. Doloi, P.S. Sridhar, Electrochemical micromachining: New possibilities for micro manufacturing. Journal of Materials Processing Technology, 2001, 113: 301-305.

18. E.S. Lee, J.W. Park and Y.H. Moon, A study on electrochemical micromachining for fabrication of microgrooves in an air-lubricated hydrodynamic bearing. International Journal of Advanced Manufacturing Technology, 2002, 20: 720-726.

19. O. Piotrowski, C. Madore, D. Landolt, The mechanism of electropolishing of titanium in Methanol-Sulfuric acid electrolytes. Journal of the Electrochemical Society, 1998, 145 (7): 2362-2369.

20. Y. Ferri, O. Piotrowski, P.F. Chauvy, C. Madore, D. Landolt, Two-level electrochemical micromachining of titanium for device fabrication. Journal of Micromechanics and Microengineering, 2001, 11: 522–527.

21. B. Ghoshal, B. Bhattacharyya, Micro electrochemical sinking and milling method for generation of micro features. Proceedings of Institution of Mechanical Engineers Part B: J Engineering Manufacture, 2013, 227(11).

22. V. Rathod, B. Doloi, B. Bhattacharyya, Influence of electrochemical micromachining parameters during generation of microgrooves. International Journal of Advanced Manufacturing Technology, 2015, 76: 51-60.

23. J. Bannard, On the electrochemical machining of some titanium alloys in bromide electrolytes. Journal of Applied Electrochemistry, 1976, 6: 477-483.

24. Y. C. Chiou, R. T. Lee, T. J. Chen, J. M. Chiou, Fabrication of high aspect ratio micro-rod using a novel electrochemical micro-machining method. Precision Engineering, 2012, 36: 193–202.

25. Y. Yang, W. Natsu, W. Zhao, Realization of eco-friendly electrochemical micromachining using mineral water as an electrolyte. Precision Engineering, 2011, 35(2): 204-213.

26. J.W. Park, E.S. Lee, C.H. Won, Y.H. Moon, Development of electrochemical micromachining for air-lubricated hydrodynamic bearings. Microsystem Technologies, 2002, 9: 61-66.

27. L. Cagnon, V. Kirchner, M. Kock, R. Schuster, G. Ertl, W. T. Gmelin, H. Kuck, Electrochemical micromachining of stainless steel by ultrashort voltage pulses. International Journal of Research in Physical Chemistry and Chemical Physics, 2003, 217: 299-313.

28. H. Rasmussen, J.A. McGeough, Theory of overpotentials in electrochemical micromachining. Journal of Materials Processing Technology, 2004, 149 (1-3): 504-505.

29. M. Sen and H.S. Shan, A review of electrochemical macro-to-micro-hole drilling processes. International Journal of Machine Tools & Manufacture, 2005, 45: 137-152.

30. R. Forster, A. Schoth, W. Menz, Micro-ECM for production of microsystems with a high aspect ratio. Microsystem Technologies, 2005, 11: 246-249.

31. V. K. Jain, Subodh Kalia, Ajay Sidpara, V. N. Kulkarni, Fabrication of microfeatures and micro-tools using electrochemical micromachining. International Journal of Advanced Manufacturing Technology, 2012, 61(9-12): 1175-1183.

32. M. Datta, L.T. Romankiw, Applications of chemical and electrochemical micromachining in the electronic industry. Journal of the Electrochemical Society, 1989, 136 (6): 2850-2857.

33. M. Datta, L.T. Romankiw, D.R. Vigliotti, R.J.V. Gutfeld, Jet and laser-jet electrochemical micromachining of nickel and steel. Journal of the Electrochemical Society, 1989, 136 (8): 225-230.

34. M. Datta, R.V. Shenoy, L.T. Rominkiw, Recent advances in the study of electrochemical micromachining. Journal of Engineering for Industry - Transactions of the ASME, 1996, 118: 29-36.

35. M. Datta, D. Harris, Electrochemical micromachining: An environmentally friendly, high speed processing technology. Electrochimica Acta, 1997, 42 (20-22): 3007-3013.

36. O. Zinger, P.F. Chauvy, D. Landolt, Scale-Resolved Electrochemical Surface Structuring of Titanium for Biological Applications. Journal of the Electrochemical Society, 2003, 150 (11): B495-B503.

37. A. Spieser, A. Ivanov, Recent developments and research challenges in electrochemical micromachining (μECM). International Journal of Advanced Manufacturing Technology, 2013, 69: 563-581.

38. M. H. Wang, D. Zhu, Fabrication of multiple electrodes and their application for micro-holes array in ECM. International Journal of Advanced Manufacturing Technology, 2009, 41:42–47.

39. C. Madore, D. Landolt, Electrochemical micromachining of controlled topographies on titanium for biological applications. Journal of Micromechanics and Microengineering, 1997, 7: 270–275.

40. D. Landolt, P.F. Chauvy, O. Zinger, Electrochemical micromachining, polishing and surface structuring of metals: Fundamental aspects and new developments. Electrochimica Acta, 2003, 48: 3185-3201.

41. X. Lu, Y. Leng, Electrochemical micromachining of titanium surfaces for biomedical applications. Journal of Materials Processing Technology, 2005, 169 (2): 173-178.

42. S. Nouraei, S. Roy, Electrochemical Process for Micropattern Transfer without Photolithography: A Modelling Analysis. Journal of the Electrochemical Society, 2008, 155: D97–D103.

43. I. Schonenberger, S. Roy, Microscale pattern transfer without photolithography of substrates. Electrochimica Acta, 2005, 51: 809–819.

44. X. Zhang, N.Qu, H. Li, Z. Xu, Investigation of machining accuracy of micro-dimples fabricated by modified microscale pattern transfer without photolithography of substrates. International Journal of Advanced Manufacturing Technology, 2015, 81: 1475–1485.

45. R. P. Frankenthal, H. D. Eaton, Electroetching of Platinum in the Titanium-Platinum-Gold Metallization on Silicon Integrated Circuits. Journal of the Electrochemical Society, 1976, 123: 703.

46. A. C. West, C. Madore, M. Matlosz, D. Landolt, Shape changes during through-mask electrochemical micromachining of thin metal films. Journal of Electrochemical Society, 1992, 139 (2): 499-506.

47. Z. Zhang, D. Zhu, N. Qu, M. Wang, Theoretical and experimental investigation on electrochemical micromachining. Microsystem Technologies, 2007, 13: 607-612.

48. D. Zhu, N.S. Qu, H.S. Li, Y.B. Zeng, D.L. Li, S.Q. Qian, Electrochemical micromachining of microstructures of micro hole and dimple array. CIRP Annals - Manufacturing Technology, 2009, 58: 177-180.

49. P. Raffelstetter and B. Mollay, On the modelling of shape evolution in through-mask electrochemical micromachining of complex patterned substrates. Electrochimica Acta, 2010, 55: 2149-2157.

50. S. Qian, D. Zhu, N. Qu, H. Li and D. Yan, Generating micro-dimples array on the hard chrome-coated surface by modified through mask electrochemical micromachining. International Journal of Advanced Manufacturing Technology, 2010, 47 (9-12): 1121-1127.

51. G.Q. Wang, H.S. Li, N. Qu, D. Zhu, Investigation of the hole-formation process during double-sided through-mask electrochemical machining. Journal of Material Processing Technology, 2016, 234: 95–101.

52. G.J. Kwon, H.Y. Sun, H.J. Sohn, Wall profile developments in through-mask electrochemical micromachining of invar alloy films. Journal of the Electrochemical Society, 1995, 142 (9): 3016-3020.

53. R.V. Shenoy and M. Datta, Effect of mask wall angle on shape evolution during through-mask electrochemical micromachining. Journal of the Electrochemical Society, 1996, 143 (2): 544-549.

54. R.V. Shenoy, M. Datta, L.T. Romankiw, Investigation on island formation during through-mask electrochemical micromachining. Journal of the Electrochemical Society, 1996, 143 (7): 2305-2309.

55. X. Chen, N. Qu, Z. Hou, Electrochemical micromachining of micro-dimple arrays on the surface of Ti-6Al-4V with $NaNO_3$ electrolyte. International Journal of Advanced Manufacturing Technology, 2017, 88: 565–574.

56. N. Qu, X. Chen, H. Li, D. Zhu, Fabrication of PDMS micro through-holes for electrochemical micromachining. International Journal of Advanced Manufacturing Technology, 2014, 72: 487–494.

57. X. Chen, N. Qu, H. Li, Z. Guo, Removal of islands from micro-dimple arrays prepared by through-mask electrochemical micromachining. Precision Engineering, 2015, 39: 204–211.

58. X. Chen, N. Qu, X. Fang, D. Zhu, Reduction of undercutting in electrochemical micro-machining of micro-dimple arrays by utilizing oxygen produced at the anode. Surface and Coatings Technology, 2015, 277: 44–51.

59. S. Qian, F. Ji, N. Qu, H. Li, Improving the Localization of Surface Texture by Electrochemical Machining with Auxiliary Anode. Materials and Manufacturing Processes, 2014, 29: 1488–1493.

60. P. Kern, J. Veh, J. Michler, New developments in through mask electrochemical micromachining of titanium. Journal of Micromechanics and Microengieering, 2007, 17: 1168–1177.

61. P.F. Chauvy, P. Hoffmann, D. Landolt, Electrochemical micromachining of titanium using laser oxide film lithography: excimer laser irradiation of anodic oxide. Applied Surface Science, 2003, 211: 113–127.

62. T. Sjostrom, B. Su, Micropatterning of titanium surfaces using electrochemical micromachining with an ethylene glycol electrolyte. Materials Letters, 2011, 65: 3489-3492.

63. H. McCrabb, A. Lozano-Morales, S. Snyder, L. Gebhart, E. J. Taylor, Through Mask Electrochemical Machining. ECS Transactions, 2009, 19: 19-33.

64. X. Chen, N. Qu, H. Li, and Z. Xu, Electrochemical micromachining of micro dimple arrays using a polydimethylsiloxane (PDMS) mask. Journal of Material Processing Technology, 2016, 229: 102–110.

65. K.H. Chun, D.S. Jin, S.H. Kim, E.S. Lee, Comparison between wire mesh and plate electrodes during Wide-pattern machining on invar fine sheet using through-mask electrochemical micromachining. Journal of Mechanical Science and Technology, 2017, 31: 1851–1859.

66. J.B. Ahn, H.Y. Ryu, J.G. Park, Fabrication of Bumping Mask for Flip-Chip Process on Stainless Steel Using Through Mask Electrochemical Micro Machining (TMEMM). ECS Transactions, 2015, 69: 1–7.

67. X. Zhang, N. Qu, X. Chen, Sandwich-like electrochemical micromachining of micro-dimples. Surface and Coatings Technology, 2016, 302: 438–447.

68. T. Baldhoff, A.T. Marshall, Characterization of Surface Films Formed on Aluminium during Mass-Transfer Limited Anodic Dissolution in Phosphoric Acid. Journal of the Electrochemical Society, 2017, 164: C46–C53.

69. G.Q. Wang, D.Zhu, H.S.Li, Fabrication of semi-circular micro-groove on titanium alloy surface by through-mask electrochemical micromachining. Journal of Material Processing Technology, 2018, 258: 22-28.

70. X.Zhang, N.Qu, Improvement in machining accuracy of micro-dimples fabricated in a sandwich-like EMM unit using a porous cathode, International Journal of Advanced Manufacturing Technology, 2018, 99 (5-8): 1661-1671.

71. M.S. Phadke, Quality engineering using robust design, 1989, Prentice Hall of India Private Limited, ISBN 0-13-745167-9, New Jersey.

72. D.C. Montogomery, Design and Analysis of Experiments, 1997, John Willey & Sons, ISBN 0-471-15746-5, Singapore.

73. J. L. Deng, Introduction to Grey System Theory. The Journal of Grey System, 1989, 1(1): 1-24.